Investigating variables affecting heap (bio)leaching through determining access to sub-surface mineral grains by micro-scale X-ray tomography

Mahdi Ghadiri

In fulfilment of the requirements for the degree of
Master of Science

Supervisor: **Dr Marijke Fagan-Endres**
Co-Supervisor: **Prof Sue Harrison**

Department of Chemical Engineering
Faculty of Engineering and the Built Environment
University of Cape Town

July 2019

Plagiarism Declaration

1. I know that plagiarism is wrong. Plagiarism is to use another's work and to pretend that it is one's own.
2. I have used the Harvard system for citation and referencing. Each significant contribution to, and quotation in, this report from the work, or works, of other people has been attributed, and has been cited and referenced.
3. This report is my own unaided work, except for assistance received from the teaching staff.
4. I have not allowed, and will not allow, anyone to copy my work with the intention of passing it off as his or her own work.

Signed by candidate

Signature

Abstract

Heap bioleaching is a hydrometallurgical technology, used to facilitate the extraction of valuable metals such as copper, gold, nickel and uranium from low-grade, typically sulphidic, ores. The process is highly complex as it is influenced by interactions of different sub-processes including flow of leaching solution around the ore particles, mass and heat transfer within and around the particles, chemical reactions, microbially-mediated reactions and microbial growth. Contact of leaching solution with mineral grains is necessary for oxidation of the sulphide minerals. However, a large fraction of the mineral grains is positioned below the surface of the ore particles and so contact with the liquid occurs through cracks and pores in the ore connected to the surface. Long extraction times and low metal recoveries typical of heap systems can be attributed to the slow leaching rate of these non-surface mineral grains as well as constraints on their accessibility. Most of the valuable grains that remain in the residue ores are non-surface grains. Therefore, investigation of the mechanism and behaviour of non-surface grain leaching and quantification of the factors contributing to their leaching is expected to be highly beneficial in the optimisation of leach conditions and recoveries.

Non-surface grain leaching within large particles cannot be investigated via traditional experimental methods reliant on bulk measurements, 2D or destructive methodologies. However, it can be studied using high resolution, non-destructive 3D X-ray micro-Computed Tomography (µCT), an imaging technique for investigation of internal structure of opaque objects. X-ray µCT has previously been developed and used for investigation of different aspects of heap leaching. In the current study, the viability of using X-ray µCT to study heap bioleaching systems and affecting variables is assessed. This required establishment of procedures for measurement and analysis of sulphide and oxide mineral recoveries and leaching penetration distances.

The feasibility of studying biotic heap leaching by X-ray µCT was explored through investigation of the relative energies required for high mineral resolution and avoidance of microbial inactivation. Specific bioleaching operating variables that were subsequently considered included: the accuracy and representivity of the X-ray µCT images, the influence of agglomeration pre-treatment, operating temperature, and type of ore on non-surface grain leaching. Addition of surfactants to the leaching solution was explored with the aim of changing surface activity to influence the penetration of the leach agent into pores and cracks in the ore.

The effects of operating conditions on non-surface mineral grain leaching was studied using mini-column experiments. Three different low-grade ores, namely a chalcopyrite-rich ore, a malachite ore and a waste rock containing pyrite were prepared for the leaching experiment. The ores were crushed using a jaw crusher and comminuted down to 100% passing 16 mm. The products were sieved into six fractions (<0.25 mm, 0.25 – 1 mm, 1 – 2 mm, 2 – 5.6 mm, 5.6 – 8 mm, 8 – 16 mm) and each fraction then representatively split into smaller portions using a rotary splitter. One portion of each size fraction was taken for XRD, AAS and QEMSCAN analyses. Mini leaching columns were designed and constructed based on the target mineral grain distribution in the ores to ensure that the mineral grains were detectable using X-ray µCT, given its resolution limitations. The columns were charged with 50 g of agglomerated or non-agglomerated ore and lixiviant was provided at a flow rate of 2.55 mL h^{-1} for a period of 5.5 months for chalcopyrite and pyrite and 26 days for malachite in incubators at 30 °C, 37 °C and 65 °C.

In order to select a surfactant suitable for use in a biological leach experiment, the effect of five different types and concentration of non-ionic surfactants on bioleaching microorganisms was studied in terms of microbial growth, ability for ferrous ion oxidation and chalcopyrite bioleaching. This was done in shake flask experiments using mineral concentrate. Based on the results of these experiments, Tween® 20 (10 mg L^{-1}) was selected to study the effect of surfactant on non-surface mineral grain leaching in the mini-columns.

Each column was scanned by X-ray µCT at 100 kV and 150 mA using a 0.38 mm copper filter and at a distance of 59.40 mm between X-ray gun and specimen. The advanced 3D analysis software Avizo® 9 was used to visualize and analyse image data. The Interactive Thresholding function in Avizo® 9 software was used for segmentation of ore particles from air and sulphide minerals from air and gangue minerals, to measure the target minerals' volume reduction during leaching. The Distance Map Algorithm was applied on a binary (segmented) image to calculate the distance of the sulphide mineral from the ore particle surface. Imaging of the whole mini-column was done before leaching and at the end of each experiment and imaging of certain sections was done at select time points during leaching to track temporal leaching dynamics. Good agreement was seen between the bulk mineral recovery data, determined using standard chemical assays, and the leaching curves generated using the X-ray µCT images for all the ores, confirming that the X-ray µCT images were a good quantitative measurement of the sulphide and oxide mineral leaching.

Liquid microbial culture experiments were used to confirm that exposure to X-ray does not affect microbial activity for energy doses between 35 and 90 kV at 200–280 µA. However, X-ray exposure was found to have a slight negative influence at higher voltages of 120 and 150 kV, temporarily reducing the specific ferrous ion oxidation and suppressing the specific growth rate of the bioleaching microorganisms. The X-ray exposure thus negatively affected both the total microbial population available for leaching (population viability) as well as the metabolic activity of the individual microorganisms (population vitality).

The effect of X-ray exposure on bioleaching cultures attached to a mineral surface was examined using pyrite-coated glass beads packed into mini-columns. The energy dosage limits identified in the liquid culture experiments were found to be compatible with the X-ray µCT imaging conditions (minimum energy dosage and sample position) required for acquisition of complete and accurate images of the columns at a resolution that allows identification of individual mineral grains. Following X-ray exposure, the performance of the exposed bioleaching mini-columns was equivalent to the unexposed control column. Similarly, the microbial activity and presence on the mineral surface appeared unchanged. Finally, the experiment was performed on the chalcopyrite ore and the microorganisms were found to still be able to convert Fe^{2+} to Fe^{3+} after 2 scanning runs. Thus, all sets of results confirm that X-ray µCT can be compatible with heap bioleaching experiments, while still permitting appropriate resolution of the mineral grains to make an X-ray µCT investigation worthwhile. However, cognisance that an upper limit of tolerable X-ray exposure exists must be taken. This may present a challenge if it is desired to image larger or denser ore samples which require a greater X-ray energy level for sufficient penetration of the sample by the X-rays and hence accurate imaging.

In chalcopyrite leaching, increasing temperature from 37 °C to 65 °C resulted in clear enhancement of leaching based on both analysis methods, with the copper recovery increasing from 20% to 64% by the end of the leaching period, and the overall sulphide mineral dissolution increasing from 24% to 67%. Increasing temperature from 37 °C to 65 °C resulted in an increased leaching penetration distance and crack development in the particles, and thus an enhancement in copper recovery and sulphide mineral dissolution. This was in addition to the thermodynamically expected increased leaching rate. The maximum leaching penetration distance, beyond which no mineral volume change is observed, at 37 °C was 1.7 mm. This increased to 2.5 mm at 65 °C. As a result of addition of 10 mg L^{-1} Tween® 20 into the leaching solution, the final copper recovery was improved by 4% to 68% and the maximum penetration distance increased to 2.9 mm. However, when the availability of sulphide mineral was not rate limiting, the copper recovery and sulphide mineral volume reduction in the mini-column with surfactant was lower than the system without surfactant. This may have been due to depression of diffusion of ferric ion to the ore surface as a result of the formation of an adsorbed surfactant layer on the mineral surface. The performance with surfactant became superior as the amount of readily leachable mineral became limiting. In the pyrite waste rock, an increase in temperature did not have any effect on the maximum penetration distance and any increase in iron recovery was only for thermodynamic reasons. Similarly to the chalcopyrite ore, during the later period of leaching when readily exposed mineral grains have been depleted, the system performed better in the presence of surfactant. The addition of surfactant increased the maximum penetration distance from 2.7 to 2.9 mm. The cumulative copper recovery of 86% was obtained for malachite ore in 26 days of acid leaching and the maximum penetration distance was 2.2 mm. This study thus demonstrates the value of the X-ray µCT technique for quantitative investigation of non-surface mineral grain leaching and confirms that the maximum penetration distance can be affected with changing operation conditions or ore type.

This study thus demonstrates the X-ray µCT technique for quantitative investigation of non-surface mineral grain bioleaching and confirms that the maximum penetration distance can be affected with changing operation conditions. Critically, the results confirm that X-ray µCT can be compatible with bioleaching microorganisms, while still permitting appropriate resolution of the mineral grains to make an X-ray µCT investigation worthwhile.

Acknowledgements

First of all, I would like to thank Allah Almighty to give me the opportunity to reach this level of science which it was not possible without Allah blessing upon me.

I would like to express my very great appreciation to Dr Marijke Fagan-Endres and Prof Sue Harrison, for the patient guidance, encouragement and advice they have provided throughout my time as their student. I have been extremely lucky to have supervisors who cared so much about my work, and who responded to my questions and queries so promptly.

Dr Megan Becker for her constructive criticism mostly in the mineral characterization part of this research. I am grateful to Dr Kirsten Corin for the QXRD analysis; Shireen Govender for helping me to prepare ores, Dr Rebecca Rogers Ackermann for Avizo software in Archaeology Department, Paul and Margaret Keanly (X-Sight X-ray Services), and for their advice and support. Financial support from the South African Minerals to Metals Research Institute (SAMMRI), NRF South Africa Research Chair Initiative (SARChI), and National Research Foundation (NRF) are also acknowledged.

A heartfelt thank you to the Centre for Bioprocess Engineering Research (CeBER) staff, Tich Samkange, Emmanuel Ngoma, and Sharon Rademeyer, for their ability to manage the labs effectively and for their technical assistance. Thank you, Sue Jobson, Candice Mazzolini. Lesley Mostert, Sandra Christian, and Ruegshana Ederies for managing administrative issues and making my life easier.

A big thank you goes out to the rest of the CeBER members for their support and friendship.

Last but definitely not least, I would like to express my heartfelt thanks to my parents and family for your prayers, love and encouragement.

Outputs of this Work

Mahdi Ghadiri, Susan T.L. Harrison, Megan Becker, Marijke A. Fagan-Endres, Mineralogical analyses with 3D X-ray micro-computed tomography enables improved understanding of heap bioleaching, SAIMM Minerals Research Showcase 3-4 August, 2017, Philippi Village, Cape Town, Oral presentation.

Mahdi Ghadiri, Susan T.L. Harrison, Marijke A. Fagan-Endres, Tracking mineral grain dissolution in heap bioleaching of low grade sulphide ore using X-ray µ-CT, 3rd Conference on Imaging with Radiation (Imgrad2017) September 13-15th, 2017 University of the Witwatersrand, Johannesburg, Oral presentation.

Mahdi Ghadiri, Susan T.L. Harrison, Marijke A. Fagan-Endres, Effect of X-Ray µCT scanning on the growth and activity of microorganisms in a heap bioleaching System. Solid State Phenomena, 262, 2017, 143-146 (Conference proceeding of International Biohydrometallurgy Symposium 2017), Poster presentation.

Mahdi Ghadiri, Susan T.L. Harrison, Marijke A. Fagan-Endres, Effect of adding surfactant in the leaching solution on the growth and activity of microorganisms in a heap bioleaching system, Biohydrometallurgy '18, Windhoek Country Club Resort, Namibia, June 12-13, 2018, Oral presentation.

Mahdi Ghadiri, Susan T.L. Harrison, Marijke A. Fagan-Endres, Quantitative measurement of the effect of operating conditions on non- surface mineral grain leaching from crushed and agglomerated low grade chalcopyrite ore, Process Mineralogy'18, Vineyard Hotel, Cape Town, South Africa, November 19-21, 2018, Oral presentation.

Mahdi Ghadiri, Susan T.L. Harrison, Marijke A. Fagan-Endres. Influence of X-ray µ-Computed Tomography on the microbial activity of a mixed thermophilic and mesophilic bioleaching culture colonising a mineral surface, Biochemical Engineering Journal, Volume 139, 15 November 2018, Pages 123-131.

Mahdi Ghadiri, Susan T.L. Harrison, Marijke A. Fagan-Endres, Effect of surfactant on the growth and activity of microorganisms in a heap bioleaching system, Minerals Engineering, Volume 138, July 2019, Pages 43-51.

Table of Contents

List of Figures

List of Tables

Glossary of Terms

Acidophile	Microorganism which thrives in acid environment, typically at pH of 3 and below.
Archaea	Grouping of unicellular microorganisms that are genetically distinct from bacteria and eukaryotes, often thriving in extreme environmental conditions.
Abiotic	Physical rather than biological; not derived from living organisms
Biotic	Relating to or resulting from living organisms
Grain	A mineral grain that consists of a single mineral type. Several grains can make a particle. In the case of a liberated grain, the terms ‘grain’ and ‘particle’ are equivalent.
Inhibition	Prevention or slowing of microbial functions in response to a chemical or physical stimulus.
Inoculum	Initial microbial cells added to the heap system from which microbial growth proceeds.
Mesophile	Microorganism that can grow in the temperature range 20-45 ^{o}C.
Metabolism	The system of chemical reactions occurring within the microbial cells, including both the breakdown of compounds via catabolism and the synthesis of compounds through anabolism.
Mineral association %	The number of pixels of a mineral type adjacent to the mineral of interest expressed as a percentage of all the pixels associated with the mineral of interest.
Particle	Several grains make up a particle. A particle usually refers to a fragment of a rock or ore, the size of which is dependent on crushing and milling conditions as well as the size class it deports to.
Planktonic	Freely suspended
PLS	Effluent leach solution
Thermophile	Microorganism that can grow at elevated temperatures i.e. above 40 ^{o}C.

Acronyms, Abbreviations and Nomenclature

2D	Two-dimensional space
3D	Three-dimensional space
AMD	Acid Mine Drainage
AC	Abiotic control
ARD	Acid Rock Drainage
BC	Biotic control
BSE	Back-scattered electron
CeBER	Centre for Bioprocess Engineering Research
EW	Electrowinning
EVs	Electric vehicles
EPS	Exopolysaccharide
HPGR	High Pressure Grinding Rolls
OPD	Ortho-phenylenediamine
PCR	Polymerase chain reaction
PLS	Pregnant leach solution
PSD	Particle size distribution
QEMSCAN	Quantitative Evaluation of Minerals by Scanning Electron Microscopy
qRT PCR	Quantitative real time polymerase chain reaction
QXRD	Quantitative X-Ray Diffraction
SEM/EDS	Scanning Electron Microscope and Energy Dispersive Spectrometry
SX	Solvent extraction
X-ray µCT	X-ray Computed Tomography
XRF	X-ray Fluorescence
Cu	Copper
Fe	Iron
Fe^{2+}	Ferrous ion
Fe^{3+}	Ferric ion
S	Sulphur
SO_2	Sulphur dioxide
SO_4	Sulphate ion
Zn	Zinc
I	Intensity of attenuated X-rays
I_0	Intensity of the incident X-rays
μ	Linear attenuation coefficient
ρ	Bulk density of the material
γ	Surface tension

θ	Contact angle
D	Diffusion coefficient
$S_{l/s}$	Spreading coefficient of liquid
Z	Bulk atomic number of the material
E	X-ray energy
a	Energy-dependent coefficients
b	Energy-dependent coefficients
Z_e	Effective atomic number
f_i	Fraction of the total number of electrons
T.20.5	5 mg L^{-1} Tween® 20
T.20.10	10 mg L^{-1} Tween® 20
T.20.20	20 mg L^{-1} Tween® 20
T.80.5	5 mg L^{-1} Tween® 80
T.80.10	10 mg L^{-1} Tween® 80
T.80.20	20 mg L^{-1} Tween® 80
P.120.5	5 mg L^{-1} Plurafac® LF 120
P.120.10	10 mg L^{-1} Plurafac® LF 120
P.600.5	5 mg L^{-1} Plurafac® LF 600
P.600.10	10 mg L^{-1} Plurafac® LF 600
L.90.XL.5	5 mg L^{-1} Lutensol® XL 90
L.90.XL.10	10 mg L^{-1} Lutensol® XL 90

Mineral chemical formulae

Biotite	$K(Mg,Fe)_3(AlSi_3O_{10})(OH,F)_2$
Bornite	Cu_5FeS_4
Chalcopyrite	$CuFeS_2$
Chlorite	ClO_2
Chrysocolla	$Cu_{2-X}Al_X(H_{2-X}Si_2O_5)(OH)$
Garnet	$X_3Y_2(SiO_4)_3$
Fe-Ti oxide	$FeTiO_3$
Jarosite	$KFe_3(SO_4)_2(OH)_6$
Limonite	$FeO(OH).nH_2O$
K-feldspar	$KAlSi_3O_8$
Malachite	$Cu_2CO_3(OH)_2$
Muscovite	$KAl_2(Si_3Al)O_{10}(OH,F)_2$
Pyrite	FeS_2
Pyrrhotite	$Fe_{(1-X)}S$ (X=0 to 0.2)
Quartz	SiO_2
Rutile	TiO_2
Sphalerite	ZnS

1 Introduction

1.1 Context of project

Processing of low-grade and complex run of mine ores has gained considerable attention in recent years due to increasing world demand for metals and depletion of high-grade ores. The conventional method for recovery of metals from high-grade ores after crushing and milling is flotation, followed by smelting and purification processes. This method is not economically viable when treating low-grade ores because of the increased expense and energy requirement per unit metal recovered when the grade of ore decreases. Furthermore, there is an increasing prevalence of complex mineral ores and minerals associated with penalty metals, both unsuitable for smelting.

The most appropriate technologies for processing of low-grade secondary (e.g. chalcocite, covellite) and primary copper sulphide (e.g. chalcopyrite) ores are dump and heap leaching (Watling, 2014). This method is also used to treat metals such as uranium, gold, cobalt, nickel, and zinc commercially from sulphide mineral containing ores (Natarajan, 2018).

With the emergence of solvent extraction-electrowinning (SX-EW) technology, refined copper produced from leaching ores has increased from less than 1% of world refined copper production in the late 1960's to 16% of world output in 2017 (ICSG, 2018). The major uses of copper are in electronics and communications, construction, industrial machinery and equipment and transportation. One of the major anticipated future uses of copper is for electrical vehicles (EVs), which contain approximately four times more copper than conventional cars. The metal is used in batteries, windings and copper rotors in electric motors, wiring, busbars and charging infrastructure. It is estimated that globally 3 million EVs were on the road in 2017 and the demand for EVs is expected to see major growth going forward, driven by technology improvements, increased affordability and the deployment of more electric chargers. Each charger requires 0.7 kg of copper, while fast chargers can add up to 8 kg of copper each. This increase will result in a greater demand for copper (ICSG, 2018).

Major heap bioleach operations for copper around the world are listed in Table 1-1. As it can be seen, most of ores are secondary sulphides such chalcocite, bornite, etc. In the case of chalcopyrite bioleaching, Mintek has also developed a high-temperature heap bioleach pilot plant (Figure 1-1) in Iran (Van Staden et al., 2007). Three independent pilot heaps, each of about 25000 tonnes, were constructed on site at the Sarcheshmeh copper mine. The pilot plant has been in operation since 2005 and 14 pilot heaps (20,000 tons) have been operated. In average, 58.5% of copper was extracted after about 380 days (Van Staden et al., 2007).

Table 1-1: Industrial heap bioleaching operations for copper (Harrison, 2016; Natarajan, 2018; Watling, 2006).

Bioheap location	Ore type	Copper tons/year	Year
Andacollo Cobre, Chile	Sulphides, oxides	21000	1996
Chuquicamata, Chile,	Low grade sulphide dump	12500	1994
Cerro Colorado, Chile	Chalcocite, covellite	130000	1993
Dos Amigos, Chile,	Chalcocite	10000	1997
Escondida, Chile	Sulphides/oxides	750000	2006
Ivan Zar, Chile	Sulphides/oxides	10000	1994
Lince II, Chile	Sulphides/oxides	27000	1991
Lomas Bayas, Chile	Sulphides/oxides	60000	1998
Los Bronces, Chile	Sulphides	46400	2006
Punta del Cobre, SA/Chile	Sulphides/oxides	7000-8000	1994
Quebrada Blanca, Chile,	Chalcocite	82000	1994
Spence, Chile	Sulphides, oxides	20000	2007
Zaldivar, Chile	Chalcocite	150000	1998
Mount Gordon Australia	Chalcocite, bornite	33000	1991
Nifty Copper, Australia	Chalcocite, oxides	16000	1997
Whim Creek and Mons Cupri, Australia	Sulphides, oxides	17000	2006
Monywa, Myanmar	Chalcocite	40000	1998
Cerro Verde, Peru	Sulphides/oxides	54000	1997
Lisbon Valley, Utah	Chalcocite/oxides	27000	2006
Morenci, Arizona	Chalcocite, pyrite	380000	2001
Skouriotissa Copper Mines, Cyprus	Sulphides/oxides	8000	1996
Jinchuan Copper, China	Chalcocite, enargite, covellite	10000	2006

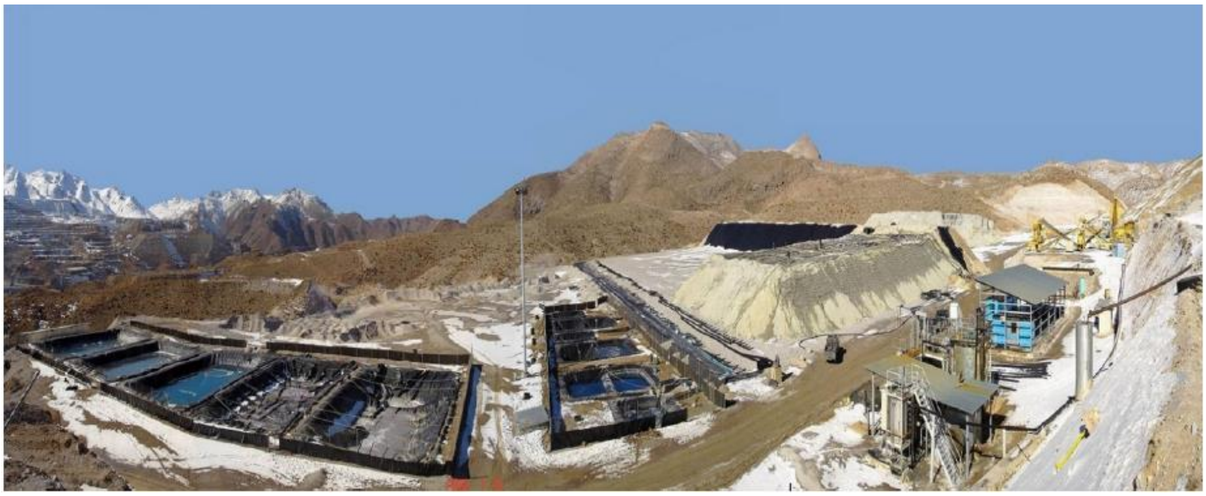

Figure 1-1: High-temperature heap bioleach pilot plant, Iran [Photograph and information provided by Mintek of Randburg, South Africa; http://www.mintek.co.za].

Heap leaching advantages include reduction of comminution costs, applicability for small to large deposits and potential for less environmental burden than conventional processes (Ghorbani et al., 2016). In heap bioleaching, microorganisms are required for the regeneration of leach reagents and control the products of the leaching reactions. This technology, though seemingly a simple process, is complicated by a collective of several sub-processes from heap to grain level (Ghorbani et al., 2011; Petersen and Dixon, 2007a). The major challenges in heap leaching are low recoveries, long extraction times from coarse particles, high acid consumption increasing the operational cost, and uneven distribution of the leaching solution (Fagan, 2014; Lin et al., 2016a; Petersen, 2016; Watling, 2006). However, there are limited fundamental and systematic studies which consider the effects of the aforementioned issues at the particle or mineral grain scale.

The contact of solution with mineral grains is necessary for the oxidative liberation of metals from the ore. Mineral grains on the ore surface are directly accessible to leaching reagent in the solution; therefore, the leaching rate of these mineral grains is relatively fast. There are other mineral grains in the ore which are indirectly accessible to leaching reagents via pores and cracks (Ghorbani et al., 2011). The slower leaching of these non-surface mineral grains is a key reason for the low recoveries and long extraction times of heap leaching. There are additionally some mineral grains which are fully occluded within the particle. Ore matrix degeneration is necessary for leaching of these grains. The position of the various mineral grains is shown in Figure 1-2. Their accessibility to the leach agent is expected to define the extent of metal recovery attainable.

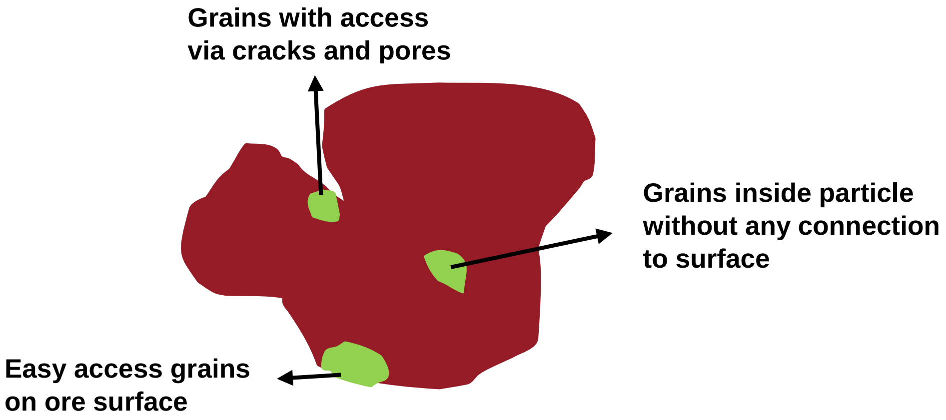

Figure 1-2: Position of mineral grains in an ore particle, classified by their ease of contact with the leaching solution.

Mineral exploitation can lead to formation of a major environmental issue known as Acid Rock/Mine Drainage (ARD/AMD). ARD contains high concentrations of acid and dissolved metals, especially heavy metals (Parbhakar-Fox and Lottermoser, 2015; Simate and Ndlovu, 2014) and can have detrimental effects on human health, plant and aquatic life (Simate and Ndlovu, 2014). The principle of ARD formation is the same as heap bioleaching for metal recovery, with oxidation of sulphide minerals in the waste ore accelerated by regeneration of leaching reagents by microorganisms. Therefore, understanding of the sub-processes and factors affecting non-surface grain leaching can provide improved ability to predict and deal with ARD issues, especially in the longer term.

Study of the internal structure and properties of coarse ores have been limited because a combination of traditional bulk chemical assays coupled with 2D SEM-EDS type hardware (e.g. QEMSCAN, MLA etc) are 2D or destructive. However, advanced analytical techniques such as high-resolution X-ray micro-Computed Tomography (µCT) has opened new avenues for further studying and understanding of non-surface grain leaching (Dhawan et al., 2012; Lin and Garcia, 2005).

X-ray µCT, a 3D non-invasive imaging technique, is proposed for the study of different aspects of coarse ore particles in bioleaching systems. The technique has been demonstrated by a number of authors on abiotic systems. Fagan-Endres et al. (2017)

used it to quantify the degree of sub-surface leaching in a bed of coarse chalcopyrite ore. Ghorbani (2012) used X-ray µCT to study the effects of two different methods of comminution on the leaching of zinc from large sphalerite ore particles under saturated conditions. Lin et al. (2016c) conducted mini-column leaching of large chalcopyrite particles and quantitatively determined non-surface mineral grain leaching at three different flowrates.

The presented work investigates further use of X-ray µCT to interrogate microscale phenomena in heap bioleaching systems. This firstly requires the establishment of the viability of using X-ray µCT to study biotic leaching systems. Therefore evaluation of X-ray µCT exposure impact on the bioleaching microbial activity will be investigated. This will be used to establish imaging conditions which permit the examination of the influence of micoorganisms on non-surface mineral grain leaching. This is critical to study, given their critical role in heap bioleaching process reactions. Different physico-chemical and solid state variable which are anticipated to affect the extent of leaching penetration in a bioleaching system are further considered. Temperature is one factor, as a critical variable due to the exothermic nature of the bioleaching reactions. In addition, ore type is investigated using a selection of oxide and low-grade sulphide ores chosen for their different physical characteristics, with mineral leaching kinetics and ore porosity expected to have significant influence on leaching penetration. A promising technology for the improvement of non-surface leaching is the inclusion of surfactant. The influence of surfactant on bioleaching population viability and vitality is thus assessed and acceptable surfactant types and dosages established. The effect of appropriate surfactant inclusion on leaching penetration is then examined. In all investigations, sub-surface mineral leaching is evaluated using measurement of leaching penetration distance and mineral recovery by X-ray µCT. The X-ray µCT analysis is evaluated by comparison with traditional bulk analytical methods throughout.

1.2 Scope and constraints

Numerous physical, chemical, biological, ore and operation parameters can affect leaching behaviour. These parameters affecting mineral oxidation and metal solubilisation are presented in Table 1-2. To ensure a manageable project scope, only select factors will be considered or measured in this study (highlighted in green). Ore type and its porosity, mineral composition and target mineral position and grain size in the ore can have significant effect on non-surface mineral grain leaching are have therefore been selected. Acid consumption by gangue minerals in the ore is also considered because it provides understanding the overall leaching behaviour. Agglomeration, temperature, and addition of surfactant to leaching solution (which affects surface tension) have the potential to directly influence non-surface mineral grain leaching. Redox potential, pH, Fe^{3+}, and the bioleaching microorganisms' population density should be monitored to ensure the leaching environment is favourable for leaching and the growth and activity of the microorganisms.

Table 1-2: Parameters affecting mineral oxidation and metal solubilisation in heap bioleaching ((Harrison, 2016), Ghorbani, 2012; Panda et al., 2015; Pradhan et al., 2008), with those to be considered within the PhD thesis scope highlighted in green.

Physical & chemical parameters	Biological parameters	Characteristics of minerals/ore	Processing or conditions
Temperature	Microbial activity	Mineral/Ore type	Pulp density
pH	Population density	Acid consumption	Heap geometry
Redox potential	Microbial diversity	Mineral dissemination	Practical weather conditions
Water potential	Spatial distribution of microorganisms	Grain size	Prolonged or Intermittent
Oxygen content and availability	Attachment	Surface area	Rest periods
Carbon dioxide content	Metal tolerance	Porosity	Lixiviant flow rates to heap
Mass transfer	Microbial adaptation ability	Hydrophobicity	Agglomeration
Nutrient availability		Galvanic interactions	
Fe (III) concentration		Formation of secondary minerals	
Light		Mineral composition	
Pressure			
Surface tension			
Presence of inhibitors			

1.3 Structure of dissertation

The general background, problem statement and project scope, presented in Chapter 1, are followed in Chapter 2 by a review of relevant literature concerning heap bioleaching, sub-processes in heap bioleaching from heap to grain level, factors affecting non-surface minerals leaching, and X-ray µCT application in heap leaching research.

Chapter 3 describes the experimental methodology for the ore preparation, mineralogical characterisation, and mini-column leaching experiments. The detailed design of the experiments is explained, including the experimental setup, controlling parameters such as temperature, ore types, agglomeration and leaching agents. The details of feed solution and relevant chemistry measurement are also introduced. The X-ray µCT system used for the experiments is presented.

In Chapter 4, mineralogical data is combined with X-ray µCT images to find an appropriate leaching setup and image analysis method, enabling identification of different minerals in the images. The X-ray µCT image reconstruction from a series of 2D projections to a 3D volume image is demonstrated with examples. A series of image processing algorithms are applied to process the reconstructed image data, including filtering algorithms to reduce the noise level, thresholding algorithms to segment and extract different phases, labelling to get quantitative data, a distance map algorithm to find the distribution of sulphide mineral grains and the pore distribution in ore particles. Error and uncertainty analysis are carried out to quantify the measurement precision in the image processing and the relevant analysis, particularly in the volume measurements.

The compatibility of bioleaching microorganisms with X-ray energy exposure is examined in Chapter 5. Initially, the X-ray effect on a mixed thermophilic culture suspended in solution is assessed using different imaging conditions. The X-ray influence on a mixed mesophilic culture colonising a mineral surface is then investigated. Finally, an optimised X-ray µCT imaging approach is applied to study a mixed culture thermophilic bioleach of a chalcopyrite-containing low-grade ore in a mini-column.

The effect of surfactant addition to the lixiviant on non-surface mineral grain leaching from low-grade chalcopyrite ore and waste rock containing pyrite is evaluated in

Chapter 6. The ore type (physical characteristics) and temperature effects on non-surface mineral grain leaching and distribution of sulphide mineral grains in ore particles are presented and discussed in Chapter 7.

In Chapter 8, the conclusions from the findings are presented. The developed method potential impact on improving the bioleaching process is described. Recommendations for further investigations within this research area are suggested.

2 Literature Review

Chapter 2 delivers the relevant body of knowledge that is available on the subject matter and show the gaps in the existing knowledge. Fundamentals of heap bioleaching and sub-processes in heap bioleaching at different levels are explained. Then, the important parameters that influence non-surface leaching are explored, including ore types and mineralogy, agglomeration pre-treatment, temperature and surfactant. After that, the role of microorganisms in heap bioleaching is explained. Challenges for extraction of copper from chalcopyrite, as the main copper resource in the world but the most reluctant to leach, is then described. Finally, X-ray µCT fundamentals, its application to heap leaching and methods for image processing are explored.

2.1 Introduction

Low-grade sulphide ores including pyrite, molybdenite, tungstenite, sphalerite, galena, arsenopyrite, chalcopyrite, hauerite and chalcocite (etc.) are usually difficult to treat with conventional mineral processing methods due to their low solubility in most leaching reagents (Dew et al., 2000; Watling, 2006). Pyro-metallurgical processing (roasting/ smelting) of these low-grade ores is difficult and costly which renders them unattractive for commercialization (Habashi, 2005; Rubio and García Frutos, 2002).

Hydrometallurgy presents an alternative processing route. It involves three stages consisting of leaching, separation/concentration, and purification taking place at near ambient temperature (Ghorbani et al., 2016). The leaching stage can be classified into two methods, namely agitation and percolation. Agitation leaching is carried out using a finely ground ore in a stirred tank reactor, while percolation leaching is defined as the selective removal of metal values from a mineral by causing a suitable solvent or leaching agent to seep into and through a mass or pile of material containing the mineral (Gupta and Mukherjee, 1990). Commercial percolation leaching is commonly grouped into in-situ, dump, heap, and vat leaching based on the deposit and ore characteristics. The degree of ore bed preparation varies for the different types (Petersen, 2016). Heap leaching is one of the well-established technologies, usually used for low- to intermediate-grade ores and it has the advantages of low investment, improved working conditions, and low relative energy consumption (Ghorbani et al., 2011). Three key applications of heap leaching are cyanide leaching of gold ores, acid leaching for copper oxide ores, and oxidative acid leaching of secondary copper sulphide ores catalysed using microorganisms (Petersen, 2016). It is estimated that 20% to 25% of the world's copper production is attributable to heap and dump leaching (Natarajan, 2018).

2.2 Description of heap bioleaching

A schematic of a heap bioleaching process is shown in Figure 2-1. As seen, metal ores (mostly copper) from the mine are crushed primarily with jaw crushers to pass about 150 mm top size. Then crushing continues using a cone crusher or high pressure grinding rolls (HPGR) to produce particles less than 25 mm (Ghorbani et al., 2011). The prepared crushed ores along with acidified solution (sometimes containing binder) is introduced into rotating agglomeration drums. In the agglomeration drums, fine ore particles are bonded to coarser ore particles via liquid bridges (Kodali et al., 2011a). The agglomeration product is stacked on the heap leach pad to a height of 5 to 20 metres (Petersen, 2016). Acidified solution and microorganisms are introduced on the top of the heap by sprinklers or drippers. The solution and microbes cause the dissolution of metals from the mineral grains in the ore as the solution passes through the heap. Air blowers are commonly used to force air flow into the heap base so that sufficient oxygen and carbon dioxide is provided for the growth of microorganisms and the leaching reactions (Brierley, 2008a). Extent of metal recovery from the heap leach pad depends on several parameters, some of which are investigated in the current project. The pregnant leach solution (PLS) containing dissolved metals generated by the chemical and microbial solubilization, is subject to solvent extraction to obtain a highly concentrated metal solution from which the metal is recovered in an electro-winning plant to generate e.g. electrolytic copper of high purity. The spent leach liquor (raffinate) is recycled to the heap stack after solution make-up. Sometimes, the quality of spent leach solution is improved by adding further nutrients and microorganisms (Watling, 2006).

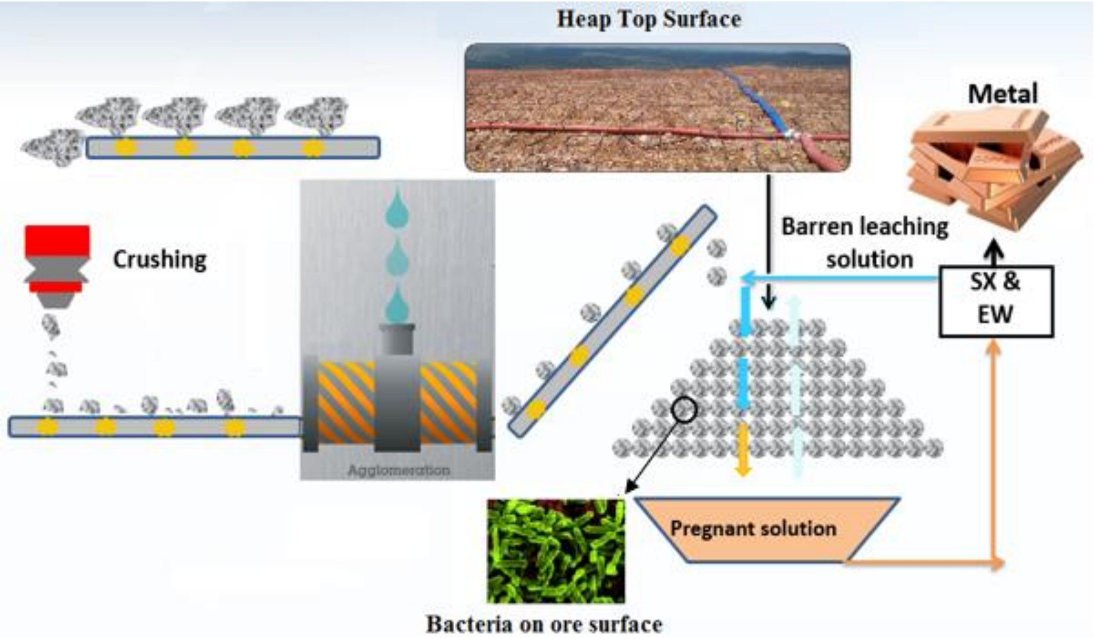

Figure 2-1: Schematic representation of heap bioleaching process to obtain metals in industrial scale [Source: adapted from (Jerez, 2011)].

2.3 Chemical and biological reactions in the heap

Figure 2-2 shows heap leaching at macro- and particle-scale levels and the role of microorganisms in the leaching of metals from ore (Petersen and Dixon, 2007a). Various reactions take place inside the heap, with reagents provided in the flowing acidic solution from the top of heap and in the gas stream from the bottom. There are four phases besides the ore, including: gas, pregnant leach solution (PLS), interstitial and attached phases within the whole ore bed (Govender et al., 2014). The division between the PLS and ore-associated phases is shown in Figure 2-2 (b). Some microorganisms cross through the phases and attach on the ore surface (sessile), whereas some microbes remain in the PLS (planktonic).

Sulphidic ores are dissolved by the combined action of electron extraction by ferric ions or proton attack (Rohwerder et al., 2003). Sulphidic ore dissolution is initiated through proton attack on the ore surface with hydrogen sulphide as reaction product. This reaction in the absence of O_2 and ferric ions can be written as follows (Tributsch and Gerischer, 1976):

$$MS + 2H^{+} \rightarrow M^{2+} + H_2S \qquad (2\text{-}1)$$

Oxygen acts as an electron acceptor in the absence of ferric ion and reaction (2-1) might proceed to elemental sulphur in the system according to reaction (2-2) (Tributsch and Gerischer, 1976):

$$H_2S_n + 3/2O_2 \rightarrow H_2S_2O_3 + [(n-2)/8]S_8 \tag{2-2}$$

The rate of reaction (2-1) is very low and is not good for dissolution of sulphidic ores. In all cases, dissolution of an ore relies on oxidative leaching via the ferric ion. Ferric ion plays a much more significant role in heap bioleaching, such that in the presence of ferrous ion the mechanism does not require oxygen (Tributsch and Gerischer, 1976).

$$MS + Fe^{3+} + H^+ \rightarrow M^{2+} + 0.5H_2S_n + Fe^{2+}(n \geq 2) \tag{2-3}$$

$$0.5H_2S_n + Fe^{3+} \rightarrow 0.125S_8 + Fe^{2+} + H^+ \tag{2-4}$$

Net reaction:

$$MS + 2Fe^{3+} \rightarrow M^{2+} + 0.125S_8 + 2Fe^{2+} \tag{2-5}$$

After oxidation of ore by ferric ion and production of elemental sulphur and ferrous ion, microorganisms impose their role on the heap bioleaching process. Iron oxidizing microorganisms reduce ferrous ion to ferric ion (reaction 2-6) and sulphur oxidizing microorganisms reduce elemental sulphur to sulphuric acid (reaction 2-7). The dissolution mechanisms and the role of microorganisms are depicted in Figure 2-2 (c) (Hansford and Vargas, 2001).

$$4Fe^{2+} + O_2 + 4H^+ \rightarrow Fe^{3+} + H_2O \tag{2-6}$$

$$2S + 3O_2 + 2H_2O \rightarrow 2H_2SO_4 \tag{2-7}$$

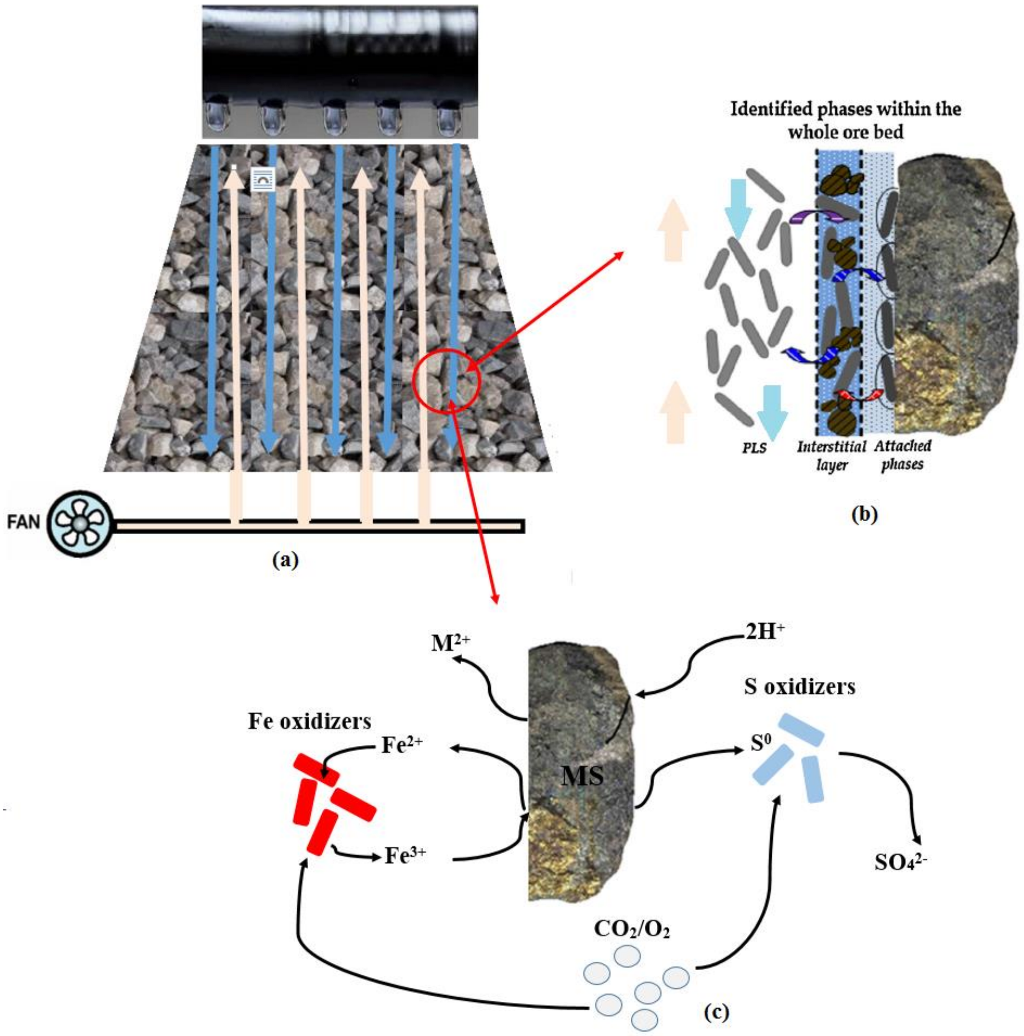

Figure 2-2: (a) Macro-scale heap bioleaching, (b) the different phases inside the heap, and (c) the reaction mechanisms and microorganisms' roles [Source: adapted from (Govender et al., 2015b; Hansford and Vargas, 2001)].

2.4 Heap bioleaching microbiology

The role of microbiology in heap bioleaching was not discovered until 1947. Colmor and Hinkle (1947) discovered microorganisms in acid mine drainage. *Acidithiobacillus ferrooxidans* was isolated and described in 1951 as the first microorganism that facilities metal oxidation (Temple and Colmer, 1951). Later, other microorganisms such as the sulphur oxidizing *Acidithiobacillus thiooxidans* and *Acidithiobacillus caldus*, and the iron oxidizing *Leptospirillum ferrooxidans*, *Leptospirillum ferriphilum*, *Sulfobacillus* and *Acidianus brierleyi* were recognized. The first commercial heap bioleaching operation was developed in Chile in the 1980s (Brierley, 2008b; Panda et al., 2015). The microorganisms involved in heap bioleaching can be classified as mesophilic, moderately thermophilic or thermophilic, based on their optimum temperature for growth (Panda et al., 2015).

2.5 Dissolution mechanisms

Initially, two direct and indirect mechanisms were proposed for dissolution of sulphidic ores by Silverman and Ehrlish (1964). In 1967 Silverman (1967) redefined his proposed mechanisms to an indirect contact leaching mechanism. No conclusive results were presented on the proposed mechanisms, or whether the presence of microorganisms increases the rate of leaching above that of pure chemical leaching at the same solution conditions. It is now generally accepted that the microorganisms' role is to generate oxidants. According to the type of sulphidic ore (acid soluble metal sulphides versus acid non-soluble metal sulphides), there are two mechanisms for bioleaching of metals. These two mechanisms are the thiosulphate and polysulphide pathways, presented in Figure 2-3 (Rohwerder et al., 2003).

2.5.1 Thiosulphate pathway

Acid non-soluble sulphidic ores such as pyrite, molybdenite, and tungstenite can only be oxidized by ferric ion. A cyclic leaching mechanism is carried out in the presence of iron and sulphur oxidizing microorganisms. Ferric ions attack the mineral surface and produce ferrous ions and oxidized metal as reaction products. Iron-oxidizing microorganisms reduce ferrous ions to regenerate ferric ions and thus an appropriate reaction media for further sulphidic ore leaching to take place. Intermediate sulphur species such as thiosulphate ($S_2O_3^{2-}$) are also formed during sulphidic ore dissolution. Sulphur-oxidizing microorganisms and ferric ion oxidize these intermediate sulphur species to sulphate (Rohwerder et al., 2003).

2.5.2 Polysulphide pathway

In comparison to the acid non-soluble metal sulphides, the dissolution of acid-soluble metal sulphides such as chalcopyrite, sphalerite, galena and arsenopyrite is quite different. As shown in Figure 2-3, the combination of ferric ions and proton attack lead to oxidization of these sulphidic ores. The products of oxidization are metal ions and intermediate sulphur species. Iron-oxidizing microorganisms reduce ferrous ions to ferric ions, like in the thiosulphate pathway. In the absence of sulphur-oxidizing microorganisms, more than 90% of the sulphide is transferred to elemental sulphur

(Rohwerder et al., 2003). The main sulphur-oxidizing microorganism function within the polysulphide pathway is to generate sulphuric acid in order to supply proton hydrolyses from elemental sulphur oxidation.

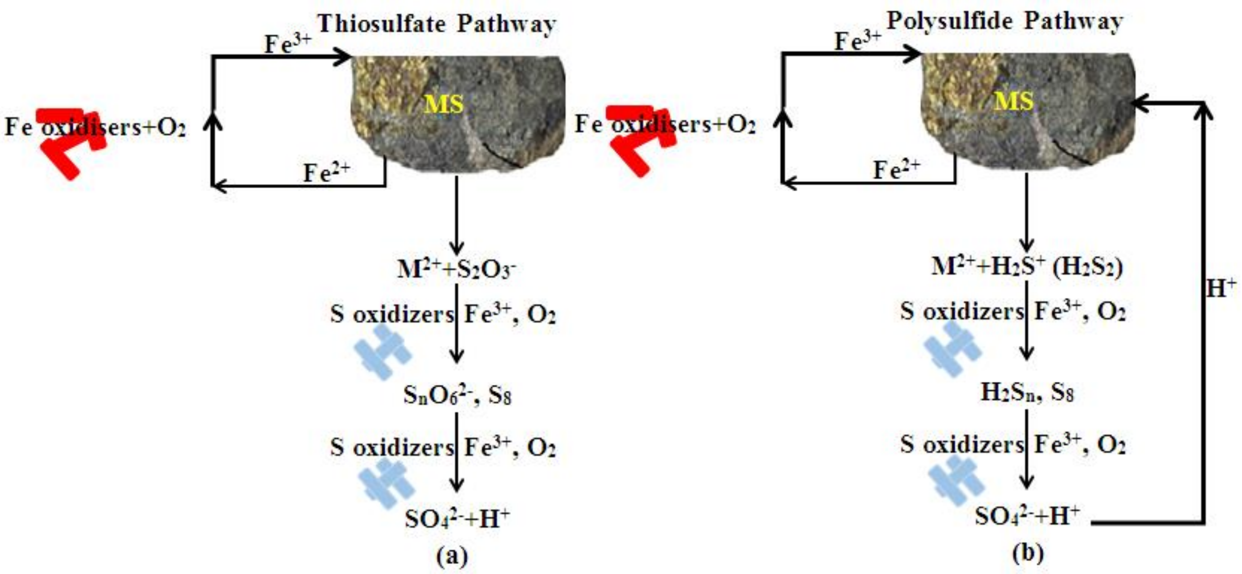

Figure 2-3: (a) Thiosulphate pathway and (b) polysulphide pathway [Source: adapted from Rohwerder et al. (2003)].

2.6 Sub-processes in heap leaching

Peterson and Dixon (2007a) categorized heap leaching from the macro to micro-scale as shown in Figure 2-4. Heap bioleaching seems to be simple system in concept, though several sub-processes at the different scales play key roles and interaction between lixiviant and the ore particle is very complex. In the following section, different scales and affecting parameters are explained in more detail.

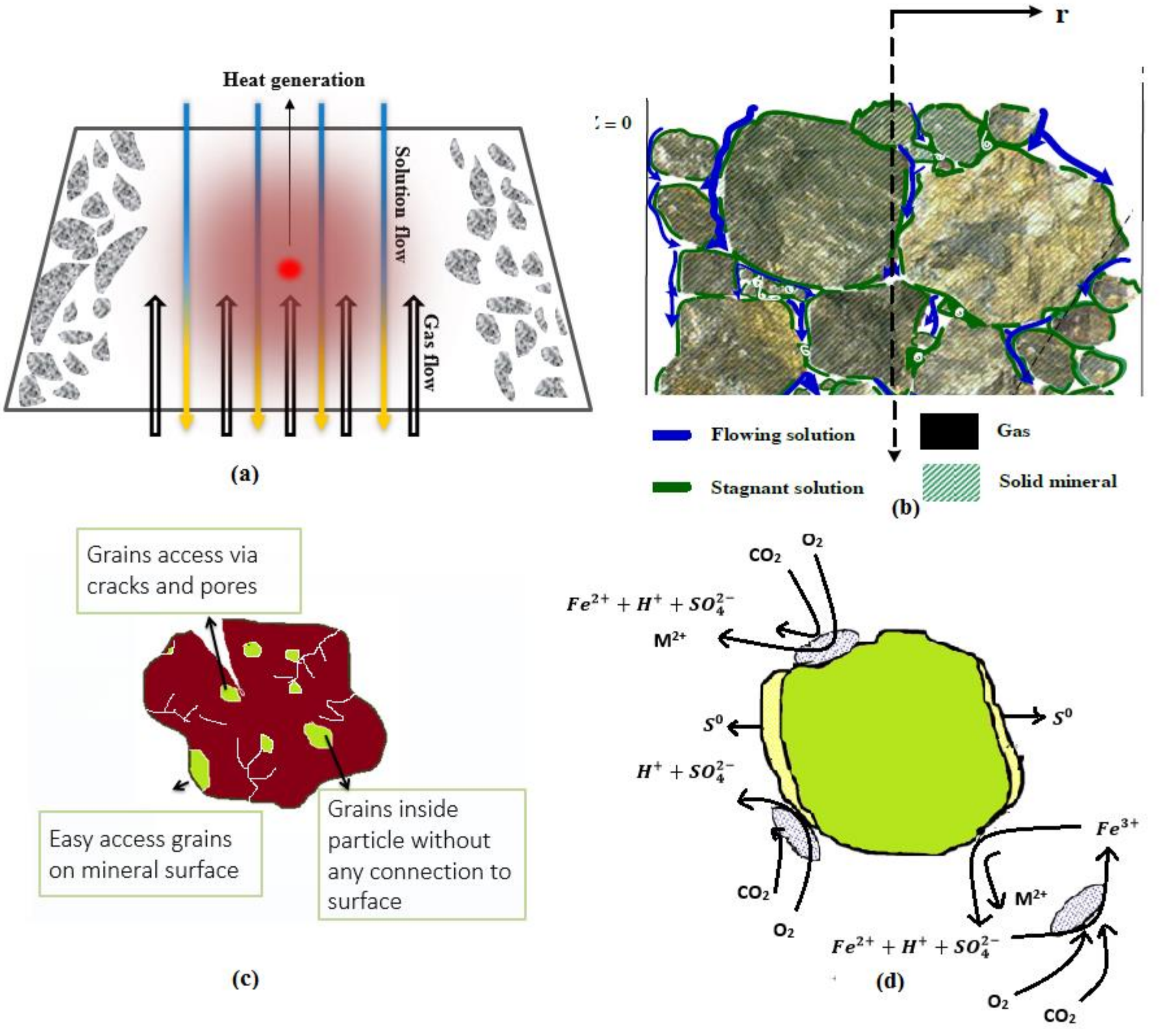

Figure 2-4: Various levels in heap bioleaching (Govender-Opitz et al., 2017; Petersen and Dixon, 2007a).

2.6.1 Heap level

Figure 2-4 (a) shows the heap level, where acidic solution and microorganisms enter from the top of the heap and percolate through the ore bed. As solution flows in the void space and contacts the ore, the oxidation of mineral takes place. Gas (air) migrates through the unsaturated void spaces of the ore bed upwards and provides suitable media for growth of microorganisms (Brierley, 2008a). The gas stream becomes saturated with water vapour as it percolates in upwards through the heap. Bioleaching reactions are exothermic (Petersen and Dixon, 2007a) and release heat in the ore bed. Therefore, solution flow, gas advection, water vapour transport, and heat balance are vital sub-processes at the heap level (Petersen, 2016).

2.6.2 Agglomerate level

A collection of particles held together by stagnant solution is referred to as an agglomerate (cluster). Diffusive mass transfer is important at the agglomerate level because the solution flow in interstitial spaces is slow. Microorganisms and dissolved reactants and products of leaching are transferred by diffusion. Only upon initial wetting, capillary forces lead to convective migration. The microorganisms' interaction with the ore surface is also important at the agglomerate level, as they provide reagent for oxidation of metal. Gas (O_2 and CO_2) uptake in the interstitial spaces, porosity of particles and attachment of microorganisms on the ore surface should be considered as important sub-processes at the agglomerate scale (Govender et al., 2015b). Availability of nutrients and temperature are also vital for the growth of the microorganisms (Petersen and Dixon, 2007a).

2.6.3 Particle level

Particle shape, propagation of mineral grains in the gangue matrix and intra-particle diffusion should be paid attention at the particle level (Ghorbani et al., 2011). Valuable metals in ore particles are distributed within a matrix of gangue minerals. Thus, mineral grains' position in ore particles must be taken into account at this level (Dobson et al., 2017; Fagan-Endres et al., 2017). The solution contents (reactants) need to penetrate through pores and cracks in particles to react with sub-surface target species and then reaction products travel out from the reaction sites again. Because of the typical low porosity of sulphidic ore particles, leaching from the sub-surface is very slow. There have been few studies focussed on leaching of non-surface minerals. In addition, the complete mineralogy of low-grade ores must be understood because mineral leaching and biological phenomena can be affected by the ore gangue matrix (Park and Levenspiel, 1977).

2.6.4 Grain level

The chemical and electrochemical interactions at the grain surface determine the leaching kinetics in the selective dissolution of one mineral over another one (Mehta and Murr, 1983). Chemical reaction is influenced primarily by temperature (activation energy) and concentration of reactants (Córdoba et al., 2008a). Galvanic interactions, resulting from interaction of different minerals, complicates the reactions. Availability of substrate surface is also important because contact leaching mechanisms is dominant at this level. Ferrous or ferric reduction, metal oxidation, sulphur oxidation and surface processes are the most important sub processes at this level (Ghorbani et al., 2016).

2.7 Important parameters to non-surface leaching

2.7.1 Ore type and mineralogy

Chemical or microbial dissolution of mineral grains and leaching efficiency is strongly dependent on the ore nature. This includes its origin, ore type, and chemical composition (Ghorbani et al., 2016; Watling, 2006). For example, different intermediates can be formed during metal sulphide dissolution and this changes sulphide mineral leaching kinetics (Ruan et al., 2013). Copper-bearing ores can be found in various forms of oxides, primary and secondary sulphides. Leaching time and efficiency changes according to ore type. Oxides such astenorite and malachite might need only hours of leaching to achieve a high extraction value, even at low temperatures, while secondary sulphides like chalcocite and covellite require months of leaching. Chalcopyrite, the world’s main copper resource, can require years of leaching (Watling, 2006).

An ore’s mineral composition is another highly important characteristic which must be considered in order to optimise heap leaching performance. Presence of gangue minerals such as silicate and limonite consume acid during initial leaching. Soluble silicate breakdown products may regenerate acid by reaction with each other during formation of various precipitates and also to form new solid silicate alteration products (Jansen and Taylor, 2003).

The target mineral grain dissemination and size in large ore particles plays a vital role in heap leaching performance because the contact of mineral grains and leaching reagent is necessary for leaching of the mineral grain to occur. Sulphide minerals also exhibit a surface rest potential and can therefore corrode by Galvanic action (Khoshkhoo et al., 2014). Galvanic interaction between pyrite and copper sulphide minerals cause the copper minerals to corrode more rapidly than the pyrite and this effect is accelerated in the presence of bacteria (Berry et al., 1978). Most ores contain pyrite and its presence can have some disadvantages such as precipitation of potentially interfering ferri-hydroxides and jarosite, and in aerated heaps it can scavenge available oxygen. However, pyrite oxidation is also advantageous as it provides acid and heat in the heap (Ghorbani et al., 2016).

2.7.2 Ore agglomeration

Agglomeration is a pre-treatment step performed before stacking in order to adhere fine particles to coarse particles or self-coalescence of fine particles. This is especially for ores having a considerable amount of fines or clay content (Dhawan et al., 2013). The main purpose of agglomeration is improvement of heap leaching efficiency and reduction of leaching time, improving the uniformity of solution distribution and prevention of clogging, pond formation, segregation, solution channelling and fine particle migration in the heap (see Figure 2-5) (Bouffard, 2005). It has the additional effect of changing the liquid flow properties around the ore particles, essentially creating a larger ore particle with an improved porous network structure. In 1979, Heinan (1979) showed a comparative test of non-agglomerated and agglomerated ore in which the percolation rate could be improved by a factor of 10 to 100 times by agglomeration which lead to the reduction of leaching time by 33%. After this improvement, most of copper and gold heap leaching systems used agglomeration as pre-treatment step (Heinen et al., 1979). It is typically considered as 14% of total heap leaching operating cost distribution (Kappes, 2002; Kappes, 2005). Belt, drum, disc and stockpile agglomerators can be used for agglomeration based on ore type and size distribution (Dhawan et al., 2013).

Nosrati et al. (2013) used X-ray µCT to study the porosity and internal structure of low-grade nickel (Ni) laterite ore agglomerates. Acid or water-based agglomeration and the change in the agglomerated ore structure after drying was examined. The results showed that both the agglomeration medium and agglomerate drying and curing play pivotal roles in structural changes within the agglomerates and hence significantly impact on the agglomerate's physicochemical and microstructural properties. In another study, the internal structure of an uranium ore was investigated and it was found that acid-bound agglomerates had the higher connected porosity than water-bound agglomerates (Hoummady et al., 2017).

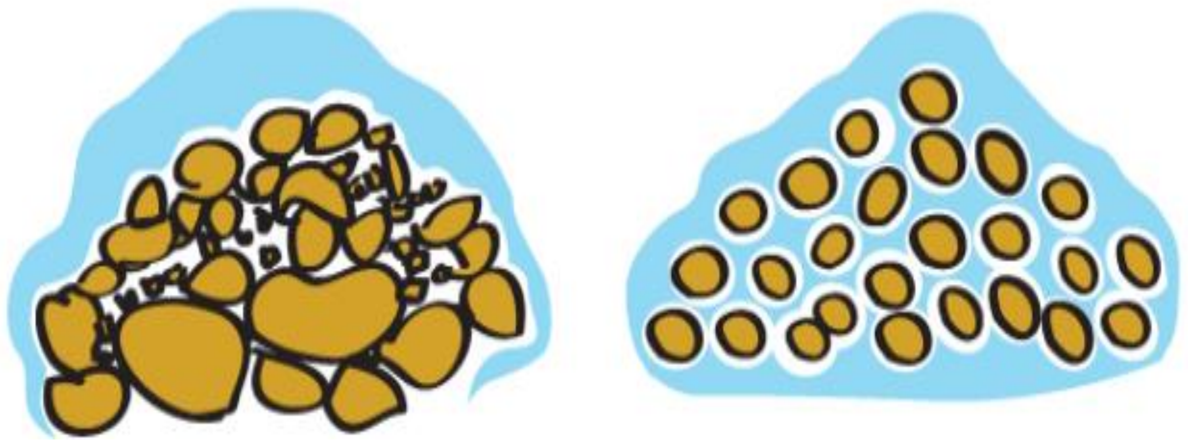

Figure 2-5: Comparison of solution percolation in an agglomerated vs. non-agglomerated ore [https://commons.wikimedia.org/wiki/File:Agglomerate-Ore-Fines.jpg].

Solid bridges, adhesion and cohesion forces are dominant for binder-assisted agglomeration, while surface tension and capillary pressure are the most influential factors for non-binder/wet agglomeration. Attraction forces between solids and interlocking bonds are size enlargement mechanisms during the agglomeration process (Bouffard, 2005; Kodali et al., 2011a).

During agglomeration the ore is first wetted, and then nucleation, growth, pseudo-layering and coalescence occur. There are two kinds of particle interaction which may happen, depending on the ore type. Newly nucleated agglomerate formation occurs when the ore has high clay content, while coarse particles are layered with fine particles in hard crushed ores like low grade sulphide ore (Bouffard, 2005; Dhawan et al., 2013). As mentioned previously, agglomerated ore has a special internal structure which can affect the non-surface leaching. Nosrati et al. (2012) studied nickel laterite agglomerates for enhanced heap leaching efficiency by X-ray micro-CT imaging. The agglomerates were shown to be comprised of a core-shell structure. They additionally demonstrated that pore spaces, sub-agglomerates and different minerals could be evaluated by using the CT scan images.

2.7.3 Surfactants

A surfactant (***surf***ace ***act***ive ***a***ge***nt***) is defined as a substance that can reduce the surface tension of a solution or interfacial free energies when used at very low concentrations. These materials are used in many industries including food, pharmaceutical, petroleum, and mining (Tan et al., 2014).

Leaching of non-surface mineral is made difficult due to inaccessibility of non-surface mineral grains as the mineral is only connected to the surface by cracks and pores. Addition of surfactant into the leaching solution promotes better wetting of the heap. Decreased dry zones or unleached regions in the heap and penetration of leaching solution into small cracks and pores of coarse particles leads to the enhancement of solution-metal contact and consequently metal dissolution and recovery (Shah, 2017). This results in shorter leaching times and higher recovery. Reduced leaching time in turn reduces leaching agent and pumping costs.

However, surfactant addition can have negative impacts on heap performance by formation of a hydrophobic layer at the solution/air or solution/solid interface and retardation of diffusion of the reactants to the mineral surface or products away from the surface (Hiroyoshi et al., 1995; O'Kane Consultants, 2000). The surfactant should also be used at very low concentrations because at high concentrations, their tendency to adsorb at interfaces may block reaction sites on the mineral surface (Schmuhl et al., 2011). Microbial activity, growth and attachment on ore surfaces can also be affected by adding surfactant to the leaching solution. Surfactant addition in the leaching solution has been known to decrease micobial attachment on an ore surface, due to the surfactant changes in the surface properties of the ore (Hiroyoshi et al., 1995). Other issues include that the surfactant is not extracted into the organic medium in the SX circuit, and it does not cause a stable emulsion to be formed during extraction (Hiroyoshi et al., 1995).

Using capillary pressure phenomena and theory (Equation (2-8)), Young's equation (Equation (2-9)), and the principle of Nernst (Equation (2-12)) can mathematically explain how surfactant reduces surface tension of solution around particles (Tan et al., 2014). The capillary pressure phenomenon is described by:

$$\Delta p = 2\gamma\left(\frac{1}{r_1} - \frac{1}{r_2}\right) \tag{2-8}$$

where Δp is the fluid flow driven force difference, γ denotes the interfacial tension, and $1/r_1$ and $1/r_2$ are curvatures of liquid levels of different pore sizes. Reduction of solution surface tension changes the liquid curvatures, and consequently affects the capillary pressure (Tan et al., 2014). Interfacial tension is defined further as follows:

$$\gamma_{sv} = \gamma_{sl} + \gamma_{lv} \cos\theta \tag{2-9}$$

$$\gamma_{lv} \cos\theta = \gamma_{sv} - \gamma_{sl} \tag{2-10}$$

$$S_{l/s} = \gamma_{sv} - \gamma_{sl} - \gamma_{lv} \tag{2-11}$$

where γ_{sv} is the gas–solid interfacial tension, γ_{sl} is the liquid–solid interfacial tension, γ_{lv} is the liquid interfacial tension, θ is the contact angle, and $S_{l/s}$ denotes the spreading coefficient of liquid.

Eq. (2-12), the spread speed can be approximately written as follow (Eq. (2-12)) at steady state condition based on the principle of Nernst (Tan et al., 2014):

$$\frac{ds}{dt} = DA\frac{c_1 - c_2}{b} \tag{2-12}$$

where $\frac{ds}{dt}$ is the diffusion rate of components, c_1 and c_2 are concentrations of the components on either side of the liquid layer respectively, b is the thickness of the liquid film on the mineral surface, A is the contact area of the solid and liquid phase and D is the diffusion coefficient.

Adding an appropriate surfactant improves the ore wetting ability of the leaching liquid based on Young's equation or the wetting equation, reducing ore surface liquid film thickness according to principle of Nernst, and finally, based on the capillary pressure phenomena and theory, there is an increase in the permeability in the heap and penetration into tiny pores and cracks (Tan et al., 2014). Vest et al. (2009) derived an equation using Fick’s law and the Washburn equation for a spherical particle which relates total leaching time to penetration length of the fluid (surface tension and contact angle).

Fatty alcohol alkoxylate was used by Vest et al. (2009) as a surfactant to improve copper extraction from a copper oxide ore. The copper extraction was enhanced by 5.4% when 100 ppm surfactant was added to the leaching solution. The effect of three fatty alcohol alkoxylates on copper extraction from a copper sulphide ore in saturated column leaching was investigated by Schmuhl et al. (2011). Adding surfactant increased the wetting of the ore particles with considerable increase in the copper yield. However, high surfactant concentrations were reported to block reaction sites on the mineral surface (Schmuhl et al., 2011). It has also been reported to decrease hydrophobicity of a chalcopyrite ore surface (Sandoval et al., 1990, 1991).

Duncan and Trussell (1964) and Duncan et al.(1964) tested the effect of various surfactants on the *Acidithiobacillus ferrooxidans*-aided leaching of chalcopyrite in shake flasks. The addition of non-ionic surfactants, particularly Tween® 20 (0.0005 – 0.012%), was found to aid the microbial leaching process. Yields of copper from chalcopyrite were increased from 38% to 85% in the presence of 0.001% Tween® 20 compared with the biotic control. In other studies Liu et al. (2015) used Tween® 20 and Tween® 80 (0.1 and 0.25 g L^{-1}) to improve cobalt leaching in a shake flask experiment. The cobalt leaching efficiency was boosted by more than 21% and the copper leaching efficiency increased by more than 8% when 0.1 g L^{-1} surfactant (Tween® 80 or Tween® 20) was added. Moreover, in such a case, the leaching time could be reduced by more than 15%. Peng et al. (2012) used Tween® 80 (10^{-3} –10 g L^{-1}) to increase copper leaching from chalcopyrite. A 16% improvement of the copper extraction was observed with the introduction of 0.01 g L^{-1} Tween 80 compared to that in the absence of Tween® 80. Lan et al. (2009) added ortho-phenylenediamine (OPD) (0.01 – 0.4 g L^{-1}) into the leaching solution with the aim of enhancement of marmatite concentrate leaching. The ore was ground to a particle size distribution of 75% passing 74 µm. With the addition of OPD to the concentration of 0.00 g L^{-1}, 0.01 g L^{-1} and 0.05 g L^{-1}, the zinc extraction rate was 66%, 71% and 76% after 22 days respectively. Moreover, with the addition of OPD at concentrations of 0.1 g L^{-1} and 0.2 g L^{-1}, the zinc extraction rate was 62% and 45% after 22 days, respectively. The decrease in zinc extraction at higher concentrations was associated with the negative effect of OPD on the iron oxidizing capacity of the bacteria. The effect of Tween® 20 on microbial attachment on chalcopyrite concentrate was studied by Hiroyoshi et al. (1995). They found that addition of surfactant increases the number cells in the solution and decreases the attached cells (Hiroyoshi et al., 1995). It was found that the absorption of the surfactant was sufficient to reduce the hydrophobicity of the particles and resulted in the enhancement of copper leaching. However, they reported that at high surfactant concentrations, their tendency to adsorb at interfaces may block reaction sites on the mineral surface. Tween® 20 at 0.4% (v/v) has also been applied purposely for microbial detachment from the mineral surface (Govender et al., 2015b; Makaula et al., 2017a). Efficient heap bioleaching requires the presence of an effective and appropriate indigenous bacterial population. The StickiBugs process has been developed at Mintek to improve bacteria inoculation in the heap. A surfactant was used in the process to facilitate attachment to inner depth of heaps (Gericke et al., 2005).

2.7.4 Temperature

The heap leaching reactions are exothermic and temperatures in heaps are typically higher than ambient, varying with position in the heap. Increasing temperature changes the microbial population from predominantly mesophilic to thermo-tolerant and moderate thermophilic microorganisms to thermophilic microorganisms (Acosta, 2014). Watling (2006) reviewed temperature enhancement on chalcopyrite concentrate leaching under the abiotic and biotic conditions, with a rapid copper leaching rate only obtained at higher temperatures. Temperature additionally has an effect on physical properties of the heap liquid including viscosity, density and solubility of copper sulphates in a saturated solution (Justel et al., 2015). It was observed that an increase in the temperature leads to the enhancement of density and solubility but the reduction of viscosity (Justel et al., 2015). Viscosity and density affect oxygen mass transfer from gas phase to liquid phase in a heap (Petersen, 2010). The high temperature is required in order to break down bonds in the chalcopyrite crystal lattice due to its high values of activation energy. Chalcopyrite activation energy is reported as 130.7 kJ mol^{-1} in the temperature range between 35 and 68 °C (Córdoba et al., 2008a).

2.8 Chalcopyrite

Chalcopyrite is the most abundant copper-bearing mineral comprising approximately 70% of copper reserves in the world (Córdoba et al., 2008a). It thus deserves particular attention. Copper is usually extracted from high-grade chalcopyrite using pyro-metallurgy routes, however, this is not economically viable for low-grade chalcopyrite ore. Hydrometallurgy routes have been successfully used for processing of low-grade oxide and secondary sulphide minerals. But, it is difficult to use a hydrometallurgy route for processing of low-grade chalcopyrite ore at industrial levels because chalcopyrite is highly refractory (Watling, 2006). The crystal structure of chalcopyrite consists of a relatively simple tetrahedron angles, close to cubic with each sulphur ion surrounded by four metal ions of copper and iron located on tetrahedron angles and in a certain order in each plane (Córdoba et al., 2008a).

There are several reasons for slow leaching rates of chalcopyrite in a heap leach, which include:

- Inaccessibility of target mineral grains in ore particles (Cathles and Apps, 1975), as a large fraction of the mineral grains are positioned below the surface of the coarse ore particles and the leaching solution has to penetrate through cracks and pores connected to the surface for oxidative dissolution to occur,
- High activation energy of the leaching reactions (Córdoba et al., 2008a),
- Limited availability of oxygen (a reactant in the leaching reactions) in a heap (Madsen and Groves, 1975; Petersen, 2010),
- Formation of compounds such as jarosite, elemental sulphur or polysulphide (Klauber, 2008) on the surface of the ore (often termed “passivation”) which act as a diffusional barrier limiting ingress and egress of leaching solution (Khoshkhoo et al., 2014), and
- The fact that the chalcopyrite ore surface becomes hydrophobic as leaching progresses (Gardner and Woods, 1979; Heyes and Trahar, 1977).

Based on the above-mentioned issues, a number of research studies have been done for improvement of low-grade chalcopyrite heap leaching, specifically to overcome long extraction times and low copper recovery.

A high temperature is required to break down bonds in the chalcopyrite crystal lattice due to its high activation energy. Cordoba (2008a) found that temperature enhancement from 38 °C to 68 °C resulted in a substantial increase in chalcopyrite chemical leaching. A chalcopyrite concentrate bioleaching study reported increased copper recovery as temperature was increased, with 16%, 23%, and 61% recovery obtained in the presence of acidophilic mesophiles (25 °C), moderate thermophiles (45 °C) and extreme thermophiles (60 °C) respectively (Natarajan, 2018).

Reductive leaching of chalcopyrite generally refers to the dissolution of chalcopyrite at low redox potential. Based on the chalcopyrite dissolution reaction using ferric ion and the Nernst equation, a higher redox potential (higher ferric/ferrous ratio) would be expected to lead to higher chalcopyrite dissolution. However, it does not happen in reality. Chalcopyrite leach kinetics reach a maximum at relatively low ferric to ferrous ratios, and leach at slower rates at more elevated solution potentials (Hiroyoshi et al., 2004; Petersen and Dixon, 2006). Peterson & Dixon (2006) found that a low operating potential is favourable for the leaching of chalcopyrite at high temperatures, whereas at low temperatures high potential leaching of pyrite is promoted. Furthermore, Khoshkhoo et al. (2017) showed that the reductive leaching mechanism does not necessarily result in higher and faster recoveries in the absence of the galvanic interaction induced by the presence of pyrite.

In order to catalyse copper extraction from chalcopyrite ore, different additives have been used. It was reported that pyrite and MnO_2 addition caused the chalcopyrite to corrode more rapidly than the pyrite or MnO_2 due to galvanic interaction (Berry et al., 1978; Jyothi et al., 1989; Nakazawa et al., 2016). The dissolution of chalcopyrite can also be accelerated by addition of soluble foreign ions such as silver (Hiroyoshi et al., 2002; Nazari et al., 2012). Based on the model of Hiroyoshi et al. (2002), chalcopyrite leaching proceeds in two steps: first, chalcopyrite is reduced by ferrous ions to form Cu_2S that is more rapidly leached; next, the intermediate Cu_2S is oxidized by ferric and/or dissolved oxygen to release cupric ions. During the chalcopyrite reduction, hydrogen sulphide is released to the liquid phase. Silver ions react with the hydrogen sulphide to form silver sulphide precipitate and decrease the concentration of hydrogen sulphide in the liquid phase, causing a rise in the critical potential of Cu_2S formation and broadening of the potential range where rapid copper extraction takes place. The results showed that the critical potential increased with increasing concentrations of silver ions. Therefore, silver catalyses chalcopyrite dissolution, but is not an economic additive (Hiroyoshi et al., 2002).

Surfactants have been found to reduce the hydrophobicity of the chalcopyrite surface caused by interfacial tension (Duncan et al., 1964; Sandoval et al., 1990; Shah, 2017; Tapera et al., 2018). Tapera et al. (2018) additionally suggested that reduction of the hydrophobicity of the chalcopyrite surface further facilitates contact of the chalcopyrite with silver ions in solution.

Some researchers have proposed use of chloride leaching solution rather than sulphate media. Perceived advantages of chloride systems are the higher solubilities of copper and iron, the ease of ferrous ion oxidation and faster leaching kinetics of chalcopyrite compared to ferric sulphate systems, and the generation of sulphur rather than sulphate as the product of sulphide oxidation. However, there are a number of difficulties in processes based on chloride systems including: (i) the corrosive nature of chloride which necessitates the use of more expensive materials for construction of reactors (Watling, 2013); (ii) less selective leaching which results in co-leaching of multiple elements and necessitates additional treatments (Bobadilla-Fazzini et al., 2017) and (iii) the difficulty of the solvent extraction and electrowinning high-grade copper from chloride solutions (Dalton et al., 1991).

2.9 X-ray micro-Computed Tomography

X-ray micro-Computed Tomography (µCT) is the measurement of attenuated X-ray photons by an X-ray detector after passing through a sample. A schematic of a CT scanner is shown in Figure 2-6. There are three important sections in a CT scanner including: the X-ray generator which emits X-ray photons; the X-ray detector which changes attenuated X-ray photons to readable information; and a sample placed between the X-ray generator and detector (Cnudde and Boone, 2013). A series of X-ray projection images is acquired and mathematically reconstructed to produce a 3D map of X-ray absorption in the volume. The 3D map is typically presented as a series of 2D slice images. Finally, image processing software is used to get data from the 3D volume (Landis and Keane, 2010).

Standard cone beam µCT is the most common lab-based CT scanner. The sample under investigation is imaged by conical X-ray beams. However, there are limitations for achievable resolution based on focal spot size, intensity of X-ray photons and the spectrum of generated X-rays. Focal spots are the area of the anode surface which receives the beam of electrons from the cathode. The resolution of a CT image depends on the size of the focal spot because it determines the number of source to detector paths. In terms of energy intensity, low energy intensity is not able to penetrate through high density materials and high energy intensity is not suitable for low density material because of its lesser sensitivity for variation of density (Cnudde and Boone, 2013).

This technique can be mathematically formulated Beer's law which expresses the transmitted intensity I of a monochromatic X-ray passing a sample (Van Geet et al., 2000):

$$I = I_0 e^{-\int \mu(s)ds} \tag{2-13}$$

where I_0 is the incident beam intensity and $\mu(s)$ is the local linear attenuation coefficient along the ray paths. Four phenomena –the photo-electric effect (low-energy phenomena), coherent (Rayleigh) scattering, incoherent (Compton) scattering (Mid-energy phenomena) and pair production (high-energy phenomena) –can affect the energy-dependent linear attenuation coefficient μ.

In mineral processing, the intensity of X-ray photons is usually lower than 200 kV. In this range the photo-electric effect and Compton scattering have more influence on the value of the linear attenuation coefficients. The effect of these phenomena can be written as follows (Han et al., 2009):

$$\mu = \rho \left(a + b \frac{Z^{3.8}}{E^{3.2}} \right) \qquad (2\text{-}14)$$

where ρ is the bulk density of the material, Z is the bulk atomic number of the material, E is the X-ray energy and a and b are the energy-dependent coefficients. The first and second terms of Eq. (2-14) correspond to Compton scatter and photoelectric absorption respectively.

For mixtures of atoms, the effective atomic number Z_e is used:

$$Z_e = (\int f_i Z_i^{3.8})^{1/3.89} \qquad (2\text{-}15)$$

where f_i is the fraction of the total number of electrons contributed by element i, and Z_i is the atomic number of element i. As described by Eq. (2-14), the linear attenuation coefficient will become increasingly dominated by the photoelectric absorption due to presence of the factor $Z^{3.8}$ in Eq. (2-15).

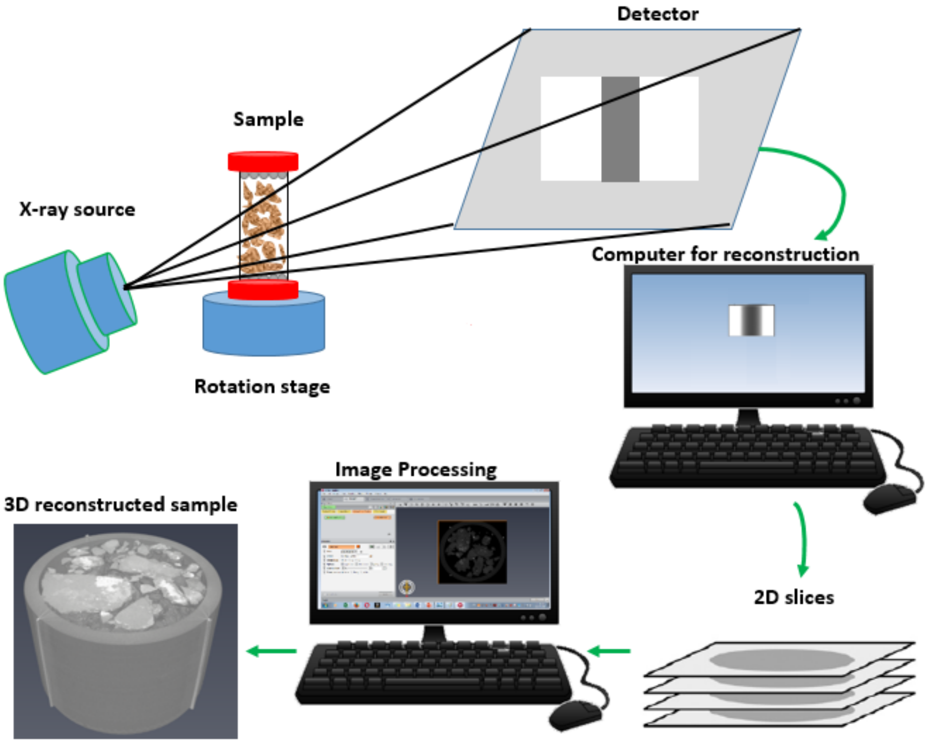

Figure 2-6: Schematic illustration of X-ray CT acquisition, reconstruction processes and image processing.

2.10 X-ray µCT application to heap leaching

A number of companies such as Bio-imaging and ARACOR have introduced non-medical application of X-ray µCT scanners with high resolution since the first introduction by EMI MARK I in 1973 (Miller et al., 1990). In 1987, X-ray µCT was used to follow bacterial-assisted removal of pyrite from lump coal. It was found that pyrite inclusions at a depth of 17 mm within the lump could be dissolved after 4 months of leaching (Spiro et al., 1987). Miller et al. (1990) identified the potential applications of the technique in mineral processing such as particle composition distribution, liberation analysis, and coal washability in 1990.

The first use of X-ray µCT in heap leaching operation was in 2003 when it was used to determine mineral exposure analysis in order to predict and determine the ultimate recovery in three different ore particle size distributions. The results showed that exposure analysis are slightly underestimated compared with the actual recoveries from column leaching experiments (Miller et al., 2003). It has since been used to examine porous network structure analysis in a column before and after leaching

(Dhawan et al., 2012), particle shape (Lin and Miller, 2005), and mineral compositions of an ore (Garcia et al., 2009).

X-ray µCT has also been applied to study the effect of comminution on heap leaching. Research undertaken includes: determination of micro-fracturing and deep internal particle fracture (Baum and Ausburn, 2011), detailed understanding of the leaching behaviour of large particles (Ghorbani, December 2012), and particle damage and exposure analysis by HPGR crushing of selected copper ores for column leaching (Kodali et al., 2011b). Garcia et al. (2009) used it to quantitatively analyse grain boundary fractures in the breakage of single multiphase particles. The results showed that preferential grain boundary fractures occurred at low energy dissipation rates for a copper ore. Nosrati et al. (2012) used the technique to visualize material micro-structural properties of nickel laterite agglomerates for enhanced heap leaching, e.g. pore distribution and interconnectivity, and defects such as cracks and voids. The results suggested that agglomerate microstructure analysis provides valuable information which may be used for possible agglomeration process optimization and improving final granule properties such as porosity, permeability, strength and re-wetting stability.

Acquiring X-ray µCT images of an ore at different time points in a leach allows for leaching progress to be tracked. Chalcocite grain dissolution in the course of leaching has been followed (Lin and Garcia, 2005). The results confirmed the leaching disappearance of chalcocite grains as leaching proceeded. Fagan-Endres et al. (2017) used it to quantify the degree of sub-surface leaching in a bed of coarse chalcopyrite ore (Dobson et al., 2017). Lin et al. (2016b) conducted mini-column leaching of large chalcopyrite particles and quantitatively determined non-surface mineral grain leaching at three different flowrates. Furthermore, they developed an automatic image processing package to process the 3D volume data.

Studies of bioleaching systems using X-ray µCT have not been conducted due to concerns that the X-ray radiation negatively affects the microorganisms. In a different field, Schmidt et al. (2015) investigated soil archaea and bacteria respiration, enzyme activity, microbial biomass, abundance and community structure in scanned using X-ray µCT and control treatments. Their results suggested that X-ray µCT had no or little effect on microorganism populations and may be compatible with soil microbiological experiments. It was found that X-ray µCT scanning at low energy doses (80-120 kV) has negligible influence on archaea and bacteria (Schmidt et al., 2015). However, Fischer et al. (2013) assessed microbial activity at 160 kV and 1000 µA energy dose which reported that the negative X-ray effect on microbes was strong.

2.11 X-ray µCT image processing

In addition to establishing the proper scanning conditions for image acquisition, careful consideration must be given to image analysis depending on what information is required. The 3D reconstructed volume is used for image analysis. The data analysis is accomplished by a series of steps. Image pre-processing and filtering is used for controlling contrast, smoothing, noise reduction and feature enhancement. Then, image segmentation of different mineral phases is performed, which is assigning to each pixel of the image a label describing to which region or material the pixel belongs. Identification and assignment of each particle or grain to a unique index (labelling) follows, and finally image quantification and analysis is completed.

2.11.1 Image filtering

It is often necessary to reduce image noise or artefacts and enhance features of interest before segmentation. Digital image filters are tools used to enhance images or highlight image features. Image processing operations implemented with filtering include smoothing (de-nosing), sharpening, and edge detection. Smoothing filters or low pass filters smooth noisy images by passing low-frequency signals and attenuating signals with frequencies higher than the cut-off frequency. However, it should be used carefully in order to prevent changing any data contained in the image, especially for quantification purposes (Avizo User's Guide, 2015). Sharpening filters or high pass filters help reinforce the contrast at edges and make details appear sharper by passing high frequencies well, but attenuate frequencies lower than the cut-off frequency. Finally, edge detection filters highlight boundaries between different materials or phases. They can be used, for instance, to directly extract feature contours and edges, or in watershed-based segmentation (Sprawls, 1992).

2.11.2 X-ray µCT partial volume effects

X-ray µCT has an intrinsic artefact when it deals with a multiphase object, such as an ore particle containing multiple mineral types, known as partial volume effect (PVE)

(Ketcham and Carlson, 2001). It makes intensity values at boundaries differ from what they really are and affects image quality. The partial volume effects may blur the transition between phases and features (Avizo User's Guide, 2015). Therefore, the PVE can have an important influence on the quantitative measurement of target mineral volumes. Figure 2-7 demonstrates that a non-existent phase is created between phase 1 and 2 whose attenuation coefficient will be a linear combination of the attenuation coefficients of each phase based on the volume occupied by each phase in the voxel. Grain size distribution in an ore, sample size, voxel size, and particle geometry all make contributions to the partial volume effect extent. It is necessary to correct PVE in image processing to enable accurate identification and quantification of the various mineral phases. One of the methods to treat PVE is using machine learning tool such as Trainable Weka Segmentation (Wang et al., 2017).

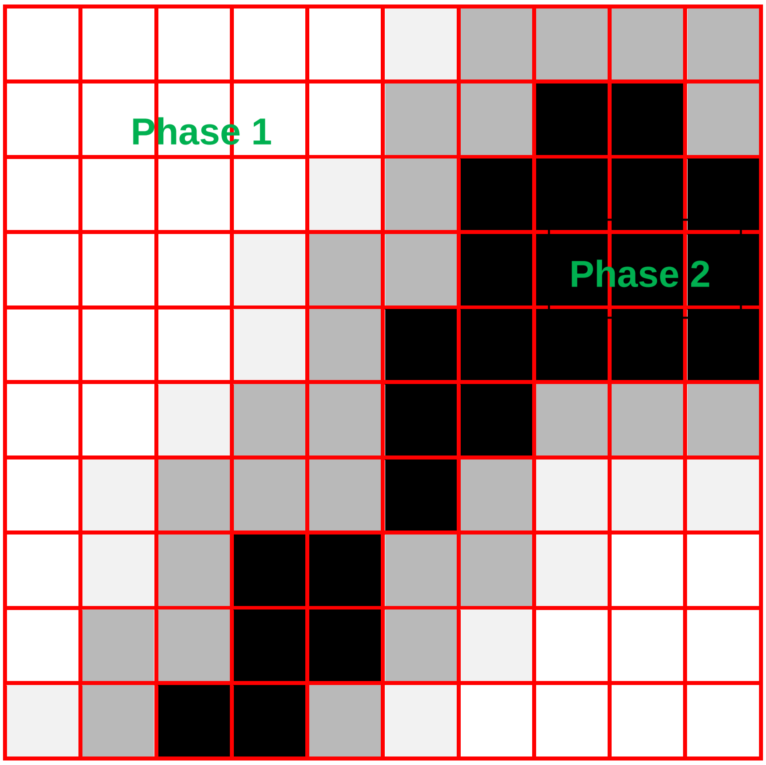

Figure 2-7: A schematic explanation of the partial volume effect in the context of X-ray µCT imaging.

2.11.3 Segmentation

There are various minerals in an ore with different atomic number and density. These each give different X-ray attenuation coefficients. Figure 2-8 shows attenuation coefficients of a number of minerals. Sulphide minerals such as pyrite and chalcopyrite have lower attenuation coefficients than zircon, while their attenuation coefficient is higher than gangue minerals like quartz and biotite. Differences in attenuation coefficient change the grey-level in the CT scan images. It is important to separate different grey levels accurately in order to measure mineral volume correctly. Therefore, image segmentation is a critically important step in image processing.

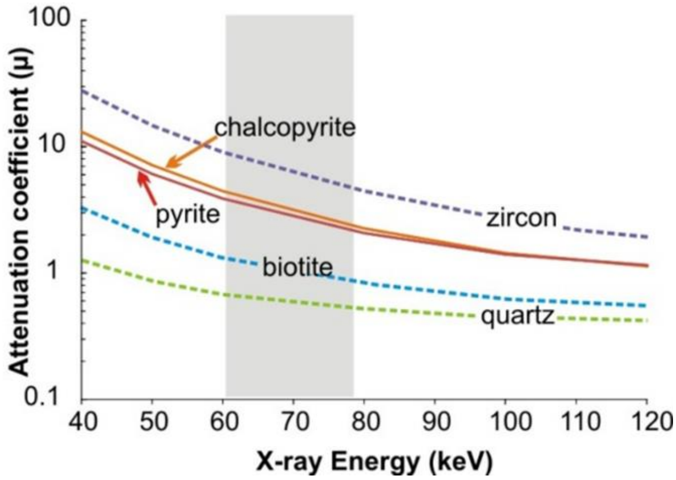

Figure 2-8: The difference in attenuation of the different minerals in the sample (Dobson et al., 2017).

Image segmentation algorithms can be based on clustering, histogram thresholding, edge detection, and region-based techniques including split-and-merge and region growing (Sridevi and Mala, 2012). Thresholding is one of the widely used techniques for monochrome image segmentation. It assumes that the images are composed of regions with different ranges of grey level. The histogram of the image can be separated into a number of peaks, each corresponding to one region and there exists a threshold value corresponding to a valley between the two adjacent peaks (Sridevi and Mala, 2012). Global and local thresholding are the two common thresholding categories (Lin, 2015). Global thresholding usually uses Otsu's algorithm (Otsu, 1979) to find the optimal value for a single global threshold to compare each pixel's grey level. Global thresholding can be applied for segmentation when there are clearly distinct differences between peaks in a histogram. Otherwise, it is possible to use local thresholding. In local thresholding, an image is divided into several sub-images and a threshold found for each sub-image to extract a region of interest. Then, the segmentation results of each sub-image are merged into a complete image again to get a good segmentation of the whole image (Firdousi and Parveen, 2014). It is applicable for an image when the gradient effect is small with respect to the chosen sub-image size. PVE is one of the crucial issues of global and local thresholding which decrease the accuracy of quantification results (Wang et al., 2017). Segmentation by simple thresholding may consequently give inaccurate results, especially in phase transition regions. It is difficult to determine correct or unique threshold in phase transition regions due to edges blurred by noise and partial volume effects and a third phase, known as the unwanted intimidate coating phase, created between two phases (Avizo User's Guide, 2015).

The watershed segmentation technique provides an effective solution for these issues in many cases. It combines region growing together with edge detection techniques. However, the direct computation of watershed segmentation always results in over-segmentation. To avoid this problem, marker-controlled segmentation has been developed to transform the input image into the watersheds of the transformed image corresponding to meaningful object boundaries. The current 3D watershed segmentation process works well for most multiphase mineral particles with a scale parameter (particle size/voxel size) greater than 30 and a density lower than 4.0 g cm^{-3} (Wang et al., 2017). The scale parameter is defined as the ratio of particle size to voxel size. It is used to identify how the particle is scaled in the image. Therefore, it is important to use other techniques in the case of lower than 30 scale parameter and density higher than 4 g cm^{-3} to get accurate mineral volume measurement.

Trainable Weka Segmentation (TWS), a machine learning tool, has been developed to extract useful features for a specific image processing procedure. To segment the input image data, TWS transforms the segmentation problem into a pixel classification problem in which each pixel can be classified as belonging to a specific segment or class (Arganda-Carreras et al., 2014). A set of input pixels that has been labelled is represented in the feature space and then used as the training set for a selected classifier. Once the classifier is trained, it can be used to classify either the rest of the input pixels or completely new image data (Arganda-Carreras et al., 2014). The process is illustrated in Figure 2-9. There are 20 features used in Weka segmentation including: Gaussian blur, Hessian, Membrane projections, Mean, Maximum, Anisotropic diffusion, Lipschitz, Gabor, Laplacian, Entropy, Sobel filter, Difference of

Gaussians, Variance, Minimum, Median, Bilateral, Kuwahara, Derivatives, Structure and Neighbours. Utilization of some features, for example Anisotropic diffusion, is time consuming. Also, some features are not efficient enough for accurate segmentation. Considering not only image segmentation results, but also computing time, Gaussian blur, Sobel filter, Hessian, Difference of Gaussians (DoG) and Membrane projections are favourable. It has been used for the segmentation of multiphase particulate systems containing fine and/or high density/high atomic number particles and the results demonstrate the utility of this improved image segmentation methodology (Wang et al., 2015). However, the local thresholding technique and Trainable Weka Segmentation are expensive and time consuming, therefore require high speed processing system (Lin, 2015) for getting data from X-ray µCT images.

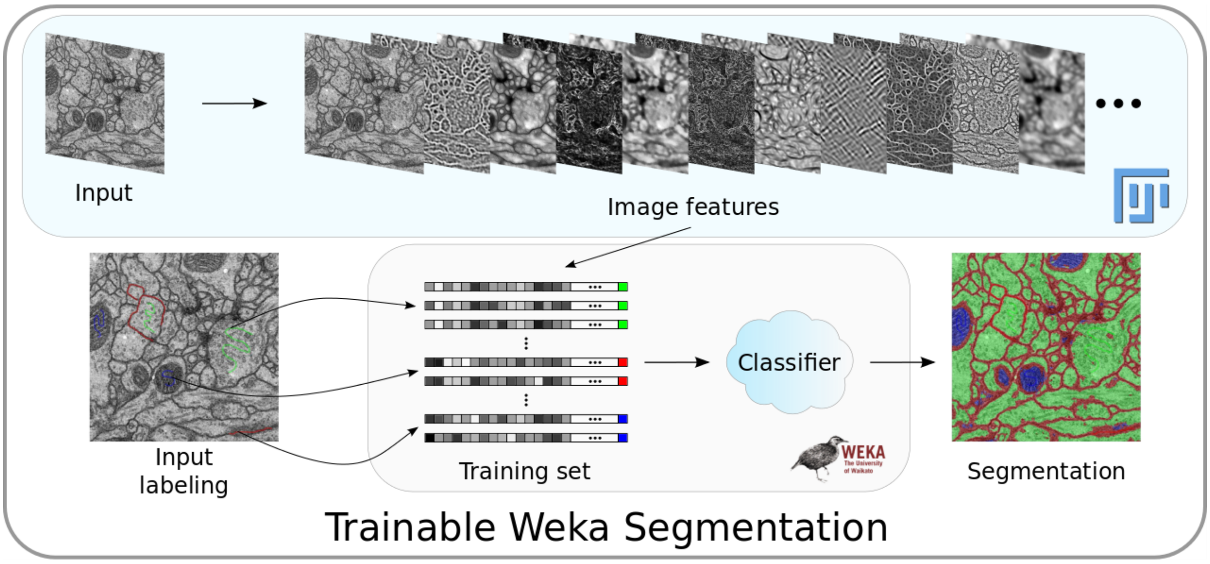

Figure 2-9: Trainable Weka Segmentation pipeline for pixel classification [with permission from (Arganda-Carreras et al., 2014)].

2.12 Research aims and objectives

The first published use of X-ray µCT in heap leaching appeared in 2003 when it was used to determine mineral exposure analysis to predict the ultimate recovery in three different particle size distributions (Miller et al., 2003). It has since been used in several leaching investigations, facilitated through the imaging of the same sample at different points in time, thereby allowing for micro-scale dynamics of the leaching process to be tracked. This circumvents the issue of leaching system heterogeneity, because the sample characteristics (such as ore particle size distribution, mineral grain distribution, local inter- and intra-particle voidage, fluid dynamics and contacting), which vary significantly within a heap structure, only change due to the effect of leaching. The aim of this study will be further investigation of using X-ray µCT in heap leaching in order to fill the knowledge gap that still exists, critically around the effect of the microbes.

The project focus is the effect of the liquid and microbial environment on the leaching penetration into coarse low-grade ores at the particle and mineral grain scale. To quantify this, the leaching of sub-surface mineral grains at different conditions relevant to a bioleaching system will be investigated using X-ray µCT. Specific factors that will be considered include agglomeration pre-treatment, addition of surfactant and effect of temperature for improvement of heap bioleaching efficiency. The parameters were selected based on their expected ability to impact the accessibility of leach solution to non-surface grains. The possibility of studying these parameters' effects on leaching performance by X-ray µCT will be examined as part of this project.

In all previous studies, the researchers supplied fresh ferric ion continuously in the feed to facilitate leaching rather than using microorganisms to regenerate the leaching reagent in-situ. This was due to concerns that X-ray exposure during CT scanning may inhibit, stress or kill the bacteria and archaea. However, it is anticipated that the association of microorganisms with the mineral surface through colonisation via generation of extracellular polymeric materials (EPS) and biofilms influences the leaching performance of biological systems over chemical systems (Govender-Opitz et al., 2017; Hansford and Vargas, 2001; Sand and Gehrke, 2006). The integration of X-ray µCT in experiments with bioleaching microorganisms may help to fill the knowledge gap that still exists regarding non-surface mineral grain leaching in the presence of microorganisms.

It is required to select an appropriate surfactant(s) for use in the heap bioleaching systems of interest, because they can have negative effects on microbial activity and growth. Most of the existing research has been done at low temperatures (30 – 45 °C). However chalcopyrite leaching needs high temperatures (typically > 68 °C) due to the high activation energy (130.7 kJ mol^{-1} for temperatures between 35 and 68°C) required to break down the bonds in the crystal lattice (Córdoba et al., 2008a). In addition to shifting the thermodynamics of the system, the higher temperature also results in shifts in the microbial population from mesophiles towards thermophiles. Thus, the applicability of the previous findings is not practicable. This study also aims to address this knowledge gap by investigating the effect of various non-ionic surfactants on the metabolic activity of mixed cultures of thermophilic microorganisms for ferrous ion oxidation and sulphur oxidation to facilitate chalcopyrite bioleaching.

2.13 Hypotheses and key questions

The following hypotheses have been formulated:

1- The biotic leaching of mineral sulphide ore can be studied using lower energy dose X-ray µCT because low energy X-ray has a negligible effect on bioleaching microorganisms.

Key questions:

- Is it possible to study biotic heap leaching by X-ray µCT technique?
- Is it possible to acquire images of the mineral ore particles at sufficiently high resolution at low energy dose to be compatible for bioleaching imaging?
- How much does the CT scan imaging affect microbial growth and metabolic activity?
- Do microorganisms have the ability to oxidise ferrous ion after CT scan imaging?

2- The inability of leaching reagents to contact non-surface mineral grains limits the maximum metal recovery because a maximum leaching penetration distance into the pores exists. The maximum leaching penetration distance can be increased through the inclusion of surfactant to the leaching solution at dosages acceptable to bioleaching microorganisms. This is as the reduction of surface tension allows increased penetration of the solution into the ore particle pore network.

Key questions:

- How is the viability and vitality bioleaching microorganisms affected by different surfactant types and concentrations?
- How does the leaching rate change as a function of distance from the ore surface?
- Does the ore porosity affect maximum leaching penetration distance?
- Do differences in pore network and extent affect the extent of leaching?
- Does the kinetics of the mineral to be leached affect maximum leaching penetration distance?
- Does addition of surfactant into the leaching solution increase leaching penetration distance?

3- Maximum leaching recovery cannot be affected by increasing temperature because there is a maximum leaching penetration distance, limiting mineral available for leaching. Conversely, increasing temperature does increase the rate of leaching.

Key questions:

- How does the leaching rate change as a function of distance from the ore surface?
- Does increasing temperature result in the enhancement of leaching rate or recovery or both?
- Does the relevant temperature range affect significantly upon solution viscosity, surface tension and other physicochemical factors affecting leaching penetration?

3 Approach to Project and Methodology

Chapter 3 describes the overall experimental design in this study including: (1) ore preparation, (2) mineralogical characterisation, (3) incubator and column design, (4) microbial culture and growth conditions, (4) density and viscosity measurements, (5) ore agglomeration, (6) SEM analysis, (7) IMC measurements, (8) surfactant addition into leaching solution effect on microbial activity and growth, (9) X-ray effect on microbial activity and growth, (10) mini-column leaching and (11) X-ray µCT imaging conditions for vials, 10 mL syringe column, and mini-columns. These are common methods applied across the subsequent research chapters.

3.1 Materials

3.1.1 Ores

Three different ores were used, namely: a Pinto Valley chalcopyrite rich ore, a malachite ore which was provided by Mintek and a waste rock containing pyrite. These ore were selected because of their different physical and mineral leaching characteristics. Ore preparation was done representatively, though it must be noted that the leaching results are not necessarily representative of the parent ore.

A chalcopyrite concentrate (71.3 wt%) was used to study the effect of surfactant on microbial activity. The ore elemental composition was 24.4 wt% copper, 21.5 wt% iron and 25.3 wt% sulphur.

A pyrite concentrate, used in suspension and to coat on glass beads, was provided by a mine from the Gamsberg Mountain in South Africa. The concentrate size fraction was 38-75 µm, determined using a Malvern Particle Size Analyser (2000). The elemental composition of the pyrite concentrate was 34.80 wt% sulphur and 47.45 wt% iron as determined by LECO Sulphur analyser (LECO) and ICP-OES respectively (Makaula et al., 2017a). Based on an XRD analysis, it comprised of 96% pyrite, 1.76% talc, 1.54% quartz and 0.51% chalcopyrite.

3.1.2 Surfactants

Five non-ionic surfactants were used, added in specific concentrations to the experimental systems. Tween® 20 and Tween® 80 were purchased from Sigma-Aldrich. Plurafac® LF 120, Plurafac® LF 600 and Lutensol® XL 90 were obtained from

BASF SE. The specifications of the surfactants are presented in Table 3-1. Surfactant concentrations of 5 mg L^{-1} and 10 mg L^{-1} were used. The Tween® 20 and 80 concentrations were extended to 20 mg L^{-1} to make sure the chosen concentrations were best with respect to microbial growth and activity. The chosen concentrations were required to be lower than the critical micelle concentration. Technical considerations that favour a low concentration include that further processing such as solvent extraction and electro-winning is required to recover the pure metal from the PLS and the surfactant should not impact on this process. The cost of surfactant also becomes significant at higher concentrations.

Table 3-1: Non-ionic surfactant specifications.

Surfactant	**Critical micelle concentration (mg L^{-1})**	**Used concentration (mg L^{-1})**	**Properties**	**Ref.**
Tween® 20	45-50	5, 10, 20	Ethoxylate of sorbitan monolaurate, based on the saturated 12C acid, lauric acid	Johnson (2013); Yeh Daniel et al. (2009)
Tween® 80	13-15	5,10,20	Ethoxylate of sorbitan mono-oleate, based on the C18:1 cis-9 acid, oleic acid	Johnson (2013); Yeh Daniel et al. (2009)
Plurafac® LF 120	70	5,10	Alkoxylated, predominantly unbranched fatty alcohols and contain higher alkene oxides alongside ethylene oxide	BASF (2008)
Plurafac® LF 600	11-12	5,10		BASF (2008)
Lutensol® XL 90	1.42×10^{-3} (mol L^{-1})	5,10	Alkyl polyethylene glycol ethers made through the Guerbet reaction of the primary aliphatic C10 alcohol with alkylene oxides ($C_{10}(PO)_1(EO)_9$)	Kong et al. (2014)

3.1.3 Microorganisms

3.1.3.1 Mixed mesophilic stock culture

A mixed mesophilic inoculum containing *Leptospirillum ferriphilum, Acidithiobacillus caldus* and archaea, including *Ferroplasma acidiphilum* and *Acidiplasma cupricumulans*, was grown on a 3% (w/v) pyrite concentrate in 0K basal salts medium (0.01 g L^{-1} $Ca(NO_3)_2$, 0.1 g L^{-1} KCl, 0.5 g L^{-1} $MgSO_4.7H_2O$, 0.5 g L^{-1} K_2HPO_4 and 3 g L^{-1} $(NH_4)SO_4$) (Kolmert and Johnson, 2001) in a 1 L batch stirred tank reactor at 35 °C, with a stirring speed of 550 rpm and air flow rate of 2 L h^{-1}. The microbial distribution of the bacterially dominated stock culture, determined by qPCR (Smart et al., 2017), is displayed in Figure 3-1 (A).

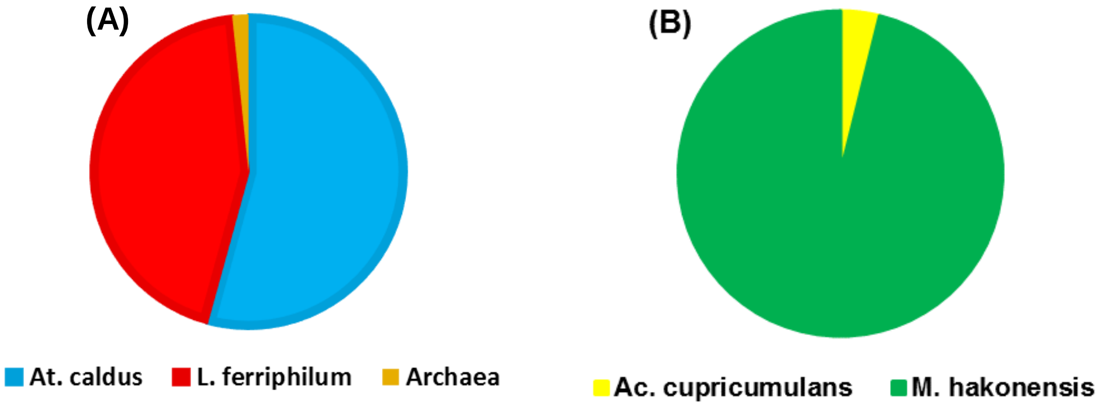

Figure 3-1: Microbial distribution of the: (A) mixed mesophilic stock culture, (B) mixed thermophilic stock culture.

3.1.3.2 Mixed thermophilic stock culture

A mixed thermophilic stock culture, dominant in *Metallosphaera hakonensis* (Bromfield et al., 2011), was maintained in a 1 L batch stirred tank reactor at 65 °C on a 3% (w/v) chalcopyrite concentrate (71.3 wt%). The ore elemental composition was 24.4 wt% copper, 21.5 wt% iron and 25.3 wt% sulphur. The stock culture was grown in a Norris basal salts medium made up of 0.4 g L^{-1} $(NH_4)_2SO_4$, 0.1 g L^{-1} KCl, 0.2 g L^{-1} K_2HPO_4, 0.5 g L^{-1} $MgSO_4.7H_2O$ and 1 mL of 1000 × stock of trace elements (Norris, 2001). This stock reactor was maintained on a basis of a weekly draw-and-fill in which 15% (v/v) was replaced with fresh media and associated concentrate. The microbial concentration was in the range of 1×10^8 to 4×10^8 cells mL^{-1}. The microbial distribution of the archaeal-dominated stock culture, determined by qPCR (Smart et al., 2017), is displayed in Figure 3-1 (B).

3.2 Ore preparation

3.2.1 Ore particle size distribution and splitting

The chalcopyrite ore sample, after primary crushing by a hydraulic rock splitter into small particles, was further reduced in size by jaw crusher. The waste rock and malachite ores were received ready crushed. The ores were sieved into six fractions (<0.25 mm, 0.25 – 1 mm, 1 – 2 mm, 2 – 5.6 mm, 5.6 – 8 mm, 8 – 16 mm). Figure 3-2 shows the resulting cumulative particle size distribution of the chalcopyrite, to which the other ores were matched. The ore variability in terms of mineral composition and particle size results in corresponding inhomogeneous leaching behaviour. Thus, leach test results that are representative of an ore body require careful preparation of ore samples to evenly distribute this variability such that leaching is repeatable. To this end, each ore size fraction was representatively split into small portions using a rotary splitter (Figure 3-3).

The different size fractions were selectively recombined to create 50 g batches of representative samples for testing. This method and the same PSD were used for preparation of all three ores. In order to measure the ore variability quantitatively, 50 g of the same batches were packed in three mini-columns (150 mm length, 20 mm diameter) and the sulphide minerals volume was determined by scanning the mini-columns using X-ray µCT. The results are shown in Figure 3-4. The maximum variation from the mean was 12.5%.

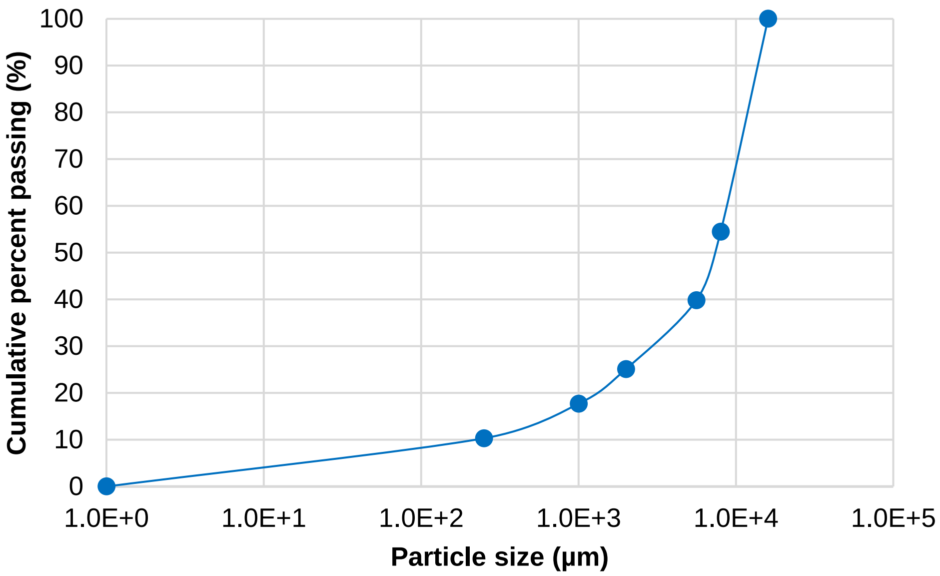

Figure 3-2: Particle size distribution of the low-grade chalcopyrite ore sample.

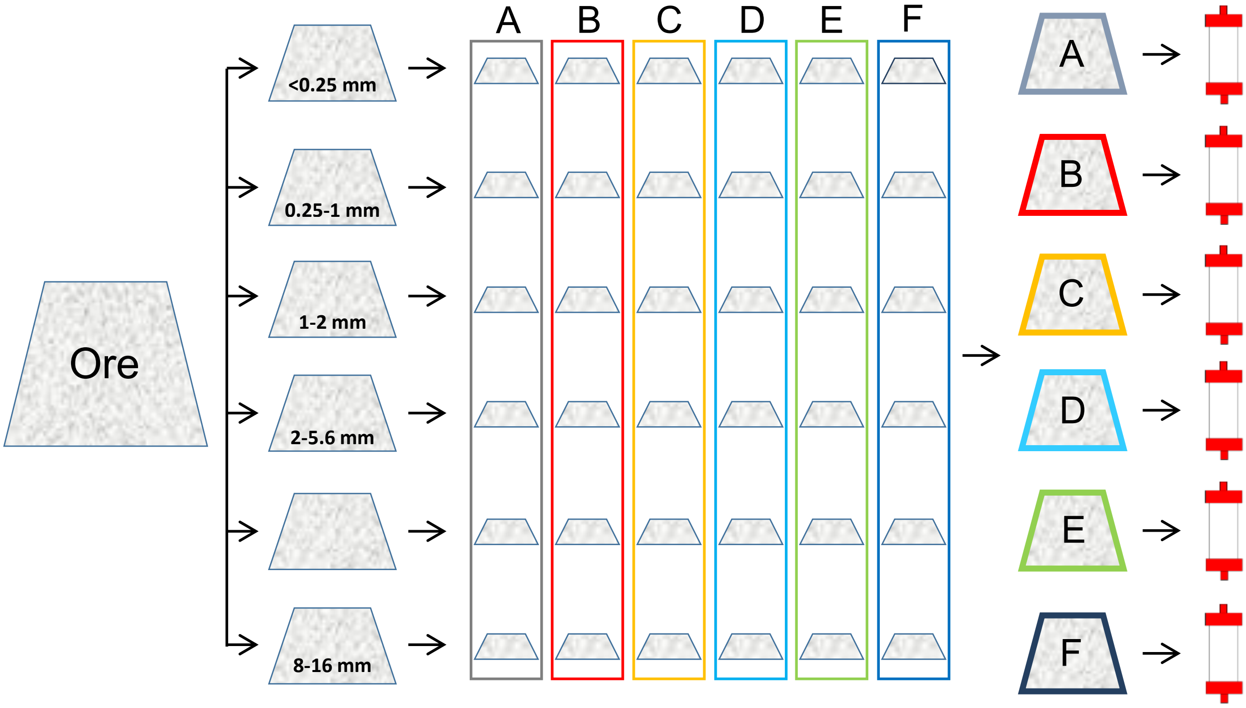

Figure 3-3: Preparation of the ore to achieve replicate and statistically representative ore mixtures.

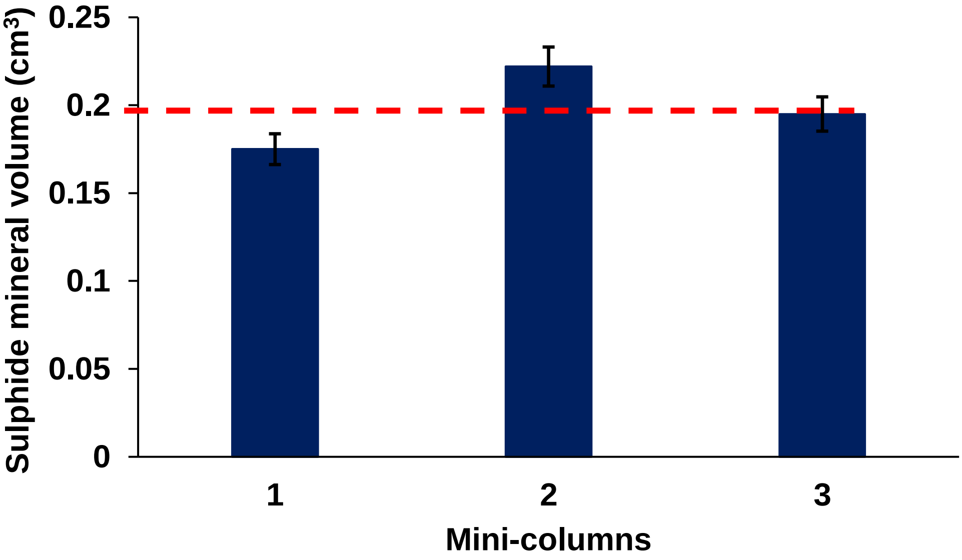

Figure 3-4: Sulphide mineral volume in three mini-columns. The error bars show the uncertainty based on relative standard deviation at the 95% confidence limit. The dashed line is the average value.

3.2.2 Ore agglomeration

Ore was agglomerated using a ratio of 2 kg acid/ton ore and 5.5 % moisture, where 0.5 % comes with the ore. This corresponded to an acid water solution prepared at a ratio of 2.6 mL water to 0.1 mL H_2SO_4 combined with 50 g of ore. The acidified water was added to the ore and then agglomerated by rotating in a bucket drum, to ensure a homogeneous clumpy sludge. The agglomerated ore was immediately packed into the experimental column. This agglomeration method has been used in various experimental work as a standard method (Chiume et al., 2012; van Hille et al., 2010).

3.2.3 Mineral-coated beads

Pyrite mineral concentrate coated onto 5 mm glass beads was used as an attachment substrate and source of energy for the microbial culture in experiments. This was selected to ensure that a reproducible mineral surface area was present across all columns and that mineral liberation did not impact the bioleaching observed in the different columns.

Glass beads of 5 mm diameter were coated with the pyrite concentrate using a non-toxic clear one-part acetoxy curing silicone sealant (Bostik™) and subsequently air dried for a minimum of 24 h (Africa et al., 2013; Makaula et al., 2017a). The mineral coated beads were sterilized by irradiation (45 kGy) prior to leaching experiments (Govender et al., 2015a).

3.3 Mineralogical characterization

One portion of each ore size fraction was used for mineralogical analysis. A pulveriser was used to prepare the ore by reducing the size to less than 75 µm.

Elemental assays of the three ores after digestion were obtained. Atomic absorption spectroscopy (AAS), performed using a Varian Spectra AA 10, was used to measure elements including Cu, Zn, Fe, Ca, Na, Mn, K and Al which are specifically important in the leaching of low-grade chalcopyrite ore. The sulphur content of the ore was quantified using a Leco analyser (LECO S632). X-ray fluorescence (XRF) was used to obtain the overall elemental composition and to validate QEMSCAN results. A Panalytical Axios wavelength-dispersive XRF spectrometer with sample-changer (56 sample capacity) and a rhodium end-window X-ray tube was used to analyse a wide range of elements.

The elemental composition of the ores, determined using AAS and Leco, is shown in Table 3-2 (chalcopyrite),

Table 3-3 (malachite), and Table 3-4 (pyrite). The percentage of copper in the chalcopyrite ore was higher in the 0-0.25 mm size fraction than the other size fractions. This could be attributed to the higher grinding ability of copper minerals and is consistent with Kodali (2011a) for a copper mineral ore.

Table 3-2: Chemical composition of the various size fractions of the low-grade chalcopyrite ore as determined by AAS and Leco.

	Content (%)					
Ore size (mm)	**Al**	**Cu**	**Fe**	**K**	**Na**	**S**
0-0.25	7.4	1.1	4.4	4.7	0.9	1.8
0.25-1	5.6	0.5	2.6	4.3	1.1	1.2
1-2	6.7	0.4	2.3	4.4	1.1	0.7
2-5.6	5.8	0.5	2.3	4.4	1.1	0.7
5.6-8	7.2	0.4	2.2	4.4	1.0	0.7
8-16	7.3	0.5	2.3	4.4	1.1	0.8

Table 3-3: Chemical composition of the smallest and largest size fractions and overall of the malachite ore as determined by AAS.

	Content (%)		
Ore size(mm)	**Fe**	**Cu**	**Mn**
0-0.25	4.2	4.0	1.0
8-16	1.0	2.3	0.1
Overall	1.5	4.7	0.2

Table 3-4: Chemical composition of the smallest and largest size fractions and overall of the waste ore containing pyrite as determined by AAS.

	Content (%)					
Ore size(mm)	**Fe**	**Ca**	**Mn**	**Zn**	**Al**	**K**
0-0.25	24.5	1.5	0.9	1.7	3.5	1.0
8-16	23.1	1.2	0.6	1.4	3.4	1.3
Overall	22.6	1.5	1.1	1.7	4.1	1.0

Quantitative evaluation of minerals by scanning electron microscopy (QEMSCAN) was used to determine elemental deportment, mineral association, and chalcopyrite and pyrite grain size distribution. The QEMSCAN unit used is located at the University of Cape Town and is based on a FEI QEMSCAN 650F with two Bruker SDD detectors. Operating conditions were set at 25 kV and 10 nÅ beam current**.** Individual ore particles (8 to 16 mm) were analysed using the Field Image analysis routine. A pixel spacing of 14.5 µm was used for the Field Image analysis and determination of grain size distribution. Ore samples were mounted in epoxy resin and prepared into polished 30 mm diameter polished resin blocks. In the bulk mineralogy routine, used for quantitative mineral composition determination, all size fractions with a certain weight percentage were mixed and ground using a pulveriser and then the ground ore was mounted in epoxy resin. The mineral composition of the ores quantified using QEMSCAN is presented in Table 3-5.

Table 3-5: Mineralogical composition of the ores as determined by QEMSCAN. Associated chemical formulae are provided in the Nomenclature section.

Chalcopyrite		**Pyrite**		**Malachite**	
Mineral	Amount (wt%)	Mineral	Amount (wt%)	Mineral	Amount (wt%)
Quartz	37.6	Muscovite	29.6	Quartz	76.8
K-feldspar	37.5	**Pyrite**	**29.4**	**Malachite**	**6.8**
Muscovite	19.1	Quartz	16.5	**Bornite**	**2. 4**
Chlorite	1.7	**Sulphide trap**	**6.3**	Muscovite	3.6
Rutile	1.2	Limonite	5.0	Fe-Ti oxide	4.5
Chalcopyrite	**1.5**	**Pyrrhotite**	**3.5**	Biotite	1.0
Pyrite	**0.7**	Garnet	3.0	Chlorite	0.4
Other sulphides	**0.3**	K-feldspar	3.0	Chrysocolla	0.1
Other	0.5	Other	3.8	Other	4.3

3.4 Mini-column design

Mini-leaching columns were designed based on the chalcopyrite grain size distribution, explained in detail in the next chapter. Glass columns, with a diameter of 20 mm and a length of 150 mm, were constructed by Glasschem (Stellenbosch, South Africa). The ends were closed with screw-cap lids with a rubber stopper and glass nipple. A peristaltic pump (Masterflex Console Drive, 7521-57) was connected to the glass nipple to allow solution to be pumped in from the top of the column, with collection of liquid out the bottom. Glass wool and 50 glass beads (4 mm diameter, Lasec) were placed at the top and bottom of the column to ensure uniform distribution of liquid in the column.

3.5 Incubator design

In order to perform the experiment to study the effect of temperature on non-surface mineral grain leaching, two 4 and 8 mini-columns wooden incubators were designed and constructed. Front, side, and top views of the 8 mini-columns incubator is shown in Figure 3-5. It includes a heater and a fan to circulate the air inside the incubator and make the temperature distribution uniform. An electronic controller keeps the temperature constant by turning the power to the heater up or down.

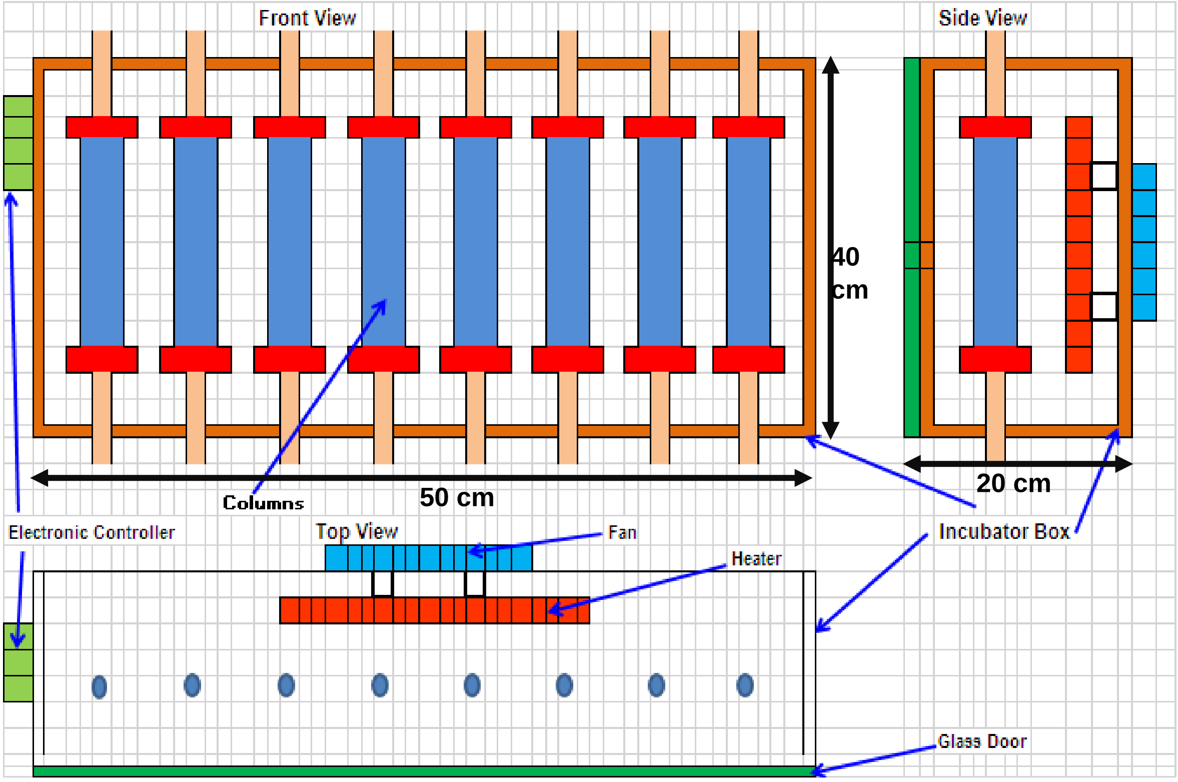

Figure 3-5: Schematic of incubator from front, side, and top views.

3.6 Analytical methods

3.6.1 Solution chemistry

A Metrohm 827 pH / redox lab meter with a Metrohm 6.0451.100 probe was used to measure redox potential. The pH was monitored using a Metrohm 713 pH meter with a Metrohm 6.0258.000 probe. The ferrous and total iron concentrations were determined using the 1–10 phenanthroline method (Komadel and Stucki, 1988).

3.6.2 Planktonic cell concentration

The unattached (planktonic) microbial concentration in the PLS was determined by direct cell counting using a THOMA counting chamber under an Olympus BX100 phase contrast microscope at 1500× magnification.

3.6.3 Isothermal microcalorimetry

Isothermal microcalorimetry (IMC) was used to study the effect of exposure to X-ray on the metabolic activity of cells on the mineral surface. It was done two days after exposure to X-ray when the microorganisms were conditioned to a leaching environment. Microcalorimetric experiments were performed using a TAM III microcalorimeter supplied by TA Instruments, USA. The TAM III was operated in static ampoule mode with 4 mL glass ampoules at 30 °C. One channel contained an ampoule with 2 mL 0K media supplemented with 0.5 g L^{-1} Fe^{2+} as the machine control. The other channels each contained ampoules with two pyrite-coated glass beads taken from: (2) the abiotic negative control, (3) the inoculated positive control not exposed to X-ray, and (4 & 5) the two inoculated experimental mini-columns post X-ray exposure (Makaula et al., 2017a). The IMC experiment was run for 5 days in order to measure the heat flow rate following insertion of the ampoules into the IMC and subsequent stabilization of the IMC system according to the procedure of Makaula et al. (Makaula et al., 2017a).

3.6.4 Visualization of microorganisms by scanning electron microscopy

Scanning electron microscopy (Tescan MIRA SEM with RAMAN confocal microscopy) was used to investigate the effect of exposure to X-ray on the cell growth and ongoing colonisation on a mineral coated bead surface (Makaula et al., 2017a). The mineral coated beads were prepared by fixing in 2.5% (v/v) glutaraldehyde for a minimum of 24 h at 4 °C. Fixed samples after washing with sterile deionized water were dehydrated through an alcohol series including 30, 50, 70, 90, 95 and 100% (v/v) ethanol using 10 min contacting times. After dehydration, critical point drying using hexamethyldisilazane (HMDS) was undertaken. The samples were then stub-mounted, sputter coated with carbon and visualised using scanning electron microscopy (Makaula et al., 2017a).

3.6.5 Viscosity measurement

An Ostwald (or Ubbelohde) capillary-tube viscometer was used to measure solution viscosity at different temperatures. Experiments were conducted in a water bath to control temperature. An Ostwald capillary-tube viscometer consists of a capillary tube in a U-shape form. The capillary tube is vertically positioned in one of the two arms of the U tube. In the arm where the capillary tube is positioned, there are two pre-marked lines above the capillary so that the time taken for a test liquid to pass the two pre-marked lines can be measured. In the other arm, there is a bulb reservoir near the bottom. To prepare a viscosity measurement, solution is drawn above the top pre-marked line by suction or other means and allowed to flow down by gravity through the capillary tube into the lower bulb reservoir. The time taken for the level of the solution to pass between the two pre-marked lines is measured using a stopwatch, which typically varies in a range of 90-250 s, depending on the magnitude of the solution viscosity. With a calibration constant provided by the manufacturer of the viscometer, the measured transit time Δt can be converted to solution viscosity (Lee et al., 2012).

3.6.6 Density measurement

To measure the density of solution, a balance was used to measure the mass of solution in a 100 mL volumetric flask in triplicate at 37 °C and 65 °C. The 100 mL volumetric flask was filled to the line with the liquid sample and put in the 37 °C room or 65 °C water bath until the solution temperature had equilibrated to the environment temperature. Increases in solution volume (beyond 100 mL) because of temperature increasing was removed from the flask. Then, the solution mass was weighed using a digital balance.

3.7 Batch leaching experiments

3.7.1 Effect of X-ray radiation on microbial growth and activity

The mixed thermophilic microorganisms were cultivated in 50 mL glass vials containing 10 mL of the ferrous supplemented (5 g L^{-1} Fe^{2+}) Norris basal medium at 65°C, agitated at 180 rpm in an orbital shaker. The initial pH was adjusted to pH 1.3. Performance of the biooxidation cultures was monitored by pH, redox potential, Fe^{2+} concentration and microbial cell counts. The glass vials containing the mixed thermophilic microbes in suspension were exposed to X-ray on the third day after inoculation. Microbial activity was compared in vials across exposure conditions and in the control samples not exposed to X-ray.

3.7.2 Effect of surfactant on microbial growth and activity

Shake flask culture experiments were conducted to examine the effect of the surfactants on microbial growth and ferrous ion oxidation. All experiments were conducted in 250 mL Erlenmeyer flasks at a 20 to 30% fill volume of Norris medium (initial pH 1.3 and 1.1), placed in orbital shaking incubators operated at 140 rpm and 65 °C. Pre-determined surfactant concentrations were added to each flask experiment. Abiotic (negative) controls which were not inoculated and biotic (positive) controls which contained no surfactant were performed for each setup. Any water lost by evaporation, determined gravimetrically, was compensated for by addition of deionized water during the experiment. Specific experiments were conducted as follows.

3.7.2.1 Effect of surfactant on ferrous ion oxidation

The effect of surfactant on the ferrous ion-oxidising capacity of the microorganisms was investigated using flasks containing 50 mL Norris medium supplemented with 5 g L^{-1} Fe^{+2} and inoculated with 1×10^{7} cells mL^{-1}. The flasks were monitored for ferrous ion concentration, redox potential, pH and microbial cell concentration at appropriate intervals.

3.7.2.2 Effect of surfactant on chalcopyrite bioleaching

Bioleaching experiments were performed in flasks containing 75 mL Norris medium and 2.25 g of chalcopyrite concentrate (3% (w/v) solids loading). The flasks were inoculated with 2×10^{7} cells mL^{-1}. The ferrous ion concentration, redox potential, pH and microbial cell concentration were monitored at appropriate intervals. The final copper concentration in solution was determined at the end of the bioleaching experiment.

3.7.2.3 Effect of surfactant on attachment

The effect of surfactant on microbial attachment to chalcopyrite was examined using a total working volume of 100 mL Norris medium with a 3% (w/v) chalcopyrite concentrate solids loading and an inoculum concentration of 2×10^{7} cells mL^{-1}. The surfactant concentration was 10 mg L^{-1}. The flasks were agitated for 4 hours, before and after which the planktonic cell concentrations were determined by direct counting, allowing attached cell concentrations to be determined by difference.

3.8 Flow-through leaching experiments

3.8.1 10 mL syringe pyrite leaching

Leaching tests were carried out in 10 mL disposable syringes which were each packed with 50 pyrite coated beads, as shown in Figure 3-6 (A).

The packed systems were first washed and conditioned with 0K media (pH=1.6) at 3 mL h^{-1} for 24 h to remove readily soluble acid-consuming minerals to allow subsequent maintenance of an acidic environment. On the second day, the systems were drained and inoculated by saturating with 30 mL 0K media supplemented with 0.5 g L^{-1} of Fe^{2+} and a mixed mesophilic microbial culture to achieve 1×10^{8} cells mL^{-1}. This culture was contacted with the mineral-coated beads by continuous recirculation for 18 h at a flowrate of 3 mL hr^{-1} in an up-flow circuit (to maintain the saturated condition). Thereafter, the systems were drained and the liquid fraction collected. The now unsaturated systems, ensuring oxygen availability, were then continuously irrigated from the top with fresh feed of 0K media at pH of 1.6, supplemented with 0.5 g L^{-1} Fe^{2+} at a flowrate of 3 mL hr^{-1}.

The experiments were operated at 30 °C for a total of 20 days. The pH, redox potential, Fe^{2+} and Fe^{3+} concentrations and cell concentration in the effluent pregnant leach solution (PLS) were monitored over this time period. The sampling was done every 24 hours. The operating conditions are summarised in Table 3-6.

Table 3-6: Operating conditions of each 10 mL syringe pyrite leaching system.

Parameter	Value
Temperature	30 °C
Media type	0K
Feed flow rate	3 mL h^{-1}
Feed solution pH	1.6
Feed solution Fe^{2+} concentration	0.5 g L^{-1}
Number of beads	50
Weight of pyrite coated	0.63 g

Four syringes were run: one un-inoculated (abiotic) negative control, one inoculated (biotic) positive control not exposed to X-ray, and two experiments which were inoculated and allowed to colonise before exposure to X-ray. The dominance of Fe^{3+} was taken as an indication of good microbial activity. Therefore, the systems were only exposed to the X-ray source when the PLS redox potential (relative to Ag/AgCl reference electrode) had increased to about 650 mV and remained stable, correlating with changes in the relative concentrations of ferrous and ferric ion.

Following X-ray exposure, the irrigation of the syringes was recommenced. While the negative and positive control columns were not imaged, they were treated in the same manner as the experimental mini-columns in all other respects.

The performance of these systems during the leaching phase was monitored in terms of pH, redox potential (relative to Ag/AgCl), Fe^{2+} and total iron concentration and cell concentration in the PLS. Further, IMC and SEM were conducted on representative beads at the end of the experiment.

3.8.2 Flow-through mini-column leaching

Ten glass mini-columns with a 20 mm internal diameter and 12 cm working length were used for the leaching of ore particles. Each mini-column was loaded with 50 g of low-grade chalcopyrite ore, malachite ore, or waste rock containing pyrite and operated as a continuous flow-through unsaturated system. The selected conditions are based on typical or best-practice or optimised operating conditions used in heap bioleaching process. The operation conditions of the ten mini-columns are shown in Table 3-7.

Prior to the introduction of feed solution, the loaded mini-columns were washed and conditioned with acidified solution (pH=1.15). For the chalcopyrite ore, feed with a pH of 1.15 was prepared containing 4.30 g L^{-1} Fe^{3+} and 8.33 g L^{-1} Fe^{2+} equivalent to 440 mV redox potential. Peterson and Dixon (2006) found that chalcopyrite leaches much more slowly at high potentials, while pyrite oxidation rate increases with increasing redox potential. There is a range of critical redox potential from 410 to 490 mV at which chalcopyrite leaching is maximized. The lower redox potential was thus selected to maximise chalcopyrite leaching while pyrite oxidation is low. Pyrite leaching was conducted using a feed solution with a pH of 1.15 and 8.60 g L^{-1} Fe^{3+}. Acidified solution with a pH of 1.20 was used for malachite leaching. For the biotic leaching, fresh feed solution of Norris media (pH = 1.6 or 1.3) supplemented with 0.5 g L^{-1} Fe^{2+} was used in duplicate (mini-columns 9 & 10). The pH was adjusted with concentrated H_2SO_4. The liquid was pumped into the top of the mini-columns from a single drip emitter point source at a flowrate of 2.55 mL h^{-1} for a period of 5.5 months for chalcopyrite and pyrite, and 26 days for malachite. Experiments were conducted in incubators at 30 °C, 37 °C and 65 °C. The lower temperature was most appropriate for the more readily leachable malachite ore. The two other temperatures are specific to mesophilic microorganisms (active at 37 °C) and thermophilic microorganisms (active at 65 °C) which are active in pyrite and chalcopyrite bioleaching.

Tween® 20 (10 mg L^{-1}) was used in order to study the effect of surfactant on non-surface mineral grain leaching. The surfactant type and concentration were based on the results of the surfactant experiments (Chapter 6). Biotic leaching was studied in two mini-columns packed with the low-grade chalcopyrite ore and inoculated using a mixed thermophilic culture. The bioleaching conditions used are based on best-practice procedures for chalcopyrite ores, detailed in literature and as used across the research group.

The mini-columns were X-ray µCT imaged in their entirety at the start and end of the experiment. In addition to this, the mini-columns were removed periodically from the flow to allow the scanning of three selected sections at 4 time points over the 165-day leaching period for pyrite and chalcopyrite and at 1 time point for malachite over the 26 day experimental period.

Table 3-7: Operating conditions of the mini-columns and feed solution characteristics (*Biotic leaching).

	Ore type	Feed	Agglomeration	pH	Temperature	Surfactant
1	Malachite	Acidified water	Yes	1.20	30 ºC	No
2	Waste rock	Fe^{3+} solution	Yes	1.15	37 ºC	No
3	Waste rock	Fe^{3+} solution	Yes	1.15	65 ºC	No
4	Waste rock	Fe^{3+} solution	Yes	1.15	65 ºC	Yes
5	Pinto Valley	Fe^{3+} & Fe^{2+} solution	Yes	1.15	37 ºC	No
6	Pinto Valley	Fe^{3+} & Fe^{2+} solution	Yes	1.15	65 ºC	No
7	Pinto Valley	Fe^{3+} & Fe^{2+} solution	No	1.15	65 ºC	No
8	Pinto Valley	Fe^{3+} & Fe^{2+} solution	Yes	1.15	65 ºC	Yes
9	Pinto Valley	Fe $^{2+}$ & nutrients*	Yes	1.15	65 ºC	No
10	Pinto Valley	Fe $^{2+}$ & nutrients*	Yes	1.15	65 ºC	No

3.9 X-ray µCT

3.9.1 Image acquisition

X-ray scans were performed using a Nikon HMX ST 225, Metris X-Tek, UK which permits resolutions of 3 to 70 µm, depending on the sample size. The mini-columns were scanned at X-SIGHT X-RAY Services in Cape Town by the candidate.

The X-ray µCT imaging system was configured to scan (i) the vials containing solution, (ii) the ore particles mounted in 30 mm diameter blocks prepared for the QEMSCAN analysis, (iii) the 10 mL syringes and (iv) the mini-columns packed with ore:

(i) The vials were positioned at a distance of 720 mm between energy source and sample. X-ray scans were performed at different energy doses (35, 90, 120 and 150 kV), flux (200-280 µA) and exposure times (1-2 hours), selected to represent the conditions required for copper sulphide mineral imaging (Hsieh, 2012).

(ii) The ore particles mounted in 30 mm diameter blocks were scanned at a voltage and current of 100 kV and 120 µA. The final pixel resolution of the images was 16.69 µm. The typical acquisition time for a single projection was 995 ms, resulting in a total scanning time of about 50 min for each sample. 2985 projections were recorded over a 180° rotation with a step size of 0.12. Scanning was done using a 0.75 mm copper filter and at distances of 83.03 mm (X-ray source to specimen) and 624.42 mm (specimen to detector).

(iii) Two of the inoculated 10 mL syringes were individually scanned with X-ray µCT on the 13th day of bioleaching for 60 min at 90 kV and 225 µA (based on the outcomes of the liquid culture experiments) using a 1 mm copper filter and at distances of 230.2 mm and 726.9 mm between X-ray source and specimen respectively. The syringe position was chosen based on the resolution required to enable differentiation of individual mineral grains (40 µm/voxel).

(iv) In the mini-column studies, the whole mini-columns were imaged at the start and end of the experiments in 5 separate sections from top (1) to bottom (5), because division into small parts permitted a smaller field of view (FOV) and thus a finer image resolution. Three regions of the mini-columns (top, middle and bottom) were scanned more regularly during the course of the leach. The imaging time points were chosen based on leaching rates observed in preliminary leaching experiments. All reasonable care was taken during handling. Each section was individually scanned with X-ray µCT for 50 min at 100 kV and 150 mA using a 0.38 mm copper filter (to reduce the effect of beam hardening and noise caused by low level energy) and at a distance of 59.40 mm between X-ray source and specimen. The scans collected 3000 projections at 0.12 angular increments on a 1900 × 1500 pixel detector. All scans were performed at the same resolution (voxels of approximately 13.40 µm × 13.40 µm × 13.40 µm).

3.9.2 Image analysis

The advanced 3D analysis software Avizo® 9 and ImageJ-Fiji (Schindelin et al., 2012) was used to visualize and analyse the image data by the candidate. An example of an original 3D X-ray µCT image for the 10 mL syringe with 50 pyrite coated beads is shown in Figure 3-6 (B). Filtered back projection reconstruction was performed to produce the 3D image using the Nikon proprietary software.

Figure 3-6: (A) a 10 mL syringe containing fifty 5 mm beads, (B) the original 3D X-ray µCT image.

Before reconstruction of the 2D projections, the centre of rotation of the image series was calculated using the software supplied by Nikon, thereby accounting for the rotation of the object not being exactly on the X-ray source axis. The projection centre of rotation needs to be precisely measured before an image reconstruction, otherwise flame-shaped artefacts will arise in the CT images which decreases the spatial resolution and makes feature recognition and analysis more difficult (Lin et al., 2018). Therefore, the 2D projection images need to be shifted and sheared correctly before applying the reconstruction algorithm. In the reconstruction software supplied by Nikon, two test slices are reconstructed and the sharpness of the reconstructed images are assessed to determine the centre of rotation (Lin et al., 2015). Figure 3-7 shows example slices for malachite and chalcopyrite ores with and without correction. As it can be seen, the quality of slices was improved clearly after applying the centre of rotation correction.

Details of the image analysis are developed in the subsequent results chapters.

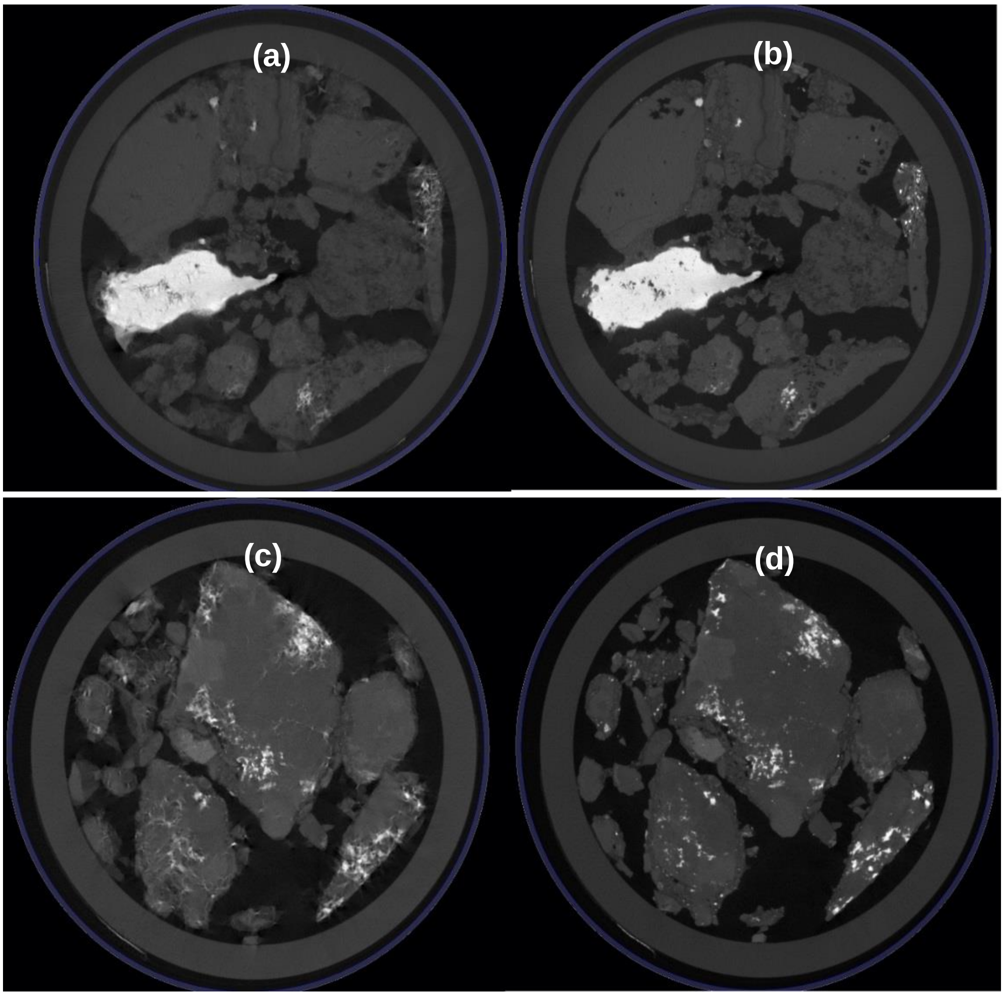

Figure 3-7: Examples of slices reconstructed with different centres of rotation for ores of malachite ((a) before and (b) after applying centre of rotation correction) and chalcopyrite ((c) before and (d) after applying centre of rotation correction).

4 Mineralogical analyses with 3D X-ray micro-Computed Tomography

The efficiency of leaching is dependent upon the whole mineral suite that makes up the ore. It is therefore important to be able to accurately identify and quantify all the metal-phases present in the ore and their mineral association. In this chapter, mineralogical analyses are used to develop accurate image processing methodologies to permit the use of X-ray µCT for the study of the selected ores. This was done using the chalcopyrite ore because it was the lowest grade and contained minerals with similar X-ray absorbance properties and hence had the greatest image analysis complexity.

Elemental deportment analysis and mineral association, chalcopyrite and pyrite grain size distribution are described based on QEMSCAN field images. Then, the method for mini-column design according chalcopyrite grain size distribution is explained. After that, mineralogical data is used to identify various minerals in the X-ray µCT image. Finally, a full series of image processing steps for selection of a suitable thresholding technique, measurement of sulphide mineral grain volume and quantification of their distribution in the ore is described.

4.1 Mineralogical characterisation

Prior to assessment of the X-ray CT images, an elemental deportment analysis and mineral association analysis was performed to anticipate the mineral differentiations that would need to be made during image processing.

An elemental deportment analysis involves the quantitative investigation of the relationship between one or more elements and the hosts, in which these elements occur in significant concentrations. These hosts generally consist of an array of minerals of which the proportions vary significantly from one rock type to another. The mineral composition and deportment of the low-grade chalcopyrite ore quantified using QEMSCAN is presented in Figure 4-1 and Figure 4-2. It was found that 95% of the copper was present as chalcopyrite. This confirmed it as a good ore for studying non-surface mineral grain leaching by X-ray CT, as it is not critical to differentiate different copper sulphide minerals in the X-ray CT scan images, a difficult task as they have similar X-ray absorbances.

Mineral association is also important because it has an influence on leaching performance by formation of some precipitates during leaching and galvanic interaction when two sulphide minerals are in contact with each other. It also affects the ease of image segmentation. Based on Figure 4-2, the chalcopyrite was mainly locked with quartz, clay minerals and K feldspar. Only 4.9% of chalcopyrite was liberated. The percentage of pyrite association with chalcopyrite was 7.43%. Of other sulphides, such as molybdenite, and sphalerite, 40.30% were associated with chalcopyrite.

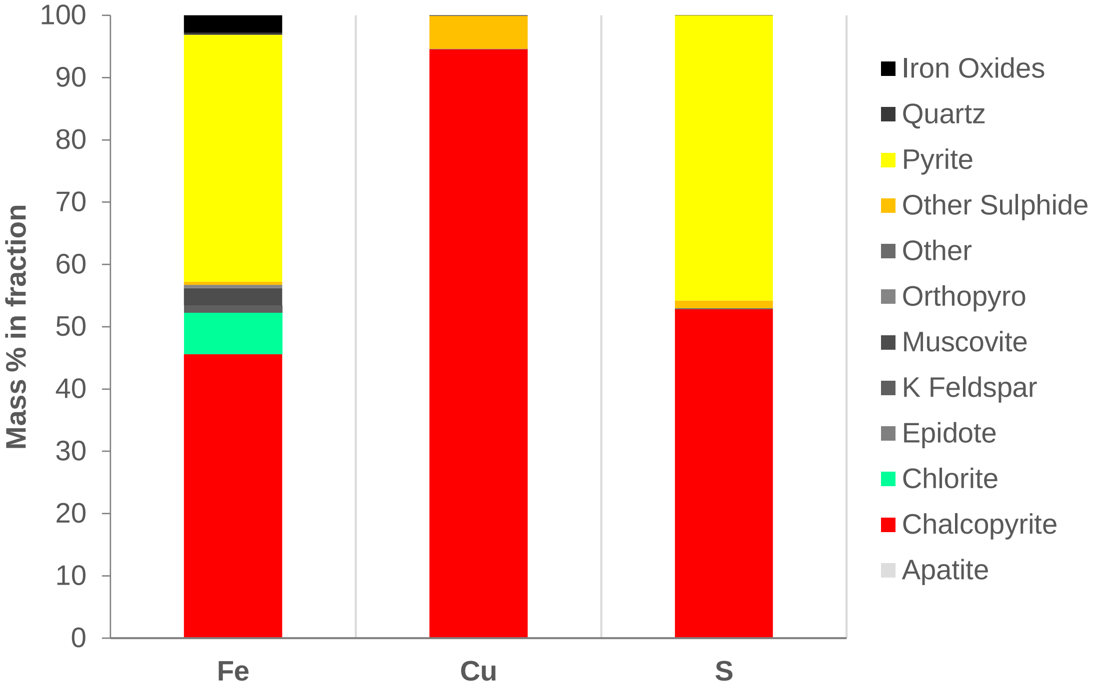

Figure 4-1: Iron, sulphur and copper deportment in the low-grade chalcopyrite ore.

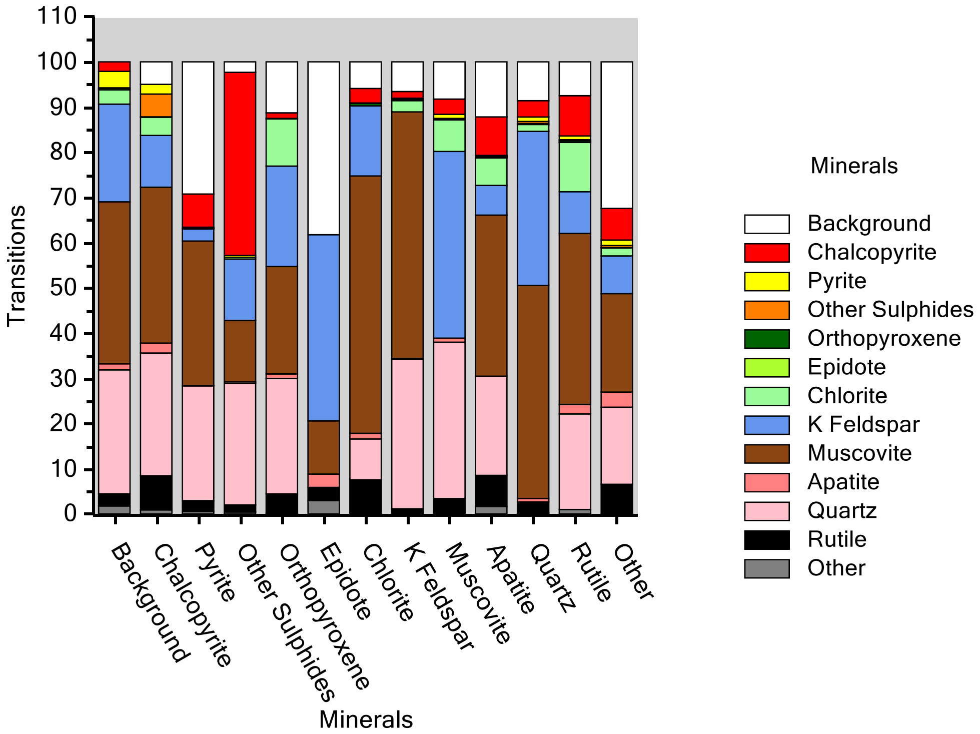

Figure 4-2: Mineral association in the low-grade chalcopyrite ore.

4.2 Leaching column design

For the leaching of mineral grains to be trackable, the image resolution needs to be chosen to match the smallest grain size. X-ray μCT resolution is determined by the sample size. Thus, the chalcopyrite and pyrite grain size distributions in the low-grade chalcopyrite ore were quantified using the QEMSCAN data. The leaching column diameter could then be designed to ensure that the sulphide mineral grains were detectable using X-ray μCT, given its resolution limitations.

The chalcopyrite grain size (Figure 4-3) was lower than pyrite grain size (Figure 4-4), and was therefore used to determine the column diameter. Approximately 91% of the chalcopyrite grains were larger than 40 μm. A 12 μm X-ray μCT resolution was therefore chosen to allow for the dissolution of all mineral grains larger than 40 μm to be quantitatively monitored while accounting for partial volume effects. The detector of the CT scanner used was 2048 pixels wide, which results in a maximum outer column diameter of 24.58 mm (Resolution [12 μm] × Pixels [2048]). The final constructed mini-column had a 24 mm outer diameter and a length of 150 mm, to accommodate sufficient ore to permit the tracking of a representative ore mass.

Copper wires or adhesive tape were affixed to the sides of the column to allow image registration for comparison of different image acquisitions.

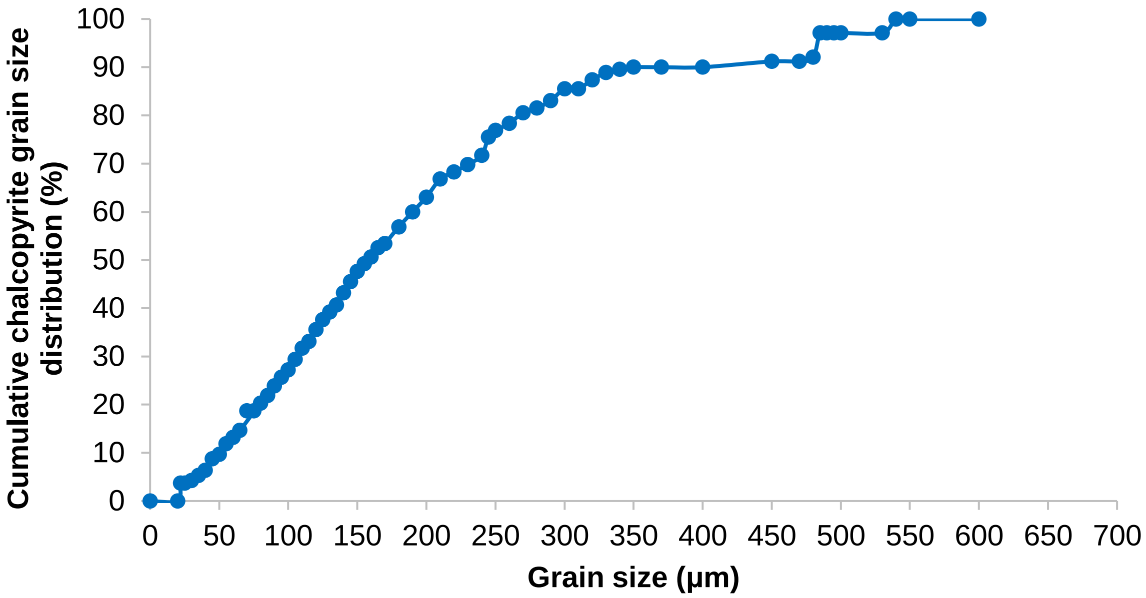

Figure 4-3: Cumulative chalcopyrite grain size distribution in the low-grade chalcopyrite ore.

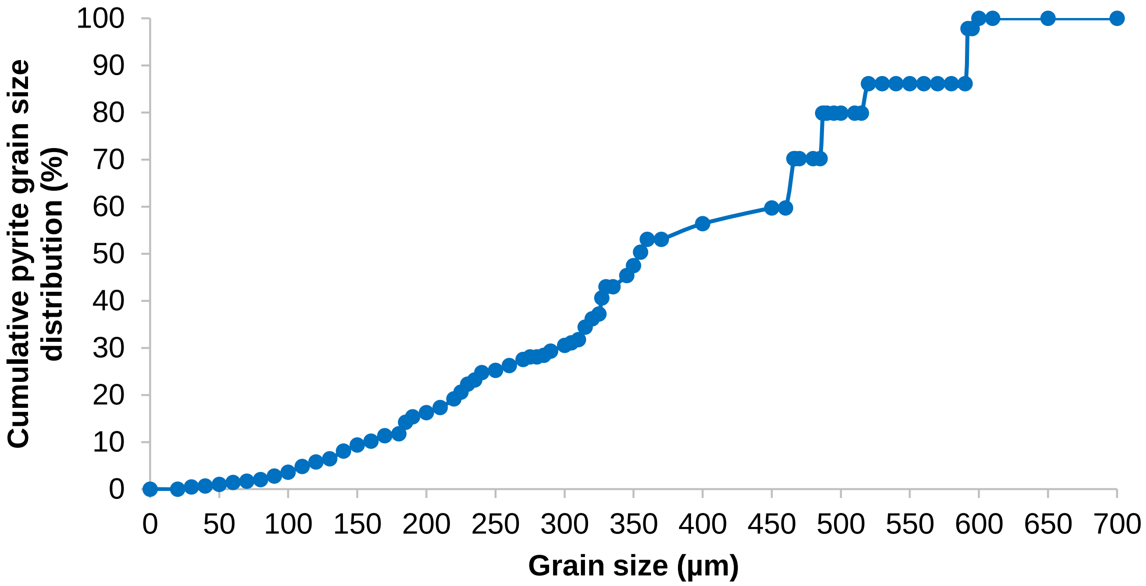

Figure 4-4: Cumulative pyrite grain size distribution in the low-grade chalcopyrite ore.

4.3 X-ray µCT analysis development

4.3.1 Mineral type identification

Tracking of the different minerals' volumes during leaching using X-ray µCT requires correct identification of the mineral grains in the images. Each mineral will have an attenuation coefficient (I) associated with it, determined by the bulk mineral density (ρ) and bulk atomic number (Z):

$$I = I_0 e^{-\int \mu(s)ds} \tag{4-1}$$

$$\mu = \rho\left(a + b\frac{Z^{3.8}}{E^{3.2}}\right) \tag{4-2}$$

where I_0 is the incident beam intensity, μ is the local linear attenuation coefficient along the ray path s, E is the X-ray energy, and a and b the energy-dependent coefficients.

A histogram for an acquisition of a volume of a mini-column is shown in Figure 4-5. There are distinct peaks in the histogram for the air and gangue minerals, which permits easy identification of these two phases. However, identification of the sulphide mineral pixels from the gangue and high-density minerals is difficult because the low number of sulphide mineral voxels in this low-grade ore results in no distinct peak. Therefore, alternative approaches to identification of the sulphide mineral volumes are required to enable measurement of volume reduction during leaching.

The QEMSCAN field image can be used to determine different mineral phases in the X-ray µCT acquisition. This is done through comparison of the QEMSCAN and X-ray µCT equivalent images of the mounted ore particles (Figure 4-8 a and c). Once corresponding voxels have been identified, the voxel intensity values for each different mineral phase in the X-ray µCT images can be determined. Table 4-1 gives the back-scattered electron (BSE) brightness for the QEMSCAN field image and the corresponding grey level for the X-ray µCT voxels for the different mineral phases.

A tiny amount of high density/atomic number minerals were identified in the scans (shown in red in Figure 4-6). These minerals are zircon or monazite based on the QEMSCAN data. The presence of these high density/atomic number minerals which do not leach were identified as being useful for registration of ore particle movement in the columns at different time points during leaching.

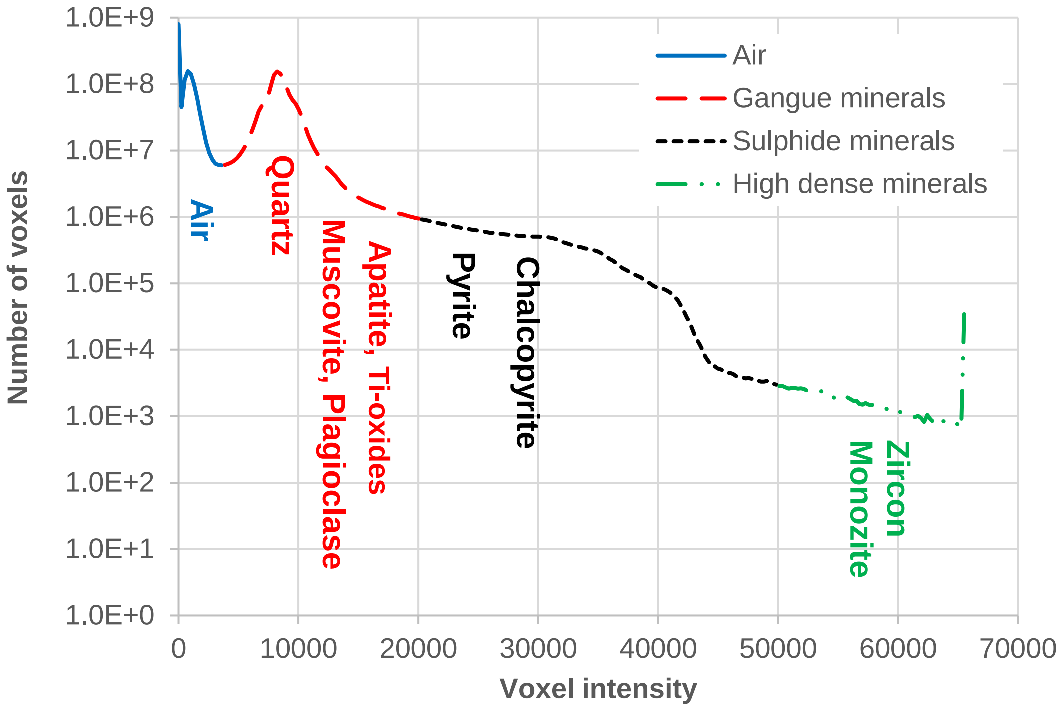

Figure 4-5: Histogram of a typical scanning volume with estimated thresholding values for ore, sulphide and high-density minerals.

Table 4-1: X-ray µCT grey level and QEMSCAN BSE brightness number for a 16-bit image of an ore column.

Phase	Grey level (X-ray)	BSE brightness number (QEMSCAN)
Air	0 – 3,500	Air = 0
Gangue minerals	3,500 – 20,000	Quartz = 10,496 Muscovite, Plagioclase = 12,544 Apatite = 14,592 Ti-oxide = 16,896
Sulphide minerals	20,000 – 50,000	Pyrite = 23,040 Chalcopyrite = 27,392
High density minerals	50,000 – 65,535	Zircon/monazite = 42,250

A 2D top view of the mini-column and a QEMSCAN field image are shown in Figure 4-6. In the X-ray µCT image, different minerals have been assigned a false colour to facilitate their distinction.

Differentiation of the sulphide minerals from each other was still found not to be possible because of the closeness of their densities. Thus, image analysis is limited to the identification of “sulphide mineral” as a group only.

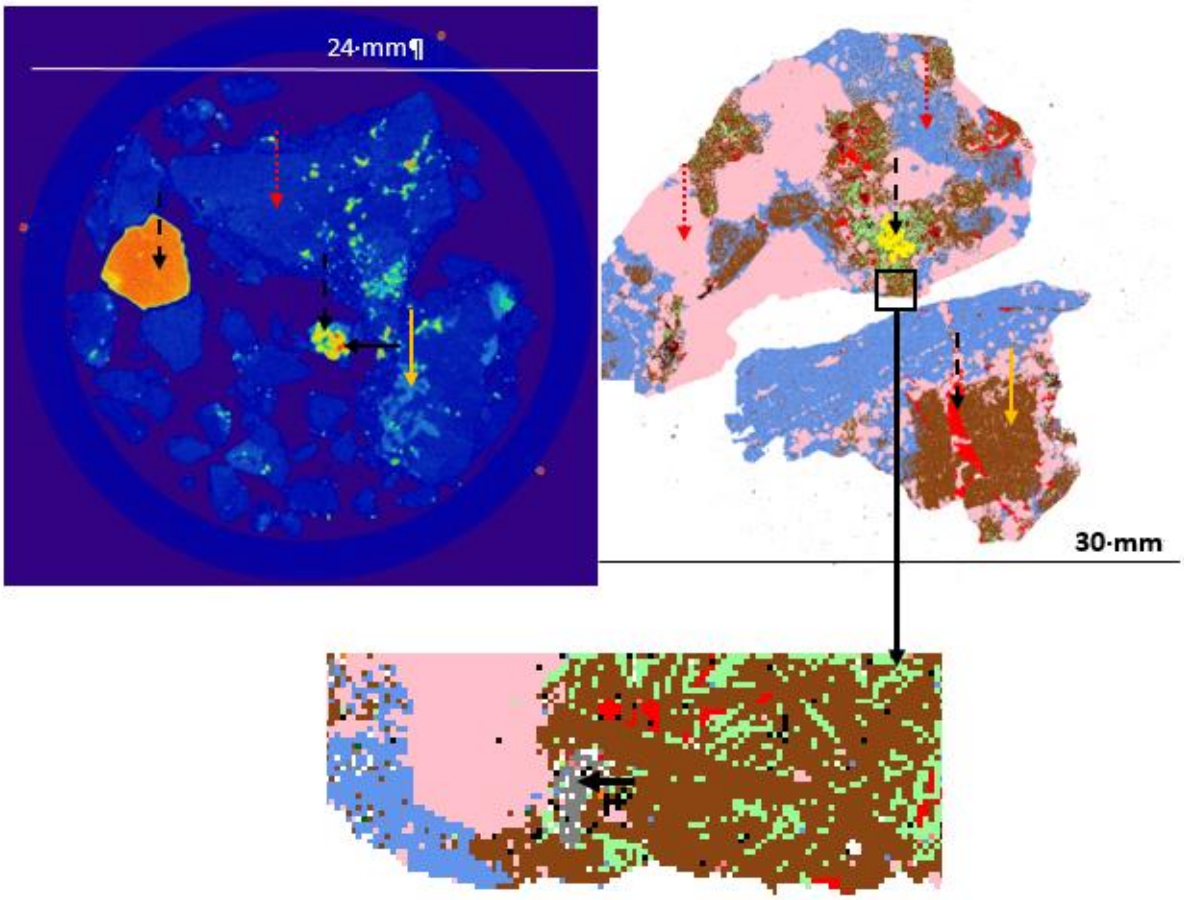

Figure 4-6: Determination of different mineral phases in an X-ray µCT image using QEMSCAN data. Gangue minerals such as quartz are dark blue (red dotted arrow). The muscovite and K-feldspar are light blue (orange solid arrow). Sulphide minerals containing chalcopyrite and pyrite are in orange (black dashed arrow), and high density/atomic number minerals including zircon or monazite are shown in red (black solid arrow).

4.3.2 Sulphide mineral grain segmentation

The establishment of X-ray µCT as a rapid, standalone and automated mineralogical analysis is challenging. It has been found that additional information using other techniques including QEMSCAN, XRF and SEM-EDS are required to effectively segment between different mineral phases in a X-ray µCT dataset (Istiadi Guntoro et al., 2019). Example side and top views and a volume-rendered 3D view of a packed mini-column reconstructed data set are shown in Figure 4-7. The sulphide mineral grains are represented by the brighter voxels, as they have high X-ray attenuation, attributed to their relatively high densities and atomic numbers. By tracking these voxels and converting this to the volume of sulphide mineral present at a given point in time, the X-ray images can be used as a measure of leaching extent.

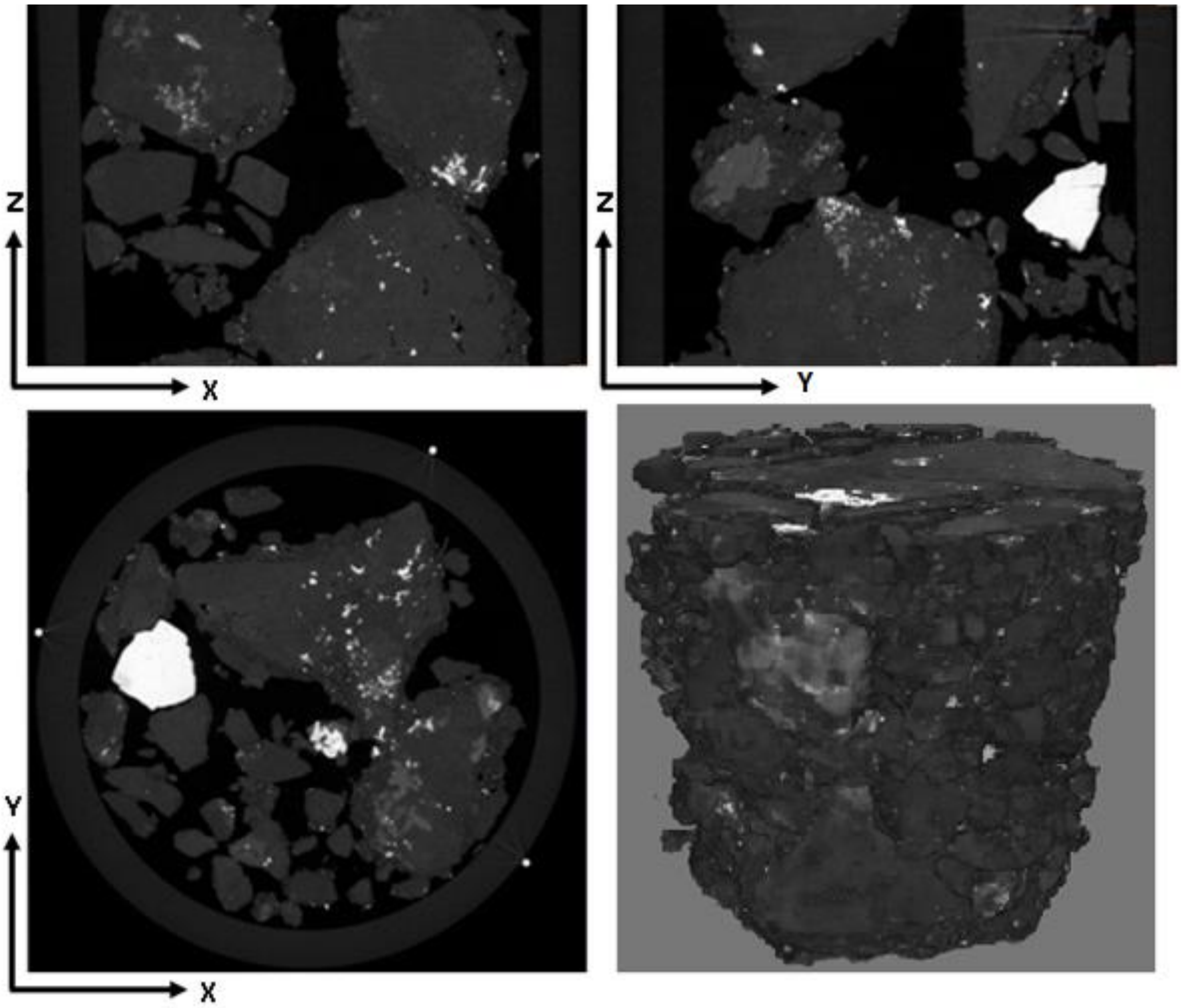

Figure 4-7: Example X-ray µCT side and top views and a volume-rendered 3D view of a mini-column packed with the low-grade chalcopyrite ore.

Segmentation involves assigning labels to image voxels to identify and separate objects in a 3D image. It is one of the most critical steps in the process of reducing images to more useful information. In mineral processing, segmentation allows the different minerals to be distinguished and for solid ore to be distinguished from any gaseous and/or liquid phases present. Accurate and quantitative processing requires segmentation which clearly identifies the minerals boundaries. However, correct or unique thresholds cannot be easily or accurately determined if edges are blurred by noise or partial volume effects. Global and local thresholding techniques and feature based classification are used to overcome this.

The suitability of different segmentation options for the thresholding of the sulphide mineral grains were evaluated by comparing the X-ray results to the equivalent QEMSCAN field image. Example resulting 2D slices are presented in Figure 4-8. Table 4-2 gives a measure of the accuracy of the different methods by comparing the total sulphide mineral area (and equivalent number of voxels) to the QEMSCAN field image.

The 3D watershed segmentation process is a local thresholding algorithm commonly used for multiphase mineral particles. However, it is appropriate for mineral grains with a scale parameter greater than 30 (mineral grain size/voxel size) and a density lower than 4000 kg/m^3 (Wang et al., 2015). The watershed segmentation's strong gradient sensitivity leads to over-segmentation of bright mineral grains, while it cannot pick small mineral grains (Lin et al., 2016c; Wang et al., 2015). Based on the resolution of the X-ray image (13.4 µm), the mineral grain size should be higher than 400 µm to segment accurately using watershed segmentation. But, as can be seen in Figure 4-3 and Figure 4-4, more than 60% of pyrite and 90% of chalcopyrite grains size are smaller than 400 µm, as is typical for low-grade sulphide ores. Furthermore, the sulphide mineral's density is larger than 4000 kg/m^3. Thus, the watershed segmentation method is not satisfactory to obtain accurate mineralogical data for the ores in this study and was not applied.

Trainable Weka Segmentation (TWS) or feature-based segmentation (Arganda-Carreras et al., 2014), which combines a collection of machine learning algorithms with a set of selected image features to produce pixel-based segmentations, is suggested for segmentation of fine or high density/high atomic number mineral grains (Wang et al., 2015). It can be used to correct partial volume effects in images. A good agreement between the TWS result (Figure 4-8 (d)) and the QEMSCAN image was achieved (error of 2.62%). However, the watershed segmentation and TWS methods are very computing memory intensive and hence time consuming for large image dataset quantitative evaluation and requiring of high-speed computing.

Lin et al. (2016c) used algorithms based on the measurement of the maximum entropy of the sulphide mineral grain phase segmentation. The Maximum Entropy algorithm is similar to the Otsu Thresholding technique. However, rather than maximizing the inter-class variance, the inter-class entropy is maximized (Kapur et al., 1985). But, the accuracy of this method depends on the ore mineralogy. In the current study, this method led to a number of gangue minerals with high intensity being identified as sulphide mineral as well as causing over-segmentation (Figure 4-8 (e)). As a result, a high error of 21.32% was found.

The Avizo® 9 Interactive Thresholding function which is based on Intensity Range Partitioning was tested for the segmentation of the sulphide and high dense/atomic number mineral grains (Figure 4-8 (f)). It resulted in accurate mineral grain phase segmentation (error of 3.3%) in comparison with the QEMSCAN results (Figure 4-8 (b)). It was additionally less computing memory intensive and hence faster than local thresholding methods and Trainable Weka Segmentation. It was therefore found to be the best segmentation method for use with this ore.

Labelling of each sulphide mineral grain was done after thresholding to extract statistical and numerical information, thus allowing the progression of leaching to be followed. Figure 4-9 shows 2D and 3D views of the thresholded and labelled images.

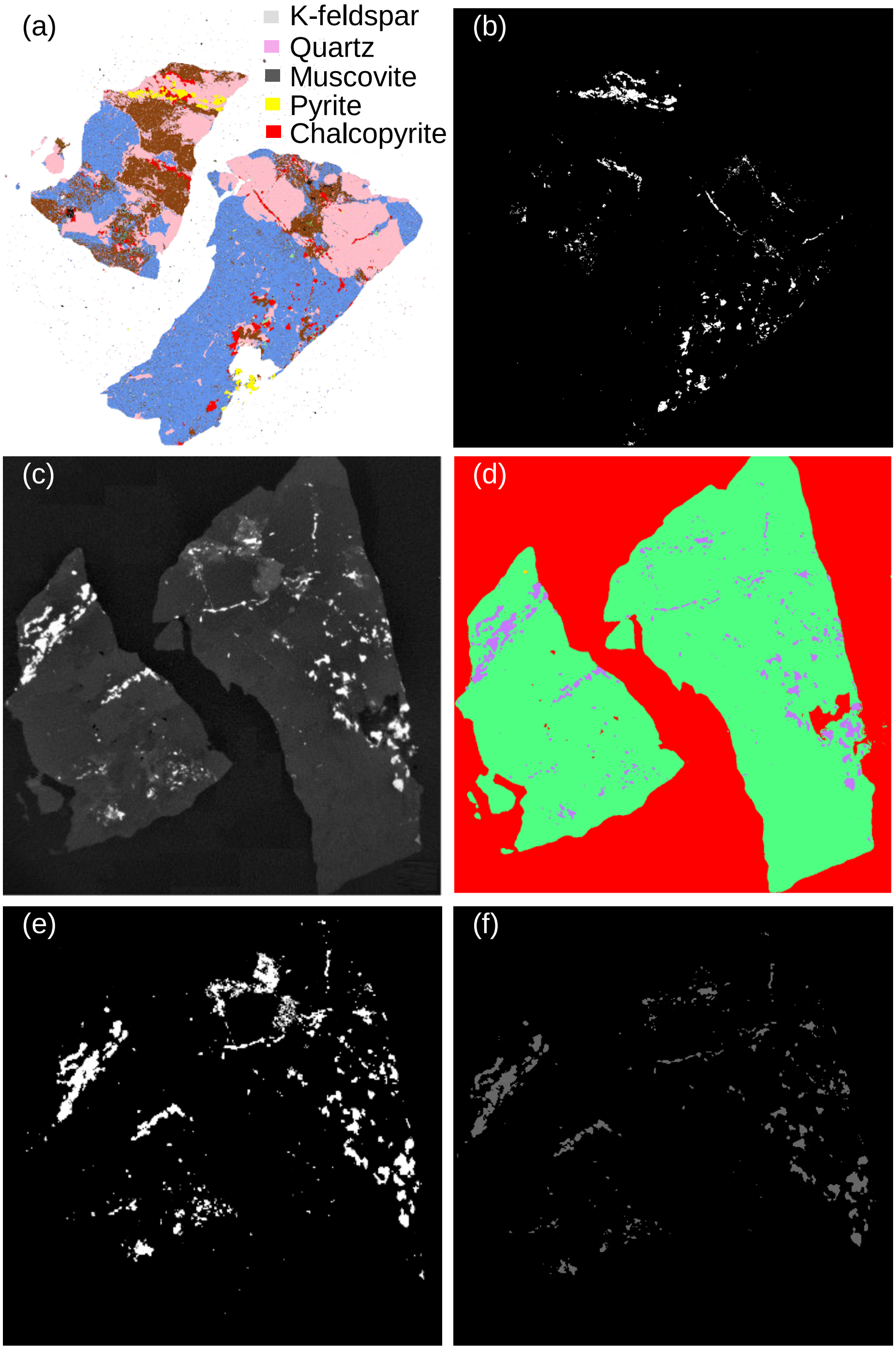

Figure 4-8: Comparison of different segmentation methods to threshold metal sulphide grains. (a) is a reference QEMSCAN image and (b) is the QEMSCAN image with the metal sulphide grains identified. (c) is the original X-ray µCT image which is then segmented using (d) TWS, (e) Max Entropy and (f) Interactive Thresholding modules.

Table 4-2: The total sulphide mineral area, number of voxels and error compared to the QEMSCAN field image calculated for the different thresholding techniques.

Thresholding technique	Area (µm^2)	Number of pixels	Error (%)
QEMSCAN	10,490,424	49895	-
Weka segmentation	10,764,534	38,598	2.62
Max entropy	12,727,447	45,636	21.32
Interactive thresholding	10,839,488	38,867	3.30

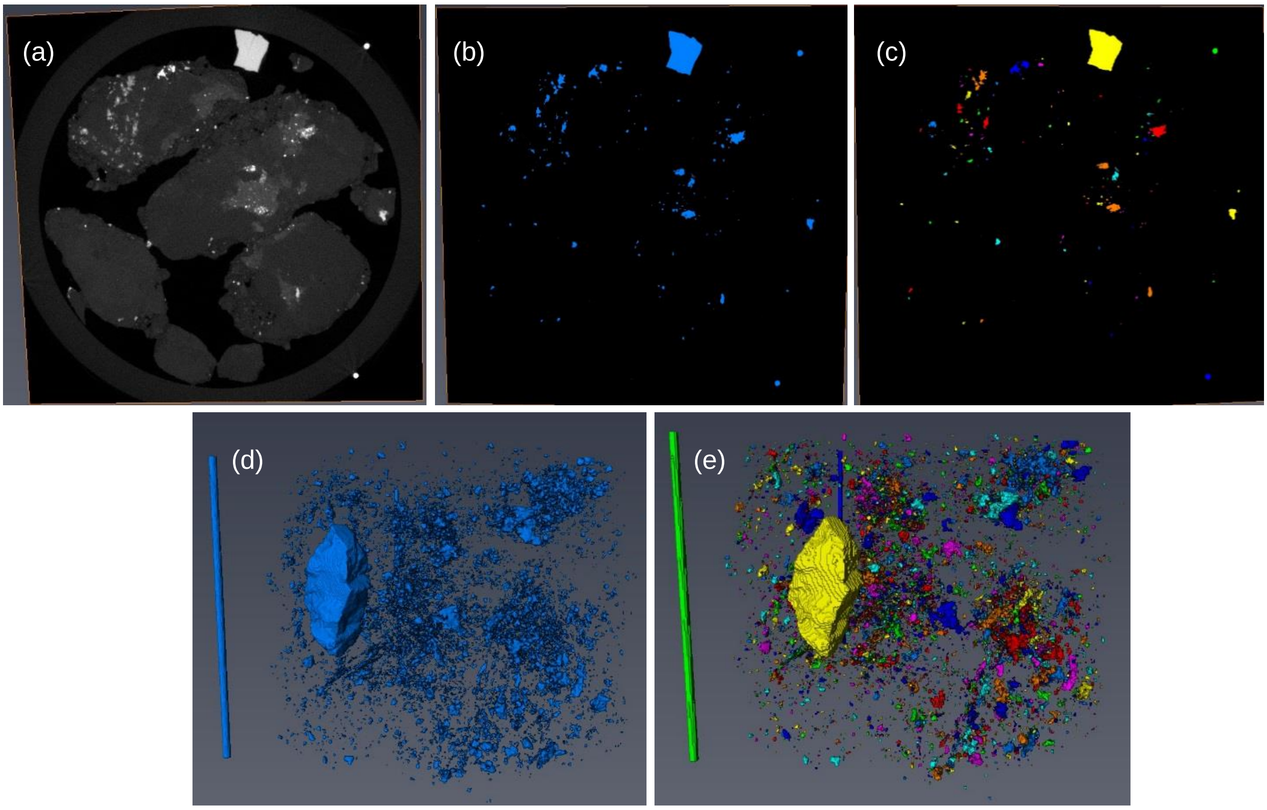

Figure 4-9: 2D (a-c) and 3D (d-e) views of thresholded and labelled images of sulphide mineral grains. An original X-ray grey level image is shown in (a). The sulphide mineral grains have been segmented in (b) and (d). Images (c) and (e) demonstrate labelling of the individual mineral grains.

4.3.3 Sulphide mineral grain distance from the ore surface

A mineral grain distance map analysis is proposed as a tool to understand positional dependence of leach performance. The procedure applied in this study to quantify the distance of the mineral grains from the ore particle surface is shown in Figure 4-10.

The Interactive Thresholding module is applied to create a binary image with the packed ore as foreground and air as background (Figure 4-10 (c)). The distance map algorithm on a binary image gives a grey level image where each voxel intensity represents the minimum distance in voxels from the object boundary. Low level intensity means that the voxel is close to the object surface while high level intensity means that part of the object is far from the object surface. The Chamfer Distance Map module was applied to the thresholded binary image (Figure 4-10 (c)) to create the distance map image. Another Interactive Thresholding module is used to separate sulphide minerals from the gangue minerals and air (Figure 4-10 (e)). Then, the distance map image is masked with this second thresholded image (Figure 4-10 (e)). This gives a grey image where each non-null intensity represents a voxel of the sulphide mineral grains and the intensity value is equal to the distance in voxels from the ore surface (Figure 4-10 (f)). The sulphide mineral grain distance from the ore surface can be quantitatively calculated using the “Multiply By Value” module on the masked image, an example result of which is presented in Figure 4-11. The accuracy of the distance values is affected by the position of the mineral grain edges relative to the voxel boundaries. This is demonstrated in Figure 4-12. An uncertainty interval of three times the voxel size results (±13.4×3 = ±40.2 μm).

The generated maps were used to extract a descriptor for the leaching solution penetration from ore surface into particles to leach target mineral grains. The maximum linear distance from the nearest ore surface (interface with air/solution) at which a change in mineral grain content is measured is termed the leaching penetration distance. This descriptor can be tracked with time. Note that separation of ore particles is not included as part of the analysis. Thus, agglomerated particles can be considered as a single solid phase, should no clear interface with air or solution be evident between the particles.

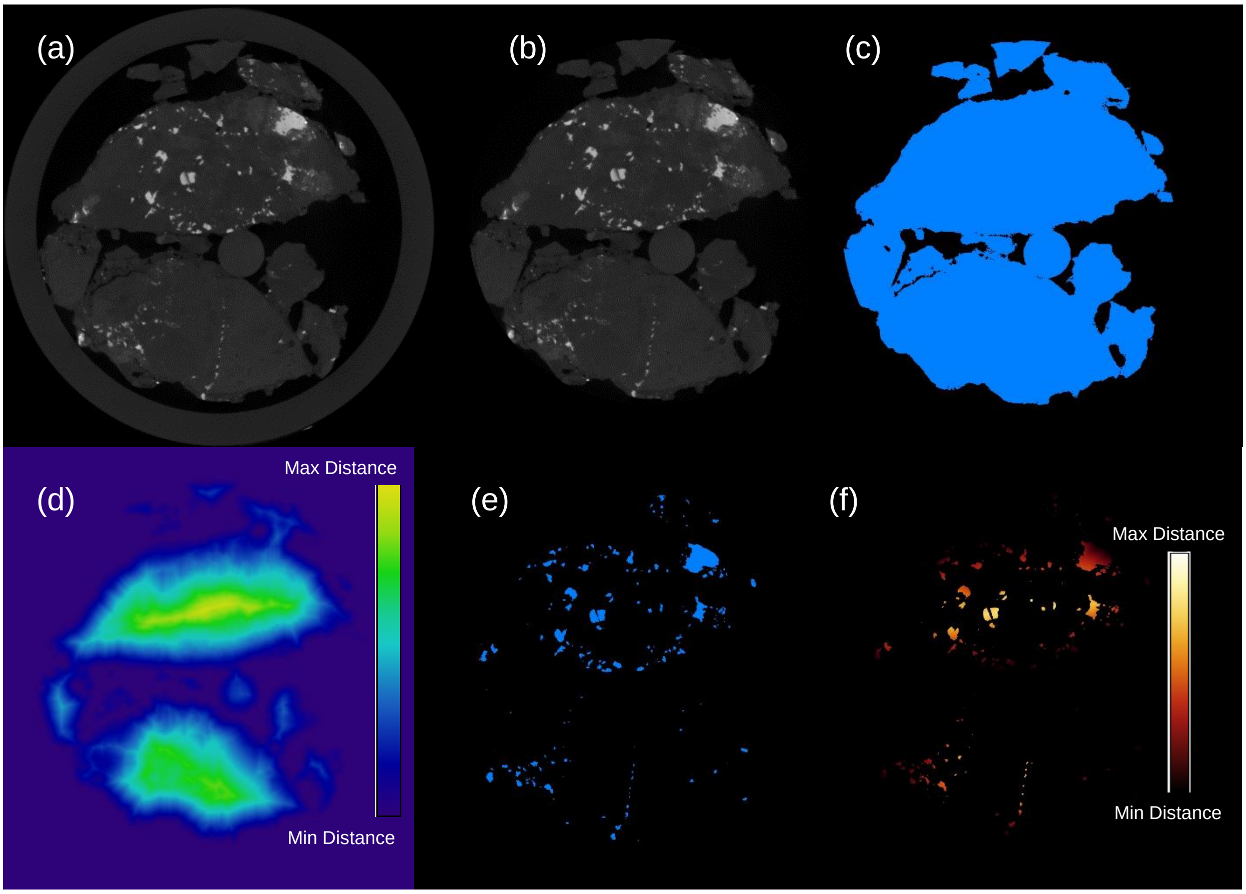

Figure 4-10: The procedure for calculation of mineral grain distance from the ore surface. The (a) original image has (b) the column wall removed. The (c) solid ore is thresholded from the background and the (d) distance of each voxel from the ore surface is found. The (e) sulphide mineral grains are thresholded from (b) and mapped onto (d) to produce (f) which finally gives the distance of the mineral from the ore surface.

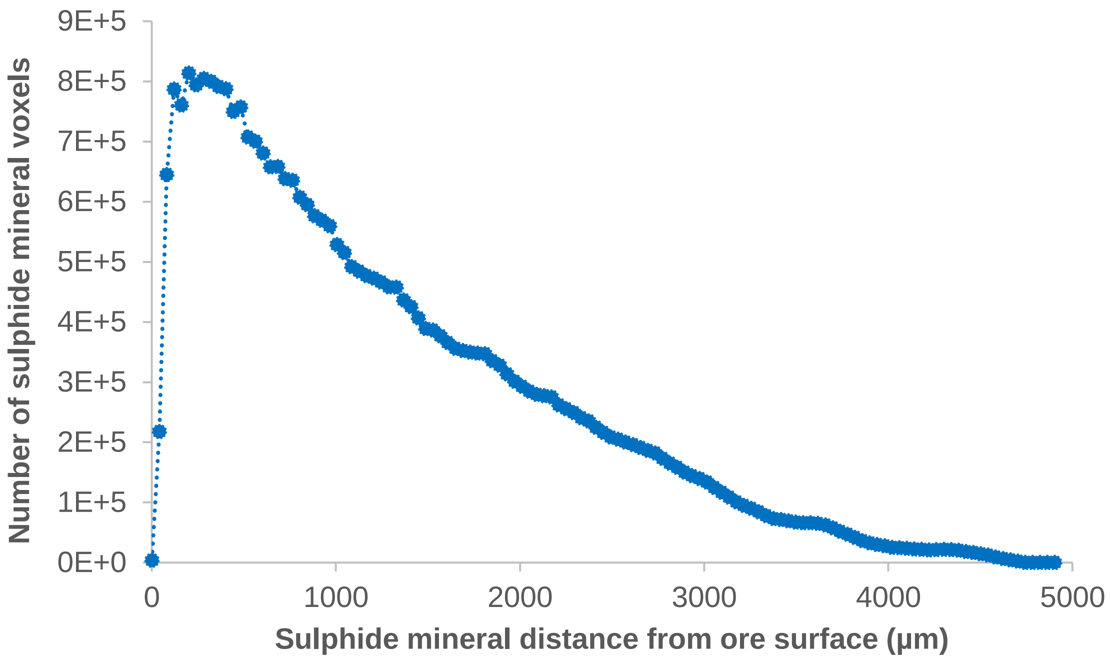

Figure 4-11: Example sulphide mineral grain positional distribution. The uncertainty for the measurement of the grain distance from the ore surface is ±40.2 μm.

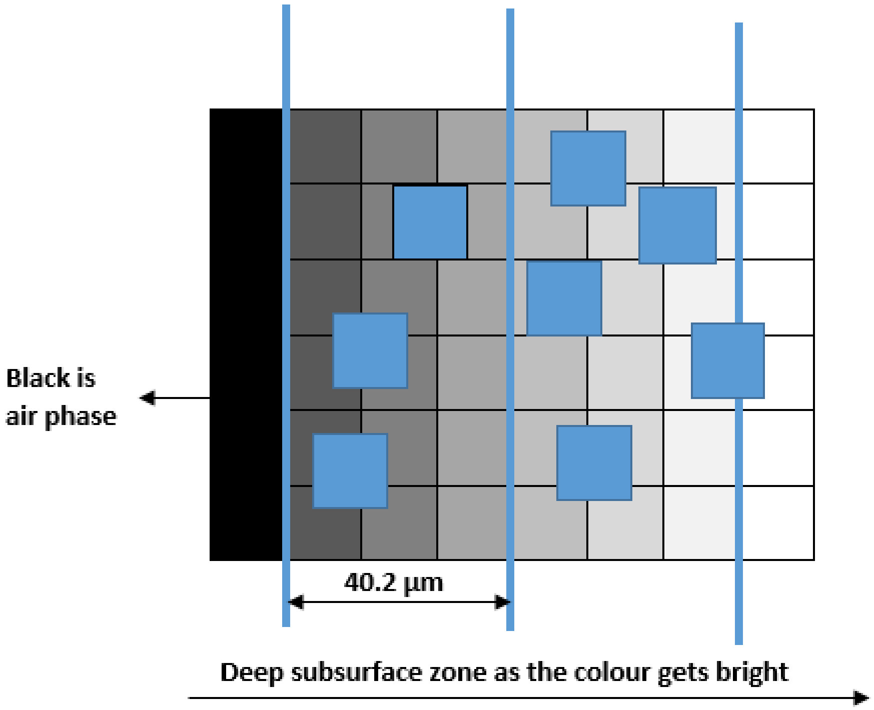

Figure 4-12: Schematic of the confidence in the measurement of sulphide mineral grain distance from the ore surface based on a voxel resolution of 13.4 μm. Grey level pixels are the ore distance map, where a lighter colour indicates a larger distance from the air (black). Blue indicates the sulphide mineral grains.

4.4 Pore volume and distribution

In order to determine pore volume and distribution, the Interactive Thresholding module is applied to create a binary image with the packed ore as foreground and air as background. The “Fill Hole” module was then applied to fill the holes (pores) in the thresholded image. Subtraction of filled image from thresholded image gives an output which is the pore volume of the ores. The pore volume and distribution were calculated using the aforementioned methods for measurement of sulphide mineral grain volume and distribution in the ore.

4.5 Uncertainty in measurement

Counting statistics can introduce uncertainties in the measurement of leaching performance of the system. Ore variability, partial volume effects, grain size and grain position in the ore particles, can all cause uncertainty in leaching extent measurement.

Standard deviation can be used as a descriptor of the measurement uncertainty at different confidence levels. Equations (4.3) to (4.6) present the method used to calculate the uncertainty at the 95.5% confidence level.

$$\overline{V_n(t)} = \frac{1}{N}\sum_{n=1}^{N} V_n(t) \tag{4-3}$$

$$s(V_n(t)) = \sqrt{\left(\frac{1}{N-1}\right)\sum_{n=1}^{N}\left(V_n(t) - \overline{V_n(t)}\right)^2} \tag{4-4}$$

$$s\left(\overline{V_n(t)}\right) = \frac{s(V_n(t))}{\overline{V_n(t)}} \tag{4-5}$$

$$\text{At the 95.5\% confidence level} = 2s\left(\overline{V_n(t)}\right) \tag{4-6}$$

where t is time, N is total number of grains, $\overline{V_n(t)}$ is the volume mean, $s(V_n(t))$ is the standard deviation, and $s\left(\overline{V_n(t)}\right)$ is the standard deviation of the mean.

The uncertainty measurement for a leaching system is a strong function of the grain size (Lin et al., 2015). Therefore, uncertainty calculations are only applicable for narrow size intervals. The standard deviation for different grain sizes, identified using the chosen segmentation method described in Section 4.3.2, was calculated and plotted against the grain volume for the chalcopyrite, pyrite, and malachite ore. These are presented in Figure 4-13, Figure 4-14, and Figure 4-15. The fitted curves can be used to estimate the standard deviation for the overall grain size distribution for the three different ores.

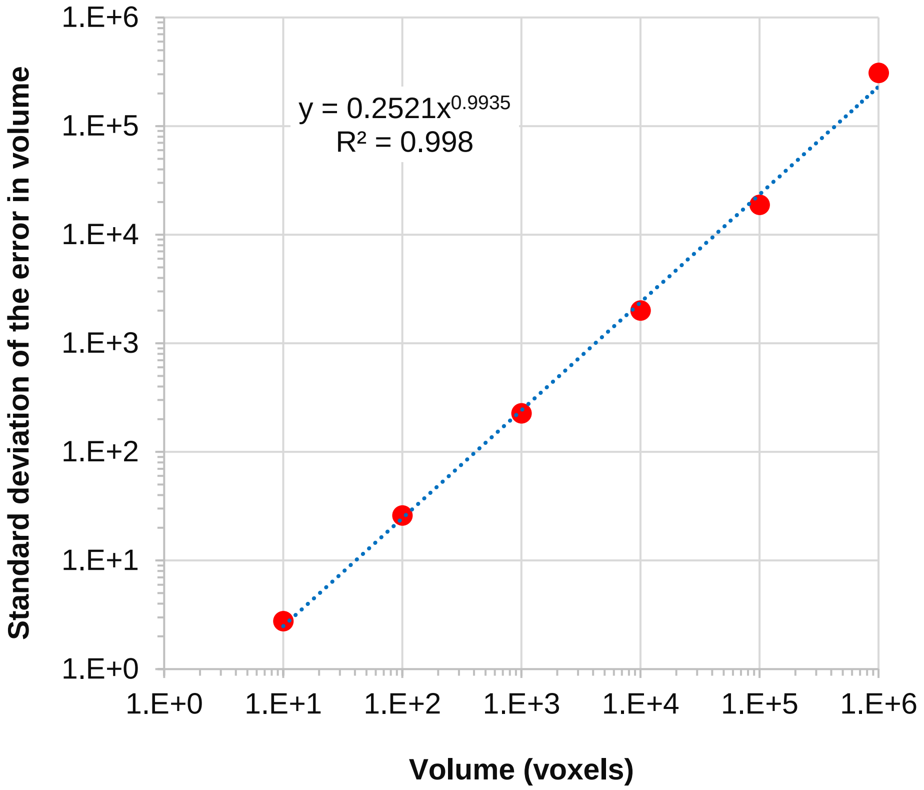

Figure 4-13: The plot of standard deviation of the error in volume for low-grade chalcopyrite.

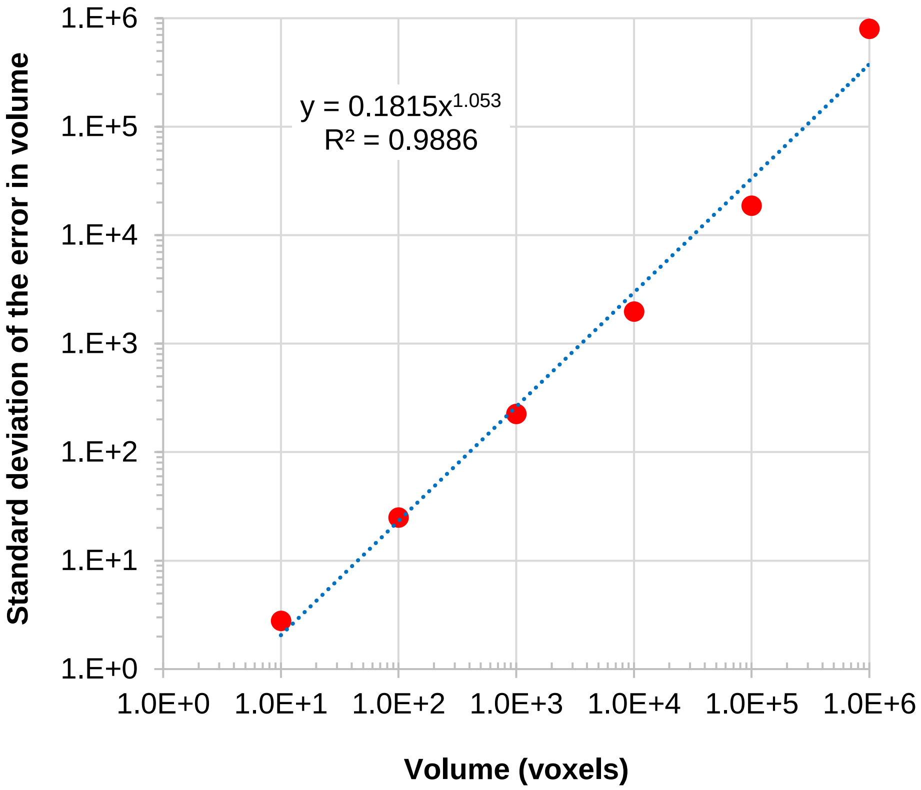

Figure 4-14: The plot of standard deviation of the error in volume for pyrite.

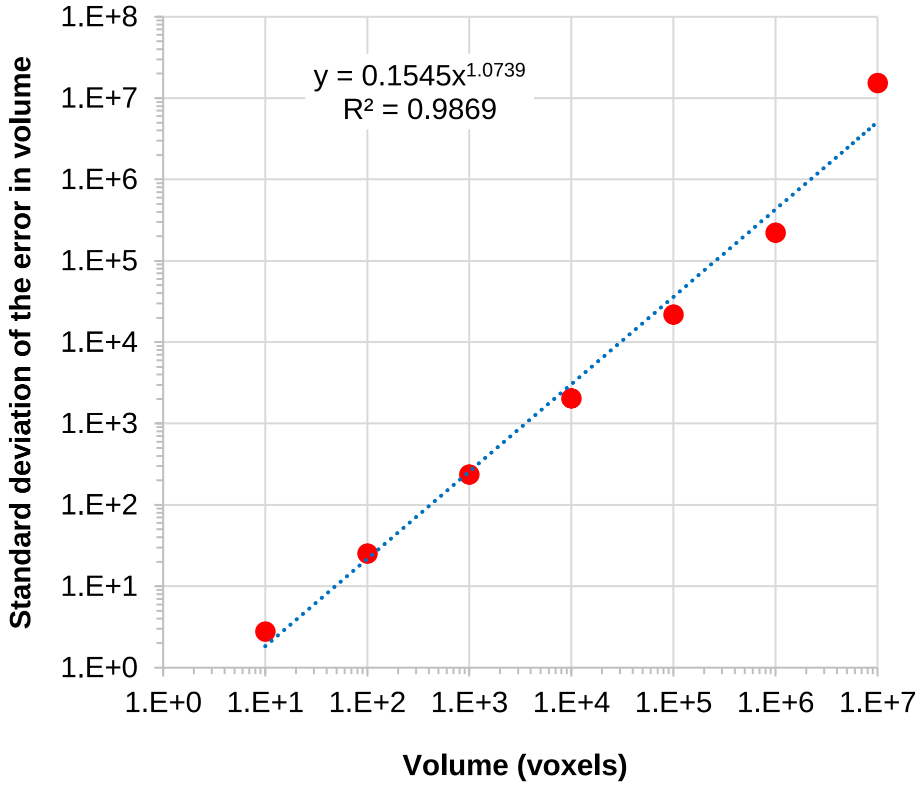

Figure 4-15: The plot of standard deviation of the error in volume for malachite.

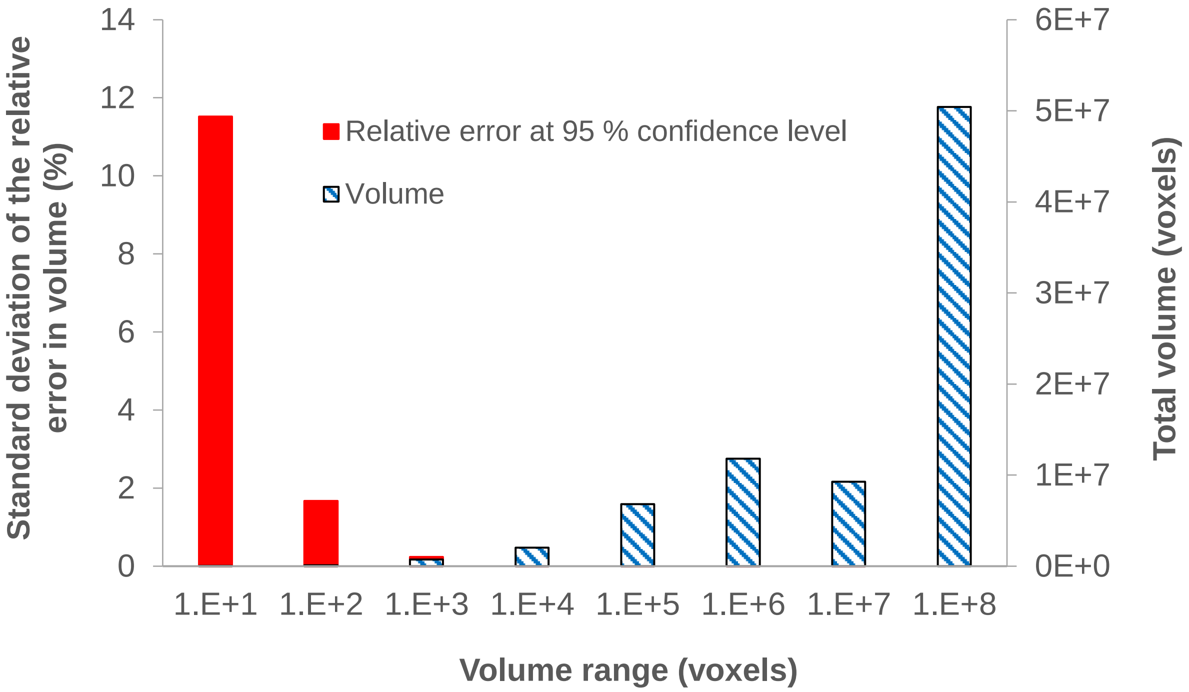

Figure 4-16: Standard deviation in the volume measurement and total volume for the different size ranges of sulphide mineral grains.

An example of the volume of sulphide minerals and standard deviation of the relative error at different mineral grain size ranges is shown in Figure 4-16. The standard deviation in the volume measurement for mineral grains with a volume greater than 1000 voxels (2406000 μm^3) was negligible. The standard deviation was higher for the smaller grains (< 1000 voxels) and was highest at 11.5% for the 0-10 voxel volume range (0-24060 μm^3). Each voxel volume was about 2406 μm^3. However, the small mineral grains only account for a tiny amount of the total sulphide mineral volume. The higher standard deviation values were therefore not considered to be an issue.

5 Feasibility of studying biotic heap leaching by X-ray µCT

The effect of X-ray exposure on microbial activity was examined in a series of experiments. Firstly, the mixed thermophilic microorganisms in their standard growth medium were cultivated in 50 mL glass vials and exposed to X-ray. The CT scanner operating conditions were changed to monitor effect of energy dose (35-150 kV), current and exposure time on microbial activity and growth. The same experiments were carried out on coated pyrite beads. Isothermal microcalorimetry (IMC), scanning electron microscopy and PLS redox potential were used to measure the metabolic activity of mineral associated cells (using heat flow from the biological system as a proxy) after the CT scan imaging. Finally, two mini-columns were run to investigate biotic leaching of copper from low-grade chalcopyrite ore using mixed thermophilic microorganisms.

5.1 Evaluation of the impact of X-ray µCT of different energies on microbial activity

The effect of X-ray µCT exposure on microbial activity in liquid culture and on an ore surface was assessed through the comparison of (i) PLS chemistry, (ii) metabolic heat generation, and (iii) microbial colonisation visualised microscopically.

5.1.1 Effect of X-ray exposure on liquid culture biooxidation

The mixed thermophilic microorganisms were cultivated in 50 mL glass vials containing 10 mL of the ferrous supplemented (5 g L^{-1} Fe^{2+}) Norris basal medium at 60 °C, agitated at 180 rpm in an orbital shaker. Figure 5-1 shows the influence of X-ray exposure on the increase in redox potential by ferrous grown liquid cultures of thermophilic bioleaching microorganisms, following exposure to imaging energies in the range of 35-150 kV for exposure times of 1-2 h. The increase in redox potential was similar for the sample exposed to X-ray and the unexposed control for doses of 35 and 90 kV for 1 hour and 90 kV for 2 hours, suggesting that the microbes' iron oxidising abilities were not affected by exposure to X-ray. However, for samples exposed to X-ray doses of 120 or 150 kV for 1 hour, the redox potential reached its maximum value one day later than the control, illustrating an inhibitory or stress effect on the microorganisms. The higher redox potential on days 3 to 5 means that the microorganisms were active and efficient in converting the ferrous ion to ferric ion and is supported by the ferrous ion concentration data in Figure 5-2.

The effect of X-ray exposure on planktonic cell growth is presented in Figure 5-3. For X-ray exposures of 90 kV or less, negligible difference in cell growth relative to the control was observed while a metabolic energy source was available, demonstrated by increasing redox potential (Figure 5-1). Exposure to 120 or 150 kV X-rays for 1 h, however, influenced the microbial growth rate compared to the control. The same maximum cell concentration was reached, as this is determined by the available nutrients and energy source. In all tests, decreased cell concentrations result in depletion of the ferrous ion metabolic energy source, as expected.

Table 5-1 compares the specific growth rate and the yield of biomass based on the ferrous ion substrate of the unexposed control to the experiments at the various X-ray exposure conditions. The yields and specific growth rates under all conditions except 120 and 150 kV were similar, lying between 1.27×10^8 to 1.35×10^8 cells g^{-1} Fe^{2+} and 0.0133 to 0.0136 h^{-1} respectively. X-ray exposure at 120 or 150 kV resulted in the reduction of both variables, to 1.17×10^8 and 1.01×10^8 cell g^{-1} Fe^{2+}, and 0.0120 and 0.0092 h^{-1} respectively.

In the liquid culture experiments, the results confirm that the microorganisms were active and viable, demonstrating cell division, after exposure to X-ray for all X-ray energy exposures tested. No detrimental effect was observed when voltages of 90 kV or less were used, thus recommending these conditions in further experiments.

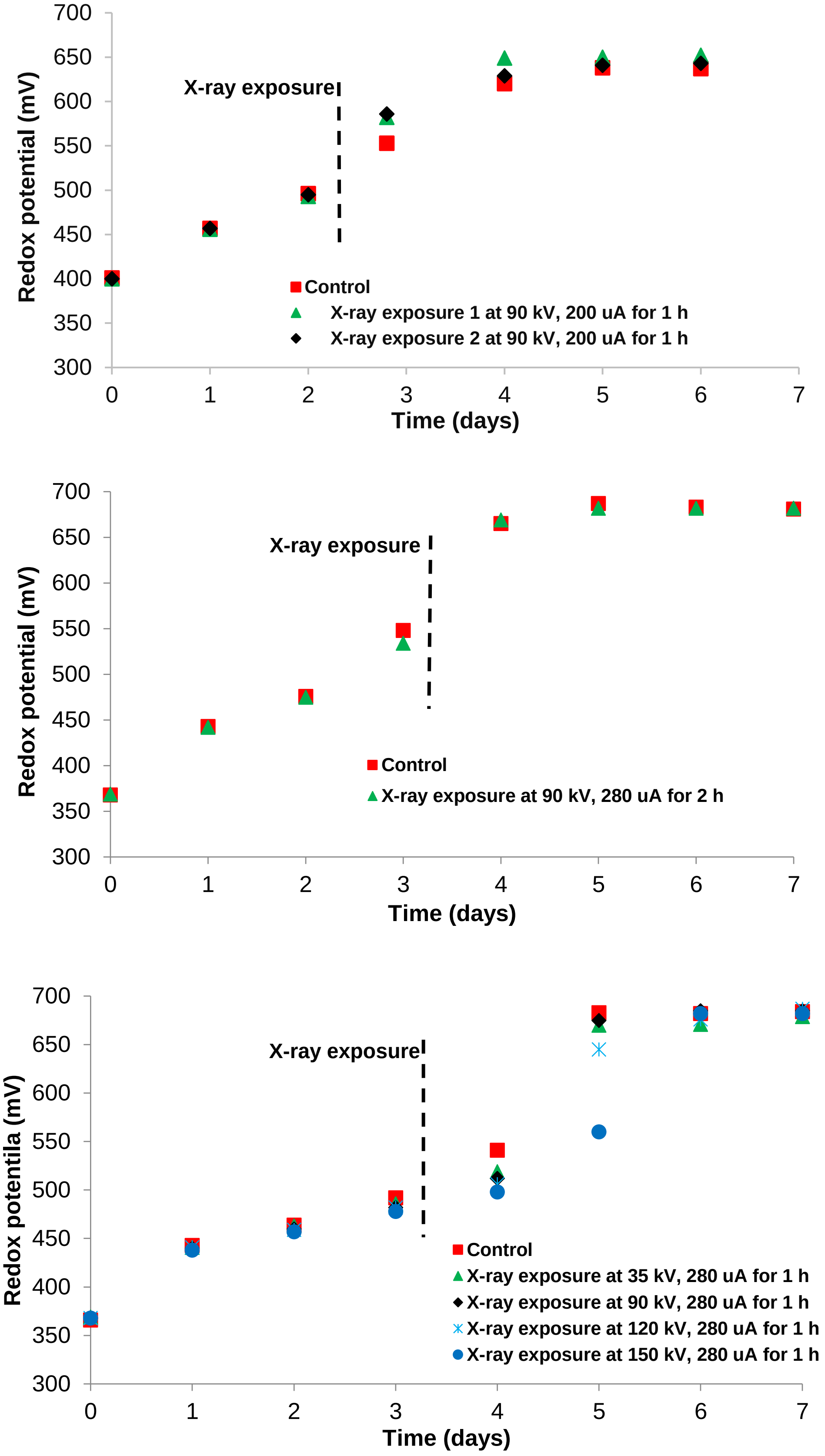

Figure 5-1: Effect of X-ray irradiation on redox potential measurements of vials inoculated with thermophilic bioleaching microorganisms grown on ferrous ion.

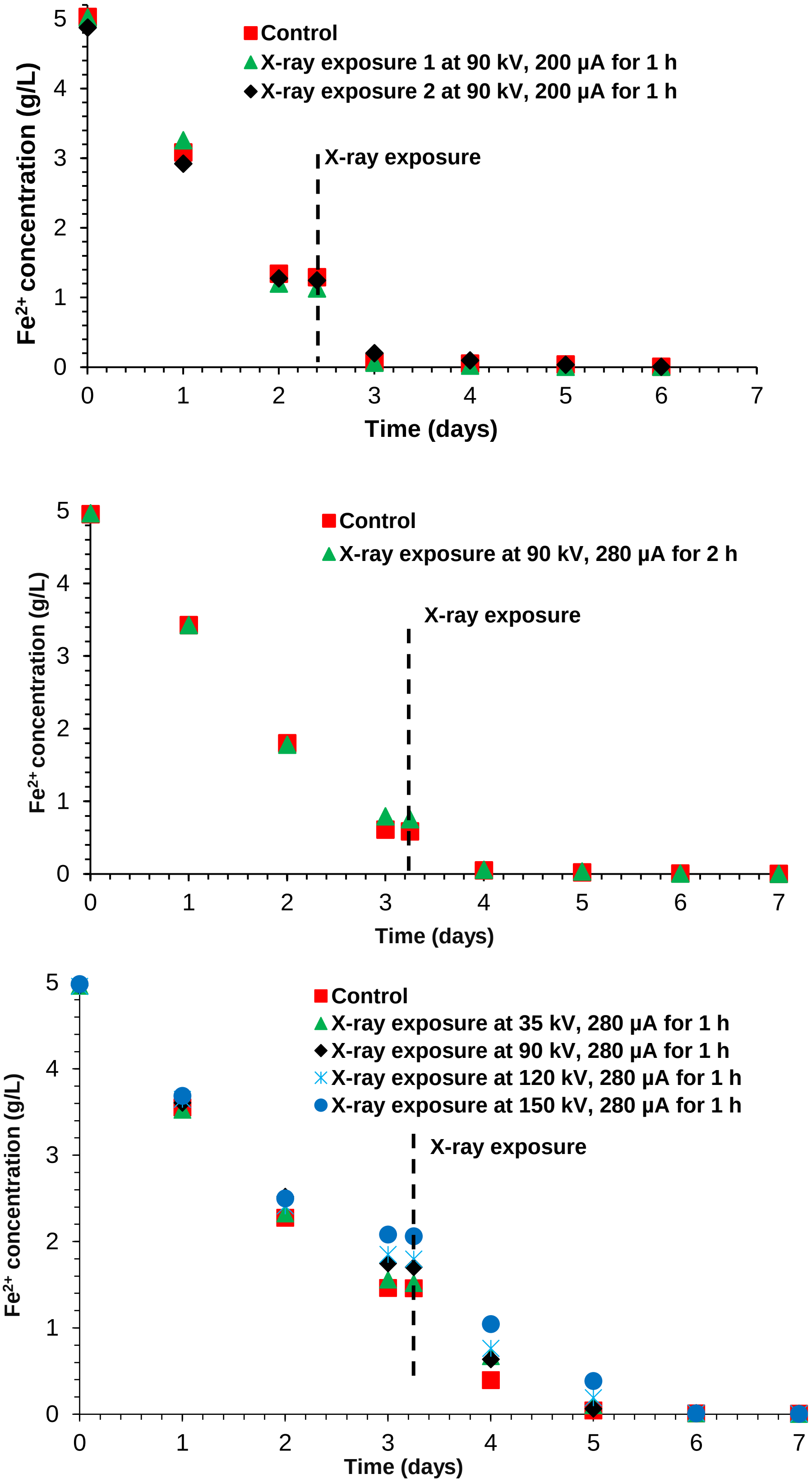

Figure 5-2: Effect of X-ray irradiation on ferrous ion concentration counts of vials inoculated with thermophilic bioleaching microorganisms grown on ferrous ion.

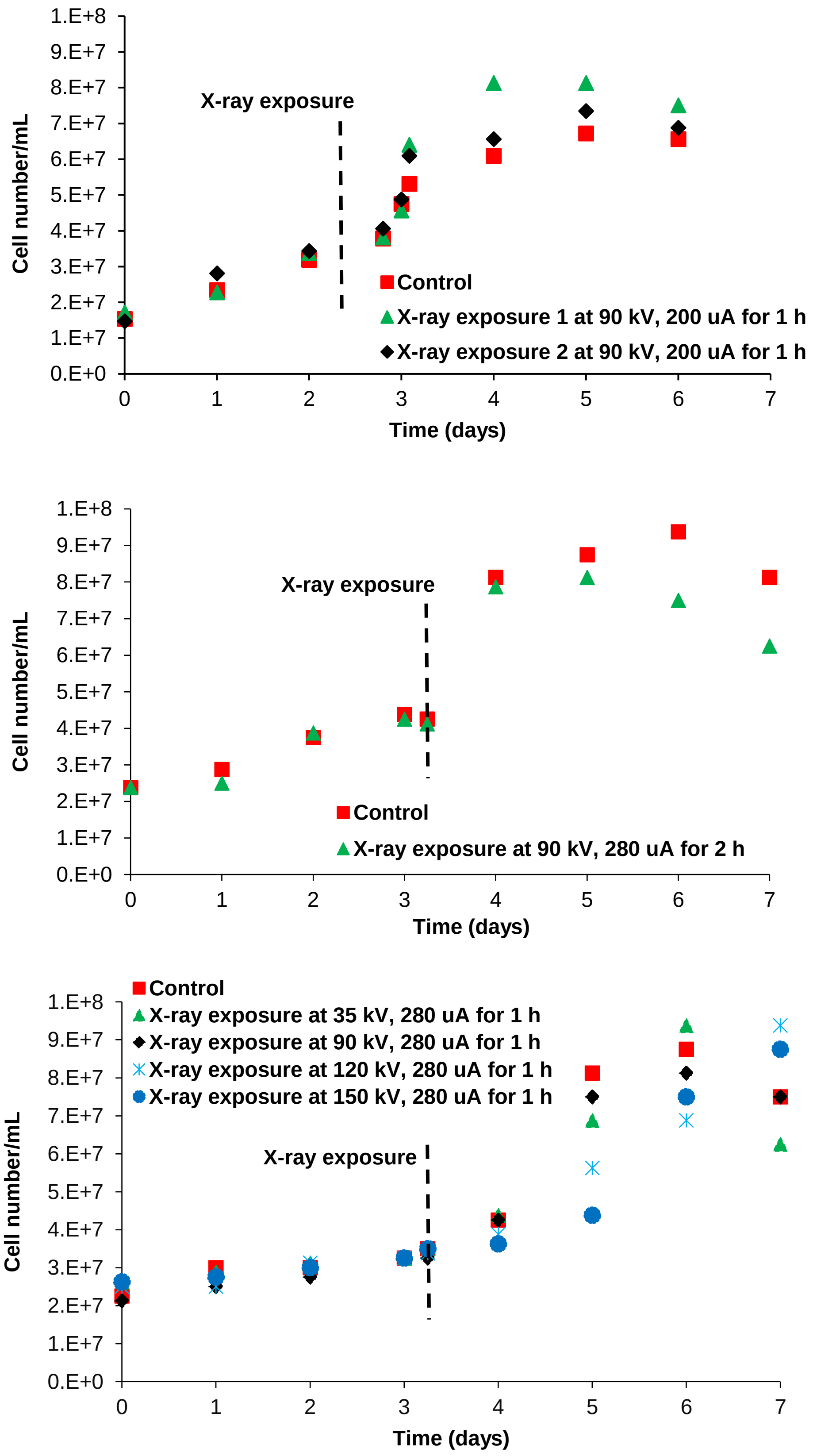

Figure 5-3: Effect of X-ray irradiation on cell number counts of vials inoculated with thermophilic bioleaching microorganisms grown on ferrous ion.

Table 5-1: Yield of biomass substrate and specific biomass growth rate for the unexposed control and experiments following X-ray exposure for vials inoculated with thermophilic bioleaching microorganisms grown on ferrous ion.

Sample	Yield biomass substrate (cells g^{-1} Fe^{2+})	Specific biomass growth rate (h^{-1})
Control	1.29×10^8	0.0136
X-ray exposure at 90 kV, 200 µA for 1 h	1.29×10^8	0.0133
X-ray exposure at 90 kV, 280 µA for 2 h	1.27×10^8	0.0136
X-ray exposure at 35 kV, 280 µA for 1 h	1.35×10^8	0.0134
X-ray exposure at 90 kV, 280 µA for 1 h	1.29×10^8	0.0135
X-ray exposure at 120 kV, 280 µA for 1 h	1.17×10^8	0.0120
X-ray exposure at 150 kV, 280 µA for 1 h	1.01×10^8	0.0092

5.1.2 Effect of X-ray exposure on bioleaching of pyrite-coated bead mini-columns

5.1.2.1 *Effluent solution chemistry and cell concentrations*

Bioleaching tests were carried out in 10 mL flow-through mini-columns (syringes) packed with 50 pyrite coated beads and inoculated with a mixed mesophilic culture. Changes in the redox potential measured in the PLS over the course of the mini-column experiments are shown in Figure 5-4. The planktonic cell concentrations measured in the PLS during bioleaching are presented in Figure 5-5.

The columns were inoculated with mesophilic microorganisms (excluding the abiotic column) on the second day. A six day lag phase was observed during which little to no change in the redox potential relative to the feed occurred. This corresponded to a period of no measurable increase in PLS cell number. On day 7 the cell concentration in the PLS started to increase, as did the redox potential. By day 9 the PLS redox potential reached circa 650 mV for the three biotic mini-columns, indicating good biological activity, in which the majority of the ferrous ion in the feed as well as any ferrous ion resulting from the pyrite leaching was converted to ferric ion.

The mini-columns were run for a further four days to ensure that the mineral surface was well colonised with an active microbial consortium, fully adapted to its environment and firmly attached on the ore surface in a biofilm before being exposed to X-ray imaging (day 13). Based on the liquid culture experiment results, X-ray imaging energy conditions of 90 kV and 225 µA for one hour were used. No detrimental effect of the bioleaching cultures had been previously observed at these conditions, while it still provided sufficient energy to image the larger ore mini-columns.

All of the biotic columns (exposed and unexposed) showed a decrease in the redox potential after the 13th day. This was also followed by a decrease in the PLS cell concentration from 5×10^6 – 6.6×10^6 cells mL^{-1} to 0.9×10^6 – 1.6×10^6 cells mL^{-1}. The fact that this drop occurred for the exposed and unexposed columns indicates that the decreases in microbial activity and concentration were not because of the X-ray exposure, but rather as a result of the brief interruption of the column irrigation and temperature control, thus removing the microorganisms from the preferred leaching conditions at which they were most active. The PLS from the inoculated columns returned to a high redox reading (640 – 670 mV) within 2 days. Following this, the exposed and unexposed inoculated mini-columns followed the same redox trend. This confirms that the microbial cultures colonised on the pyrite surface were still active (demonstrated through ferrous ion oxidation) after exposure to X-ray energy at 90 kV and 225 µA for one hour.

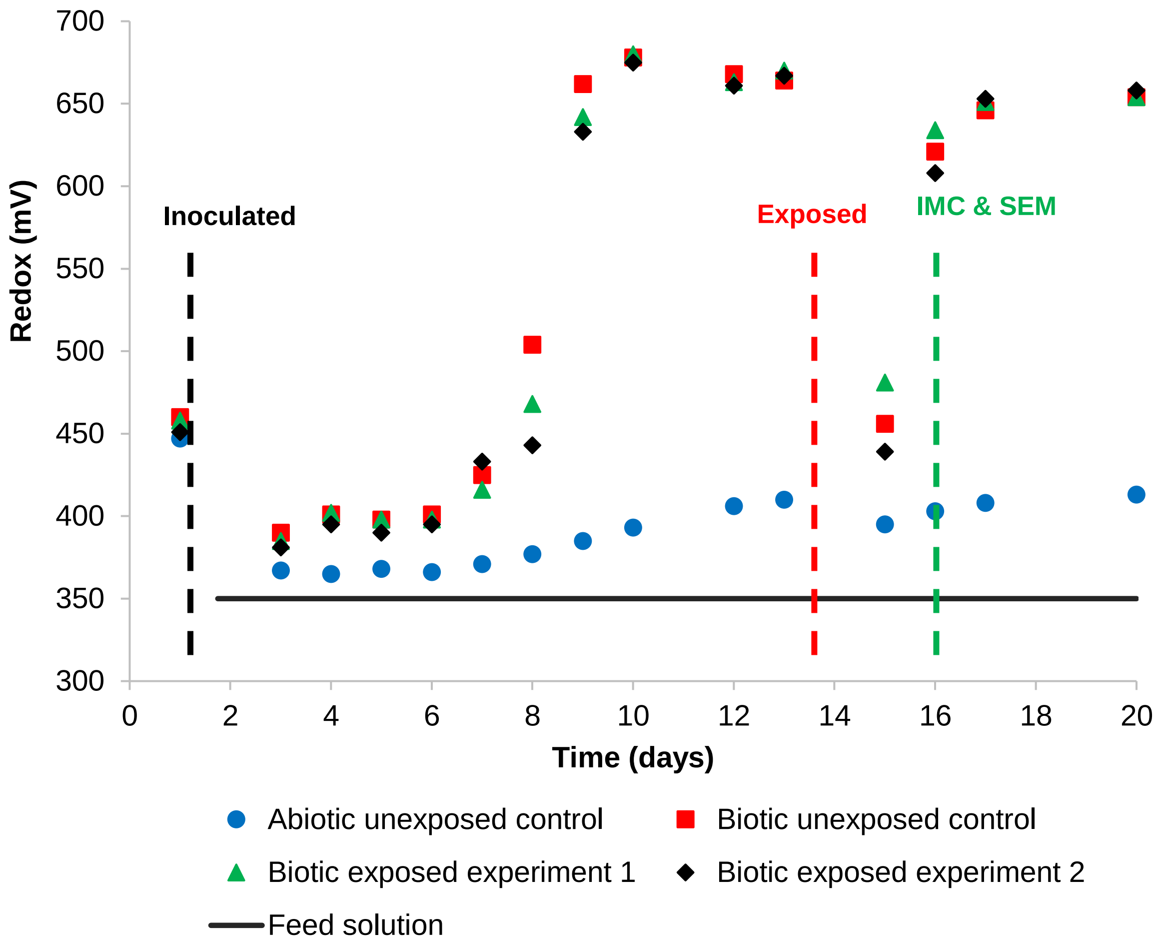

Figure 5-4: Measured PLS redox potential of the pyrite-coated bead mini-columns without and with exposure to X-ray (90 kV) over the course of the experimental period. The phases of the experimental period are indicated, showing the inoculation point, microbe-mineral contacting time of 18 h, X-ray exposure point and the day when beads were removed for IMC and SEM analysis.

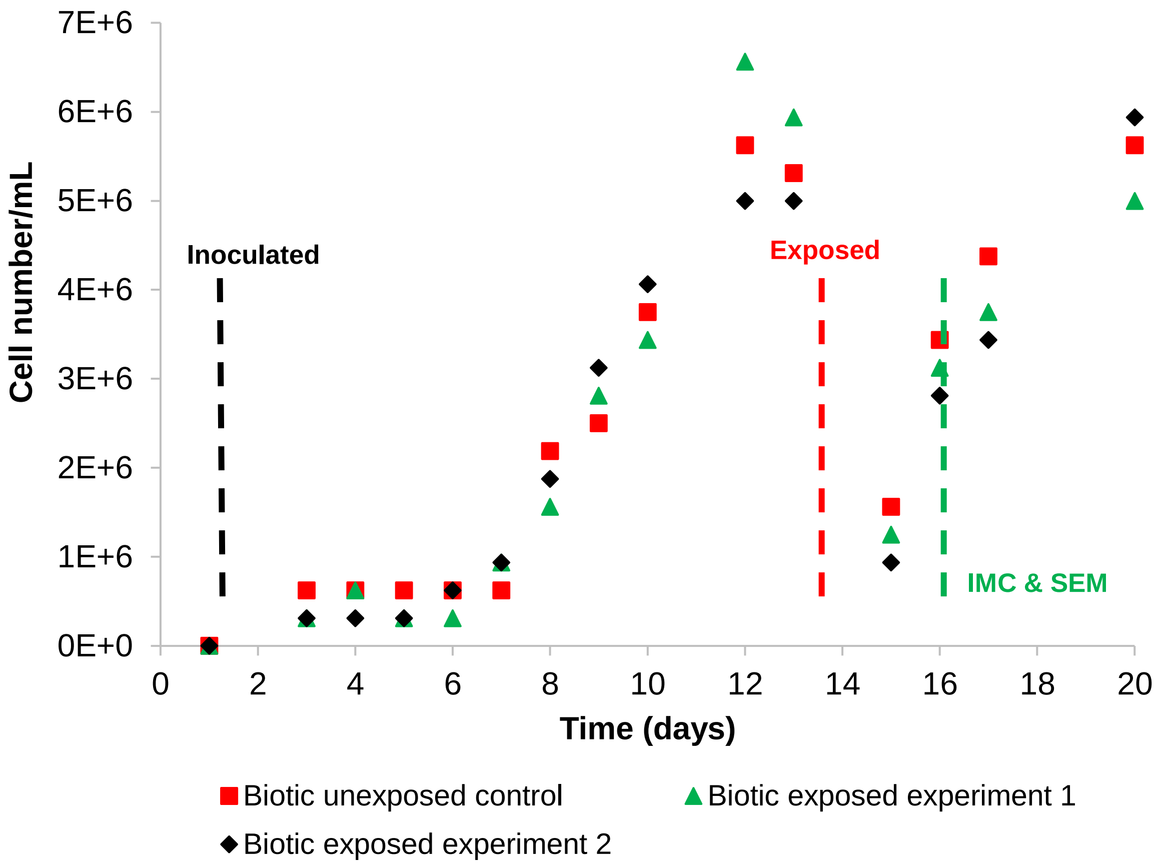

Figure 5-5: Measured PLS cell concentration of the pyrite-coated bead mini-columns without and with exposing to X-ray over the course of the experimental period experimental period. The phases of the experimental period are indicated, showing the inoculation point, microbe mineral contacting time of 18 h, X-ray exposure point and day on which beads were removed for IMC and SEM analysis.

5.1.2.2 *Microbial attachment to the pyrite mineral surface*

To examine the effect of exposure to X-ray energy on the microorganisms' health and colonisation of the ore surface, the surface morphology of the pyrite-coated beads after exposure to X-ray was visualised using SEM. Figure 5-6 presents representative SEM views of pyrite coated beads that were exposed or not exposed to X-rays respectively. Attached microorganisms can be observed on the mineral surface in both cases. The rod-shaped bacteria seen in Figure 5-6 are likely *At. Caldus* which was the dominant microbial species present in the culture. A layer of a polymeric substance (EPS) on the surface of the pyrite concentrate containing a dense population of microorganisms (white arrows) is visible on the SEM images of both exposed and unexposed beads. The ample presence of the cells on the exposed pyrite coated beads supports the evidence already presented that the X-ray exposure was not detrimental to the colonisation of the microorganisms.

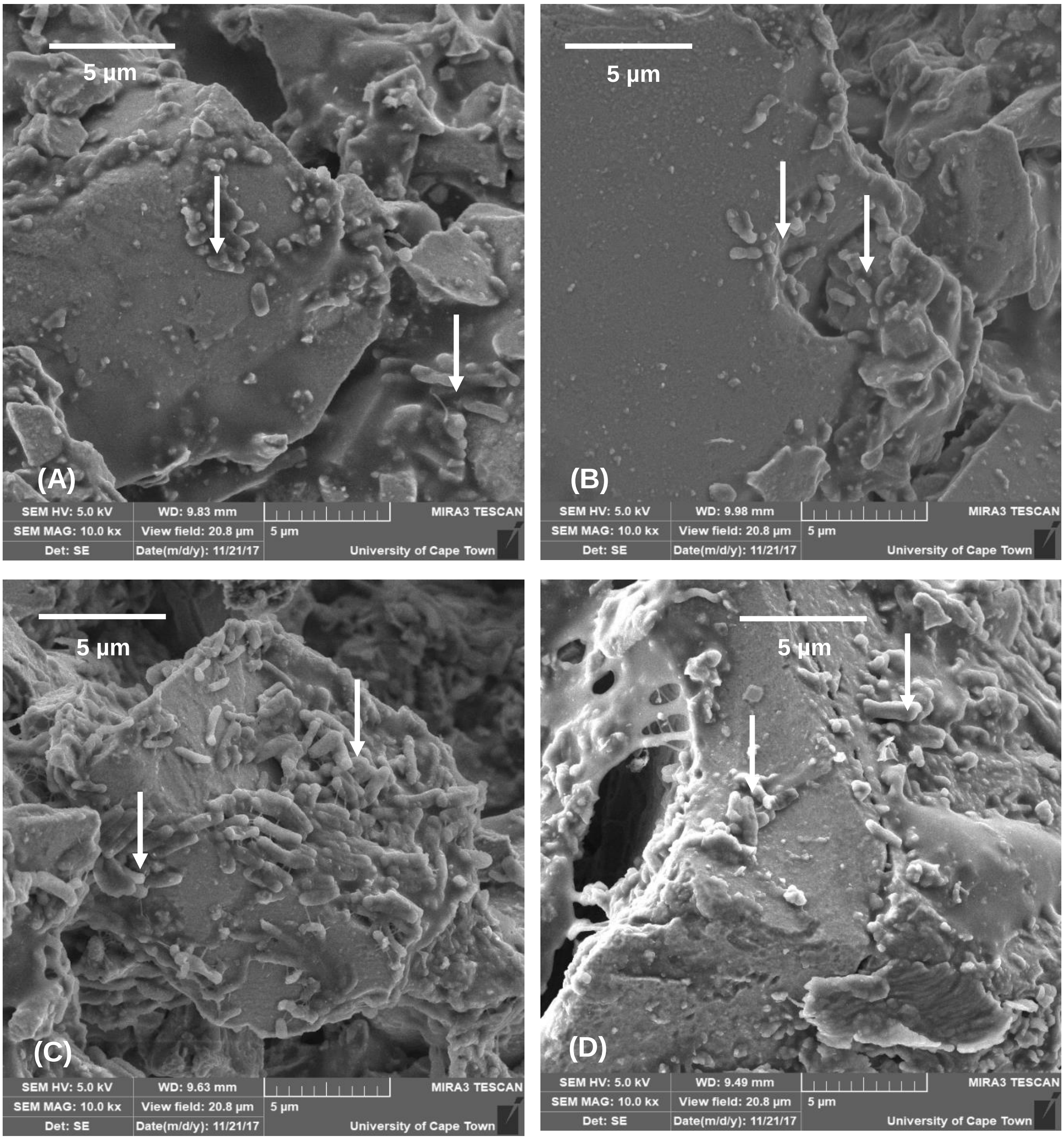

Figure 5-6: Scanning electron micrographs of cells present on the pyrite mineral concentrate coated glass beads 2 days after exposure to X-ray (day 16). Micrographs (A) and (B) show unexposed samples and (C) and (D) show X-ray exposed samples. White arrows indicate observed dense populations of microorganisms and the presence of EPS.

5.1.2.3 Metabolic activity on the pyrite mineral surface

Isothermal microcalorimetry was used to confirm that the attached cells were metabolically active on the ore surface after exposure to X-ray µCT. The power-time curves representing the metabolic activity of the microorganisms on the pyrite-coated bead surface for unexposed and exposed beads are presented in Figure 5-7.

The biotic beads exhibited an initial increase in the heat flow after which a maximum value was reached. Following this, oxygen limitation in the sealed ampoules impacted the metabolic rate, resulting in a decrease in heat flow (Makaula et al., 2017a). As seen in Figure 5-7, the heat flow for the abiotic pyrite coated beads was approximately zero (the negative values are a baseline drift by the instrument) confirming that there was no microbial activity present on the ore surface nor was there any chemically facilitated leaching of pyrite occurring owing to the absence of leach agents. For the inoculated beads, the heat flow rate during the initial period of increasing heat as well as the maximum heat flow values were similar for the unexposed and exposed samples (33 µW vs 33.5 ± 1.5 µW respectively). This further confirms that the X-ray exposure at 90 kV and 225 µA did not have any lasting effect on the overall metabolic activity of the bioleaching microorganisms which colonised the mineral surface.

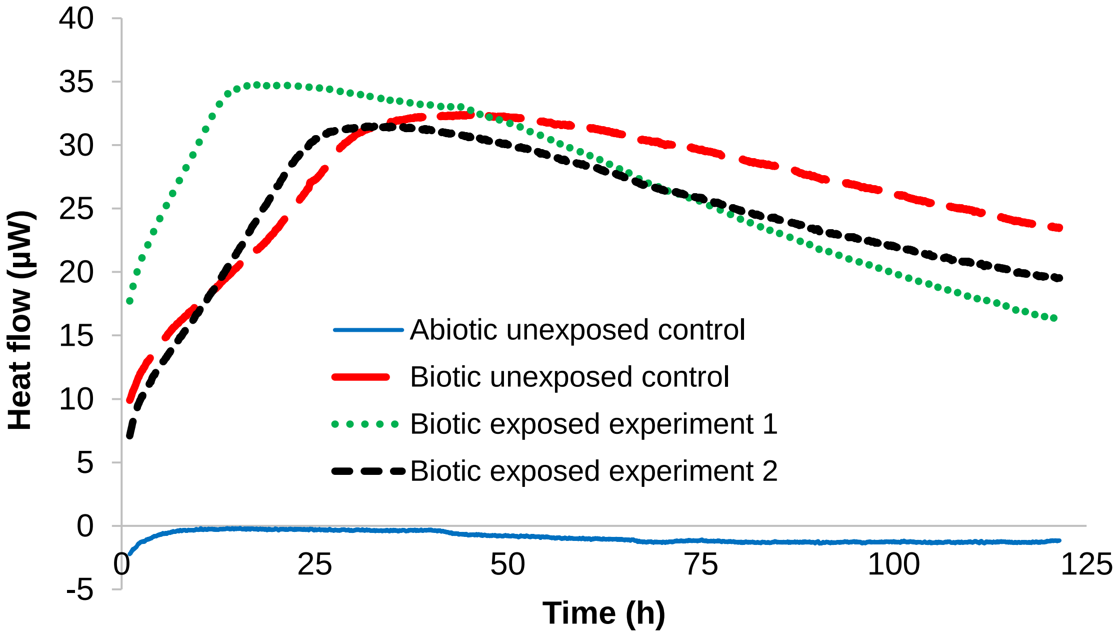

Figure 5-7: Metabolic heat flow from the X-ray exposed and unexposed bioleaching microorganisms on pyrite-coated beads 2 days after X-ray exposure (day 16).

5.2 Chalcopyrite bioleaching

Following establishment that X-ray imaging of bioleaching systems is possible without detrimentally affecting the bioleaching cultures, the biological leaching of 50 g mini-columns of low-grade chalcopyrite ore at 65 °C was monitored using X-ray µCT. The aim of the tests was to determine what effect biological leaching has on sub-surface mineral dissolution, versus in comparison to purely chemical conditions.

Changes in the PLS redox potential as a function of time are given in Figure 5-8 for the two bioleaching mini-columns run. Feed solution containing 0.5 g L^{-1} Fe^{2+} was introduced from the top into the mini-columns after acid washing for 24 hours and 18 hours of inoculation using mixed thermophilic microorganisms. In the first 7 days after inoculation the redox potential of both biotic mini-columns 1 and 2 increased from 370 mV to just less than 600 mV. This redox increase was an indication of an active microbial community ensuring rapid oxidation of Fe^{2+} to Fe^{3+}, supported by the ferrous ion data shown in Figure 5-9. There was a reduction in the redox of biotic mini-column 2 after 7 days, suspected to be due to an issue with the inoculation. This was addressed by addition of 1 mL of the stock culture from the top of mini-column. Thereafter, the redox potential was maintained between 550 and 600 mV. The redox potential increased to more than 600 mV at some points. The inherent variation of the lower redox potential of biotic mini-column 2 may have been caused by the slow detachment of the microorganisms. This inherent variation may be ignored because it was shown that the slow dissolution of the chalcopyrite was the rate limiting effect in the leaching reactions and had no impact on the copper extraction (Vries, 2013). The interruption of the biotic mini-columns for scanning led to decreases in redox potential and consequently increased Fe^{2+} concentration in the PLS solution (previously explained in Section 5.1.2.1).

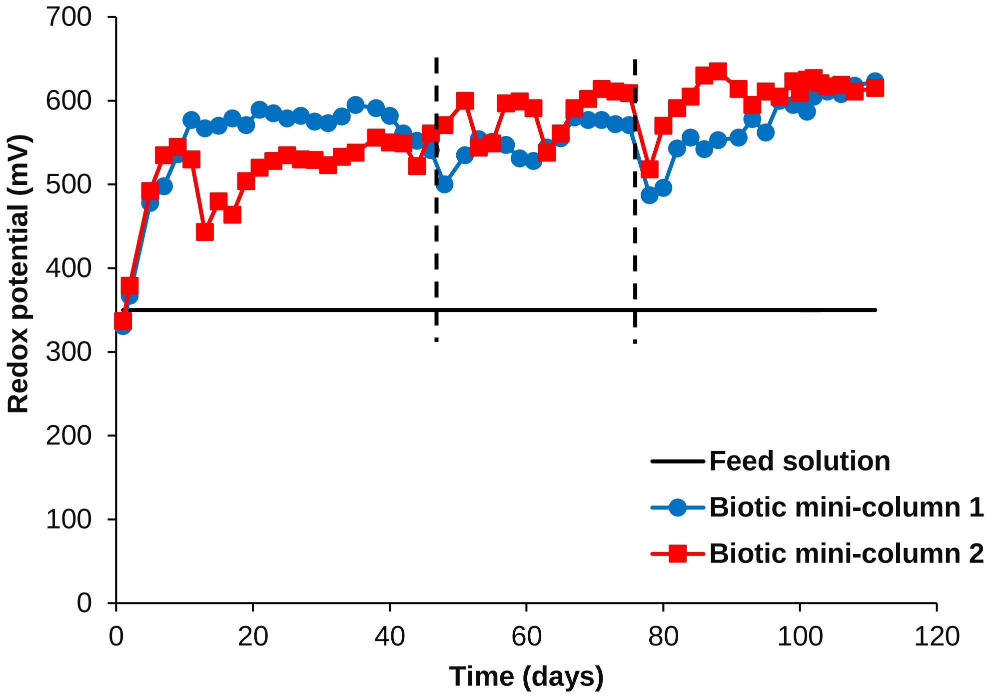

Figure 5-8: Redox potential of the PLS for the two chalcopyrite ore bioleaching mini-columns. Dashed lines indicate when the mini-column was exposed to X-ray imaging.

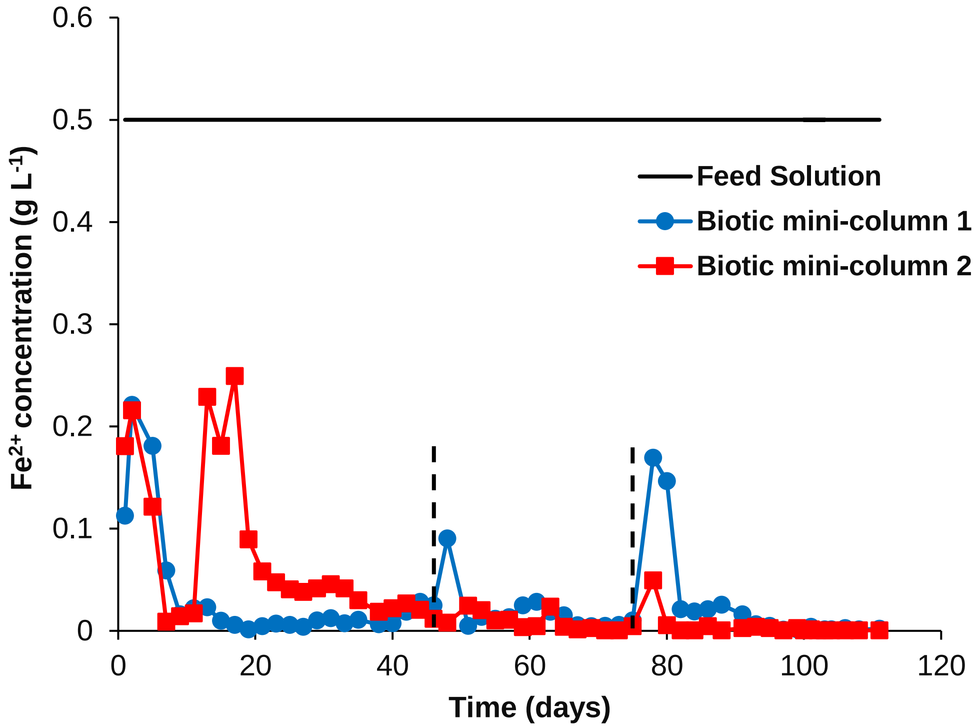

Figure 5-9: Fe^{2+} concentration of the PLS for the two chalcopyrite ore bioleaching mini-columns. Dashed lines indicate when the mini-column was exposed to X-ray imaging.

The copper recovery measured by AAS and the sulphide mineral volume reduction based on the X-ray µCT image analysis for the two biotic mini-columns and abiotic ferric leaching mini-column at 65 °C (analysed further in the subsequent chapter) are presented in Figure 5-10. Based on the AAS data, two distinct copper recovery regions can be observed following the initial lag until day 20. In the first period, between days 20 and 63, the copper recovery rate was high, the recovery increasing to 29% and 26% for mini-columns 1 and 2. This was followed by a decrease in the copper recovery rate, with the recovery only increasing to 39% and 43% for mini-columns 1 and 2 by the end of the experiment (111 days). These dissolution curves are in line with literature, which suggest that the bioleaching process takes place in three distinct phases: low dissolution observed up to circa day 15, maximum dissolution in the form of an exponential rise between circa days 15 and 63, and finally the levelling off of the process or stationary phase (Rodríguez et al., 2003; Vries, 2013a).

The abiotic ferric leaching results had a higher copper recovery than the biotic leaching. The leaching rate was high for the first 10 days because of ample availability of ferric ion in the leaching solution (4.3 g L^{-1}), whereas the bioleaching microbial community is not yet fully active to provide ferric ion for the oxidation of the sulphide minerals. The leaching rate increased in the biotic mini-columns following the lag to have approximately the same slope as the abiotic mini-columns until day 63. However, the subsequent decrease in the leaching rate in the biotic mini-columns meant that the rate of biotic leaching once again became less than in the ferric leach system. This may be due to a number of reasons. As presented in Figure 7-2, the ore particles had negligible porosity, suggesting that the archaea with size of 0.9 to 1.1 µm (Takayanagi et al., 1996) would not be able to move to the deep sub-surface regions and facilitate the bioleaching of this chalcopyrite, but only to produce lixiviant. Furthermore, crack development was not observed in the biotic leaching, though this may be because less leaching and hence degradation of the ore matrix was achieved. The feed pH was 1.30 for the biotic leaching while it was 1.15 for the abiotic system which would not be sufficient to dissolve gangue minerals such as biotite and so create cracks and pores to make the environment better for sub-surface bioleaching oxidation.

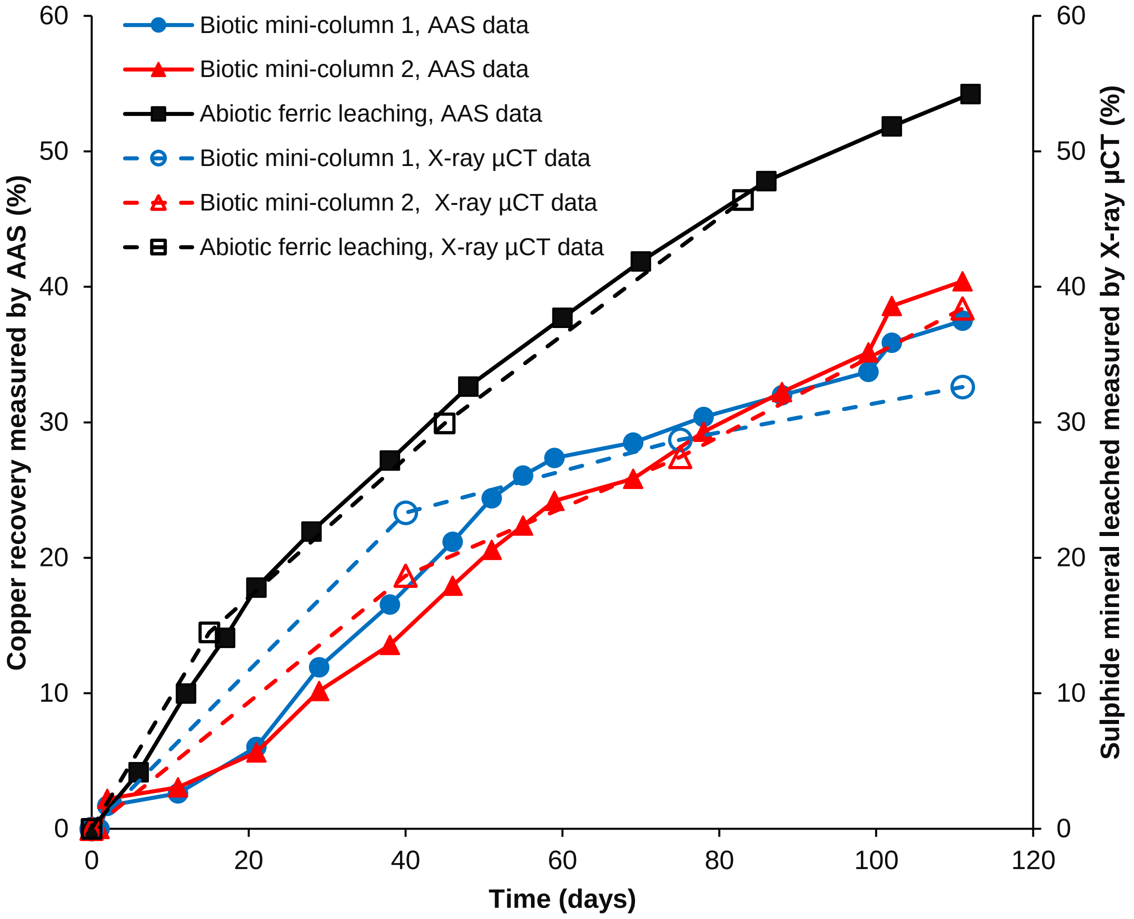

Figure 5-10: Comparison of copper recovery for the low-grade chalcopyrite ore bioleaching mini-columns, measured by spectroscopy (solid lines) and sulphide mineral leached based on image measurement (dashed lines).

Similar results were obtained for the sulphide mineral volume reduction for the two bioleaching mini-columns. However, there was a slight difference in the sulphide mineral volume reduction when it was compared with copper recovery measured by AAS. For example, the sulphide mineral volume reduction was 33% and 38% for mini-columns 1 and 2 at the end of experiment. This difference could be because the volume reduction was a sum of only three sections of the mini-column, but the copper recovery data was for the whole mini-columns. The sulphide mineral reduction will also have included e.g. pyrite dissolution effects. Acknowledging the reasons for the slight differences in bioleaching extent, the X-ray µCT image data can be used for detailed investigation of copper recovery from the ore particles based on their distribution in particles as well as their distance from the ore surface.

The distributions of the copper mineral distance from the ore surface for biotic mini-columns 1 and 2 are given in Figure 5-11 and Figure 5-13 and the sum of three tracked sections in Figure 5-12 and Figure 5-14 respectively. Maximum leaching penetration distances of 2 mm and 2.1 mm were found for biotic mini-column 1 and 2. The amount of copper recovery decreased significantly in biotic mini-column 1 when the distance was more than 1.2 mm. However, the copper recovery in deeper subsurface zones is higher in biotic mini-column 2. It may be the reason for the faster rate of copper recovery in biotic mini-column 2 in the later stages of the chalcopyrite bioleaching experiment (Figure 5-10).

The sulphide mineral content of biotic mini-column 1 decreased considerably during the first 40 days, but there was only a small amount of leaching during the last 70 days and the maximum penetration distance did not change. The maximum penetration distance was 1.3 mm for biotic mini-column 2 after 40 days and had increased to 2.1 mm by 110 days. The maximum penetration distance for the biotic leaching columns was 400 µm lower than for abiotic ferric leaching. As previously postulated, this was likely contributed to by an absence in crack development, because the archaea were only able to be present on the ore surface (and not below) and because the redox potential in the biotic system was not as favourable as the ferric leach.

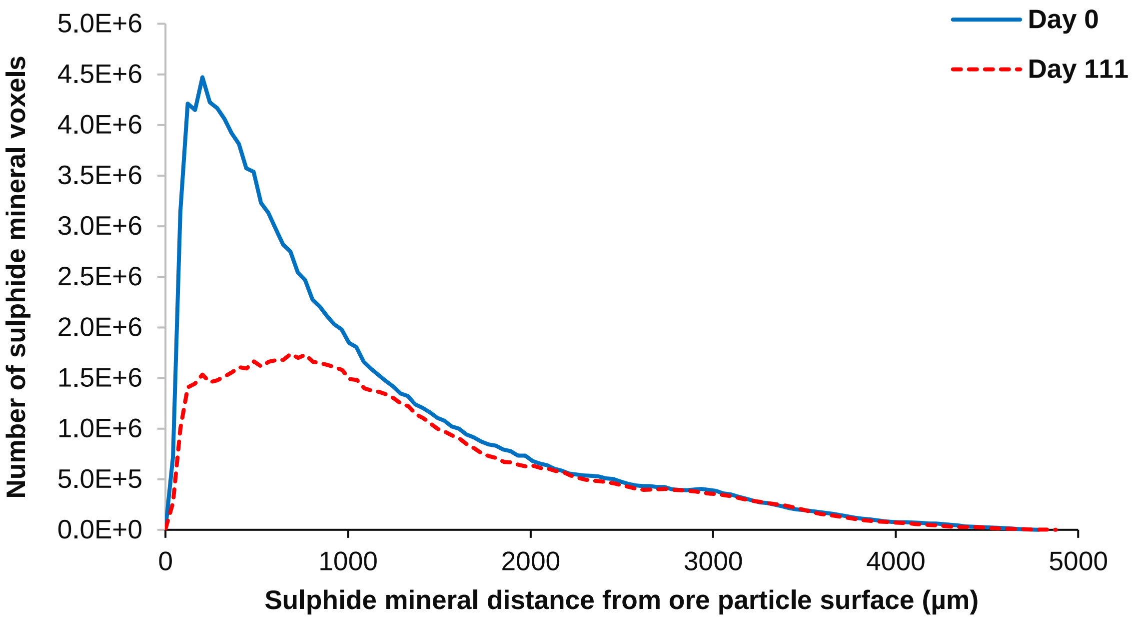

Figure 5-11: Change in distribution of sulphide minerals as a function of position and time for biotic mini-column 1. The uncertainty in the grain distance from the ore surface is ±40.2 µm.

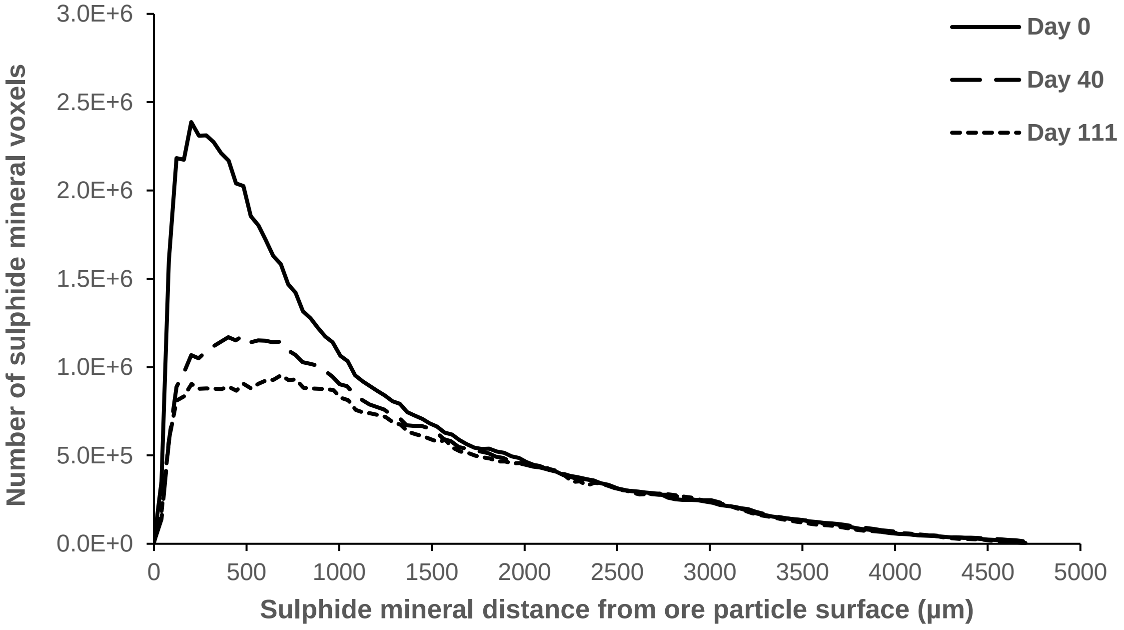

Figure 5-12: Change in the distribution of sulphide minerals as a function of position and time for biotic mini-column 1 (sum of three tracked sections). The uncertainty in the grain distance from the ore surface is ±40.2 µm.

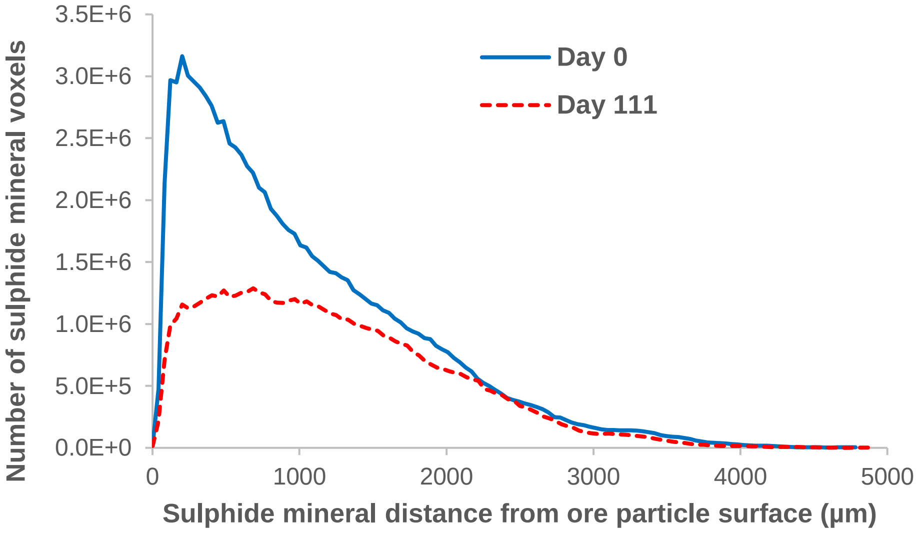

Figure 5-13: Change in distribution of sulphide minerals as a function of position and time for biotic mini-column 2. The uncertainty in the grain distance from the ore surface is ±40.2 µm.

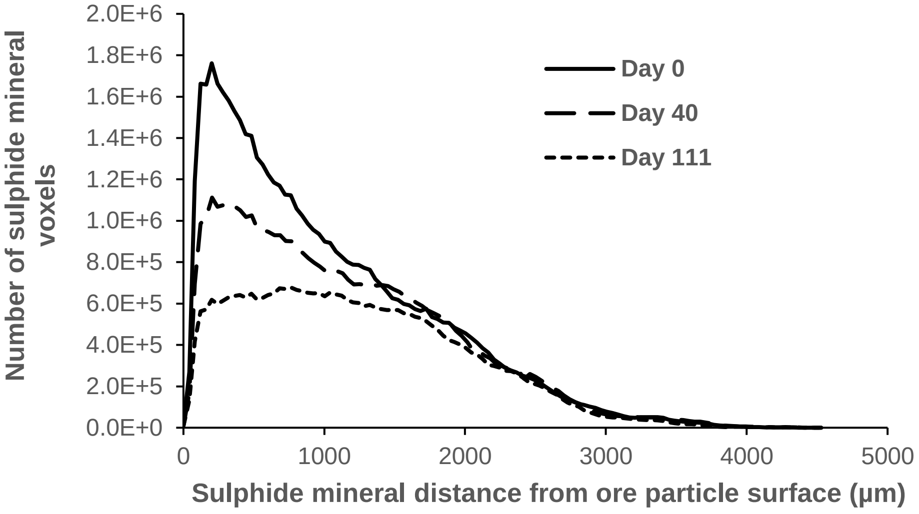

Figure 5-14: Change in the distribution of sulphide minerals as a function of position and time for biotic mini-column 2 (sum of three tracked sections). The uncertainty in the grain distance from the ore surface is ±40.2 µm.

5.3 Summary

A premise for bioleaching studies integrating X-ray µCT is that the metabolic activity of microorganisms is not affected by X-ray energy doses. This study therefore evaluates the compatibility bioleaching microorganisms with X-ray energy exposure. Feasibility studies of heap bioleaching process using X-ray µCT were successfully conducted in liquid culture, on pyrite coated beads, and low-grade agglomerated chalcopyrite ore, confirming that the technique can be used to investigate non-surface mineral grain leaching in biotic leaching processes.

The X-ray effect on a mixed thermophilic culture suspended in solution was assessed using imaging conditions of 35-150 kV, 200-280 µA and 1-2 hours. Microorganisms were unaffected between 35-90 kV and 200-280 µA while there was some detrimental effect at 120 and 150 kV. The X-ray influence on a mixed mesophilic culture colonising a mineral surface was investigated at 90 kV and 225 µA for a 1 hour exposure time. The system was monitored before and after exposure through measurement of: redox potential of the effluent solution, microbial cell concentration, heat output from the colonised surface using isothermal microcalorimetry (IMC), and cell attachment on the ore surface using scanning electron microscopy (SEM). The redox and cell concentration measurements showed insignificant differences between exposed and unexposed samples. Equivalent heat generation and good colonization of the mineral surface was demonstrated, confirming continued microbial activity post exposure, hence recommending its use in support of bioleaching studies.

Bioleaching of low-grade chalcopyrite ore using thermophilic microorganisms was performed to measure copper recovery and penetration distance. The results showed that maximum leaching penetration distances of 2 mm and 2.1 mm were found for biotic mini-column 1 and 2. The sulphide minerals recovery of 39% and 43% was obtained for mini-columns 1 and 2 by the end of the experiment. In addition, microorganisms were active and able to oxidise ferrous to ferric ion.

6 Surfactant effect on non-surface mineral grain leaching

The first section of this chapter investigates the effect of various non-ionic surfactants on the metabolic activity of mixed cultures of thermophilic bioleaching microorganisms. This fundamental work, which considers aqueous ferrous ion oxidation and leaching of chalcopyrite concentrate, is necessary to recommend surfactants (and associated concentrations) that are suitable for subsequent use with whole ores. In the second part, the selected surfactant, at its optimum concertation, was used in the mini-column leaching of chalcopyrite and pyrite ore to study its effect on non-surface mineral grain leaching and penetration.

6.1 Shake flask experiments

6.1.1 Effect of surfactant on microbial growth and ferrous ion oxidation

The effect of the addition of 5 or 10 mg L^{-1} of each surfactant on the ferrous ion-oxidising capacity of the thermophilic microorganisms at 65 °C is presented in the form of profiles of pH, redox potential, ferrous ion concentration and cell concentration with time in Figure 6-1 and Figure 6-2.

The biotic control, inoculated but with no addition of surfactant, showed an increase in pH with time. An increase in pH was not observed in the abiotic (un-inoculated) control. This is because microbial ferrous ion oxidation consumes acid (Equation 6-1) which leads to the increase in solution pH. The same trend in pH as seen with the biotic control was observed for the cultures containing 5 mg L^{-1} of Tween® 20, Tween® 80, Plurafac® LF 120 or Lutensol® XL 90 and solutions containing 10 mg L^{-1} of Tween® 20 or Lutensol® XL 90. In all these cases, the pH increased from the starting values of pH 1.25 – 1.28 to a maximum pH of circa 1.50. The increase in pH for the solutions containing 5 mg L^{-1} of Plurafac® LF 600 and 10 mg L^{-1} of Tween® 80 or Plurafac® LF 120 was depressed, achieving a maximum of pH 1.4. This indicates reduced, but still positive, microbial activity.

$$2Fe^{2+} + 2H^{+} + 0.5O_2 \xrightarrow{microorganisms} 2Fe^{3+} + H_2O \qquad (6\text{-}1)$$

The redox potential provides a measure of the ferric to ferrous ion ratio according to the Nernst equation. The redox potential of the abiotic control increased from 360 mV to 430 – 440 mV, where after no further increase in the redox potential was observed. The inoculated cultures containing 5 mg L^{-1} Tween® 20, Tween® 80, Plurafac® LF 120 or Lutensol® XL 90, or 10 mg L^{-1} Tween® 20 and the positive (inoculated) control without surfactant exhibited an increase in redox potential from 450 – 460 mV to a maximum of 660 – 670 mV on day 4. This indicates that the microorganisms were active and efficient in converting the ferrous ion to ferric ion and is supported by the ferrous ion concentration data (Figure 6-2 c). The culture containing 10 mg L^{-1} of Lutensol® XL 90 displayed a lag, requiring 5 days before the redox potential increased to its maximum value. The reduced increase in redox potential and associated slower reduction in ferrous ion concentration was observed for the cultures containing 5 mg L^{-1} of Plurafac® LF 600 and 10 mg L^{-1} of Tween® 80 or Plurafac® LF 120.

In all cases, an increase in cell concentration from the initial inoculation concentration was not observable until after day 3. The increase in cell concentration after this period corresponded with the pH and redox maxima described.

Overall, the results indicated that the addition of 5 mg L^{-1} Tween® 20, Tween® 80, Plurafac® LF 120 or Lutensol® XL 90 did not have a measurable effect on ferrous ion oxidation and microbial activity, whereas Plurafac® LF 600 clearly inhibited microbial growth and ferrous ion oxidation at 5 mg L^{-1}. At a surfactant concentration of 10 mg L^{-1}, all surfactants except Tween® 20 had a negative effect on ferrous ion oxidation and microbial growth. The redox potential required an extra two days to reach its maximum on day 5 in the presence of 10 mg L^{-1} Lutensol® XL 90, while in the presence of 10 mg L^{-1} Plurafac® LF 120 and Tween® 80 the redox potential did not exceed 450 mV over the duration of the experiment. The microbial growth inhibition may be due to the surfactant damaging to the microorganisms' membranes at this concentration (Florian and Sand, 2012). Surfactants are well recognised as agents causing cell disruption at high concentrations through membrane destabilisation (Harrison, 1991). This has been demonstrated for anionic, cationic and non-ionic surfactants (Anand H. et al., 2007; Harrison et al., 1991).

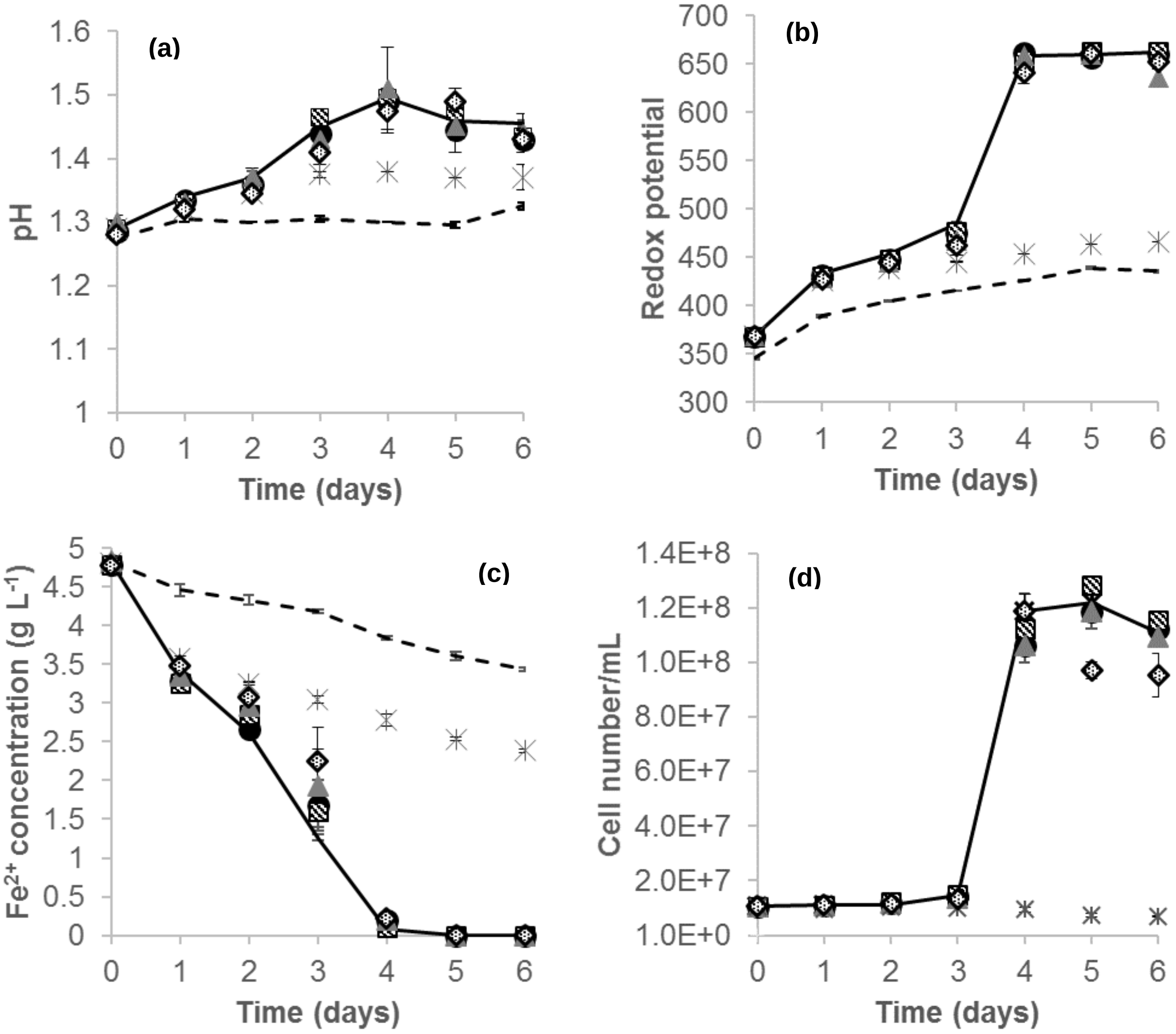

Figure 6-1: (a) pH, (b) redox potential, (c) ferrous ion concentration and (d) cell concentration in flasks used to study the effect of surfactant on ferrous ion oxidation at 65 °C. The flasks were: abiotic control (---), biotic control (—), 5 mg L^{-1} Tween® 20 (●), 5 mg L^{-1} Tween® 80 (▧), 5 mg L^{-1} Plurafac® LF 120 (▲), 5 mg L^{-1} Plurafac® LF 600 (∗), 5 mg L^{-1} Lutensol® XL 90 (◈).

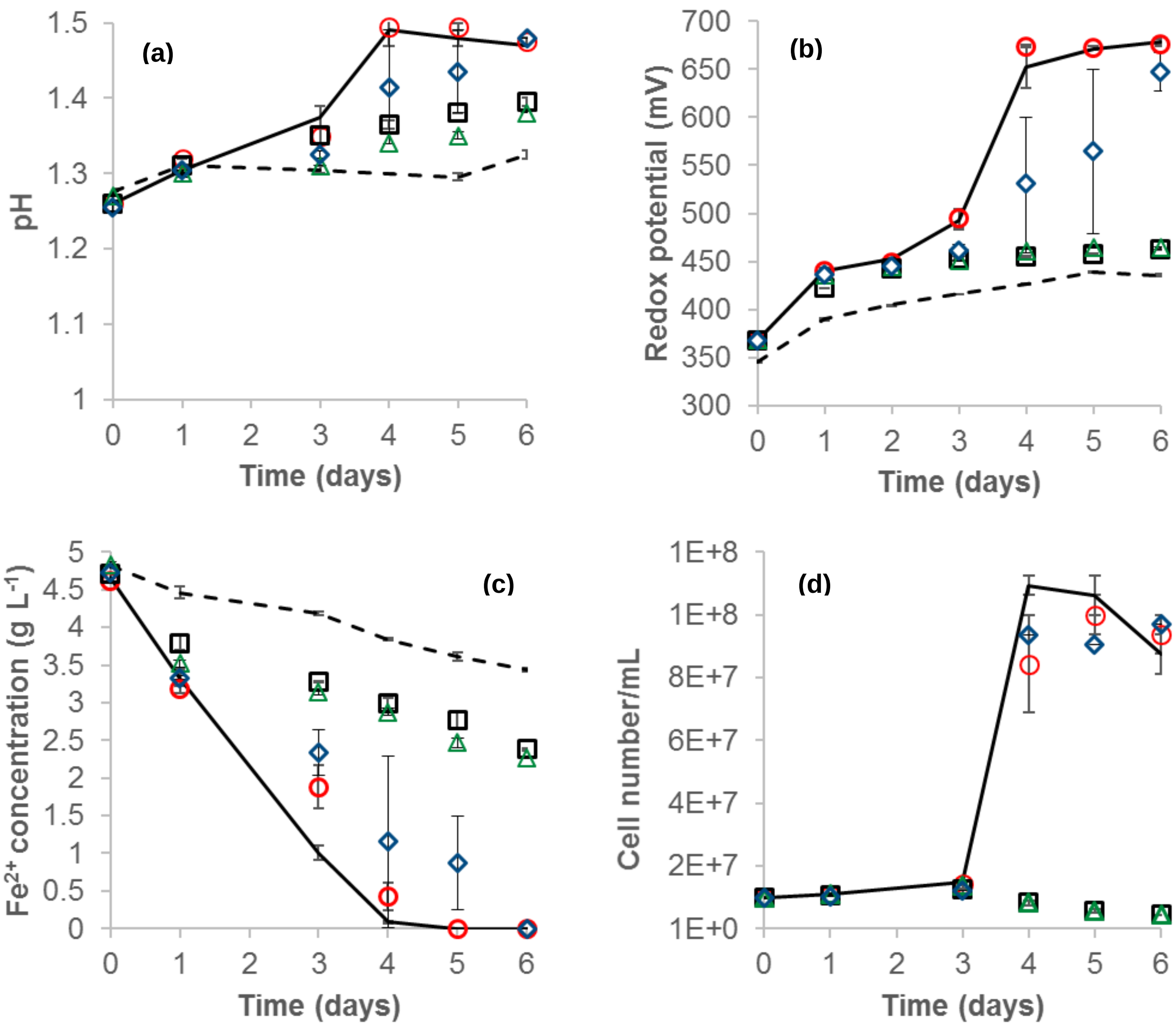

Figure 6-2: (a) pH, (b) redox potential, (c) ferrous ion concentration and (d) cell concentration in the flasks used to study the effect of surfactant on ferrous ion oxidation at 65 °C. The flasks were: abiotic control (-- -), biotic control (—), 10 mg L^{-1} Tween®20 (○), 10 mg L^{-1} Tween® 80 (□), 10 mg L^{-1} Plurafac® LF 120 (△), 10 mg L^{-1} Lutensol® XL 90 (◇).

6.1.2 Effect of surfactant on bioleaching of chalcopyrite concentrate

Figure 6-3 and Figure 6-4 show the pH, redox potential, total iron concentration and cell concentration profiles from the experiments used to study the effect of surfactant on chalcopyrite bioleaching. In the biotic control and experiments containing 5 mg L^{-1} or 10 mg L^{-1} Tween® 20, Plurafac® LF 120, Lutensol® XL 90 or 5 mg L^{-1} Tween® 80, two clear phases can be distinguished in the pH trend. During the first phase (until day

6), there is an increase of the pH due to the acid neutralising capacity of the mineral or acid leaching of mineral sulphides present or both. The first phase is followed by a gradual decrease in pH, attributable to the activity of sulphur-oxidizing microorganisms and associated acid production. Subsequent to this phase (after day 15), the pH remained constant at around pH 1.4. A continued increase in pH was observed only for the abiotic control and the experiments containing 5 or 10 mg L^{-1} Plurafac® LF 600 or 10 mg L^{-1} Tween® 80. This is in alignment with reduced microbial activity and associated acidification, signifying that these surfactants inhibited the bioleaching microorganisms.

The results of the Tween® experiments and biotic control were most similar. However, in the experiments with Plurafac® LF 120 and Lutensol® XL 90, the initial increase in pH associated with acid leaching was slower and the maximum pH lower. Surfactants form a layer on the mineral surface, the thickness of which depends on the surfactant concentration in the solution and its molecular structure. The adsorbed layer can depress the diffusion of leaching reagent from solution to the mineral surface and cause the depression in the chemical leaching (Hiroyoshi et al., 1995). Therefore, the observed differences in the pH trends across various surfactants suggest possible differences in the structure of the adsorbed layer.

There was no increase in redox potential (maximum 400 mV) for the abiotic control, or the cultures containing 5 or 10 mg L^{-1} Plurafac® LF 600 or 10 mg L^{-1} Tween® 80, which correlates with an absence of microbial activity or growth. For the biotic control, after a lag phase in microbial activity of 8 days, the redox potential increased from 425 mV on day 8 through 500 mV on day 9 to a highest value of 665 mV on day 18 (Figure 6-3 & Figure 6-4 (b)). The more gradual increase in redox potential in the chalcopyrite leaching experiments, compared to ferrous oxidation shown in Figure 6-1 and Figure 6-2, is a result of the ongoing mineral leaching by ferric ion and ferrous ion oxidation over this period. The increase in the microbial concentration occurred between day 6 and day 11 in the biotic control (Figure 6-3 & Figure 6-4 (d)). Adding surfactants into the leaching solution reduced the lag in both microbial cell growth and redox potential lag by two days for Tween® 20 and 80 and by one day for Plurafac® LF 120 and Lutensol® XL 90.

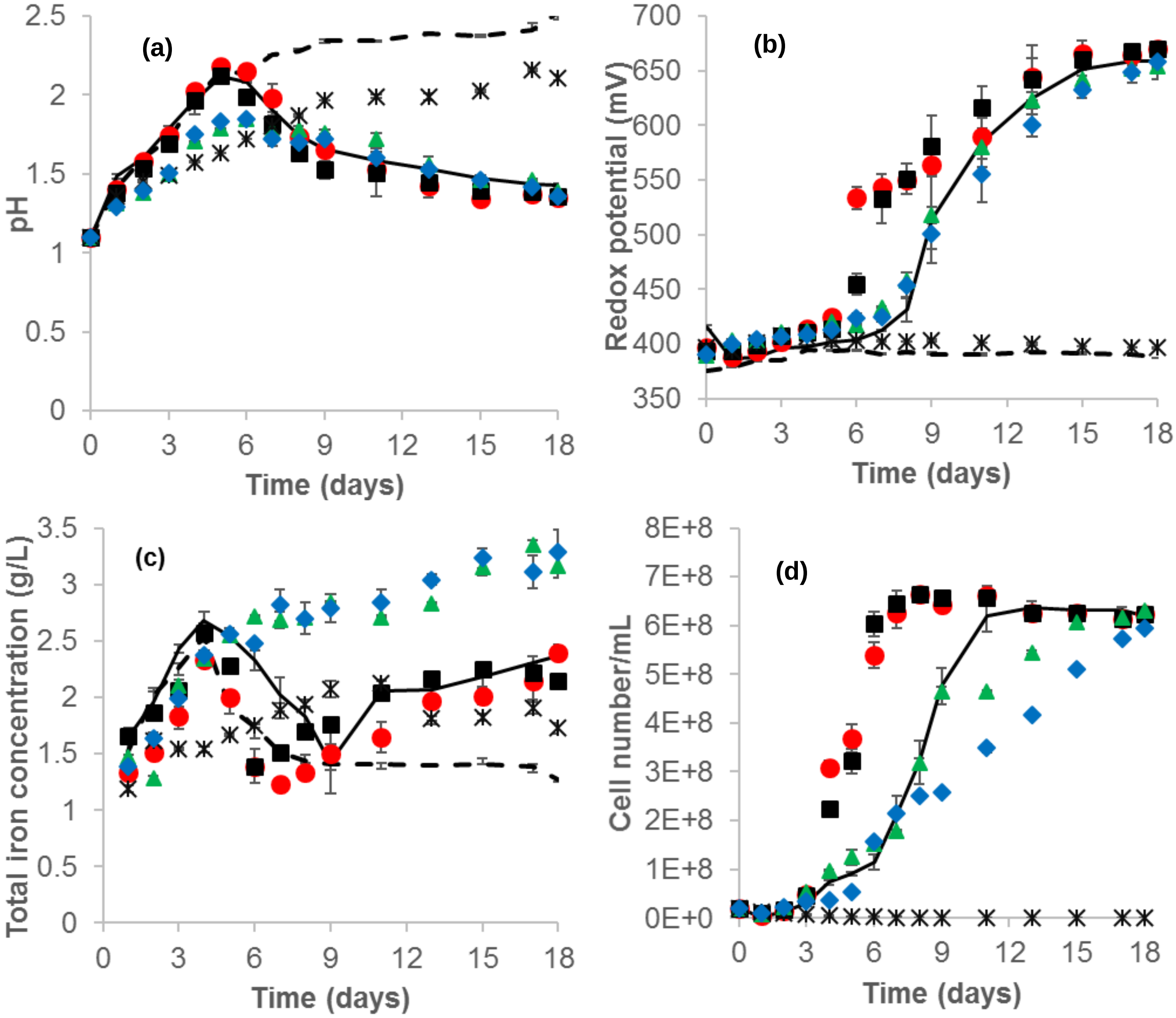

Figure 6-3: (a) pH, (b) redox potential, (c) total iron concentration and (d) cell number in the flasks used to study the effect of surfactant on chalcopyrite bioleaching at 65 °C. The flasks were: abiotic control (- - -), biotic control (—), 5 mg L^{-1} Tween® 20 (●), 5 mg L^{-1} Tween® 80 (■), 5 mg L^{-1} Plurafac® LF 120 (▲), 5 mg L^{-1} Plurafac® LF 600 (✳), 5 mg L^{-1} Lutensol® XL 90 (◆).

The total iron concentration results showed an initial increase in iron concentration in the solution, associated with the chalcopyrite solubilisation, followed by a later reduction, attributable to precipitation of the iron out of solution. The iron precipitation could have resulted from the pH increase, exceeding pH 2.0, and the high temperature (65 ˚C) accelerating the precipitation. The later decrease in solution pH because of the activity of the sulphur-oxidizing microorganisms can be correlated with an increase in total iron concentration in some of the experiments (Plumb et al., 2008; Xia et al., 2013).

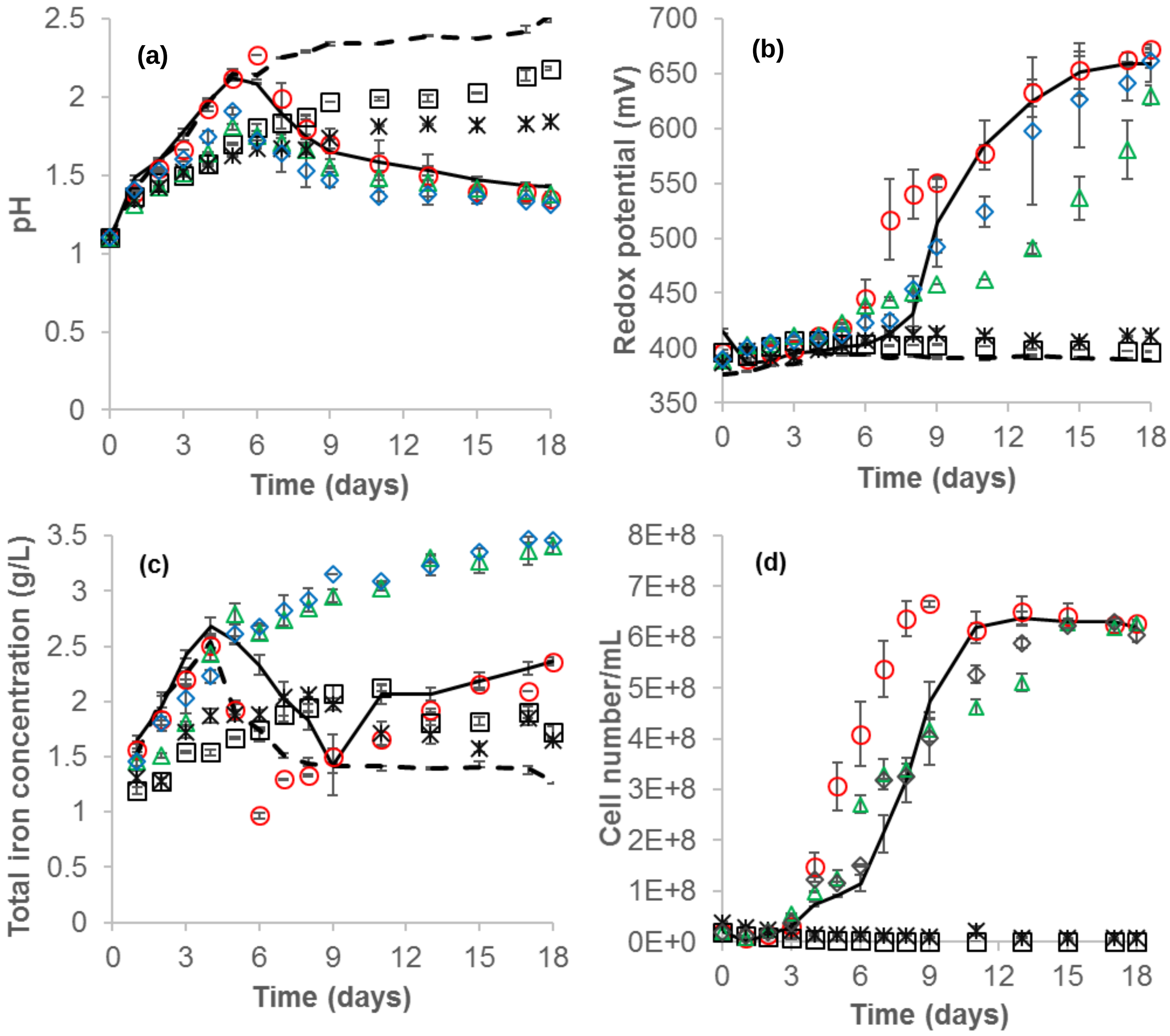

Figure 6-4: (a) pH, (b) redox potential, (c) total iron concentration and (d) cell number in the flasks used to study the effect of surfactant on chalcopyrite bioleaching at 65 °C. The flasks were: abiotic control (- - -), biotic control (—), 10 mg L^{-1} Tween® 20 (○), 10 mg L^{-1} Tween® 80 (□), 10 mg L^{-1} Plurafac® LF 120 (△), 10 mg L^{-1} Plurafac® LF 600 (∗), 10 mg L^{-1} Lutensol® XL 90 (◇).

The effect of Tween® 20 on the bioleaching of chalcopyrite was studied over an extended concentration range to 20 mg L^{-1}, as no negative effect had been observed at 5 mg L^{-1} or 10 mg L^{-1}. The pH, redox potential, total iron concentration and cell number measurements are shown in Figure 6-5. The data indicates that when the

Tween® 20 concentration was increased to 20 mg L^{-1}, microbial growth was inhibited. This leads to the recommendation that surfactants should be used at as low a concentration as practicable for the bioleaching of metals from ores. High surfactant concentrations have been reported to decrease leaching reagent diffusion to the ore surface by formation of a surfactant layer around the ore (Hiroyoshi et al., 1995) and to damage cell membranes (Florian and Sand, 2012; Harrison et al., 1991; Partearroyo et al., 1990). Further, the surfactant tendency to adsorb at interfaces may block reaction sites on the mineral surface (Schmuhl et al., 2011).

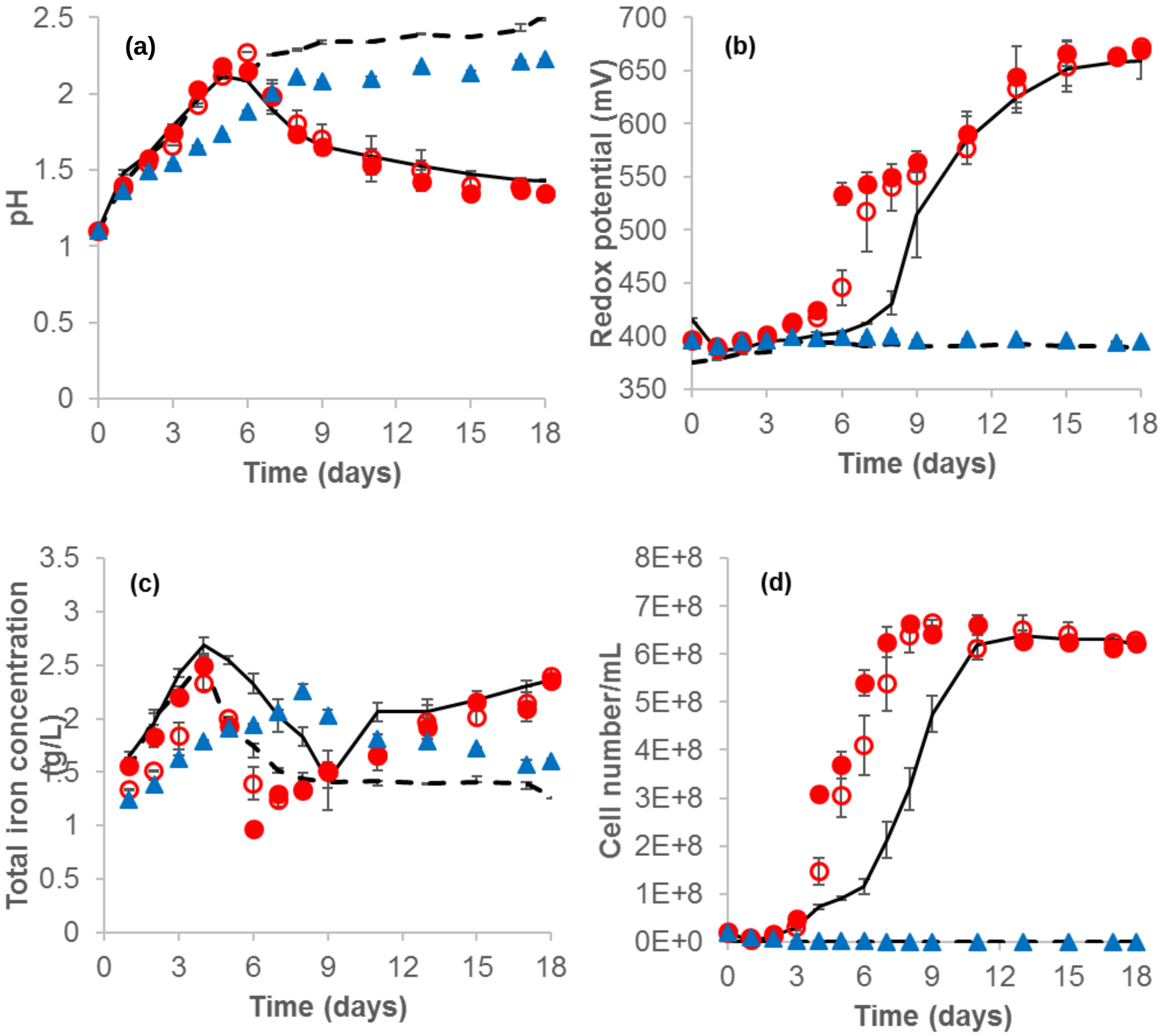

Figure 6-5: (a) pH, (b) redox potential, (c) total iron concentration and (d) cell number in the flasks used to study the effect of various Tween® 20 concentrations on chalcopyrite bioleaching at 65 °C. The flasks were: abiotic control (- - -), biotic control (—), 5 mg L^{-1} Tween® 20 (●), 10 mg L^{-1} Tween® 20 (○), 20 mg L^{-1} Tween® 20 (▲).

Figure 6-6 presents the final copper extractions achieved in the chalcopyrite bioleaching experiments. In the absence of surfactant, copper recovery was 49.3% and 72.6% for the abiotic and biotic leaching controls respectively. The abiotic leaching result is expected owing to the chemical oxidation of ferrous ion at the high temperature conditions. The chemical ferrous ion oxidation rate (initial Fe^{2+} concentration of 89.53 mM) at 65 °C was 0.46 mM Fe^{2+} h^{-1} and specific microbial Fe^{2+} utilization rate at 65 °C was 8.38 mol Fe^{2+} (mol C)$^{-1}$ h^{-1} (Searby, December 2006). For some of the experiments (containing 20 mg L^{-1} Tween® 20, 10 or 20 mg L^{-1} Tween® 80, and 5 or 10 mg L^{-1} Plurafac® LF 600), the copper recovery was lower than the abiotic leaching control. This suggests that the adsorbed layer of surfactant may cause the depression of chemical leaching at these higher surfactant concentrations, in addition to the previously reported inhibition of microbial growth. In the worst case, addition of 20 mg L^{-1} Tween® 80 decreased the copper recovery to 36.6% (12.6% lower than the abiotic control).

The copper recovery in the presence of Tween® 20, Lutensol® XL 90, or Plurafac® LF 120 at concentrations of 5 mg L^{-1} and 10 mg L^{-1} was similar to the biotic control. This indicates that the absorbed surfactant did not limit the leaching rate at these concentrations significantly. For these three surfactants, the copper recovery was a few percentage points higher at surfactant concentrations of 10 mg L^{-1}. The 10 mg L^{-1} Tween® 20 data shows an enhancement of the copper recovery by 2.4% relative to the biotic control. Liu et al. (2015) reported that Tween® 20 can disperse the sulphur product from the mineral surface and accelerate the bio-oxidation, thus accelerating the corresponding reaction kinetics.

The data therefore suggest that an optimal surfactant concentration exists at which the copper recovery is maximised, and below or above which it may be reduced. A higher molecular weight surfactant resulted in the reduction of the copper leaching efficiency, hence recommending lower weight surfactants. Further, while the benefit of surfactant addition observed with the finely milled concentrate used here is small, larger benefits are expected with crushed low-grade ore, owing to the need to access intra-particle or sub-surface mineral grains.

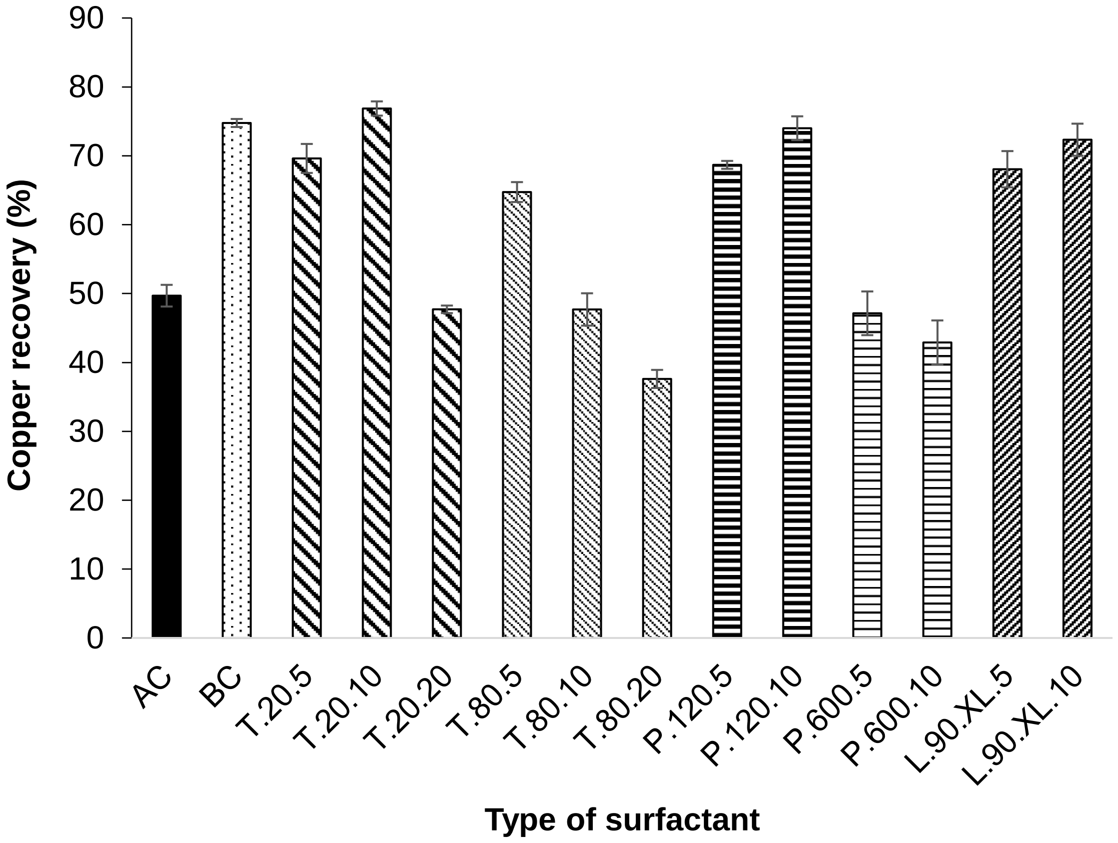

Figure 6-6: Effect of surfactant addition on copper recovery from chalcopyrite concentrate on day 18. AC and BC are abiotic control and biotic control respectively.

6.1.3 Effect of surfactant on cellular attachment to a mineral surface

There is competition between cellular attachment and surfactant adsorption on to an ore surface. Attachment data of thermophilic microorganisms to the chalcopyrite concentrate in the presence of 10 mg L^{-1} surfactant is presented in Figure 6-7, using the approach of Bromfield et al. (Bromfield et al., 2011). In the absence of surfactant, about 96% of the inoculated cells adhered to the mineral surface over the 4 h incubation. The addition of surfactant depressed the cell adhesion in all cases, with more of the microorganisms remaining planktonic. Addition of 10 mg L^{-1} Tween® 20 and Tween® 80 reduced cell attachment from 96% to 46% and 40% respectively. Plurafac® LF 600 (10 mg L^{-1}) reduced attachment to only 26% while more than 50% of cells were able to attach to the ore surface in the presence of Plurafac® LF 120 (10 mg L^{-1}) and Lutensol® XL 90 (10 mg L^{-1}). The results are consistent with the finding of Hiroyoshi et al. (1995) who found that addition of surfactant increased the number of planktonic cells in solution and decreased the attached cells, but still improved copper leaching at a low surfactant concentration.

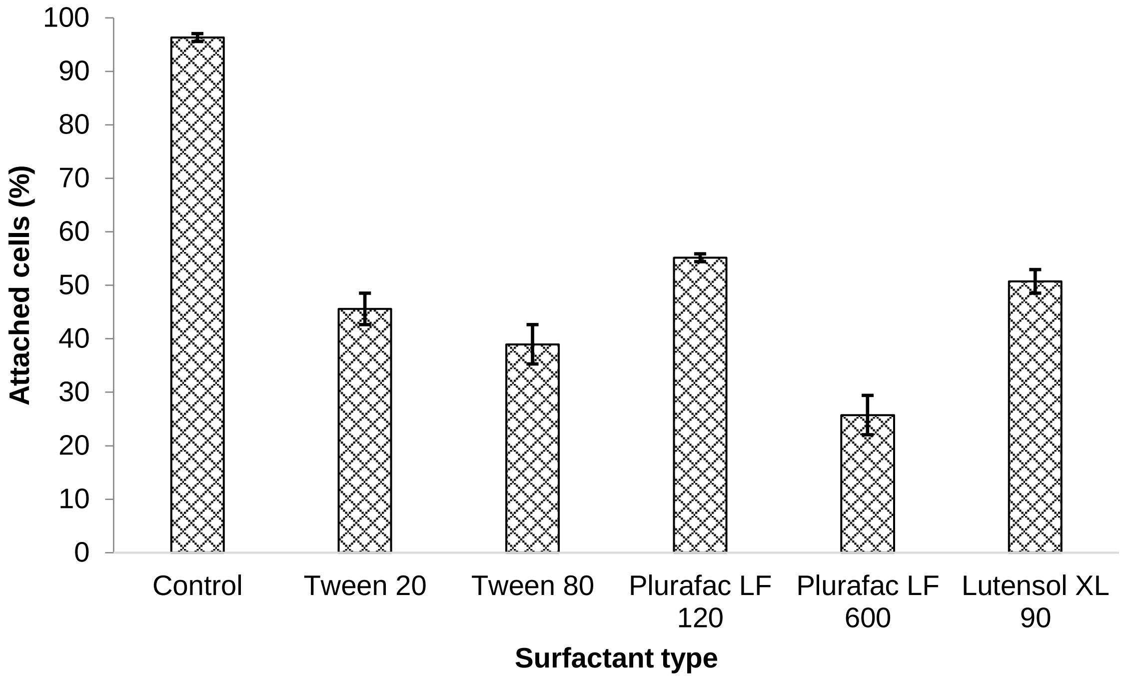

Figure 6-7: Effect of surfactant addition on the attachment of thermophilic bioleaching cells to a chalcopyrite concentrate surface.

6.1.4 Surfactant choice

The thermophilic microorganisms were able to grow and oxidise ferrous ion in the presence of 5 and 10 mg L^{-1} Tween® 20, 5 mg L^{-1} Tween® 80, 5 mg L^{-1} Plurafac® LF 120, and 5 and 10 mg L^{-1} Lutensol® XL 90. Conversely, 10 mg L^{-1} Tween® 80 and Plurafac® LF 120, and 5 and 10 mg L^{-1} Plurafac® LF 600 inhibited both the growth and ferrous ion oxidation by microorganisms. In order to choose the best surfactant and the optimum concentration it is required to consider the chalcopyrite bioleaching results. In chalcopyrite bioleaching, microbial activity and growth was not inhibited when the concertation of different surfactants (including Tween® 20, Plurafac® LF 120, and Lutensol® XL 90) was at 5 to 10 mg L^{-1} and there was even an increase in the copper recovery. However, it was found that 20 mg L^{-1} Tween® 20, 10 or 20 mg L^{-1} Tween® 80, and 5 or 10 mg L^{-1} Plurafac® LF 600 inhibited microbial growth and activity. Surfactants diminish the surface tension of the culture medium and the oxygen concentration at saturation and thus result in a limitation in the microbial activity at high surfactant concentration (Torma et al., 1976).

Although Tween® 20, Plurafac® LF 120 and Lutensol® XL 90 at 10 mg L^{-1} showed good performance in terms of copper recovery, Tween® 20 at 10 mg L^{-1} was selected as the best surfactant. This was because Tween® 20 was the only surfactant in whose presence microorganisms were able to convert ferrous ion to ferric ion and be active in the ferrous ion oxidation experiment in the presence of 10 mg L^{-1} surfactant.

This choice is supported by many previous research studies. In Sandoval et al. (1990), the addition of the Tween® 20 (10 mg L^{-1}) improved copper extraction from chalcopyrite when sufficient Fe^{3+} was present in the leaching solution. They found that Tween® 20 additions beyond 25 mg L^{-1} did not increase leaching. Yields of copper from chalcopyrite were increased from 38% to 85% in the presence of 0.001% Tween® 20 compared with a biotic control (Duncan and Trussell, 1964; Duncan et al., 1964). In other studies, Liu et al. (2015) used Tween® 20 (0.1 and 0.25 g L^{-1}) to improve cobalt bioleaching in shake flask experiments. The cobalt leaching efficiency was boosted by more than 21% and the copper leaching efficiency increased by more than 8% when 0.1 g L^{-1} Tween® 20 was added. Moreover the leaching time could be reduced by more than 15% (Peng et al., 2012). Hiroyoshi et al. (1995) reported that adding 20 mg L^{-1} of Tween® 20 was favourable for the copper extraction from chalcopyrite. The author believed that indirect leaching played the main role in the bioleaching, and the catalytic effect was attributed to the decrease in the bacterial adhesion to the chalcopyrite surface. The Tween® 20 concentrations used vary widely across the literature (0.0005 – 0.012 %) which could be due to differences in operating conditions, especially temperature. All previous studies have been done in the range of 25 – 50 °C.

6.2 Mini-column leaching

Pregnant leaching solution pH, redox potential, and Fe^{2+} and Fe^{3+} concentrations were monitored over the experimental period to evaluate the surfactant effect on iron leaching from pyrite (waste rock) and copper from chalcopyrite (low-grade agglomerated ore). Tween® 20 was used at a concentration of 10 mg L^{-1}, based on the shake-flask experiment findings. The mini-columns were operated at conditions suited to the two mineral types, as presented in the previous chapters (Section 3.8.2).

6.2.1 Pyrite

The results for the pyrite ore are presented in Figure 6-8. The overall trends in the pyrite ore effluent chemistry are described in the subsequent chapter. After introducing the feed solution containing Fe^{3+}, the pH decreased to around 1.0. After day 35 the pH fluctuated between 1 and 1.05. The pH in the effluent of the mini-column without surfactant was 0.01 to 0.03 pH units lower than in the mini-column with surfactant. Thus, more acid was produced during leaching when surfactant was added. The mini-column with surfactant also exhibited a slightly higher pyrite oxidation rate, with a lower redox potential (6 to 10 mV) and consequently corresponding low amount of Fe^{3+} observed. Addition of surfactant therefore appeared to have a positive effect on pyrite leaching.

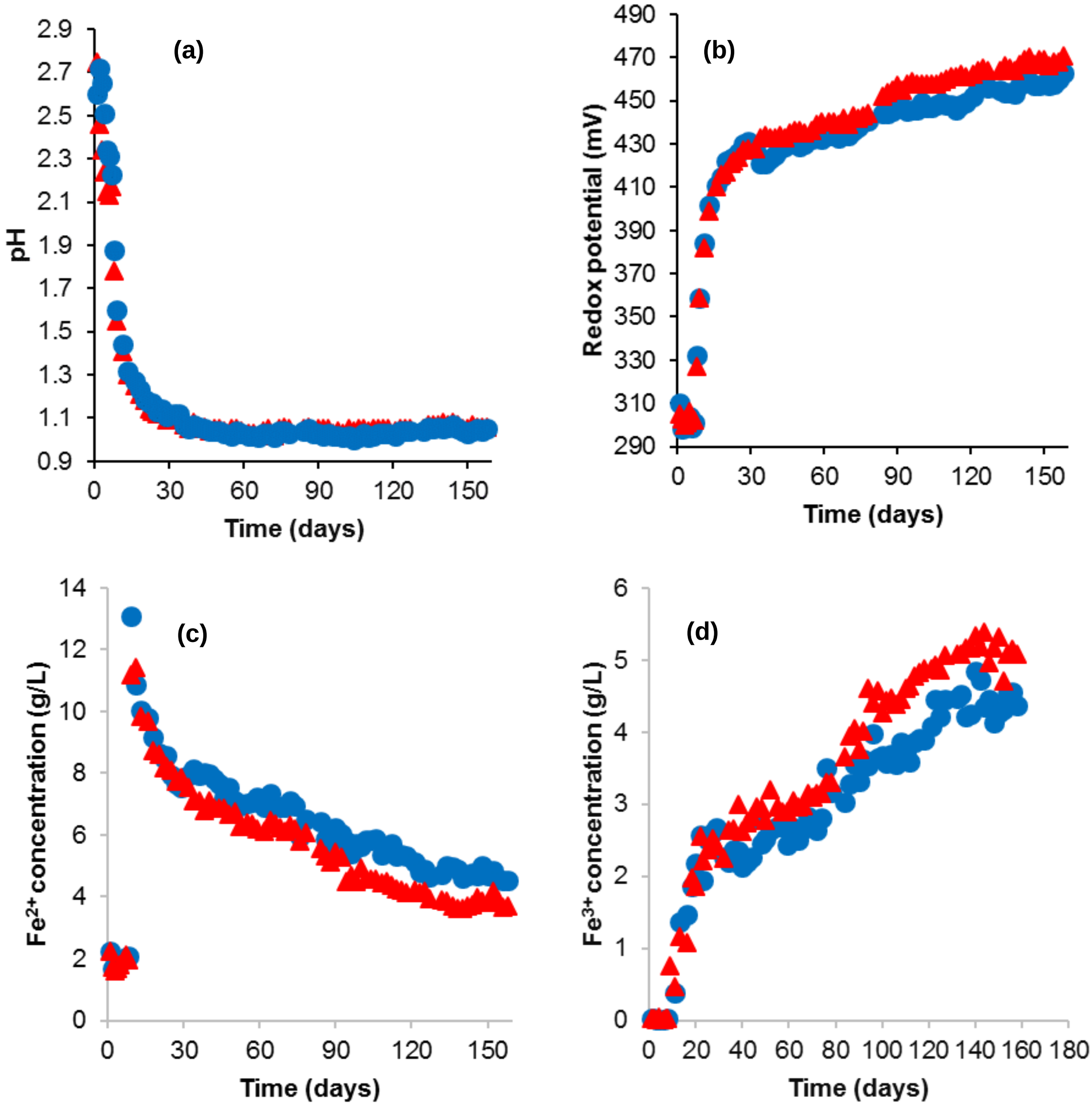

Figure 6-8: Changes of (a) pH profile, (b) redox potential (mV), (c) ferrous ion concentration (g L^{-1}) and (d) ferric ion concentration (g L^{-1}) during leaching of pyrite-containing waste rock at 65 °C with (●) and without (▲) 10 mg L^{-1} Tween® 20.

The cumulative iron extraction from the waste rock containing pyrite was the same in both the mini-columns with and without surfactant until day 18, as shown in Figure 6-9. Then, the difference in iron recovery increased between the two mini-columns, with the system without surfactant performing best. This was likely due to a surfactant layer formed on the hydrophobic ore surface leading to a decrease in leaching in the mini-column with surfactant. A maximum extraction difference of 5.5% was obtained around day 50. Subsequent to this, the gap between the two iron recovery curves steadily reduced until end of the experimental period. A final cumulative iron recovery of 70% was found for both mini-columns (Figure 6-9).

Change in sulphide mineral grain content as a function of distance from the particle surface for whole mini-column at the beginning and end of experiment as well as the sum of the three tracked sections are illustrated in Figure 6-10 and Figure 6-11 respectively. In spite of the similar recoveries, a higher maximum penetration distance of 2.9 mm was observed in the mini-column with surfactant, compared to 2.6 mm without. The pyrite was leached to a distance of 1.5 mm from the ore surface during the first 11 days. The penetration distance had increased to 2.7 mm by day 45. Subsequently, there was a 0.2 mm increase in the penetration distance by 114 days until end of the experiment. The increase in penetration distance is consistent with the surfactant reduction of solution surface tension, enabling a deeper penetration in the ore particles (Vest et al., 2009).

The similar leaching recoveries, even with the increased penetration distance, can be attributed to the relatively high total pyrite content of the sample (30%) and the fact that only a small percent of the pyrite was found beyond 2.6 mm from the surface. Therefore, the availability of mineral grains was not a critical issue and the surfactant addition effect on the leaching was slight.

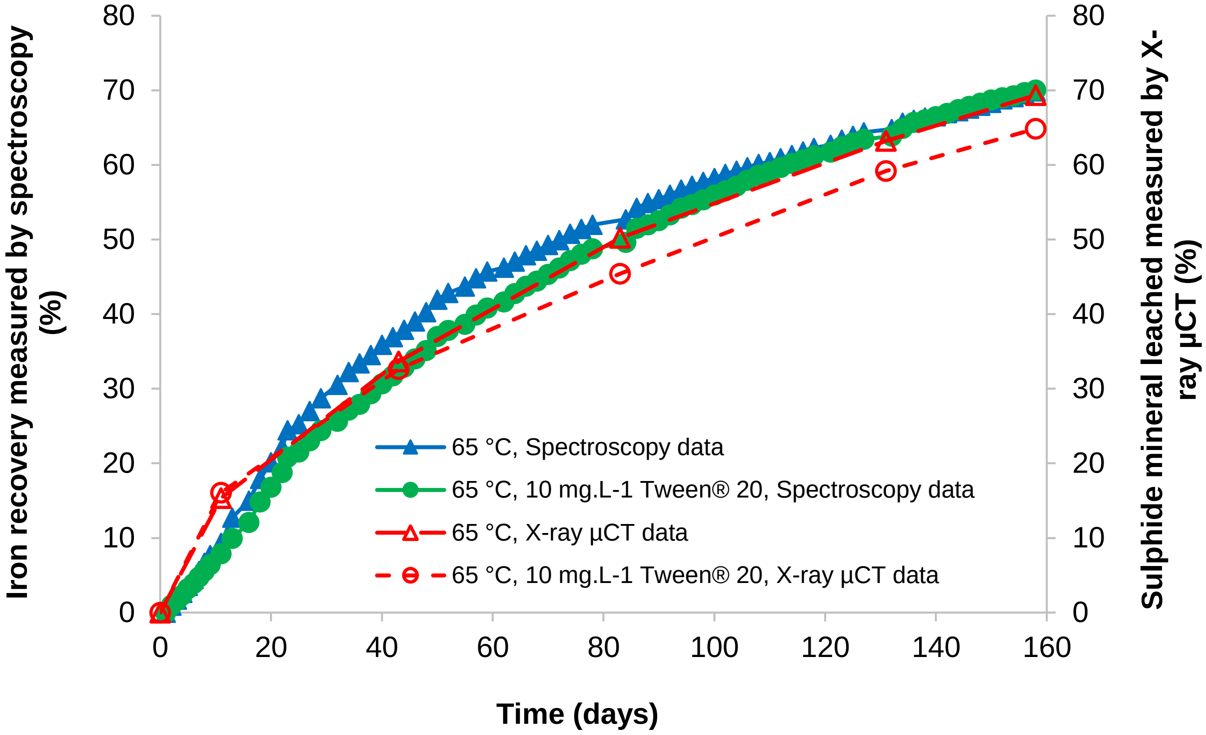

Figure 6-9: Comparison of iron recovery from the pyrite-containing waste rock measured by spectroscopy (solid lines) and sulphide mineral leached based on image measurement (dashed lines).

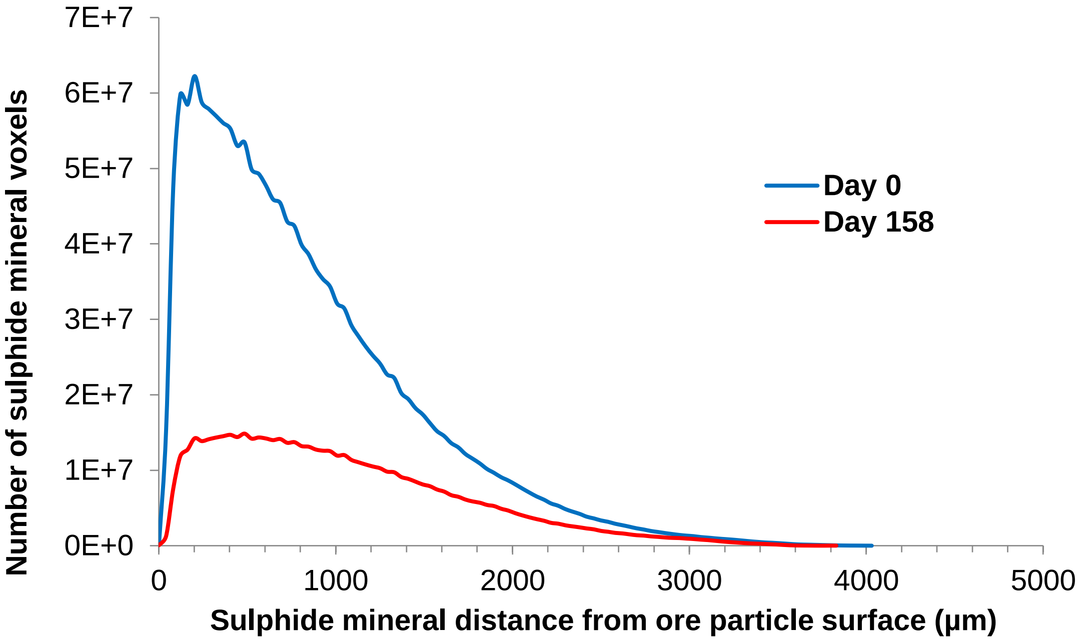

Figure 6-10: Change in the distribution of sulphide minerals in the pyrite-containing waste rock as a function of position and time for the mini-column with 10 mg L^{-1} Tween$^{®}$ 20 added to the feed solution. The uncertainty measurement in grain distance from the ore surface is ±40.2 µm.

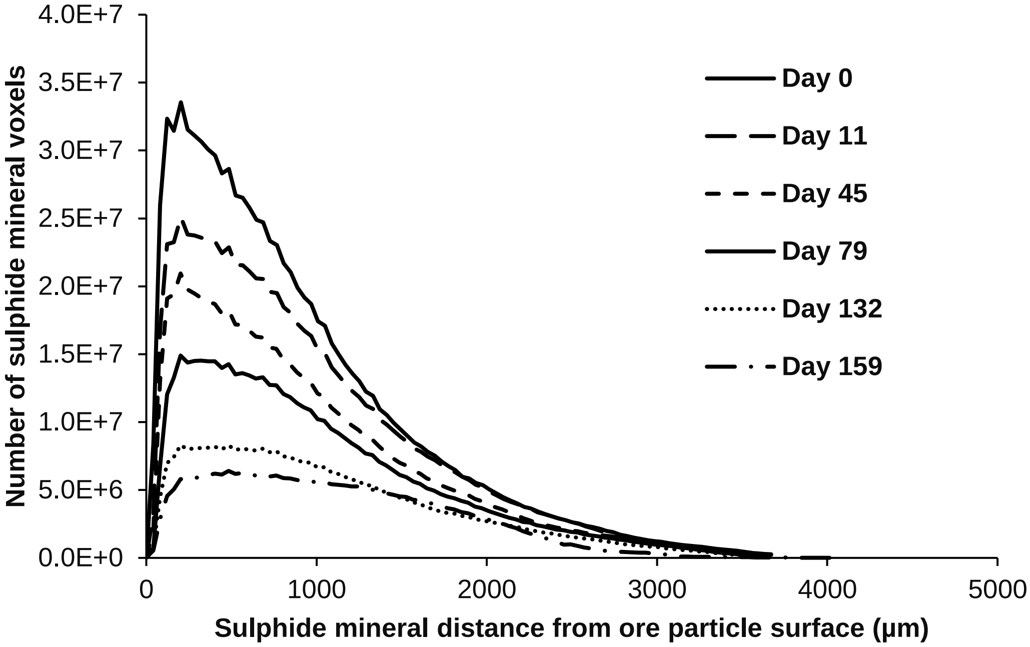

Figure 6-11: Change in the distribution of sulphide minerals as a function of position and time for the pyrite-containing waste rock mini-column with 10 mg L^{-1} Tween® 20 added to the feed (the sum of three tracked sections). The uncertainty measurement in grain distance from ore surface is ±40.2 µm.

The cumulative target metal recoveries at different distances from the ore particle surface for the mini-columns operated with and without surfactant are given in Figure 6-12. There was a decrease in pyrite leaching with increasing distance from the ore surface. The downward slope from the ore surface for both mini-columns is indicative of an increasing effect of diffusion control on the rate of recovery. This is consistent with the existence of lower porosities further from the agglomerate surface (refer to Chapter 7). In the pyrite leaching system, pyrite recovery was the same in the systems with and without surfactant for distances less than 1 mm from the surface. This value is close to the distance at which the higher agglomerate particle porosity region ends, indicating that agglomerate rims of fine particles were circa 1 mm thick. Beyond this depth, the surfactant resulted in higher recoveries. The gap between the two curves became wider with increasing the distance from the ore surface. The results therefore confirmed that there is potential advantage to surfactant addition for recovery of mineral grains at deeper zones of the particles of this ore. They also suggest that the surfactant benefit applies to the larger ore particles, rather than more porous fine agglomerate regions (clusters or rims).

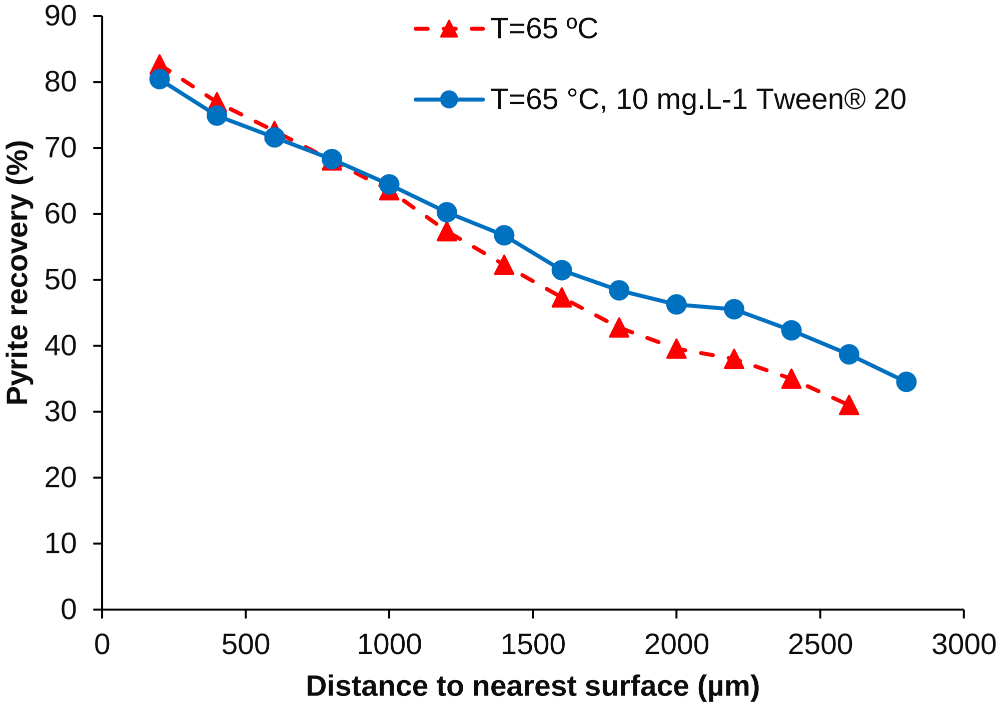

Figure 6-12: Comparison of the pyrite recovery at different distance to surface values for the pyrite-containing waste rock.

6.2.2 Chalcopyrite

The solution chemistry results for the chalcopyrite ore leaching with surfactant are given in Figure 6-13. The trends in the chalcopyrite ore effluent chemistry are described in the subsequent chapter. No difference was observed in the effluent chemistry between the columns without and with surfactant. This is likely as the chalcopyrite content of the ore was so low and thus reagent consumption was small.

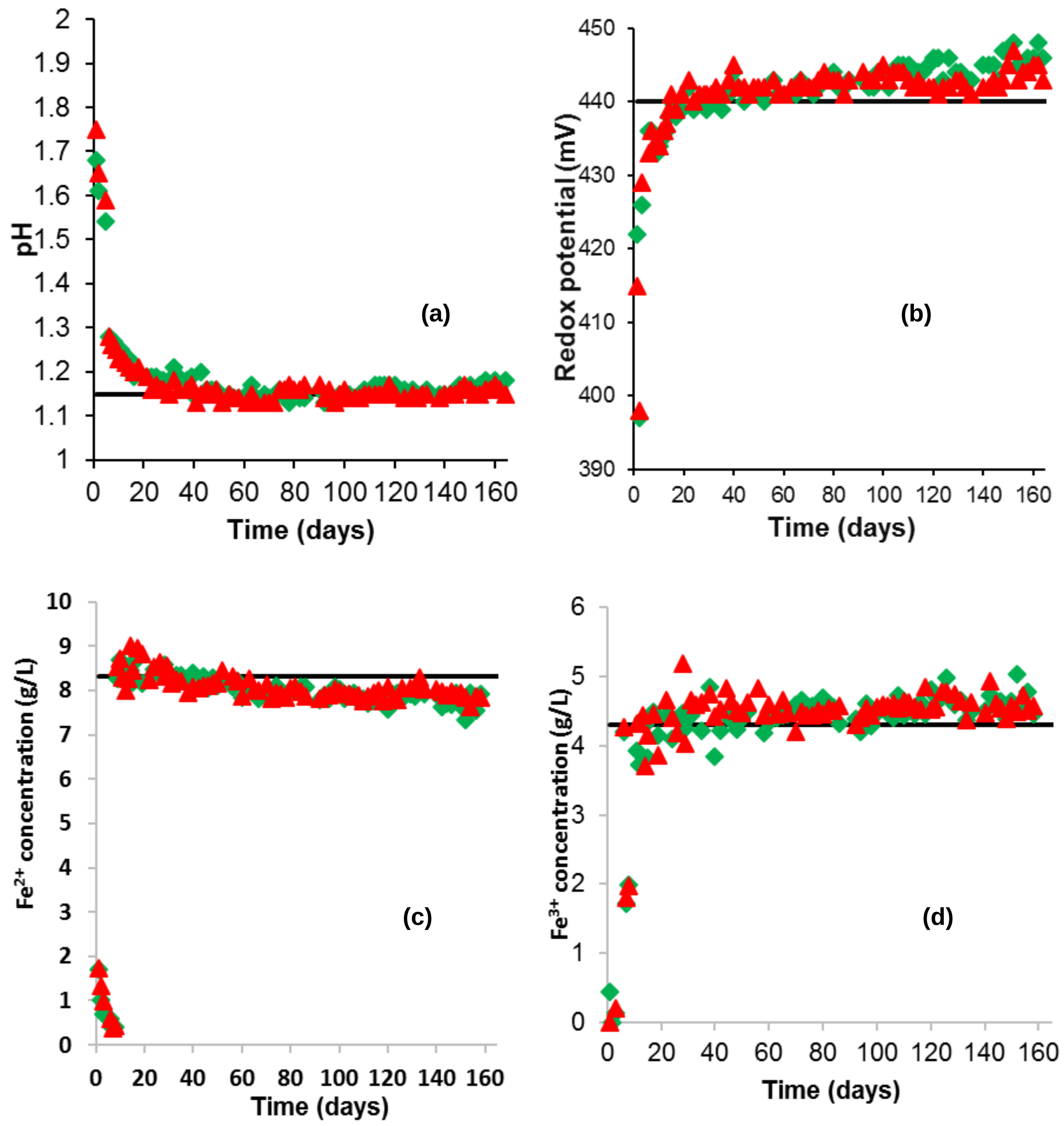

Figure 6-13: Changes of (a) pH profile, (b) redox potential (mV), (c) ferrous ion concentration (g L^{-1}) and (d) ferric ion concentration (g L^{-1}) during leaching of low-grade chalcopyrite ore at 65 °C. Feed solution (—), without surfactant (♦), and with 10 mg L^{-1} Tween® 20 (▲).

The cumulative copper recoveries for the chalcopyrite ore mini-columns with and without surfactant are shown in Figure 6-14. When 10 mg L^{-1} Tween® 20 was added, 16% copper recovery was achieved over the first 16 days, the same as from the mini-columns without surfactant. Thus, there was no evident benefit to surfactant addition during the initial period of rapid leaching. In the period subsequent to this until day 47, the column without surfactant leached at a slightly faster rate by both analysis measures. By the X-ray μCT measurement, this resulted in a better overall performance for the column without surfactant, with 63% sulphide mineral volume reduction obtained for the mini-column with surfactant compared with 67% without surfactant by day 165. However, the copper recovery data shows that from day 58 onwards, the copper recovery rate was greater in the mini-column containing surfactant. By day 165, 68% of the copper had been recovered in the mini-column containing surfactant versus 64% in the mini-column without. According to Figure 6-15, the penetration distance for the mini-column with 10 mg L^{-1} Tween® 20 surfactant was even greater at 2.9 mm.

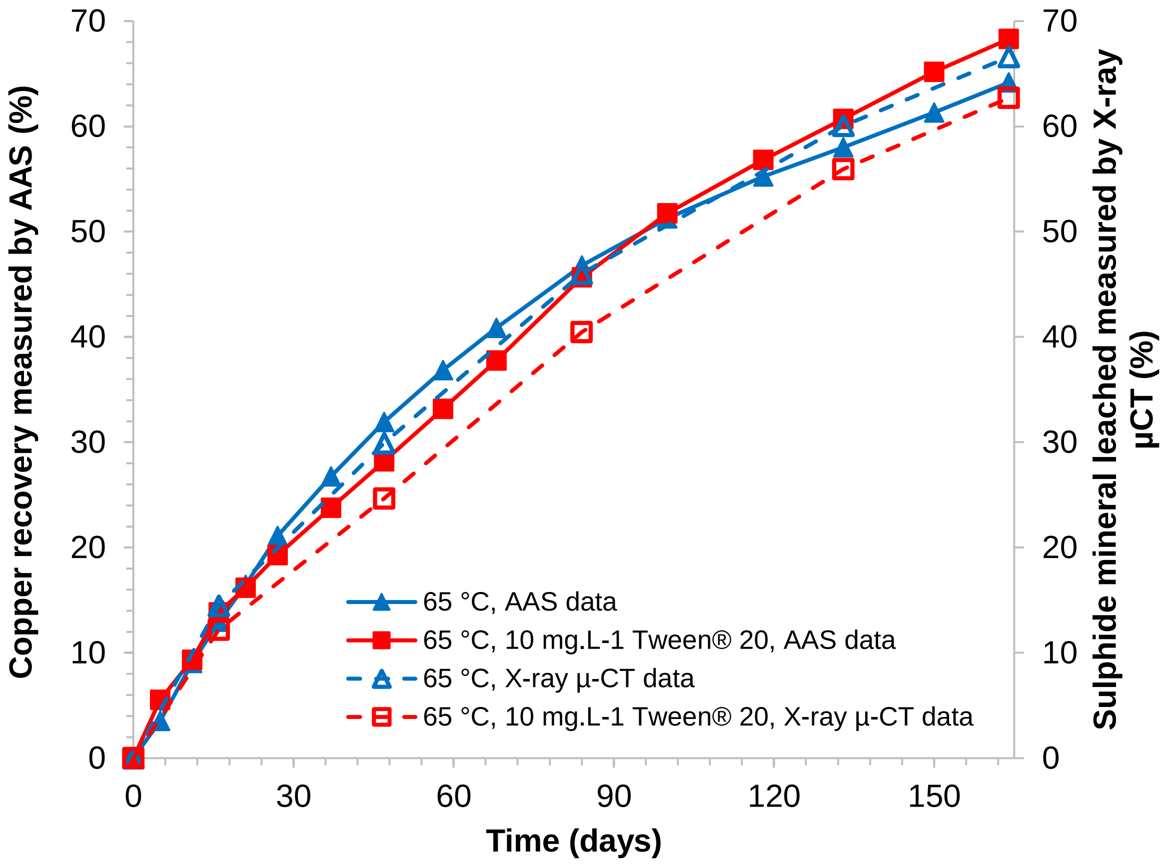

Figure 6-14: Comparison of copper recovery from the low-grade chalcopyrite ore, measured by AAS (solid lines) and sulphide mineral leached based on image measurement (dashed lines).

The fact that the copper recovery rate was at times slower in the mini-column with surfactant was counter to expectations. Surfactants form a layer on the mineral surface, the thickness of which depends on the surfactant concentration in the solution and its molecular structure. The adsorbed layer has been reported to depress the diffusion of leaching reagents from solution to the mineral surface and cause the depression in the chemical leaching (Hiroyoshi et al., 1995). This suggests that while the availability of the mineral is not rate limiting, presence of surfactant in the leaching solution can reduce the copper recovery rate. However, as the leach progressed the difference in the copper recovery decreased, presumably as the readily available mineral was depleted. The two mini-columns had the same copper recovery on day 100 which was followed by a higher recovery in the mini-column with surfactant. At the end of the experimental period, the presence of surfactant resulted in a higher overall copper recovered of approximately 4%. The data presented in Figure 6-15 confirmed that the penetration distance for the mini-column with surfactant was 400 µm higher than the mini-column without surfactant. Thus, the surfactant was successful in increasing the affinity between the solid and liquid by reducing the surface tension, allowing acid to ingress further into sub-surface regions of ore particles, and ultimately improving the final copper recovery. Therefore, sulphide mineral dissolution for the mini-column with surfactant was higher than the mini-column without surfactant when the availability of sulphide mineral grains was rate limiting.

The sum of three tracked sections' sulphide mineral distribution at different time points for the mini-column operated at 65 °C with 10 mg L^{-1} surfactant is shown in Figure 6-16. The mineral grain recovery to a distance of 1.5 mm from the particles' surface was recorded after 15 days and even 45 days. Then, the penetration distance increased to 2.3 mm by day 83, further increasing to about 2.6 mm on day 132. The reduction in the mineral content at deeper zones was high and there is a sharp peak at all times close to the particle edge. This was not seen in the mini-column without surfactant. It suggests that sub-surface leaching was better distributed throughout the ore volume throughout the leaching period in the presence of surfactant.

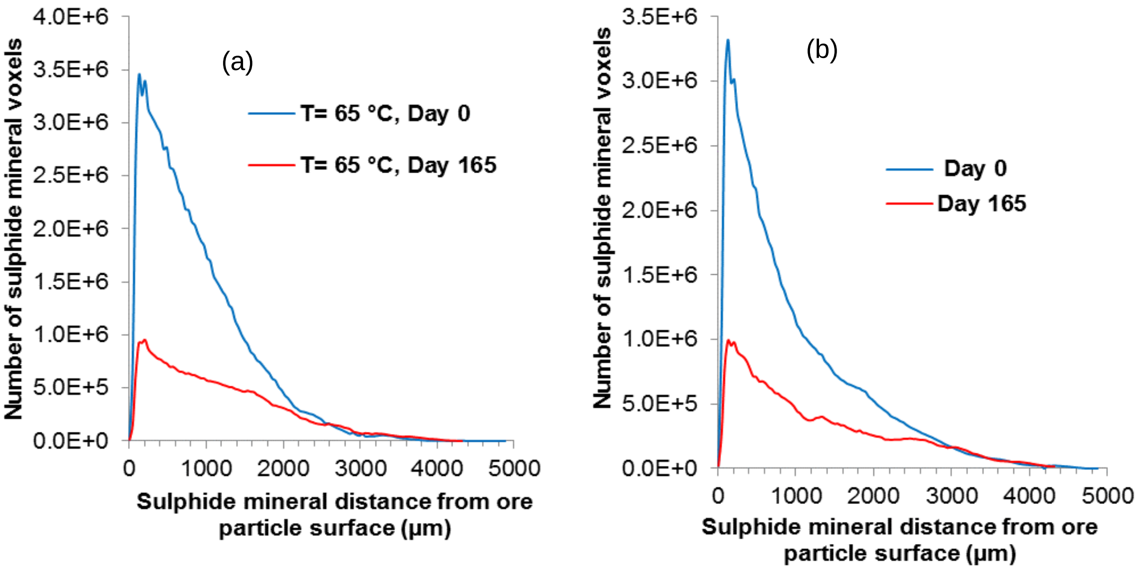

Figure 6-15: Change in distribution of sulphide minerals as a function of position and time for the low-grade chalcopyrite ore mini-column without (a) and with (b) 10 mg L^{-1} Tween® 20 added to the feed. The uncertainty measurement in grain distance from the ore surface is ±40.2 µm.

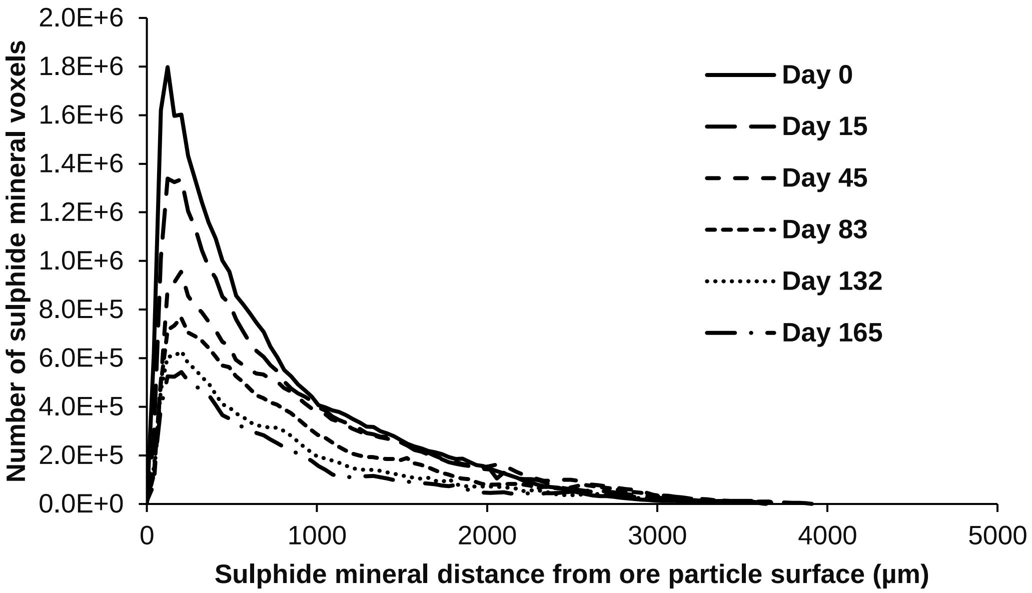

Figure 6-16: Change in distribution of sulphide minerals as a function of position and time for the low-grade chalcopyrite ore mini-column with 10 mg L^{-1} Tween® 20 added to the feed (the sum of three tracked sections). The uncertainty measurement in grain distance from the ore surface is ±40.2 µm.

The cumulative target metal recoveries at different distances from the agglomerated ore particle surface for the mini-columns containing the chalcopyrite ore and operated with and without surfactant are provided in Figure 6-17. The copper recovery was slightly higher up to a distance of 1.4 mm for the column without surfactant than with surfactant. However, the copper recovery decreased rapidly and substantially at deeper distance values in the column without surfactant. There was a more gradual reduction in copper recovery, from 70.02% to 48.50%, for the mini-column with surfactant in the distance range to 2.2 mm, followed by a sharp decrease. The gradual decline meant that the recovery was greater in the system with surfactant at distances of 1.6 mm and beyond. This confirmed that addition of surfactant increased copper recovery in regions further from the ore surface. The sharper recovery drop beyond 2.2 mm had a similar recovery rate decrease to the mini-column without surfactant, which suggests that the surfactant influence is only up to a certain critical distance.

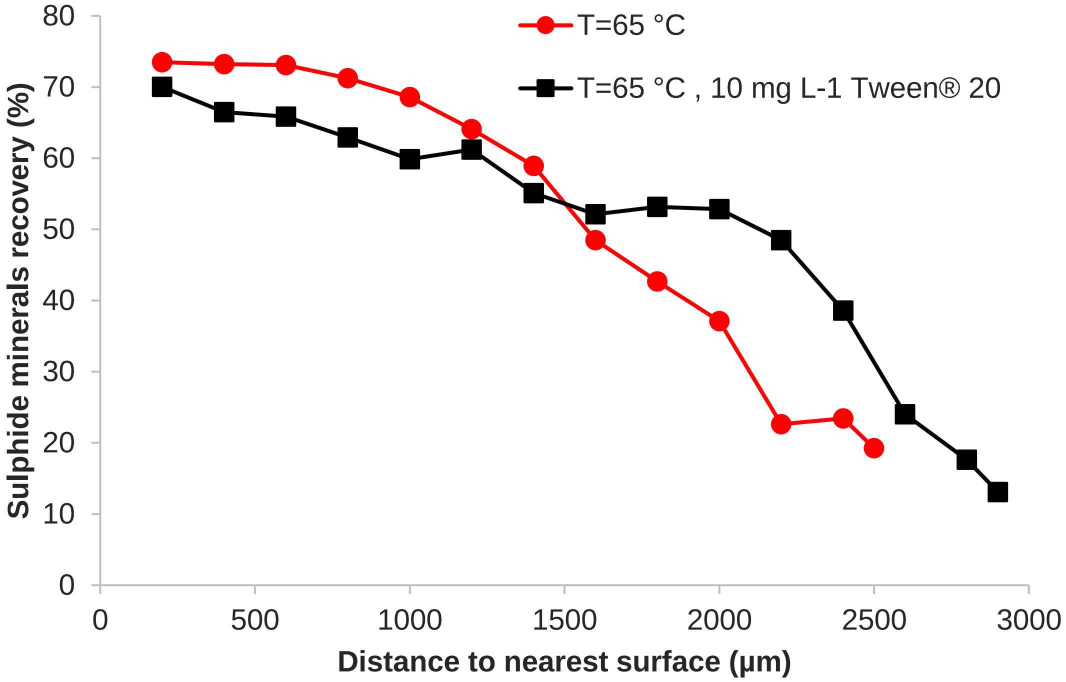

Figure 6-17: Comparison of the copper recovery at different distance to surface values for the low-grade chalcopyrite ore with and without surfactant.

Addition of surfactant into the feed solution thus appears to have had the same influence on iron recovery from pyrite as on copper recovery from chalcopyrite. The surfactant initially decreased target metal recovery due to the formation of a layer on the ore surface during the period when the availability of mineral grains was not the rate limiting factor, but rather reaction kinetics was rate limiting. The surfactant later improved the metal recovery rate when the diffusion kinetics become rate limiting in the system. Inclusion of surfactant was also evidenced to improve the penetration of leaching, through higher penetration depths and improved recoveries at greater depths. However, no significant difference in the final recoveries of the target metals was observed in the systems with and without surfactant. Differences may have emerged if the columns were run for longer periods of time, due to the access to deeper mineral grains eventually outweighing the apparent decrease in the leaching kinetics with surfactant addition. Vest (2009) have demonstrated that addition of 100 mg L^{-1} non-ionic surfactant in 2% H_2SO_4 leaching solution (EVD61549) improved copper recovery from a low-grade copper oxide ore (Cu=0.916%) by 3.5% to 5.4% over 36 days under unsaturated conditions. The addition of 100 mg L^{-1} fatty alcohol alkoxylate type wetting agents in ferric sulphate chalcopyrite leaching (13-19 mm particle size distribution) was investigated by Schmuhl et al. (2011). Addition of surfactant resulted in approximately 2% copper recovery enhancement at 25 °C over the 14 day experimental period (saturated conditions). Shah (2017) used two surfactants, MC1000 (50 mg L^{-1}) and DP-HS-1002 (25 mg L^{-1}) provided by BASF, to improve copper recovery from a copper oxide ore. The ore particle size distribution was: -0.245 mm (19.5%), 0.254-6.35 mm (20.09%), 6.35-12.70 mm (19.31%), 12.70-19.05 mm (19.72%) and 19.05-25.40 mm (21.38%). The leaching was done using acidified solution (1% H_2SO_4) for 54 days at saturated conditions. The columns with surfactant were both shown to have achieved approximately 91% to 92% of copper extraction as compared to 89% for the column without surfactant. In all cases there is only slight improvement in copper recovery reported, consistent with the results reported in this study. However, previous work only assessed the effect of surfactant on copper recovery using chemistry results. According the results, it was found that the improvement came from increased penetration difference and it was most significant when the easy to leach material is depleted.

6.3 Summary

The presence of surfactants in the lixiviant solution has the potential to improve solution penetration into small pores and cracks of large ore particles by decreasing surface tension, thereby enhancing access of lixiviant to internal mineral grains and associated metal recovery from low grade sulphide ores.

Firstly, the effect of surfactants on the growth and activity of microorganisms implicated in bioleaching was considered. This is because of the microorganisms' principal role in the regeneration of leaching reagents and facilitating metal recovery from an ore. The effect of surfactant addition on ferrous ion oxidation and microbially-mediated leaching of chalcopyrite by a mixed thermophilic microbial culture was investigated using five non-ionic surfactants: Tween® 20, Tween® 80, Plurafac® LF 120, Plurafac® LF 600 and Lutensol® XL 90 at concentrations of 5, 10 and 20 mg L^{-1}. The addition of 5 and 10 mg L^{-1} Tween® 20 showed no negative effect on microbial ferrous ion oxidation and chalcopyrite bioleaching. Further, its presence was observed to reduce the initial leaching lag time. Microbial ferrous ion oxidation was inhibited in the presence of 10 mg L^{-1} Plurafac® LF 120 while a partial inhibition was observed with 10 mg L^{-1} Lutensol XL 90. Plurafac® LF 600 at 5 and 10 mg L^{-1} and Tween® 80 at 10 mg L^{-1} inhibited microbial growth completely, and thereby leaching, hence precluding it from a role in bioleaching.

The data suggested that an optimal surfactant concentration exists at which the copper recovery is maximised, and below or above which it may be reduced. A higher molecular weight surfactant resulted in the reduction of the copper leaching efficiency, hence recommending lower weight surfactants. It was concluded that Tween® 20 at 10 mg L^{-1} had the best performance in terms of microbial activity and copper recovery and it was used in the mini-column leaching experiments.

In the mini-column experiment, adsorption and formation of a layer on the ore surface led to reduction of target metal recovery during the period when the availability of mineral grains was not the rate limiting factor, but rather reaction kinetics were rate limiting. However, the surfactant had a positive impact on the process performance when the diffusion kinetics become rate limiting in the system. Enhancement of maximum penetration distance was another phenomenon which occurred in the system. Thus, a benefit of inclusion of surfactant was improvement of recoveries at greater depths.

7 Ore type and temperature effect on non-surface mineral grain leaching

This chapter focuses on the ore type and temperature effect on non-surface mineral grain leaching. Firstly, bulk leaching measurements obtained for malachite at 30 °C, pyrite 37 °C and 65 °C, and chalcopyrite at 37 °C and 65 °C are presented. This is followed by examination of the differences in non-surface mineral grain leaching, target metal recovery and penetration distance for the three different ores at the various temperature conditions. All experiments in this chapter were conducted in the flow-through mini-columns (OD= 24 mm).

7.1 Ore type

Dissolution kinetics strongly depend on an ore's nature, including its mineral composition, texture, porosity and its origin (Ghorbani et al., 2016). To investigate the importance of ore type, three different ores were selected to examine the non-surface grain leaching: a malachite ore, a chalcopyrite ore and a waste rock containing pyrite. The different mineral ores were chosen due to their differing leaching mechanisms and kinetics and thus anticipated different leaching rate controlling limitations. In addition, the target minerals were locked in differing gangue matrices. The same particles size distribution (<0.25 mm, 0.25 – 1 mm, 1 – 2 mm, 2 – 5.6 mm, 5.6 – 8 mm, 8 – 16 mm) was used for all three ores.

The main copper minerals in the malachite ore were malachite (6.82%) and bornite (2.44%). Malachite is a basic copper carbonate mineral with the nominal formula $Cu_2(OH)_2CO_3$ that contains 57.5% copper. It is known to be easily soluble in dilute acids (Nicol, 2018). Bornite (Cu_5FeS_4) is secondary sulphide minerals which can be leached using oxygen as oxidant in acidified solution, although it is much slower oxidant (Pesic and Olson, 1984). Quartz (76.8%) was the dominant gangue mineral.

Pyrite, as a secondary sulphide, is oxidized in water by ferric ions and dissolved oxygen to form a very acidic and heavy metal-laden leachate. It is a major contributor to acid rock/mine drainage (which is biologically mediated) and can also have positive or negative influence on extraction of other sulphide minerals from an ore body. The waste rock used in the study contained approximately 30% pyrite. The main gangue minerals were muscovite (29.57%) and quartz (16.53%).

Finally, the more complex low-grade chalcopyrite ore was chosen as it is the most difficult and reluctant copper mineral for leaching and commercially reliant on inclusion of bioleaching microorganisms. The ore contained much less leachable mineral, comprising only 1.52% chalcopyrite, 0.66% pyrite and 0.3% other sulphide minerals. The sulphide minerals were disseminated in gangue minerals including quartz (37.57%), K-feldspar (37.47%) and muscovite (19.06%).

7.1.1 Porosity

The porosity of ore influences the leaching of non-surface mineral grains because it determines if mineral grains inside the ore are accessible to leaching solution (Dhawan et al., 2013). Furthermore, agglomeration results in the formation of a porous structure between particles but within the agglomerate.

3D views of the internal porosity of volumes of the agglomerated pyrite, agglomerated and non-agglomerated chalcopyrite, and agglomerated malachite ores are presented in Figure 7-1. The number of pores is plotted as a function of distance from the ore particle surface in Figure 7-2. The average measured intra-porosities were 1.06% for the agglomerated malachite, 0.066% for the agglomerated pyrite, 0.43% for the agglomerated chalcopyrite and 0.0094% for the non-agglomerated chalcopyrite. The substantial differences observed in the pores' distribution for the three different ores confirmed the importance of the type of ore and its mineralogy on potential lixiviant contact.

Accessibly of target mineral grains was anticipated to be the highest for the malachite ore due to its relatively high porosity. A good porosity was maintained even beyond 3000 µm from the ore surface, indicating that the ore itself was porous in addition to high porosity agglomerate rims having formed. The maximum porosity was observed circa 750 µm distance from ore surface.

The pyrite agglomerates had the lowest porosity, with the maximum also occurring earlier at circa 500 µm. A very low porosity was recorded beyond 1500 µm from the surface. The low porosity of these agglomerates could be because pyrite is hydrophobic at pH values lower than 4 (Kocabag et al., 1990). This would have caused decreased adsorption of acidified solution onto the ore and consequently affected the formation of bridges and porous structures between fine particles as well as fine particles around large particles.

The porosity of the agglomerated chalcopyrite ore was less than half that of the malachite, but was two orders of magnitude larger than the pyrite. The maximum distribution of pores was placed around 500 µm from the ore edge. The porosity decreased with increasing distance value until circa 2000 µm. The non-agglomerated chalcopyrite porosity results showed that the ore itself had a very low porosity. Therefore, the porosity seen in the agglomerated ore was because of the pores formed between the aggregated particles, confirmed by its ‘rim’ location. Quaicoe et al. (2013) investigated the effect of ore mineralogy and particle size distribution on required binder dosage, behaviour of agglomeration and product properties. It was observed that binder dosages required for effective agglomeration were greater for clays than oxide minerals. Quartz, kaolinite and smectite displayed slower growth behaviour in comparison with hematite. It was also demonstrated that the pore volumes (porosities) of the oxide granules were noticeably more than those of the clay granules. This is consistent with the high porosity of the malachite agglomerate versus the chalcopyrite agglomerate.

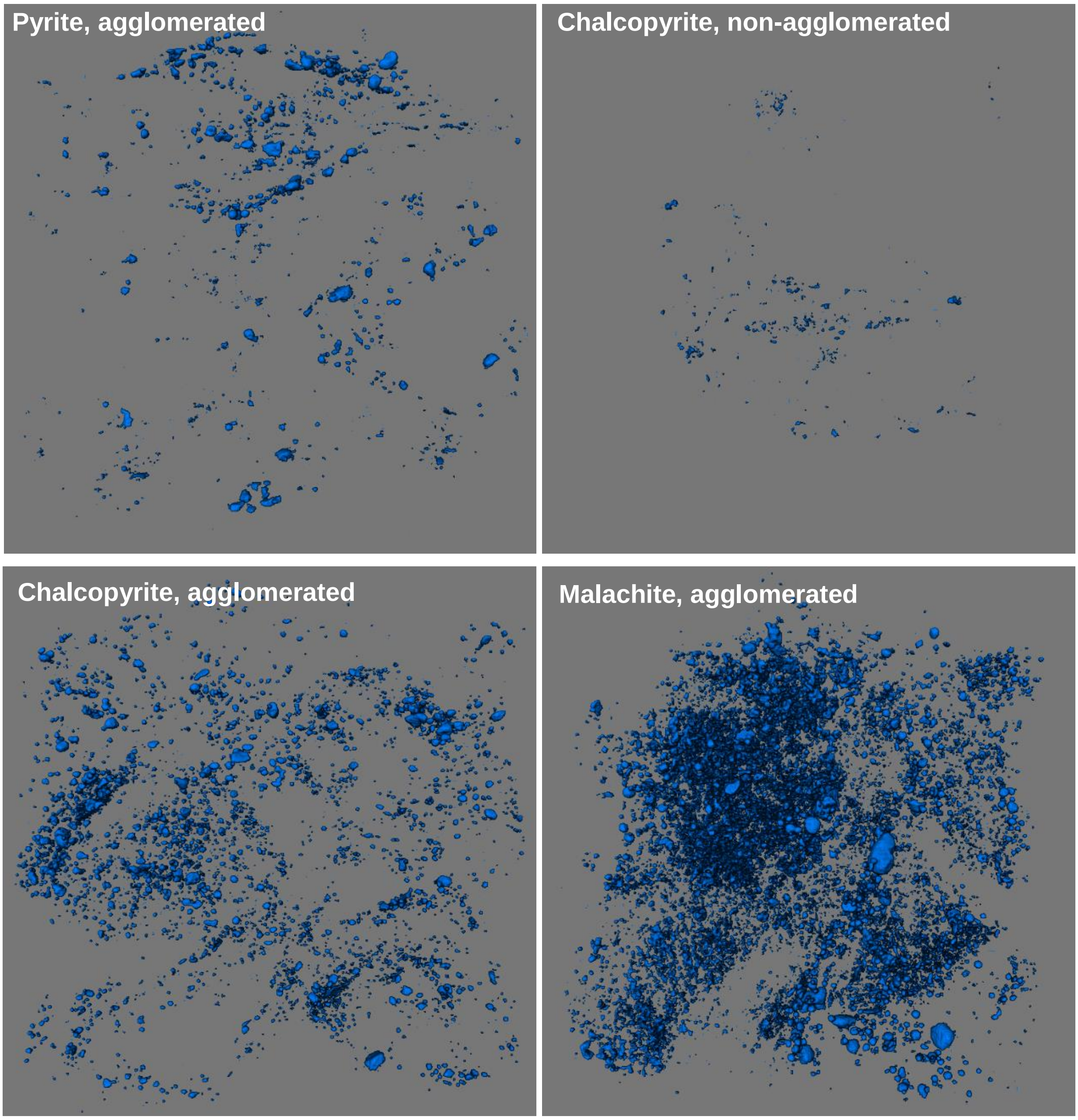

Figure 7-1: 3D views of the pore distribution for the different ores.

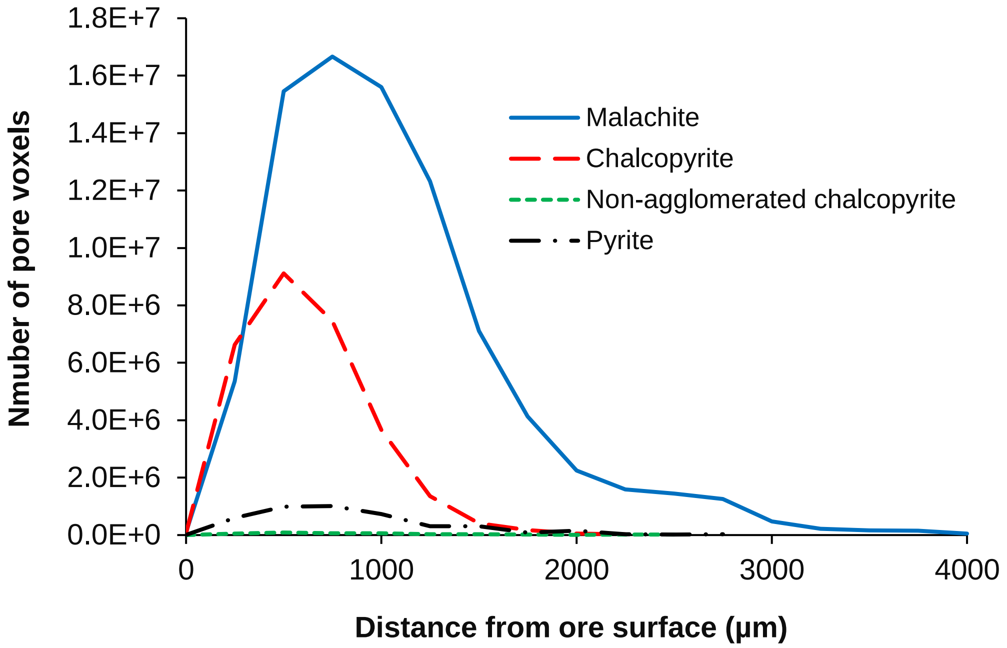

Figure 7-2: Comparison of the pore distribution for the various ores at different distance to surface values. The uncertainty in the pore distance from the ore surface is ±40.2 μm.

7.2 Leaching results

7.2.1 Malachite

Copper oxide minerals such as malachite ($Cu_2(OH)_2CO_3$) contain copper in the divalent state. These are completely soluble in sulphuric acid at room temperature. Typical reaction of malachite with sulphuric acid is as follows (Nicol, 2018):

$$Cu_2(OH)_2CO_3 + 2H_2SO_4 \rightarrow 2CuSO_4 + CO_2 + 3H_2O \qquad (7\text{-}1)$$

The effect of leaching time on the dissolution of malachite is shown in Figure 7-3. Clearly, the copper recovery increased with increasing leaching time with the initial dissolution of copper being very rapid. After 10 days, about 70% copper recovery had been achieved. This increased to 87% after 26 days. According to Figure 7-4, there was a rapid decrease in pH from circa 4 to 1.84 during first 6 days, after which the pH gradually falls to 1.22 at end of the experiment. The rate of decrease in pH was thus consistent with increase in copper recovery. The malachite ore contained 2.44% bornite based whose leaching rate using acidified solution is slow (Pesic and Olson, 1984). The slower leaching and hence flattening off of the copper recovery curve towards the end of the leaching period could be attributed to the presence of the bornite in the ore.

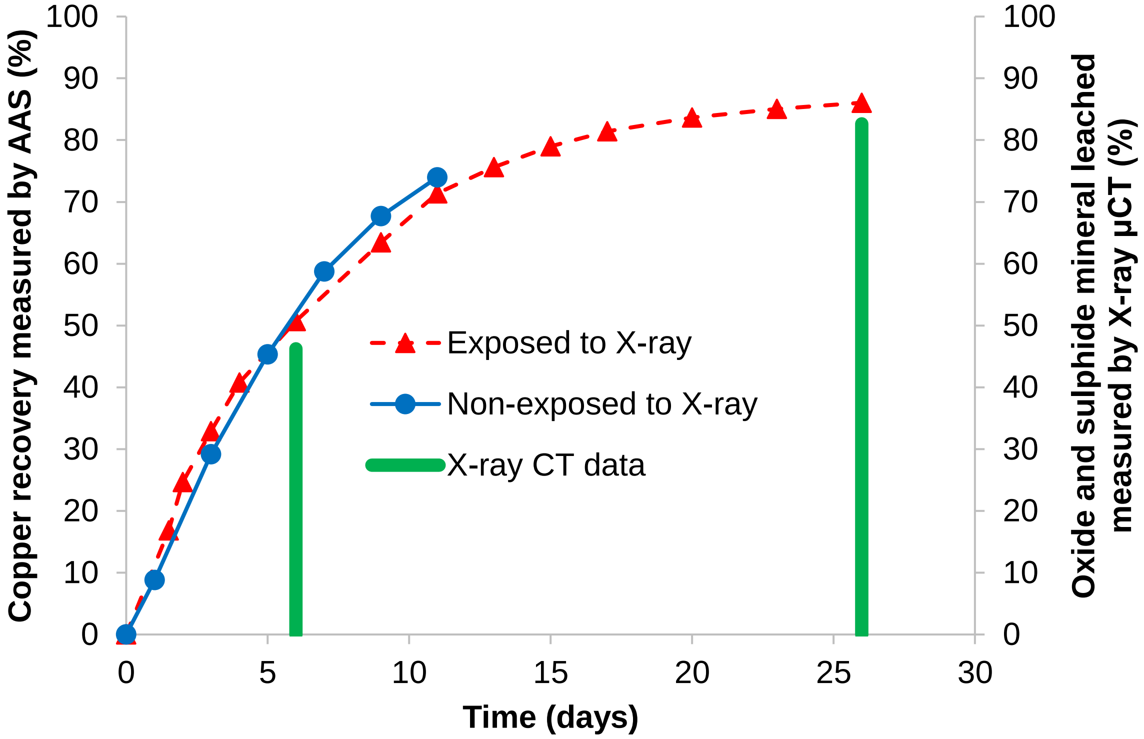

Figure 7-3: Comparison of copper recovery measured by AAS (solid and dash lines) and oxide and sulphide mineral leached based on image measurement (green columns) for the malachite ore.

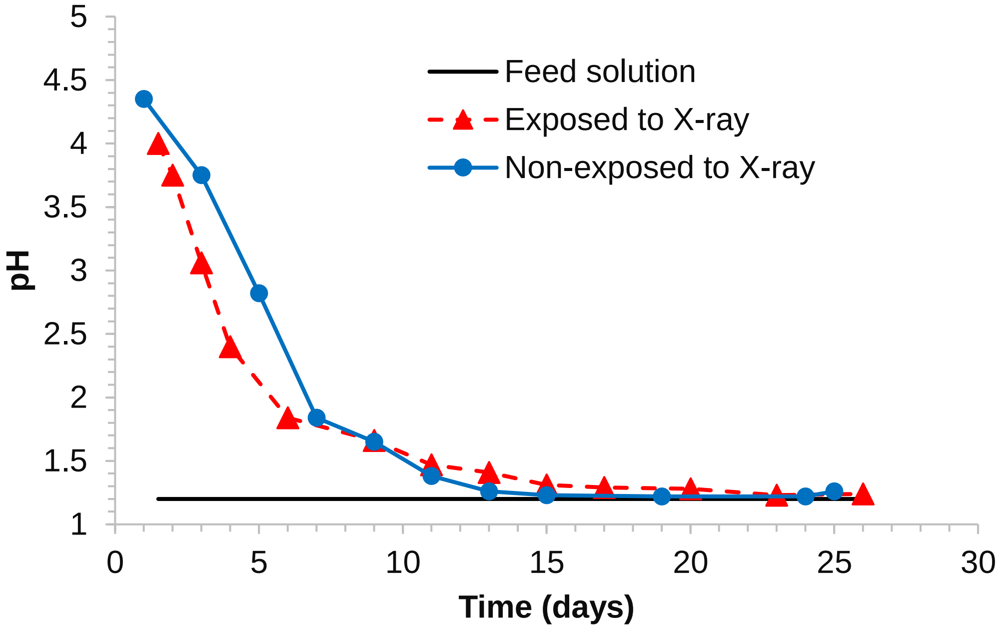

Figure 7-4: Changes in effluent pH over malachite leaching period.

Figure 7-3 shows that the oxide and sulphide recovery measured using the X-ray µCT images was consistent with copper recovery measured by AAS, though about 3 to 4% lower than the bulk measurement results. The oxide and sulphide recovery can be investigated in more detail using the image quantification data. Three-dimension views of the copper mineral grains in the five sections of the mini-column from top (Section 1) to bottom (Section 5) are presented in Figure 7-5. The images make evident that the remaining copper in the residue ore is mostly from large mineral grains. The amount of copper leached from the different sections on days 6 and 26 is illustrated in Figure 7-6. On day 6, the recoveries ranged widely, from 27% (Section 5) to 69% (Section 4). The high recovery in Section 4 can be attributed to the largest grain size being found there, in the range of 10^6 to 10^7 voxels (Figure 7-7). By comparison, the maximum mineral grain size is 10^8 voxels in the other sections. By day 26, the leaching extent was more similar for all the sections. The lowest copper recovery was obtained for the top section which contained the largest grain (79%, Section 1) and Section 3 (79%) and highest for Section 2 (97%).

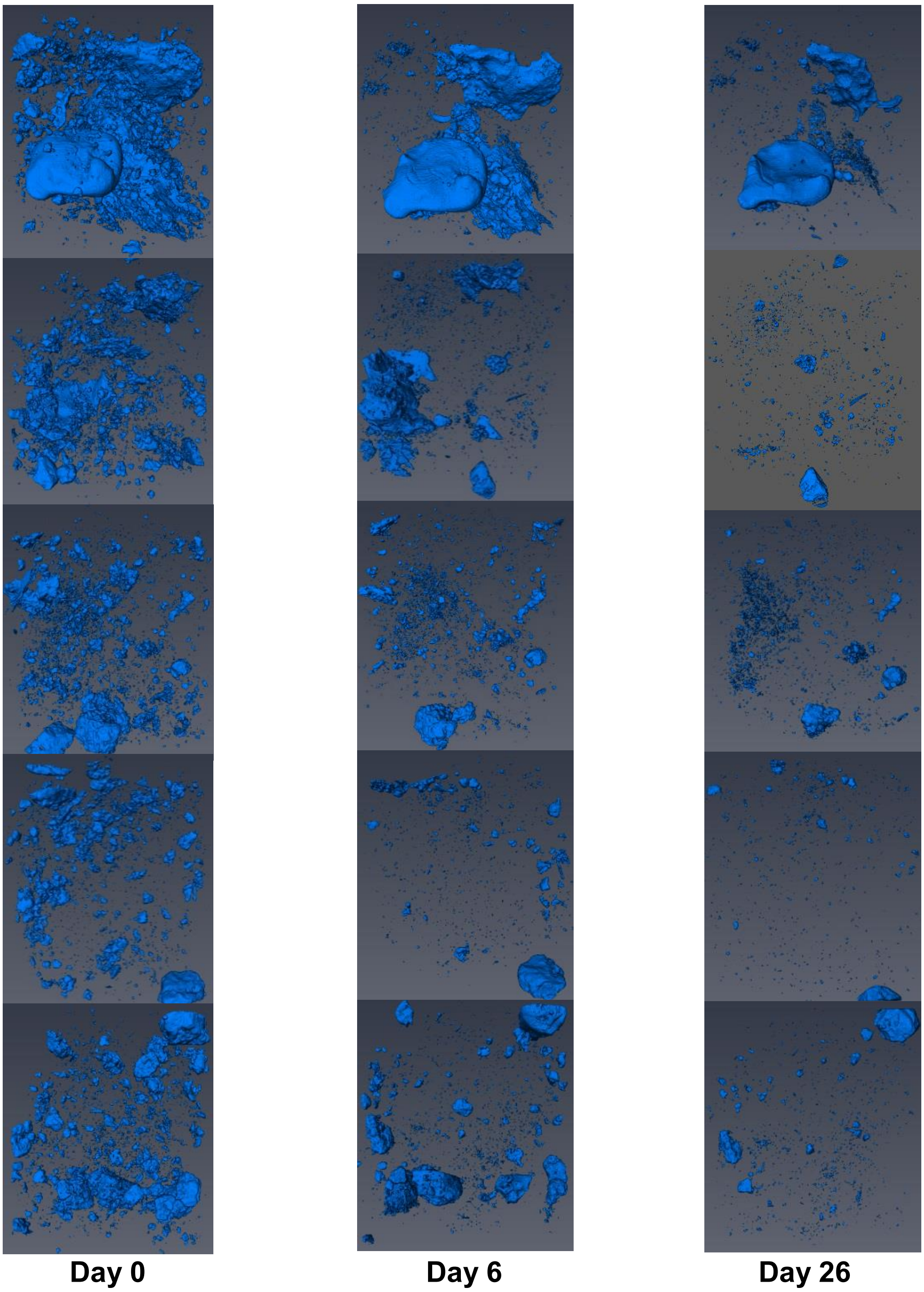

Figure 7-5: 3D views of the malachite copper mineral grain volume in 5 sections of mini-column (from top to bottom) on days 0, 6, and 26.

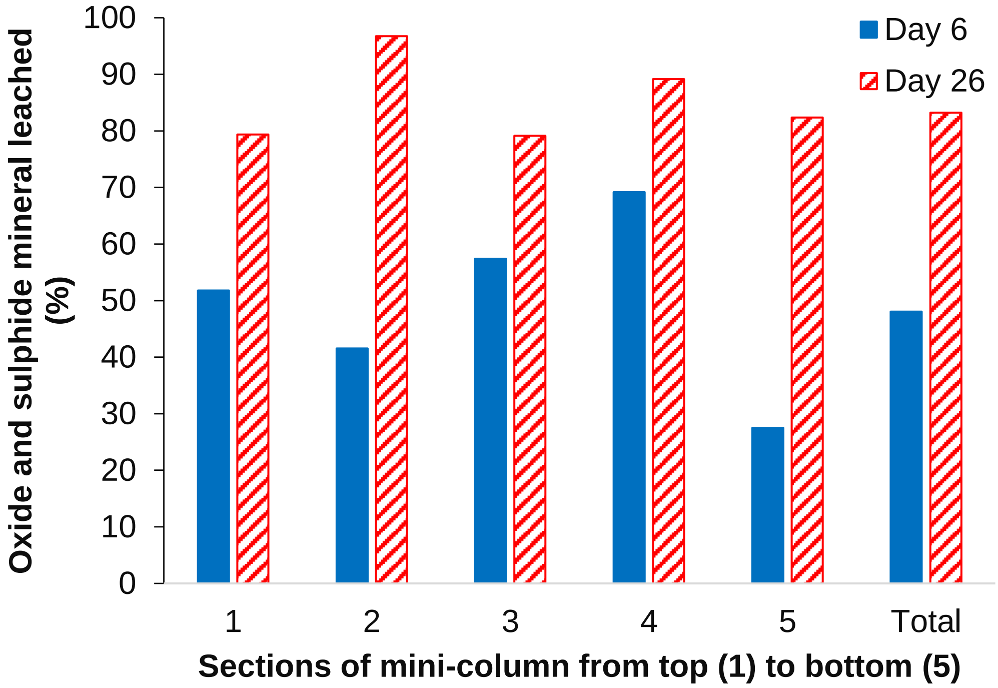

Figure 7-6: Oxide and sulphide mineral leached from various sections of mini-column containing malachite ore on days 6 and 26.

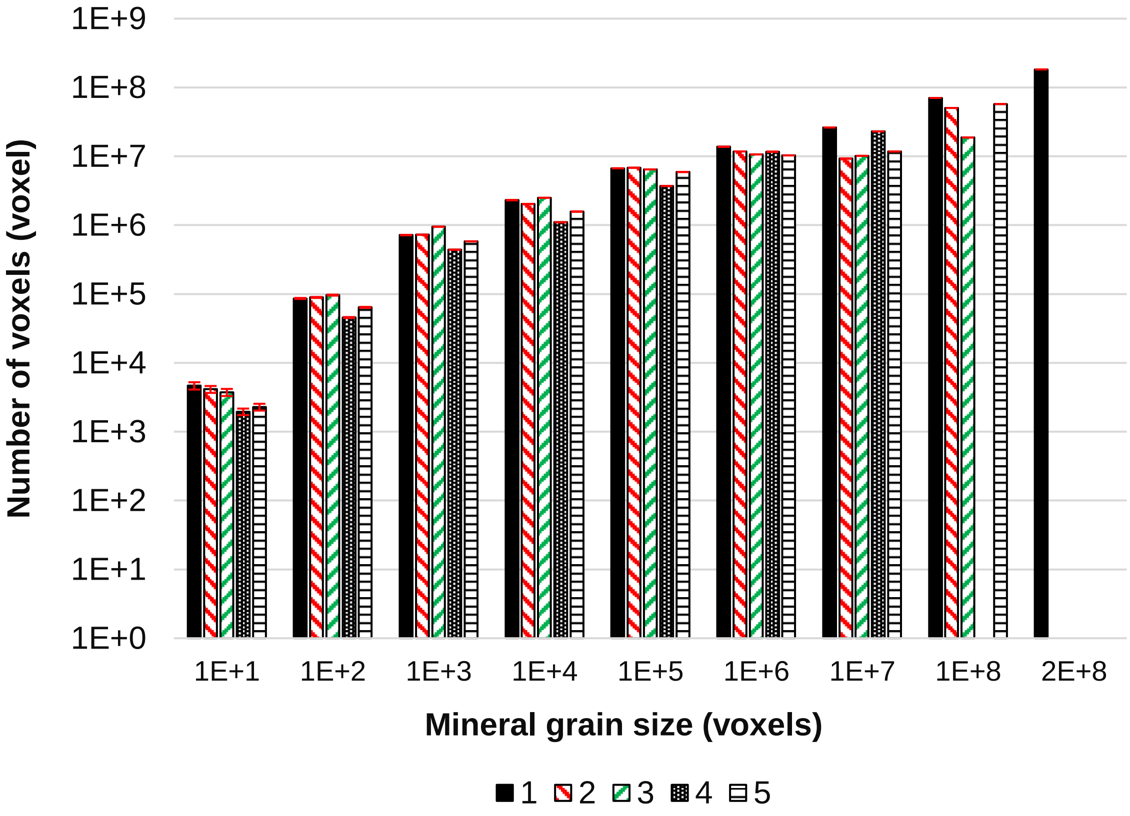

Figure 7-7: Mineral grains in specific size ranges for the five sections of the mini-column packed with malachite ore on day 0.

The distributions of the copper mineral distance from the ore particle surface at the different time points are shown in Figure 7-8. Figure 7-9 shows that the copper mineral grains were positioned less than 2000 µm from the surface for section 2 to 5 and that the existence of large mineral grains in the top most section was responsible for the overall larger maximum distance from the ore surface. The maximum distance decreased to approximately 1800 µm over the experimental period. This meant that the deeper minerals had been leached, or that the large mineral grains became smaller as leaching progressed. Figure 7-10 confirms that distance from the ore particle surface did not influence the rate of copper recovery, except initially at the farthest distance which was attributed to the large grains in Section 1. This indicates that contact between the mineral grains and leaching solution was not an issue for this ore, supported by the high porosity data. The dissolution of malachite was thus controlled by chemical reaction rather than diffusion. Another study by Nicol (2018) also showed that the kinetics of malachite dissolution were governed by rate-determining surface chemical reaction. However, Bingöl and Canbazoğlu (2004) found that their malachite leaching comprised two steps, an initial, very rapid dissolution followed with a slower second step.

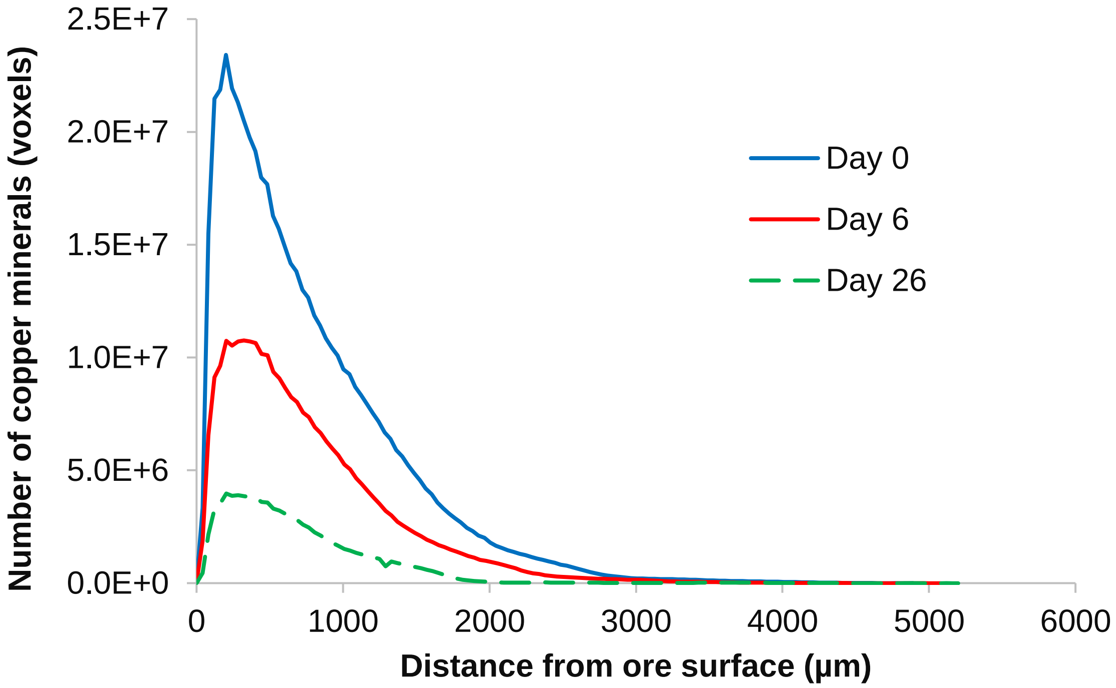

Figure 7-8: Change in the distance of mineral grains from the edge of the ore particle as a function of time for the malachite ore. The uncertainty in the grain distance from the ore surface is ±40.2 µm.

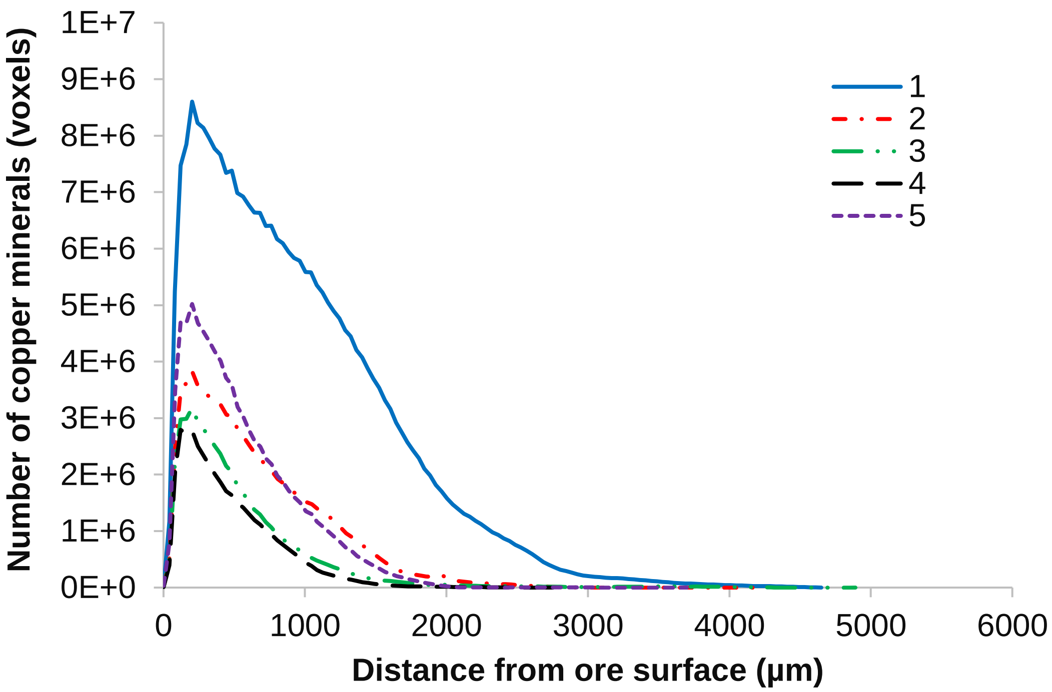

Figure 7-9: Distribution of mineral grains from the edge of the ore particle before start of the leaching for 5 sections of malachite ore. The uncertainty in the grain distance from the ore surface is ±40.2 µm.

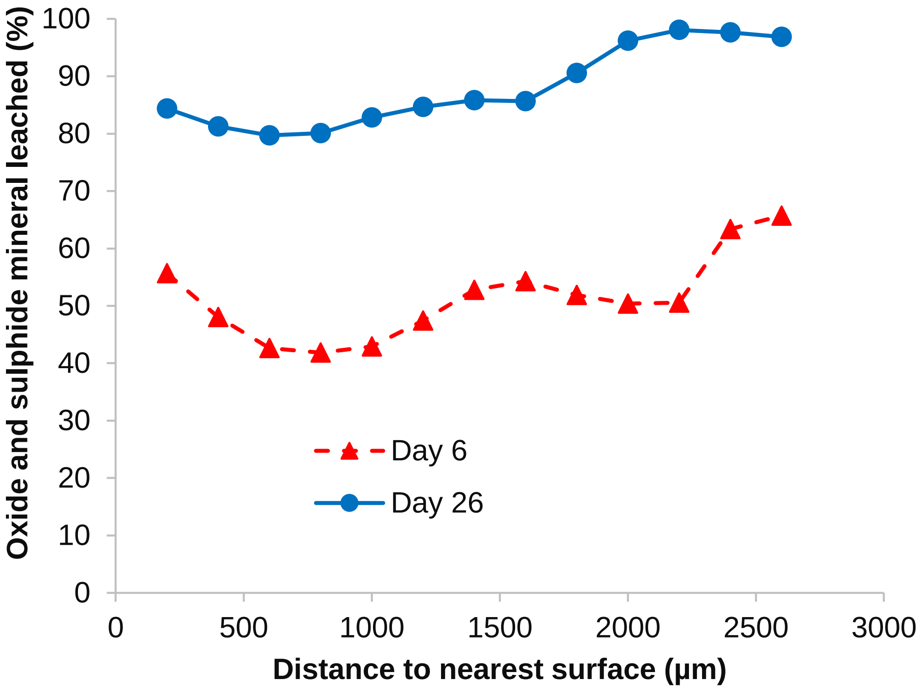

Figure 7-10: The oxide and sulphide mineral leached at different distances against the average initial mineral grain size on days 6 and 26.

7.2.2 Pyrite

Pyrite leaching was performed at 37°C and 65°C using a ferric leach. Changes in pH, redox potential, ferrous ion (Fe^{2+}), and ferric ion (Fe^{3+}) concentrations of the effluent solution of the mini-columns over the leaching period are shown in Figure 7-11.

There was acid consumption by some gangue minerals such as calcite and limonite during the acid wash (pH=1.15) over the first 7 days. The pH decreased from 2.04 to 1.71 for the 37 °C mini-column and from 2.75 to 1.88 for the 65 °C mini-column. Further pH decreases to 1.1 for the 37 °C mini-column and about 1 for the 65 °C mini-column occurred subsequent to the introduction of the feed solution containing 8.6 g L^{-1} ferric ion at a pH of 1.15. Equation (5-2) shows how this decrease may be accounted for by pyrite ferric leaching which produces a hydrogen ion and so reduces the pH of the solution (Li et al., 2017):

$$FeS_2 + 14Fe^{3+} + 8H_2O \rightarrow 15Fe^{2+} + 16H^+ + 2SO_4^{2-} \qquad (5\text{-}2)$$

The solution redox potential was approximately 330 and 300 mV during the acid wash for the 37 °C and 65 °C mini-columns respectively. Reduction in the pyrite oxidation rate over the experimental period results in an upward gradual trend of the redox potential. The redox potential for the 65 °C mini-column increased rapidly between days 7 and 15. There was then a gradual increase until the end of experiment at which time the highest recorded redox potential of 464 mV was recorded. The increase in redox potential in the PLS corresponded to a decreased Fe^{2+} concentration in solution coupled with an increase in the Fe^{3+} concentration, shown in Figure 7-11 (c and d). This meant that the pyrite oxidation rate decreased over the experimental period. In addition, the results showed that the redox values at 65 °C were lower than at 37 °C, indicating that increasing temperature increased pyrite ferric oxidation, producing more Fe^{2+} in the system.

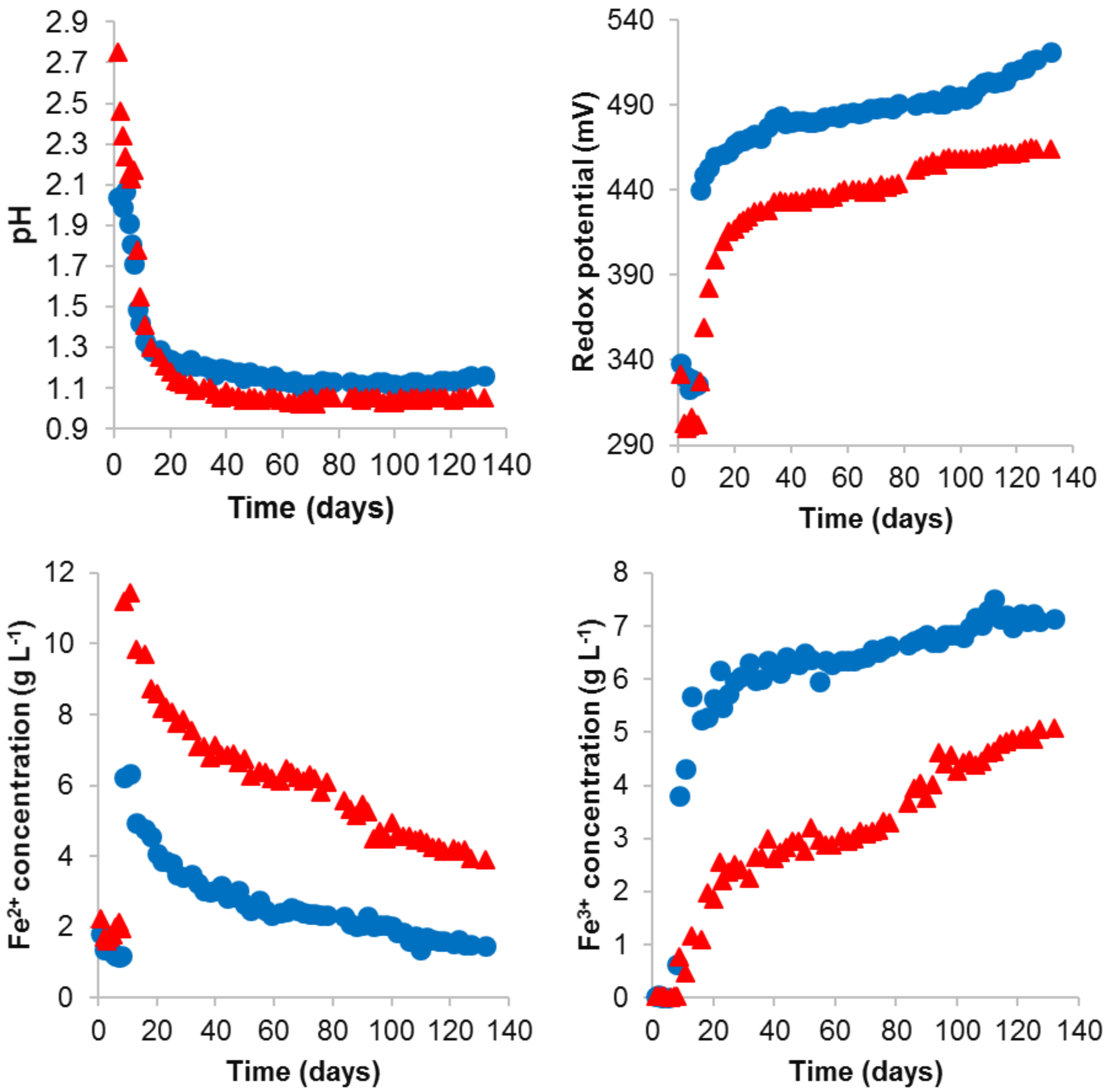

Figure 7-11: Changes in (a) pH profile, (b) redox potential (mV), (c) ferrous ion concentration (g L^{-1}) and (d) ferric ion concentration (g L^{-1}) during pyrite leaching at 37 °C (●) and 65 °C (▲).

Iron recovery for the different temperature conditions is given as a function of time in Figure 7-12, based on the spectroscopy data as well as the overall percentage sulphide mineral leached calculated through measurement of the mineral volume in the X-ray µCT images. As thermodynamically expected, increasing the temperature accelerated the pyrite dissolution rate, consistent with thermodynamics (Antonijević et al., 1997). Ahonen and Tuovinen (1991) showed that a leaching rate enhancement from 0.11 % day^{-1} to 4.54 % day^{-1} when temperature rose from 4 °C to 37 °C, confirming a strong temperature dependence for pyrite dissolution.

A rapid dissolution occurred over the first 20 days of the test. After this time, the dissolution rate decreased until the end of the experiment for both temperatures. The maximum recovery reached was 32% for 37 °C and 66% for 65 °C based on chemistry data. The recovery was 33% for 37 °C and 68% for 65 °C according to image quantification data. Thus, the calculated percentage iron released showed a general consistency between the two quantification methods.

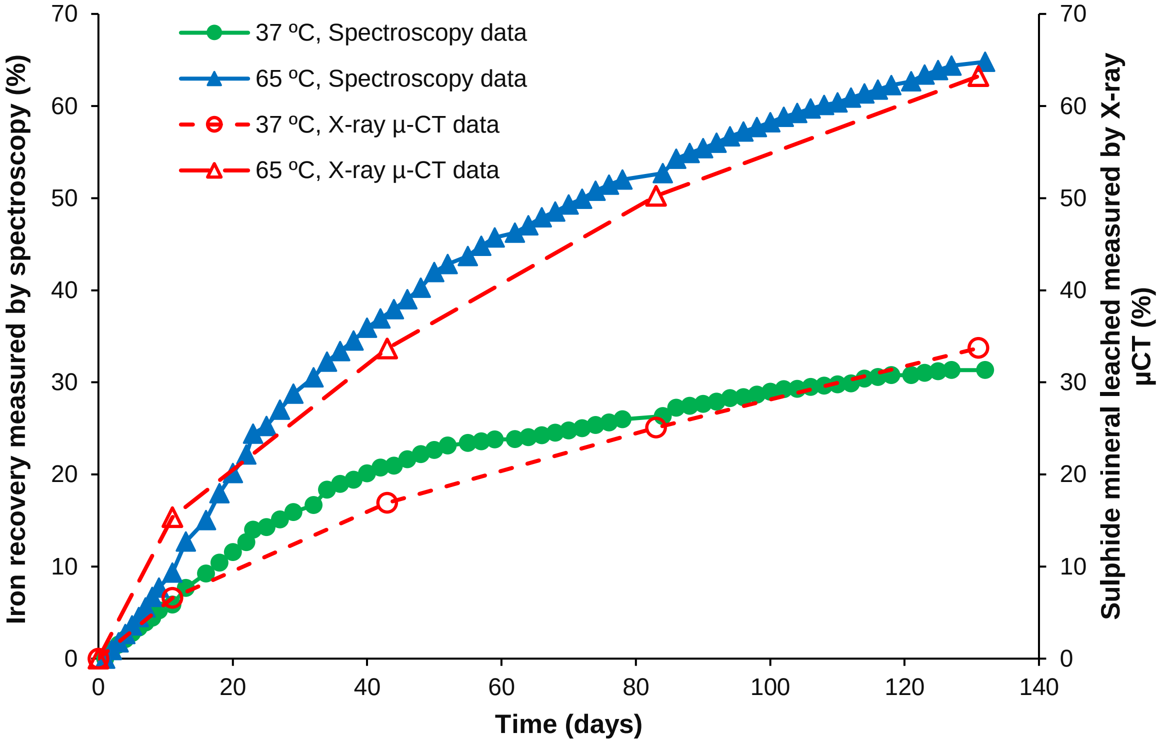

Figure 7-12: Comparison of iron recovery measured by spectroscopy (solid lines) and sulphide mineral leached based on image measurement (dashed lines) for the pyrite containing waste rock.

The distribution of the sulphide mineral grains as a function of distance from the ore particle surface at 37°C on days 0 and 132 and at 65 °C on days 0 and 159 are given in Figure 7-13 and Figure 7-15 and also the sum of three tracked sections at different time points in Figure 7-14 and Figure 7-16. The maximum leaching penetration distance was 2700 µm for both temperature conditions. This means that an increase in temperature did not have an effect on the maximum penetration distance. Based on Figure 7-14 and Figure 7-16, the leaching can be clearly seen to progress deeper into the ore with time. In the 37 °C mini-column, mineral leaching was observed to a distance of approximately 0.75 mm by day 11 and to 1.5 mm by day 45. The same leaching penetration was achieved at day 79 and 133. However, in the 65 °C mini-column mineral was leached at the distance of 1.5 mm from the ore edge by 11 days, with mineral recovery extending to a penetration of 2.5 mm by day 79.

The percentage of iron recovery as a function of distance from ore edge was plotted in Figure 7-17. This shows a reduction in iron recovery with increasing distance from the ore surface for the 65 °C mini-column, with the iron recovery decreasing from 83% to 32% as the distance increased from 200 µm to 2600 µm. Below the maximum penetration distance, the recovery at 37 °C remained between 29-34% at all distances.

There are two kinetic regimes which can control the leaching process, namely chemical reaction or diffusion through the reaction products. The regime is dependent on factors including operating conditions, ore type and size (Dixon and Hendrix, 1993; Ghorbani et al., 2013). The chemical reactions are primarily a function of temperature and are influenced by the activation energy, concentration of reactants, and size of mineral. The waste rock used in the current study had about 30% disseminated pyrite. This meant that inaccessibility of mineral grains should not have been initially rate limiting with the rate of reaction being controlling at the early stage of the leaching process. However, the leaching kinetics are expected to shift to a combination of reaction-diffusion rate limitation following depletion of accessible mineral grains. Diffusion of the lixiviant into the deeper subsurface zones then becomes the dominant kinetic factor in the leaching process.

The leaching from the mini-column operated at 37 °C was mainly reaction limited as the iron recovery is the same for entire range of distance values. Increasing temperature did increase the rate of leaching, as demonstrated in Figure 7-12. However, the higher leaching rate at the ore particle surface compared to that at larger distances from the ore surface indicates that leaching at the higher temperature became limited by access to the lixiviant. This points to either a partially diffusion-controlled system or a bias due to more completely occluded (inaccessible) pyrite mineral grains existing further from the ore particle surface. This conclusion is supported by the rapid and slow leaching periods evident in Figure 7-12. In the first period, easy leachable minerals lead to comparatively rapid iron extraction. The extraction rate then decreased in the second period, due to the depletion of rapidly leachable and more accessible minerals.

Changes in solution physicochemical factors such as density and viscosity may also have affected the leaching rate. Changes in density and viscosity with increase in temperature are shown in Figure 7-18 and Figure 7-19. With increasing temperature from 37 °C to 65 °C, the density decreased from 1027.64 kgm^{-3} to 1012.70 kgm^{-3} and the viscosity from 0.8108 cP to 0.5027 cP. The reduction of these physicochemical factors with temperature increasing did not have influence on the final maximum penetration distance for this ore. However, they may have contributed to the faster progression of the leaching front into the particles at the higher temperature.

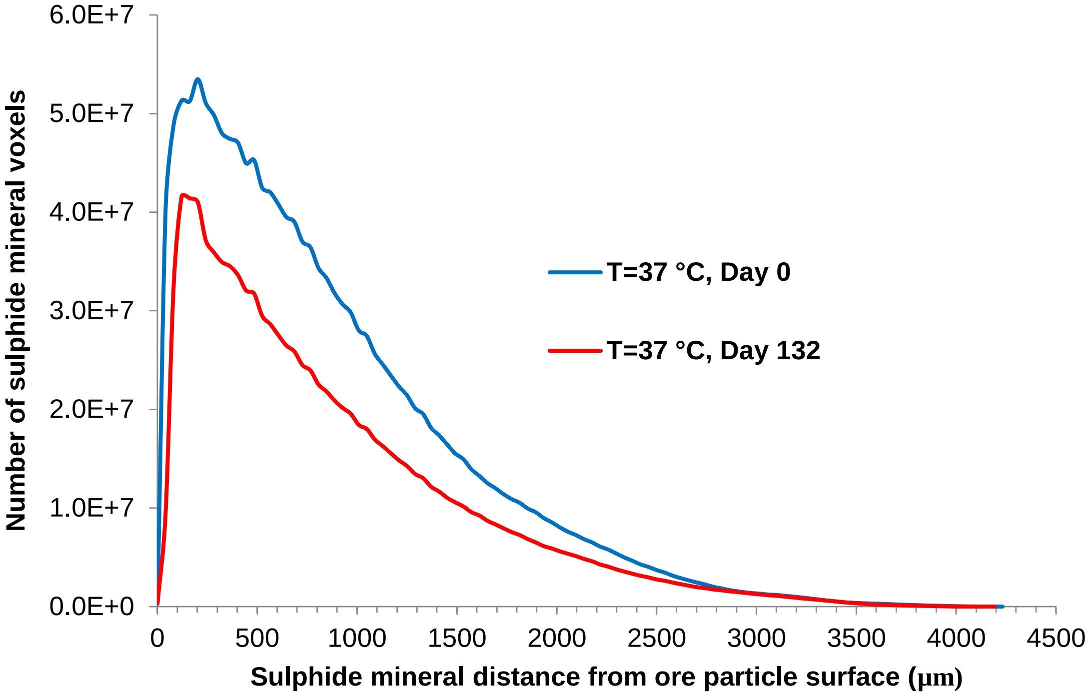

Figure 7-13: Change in the distribution of sulphide minerals as a function of position and time for the waste rock containing pyrite at 37 °C. The uncertainty in the grain distance from the ore surface is ±40.2 µm.

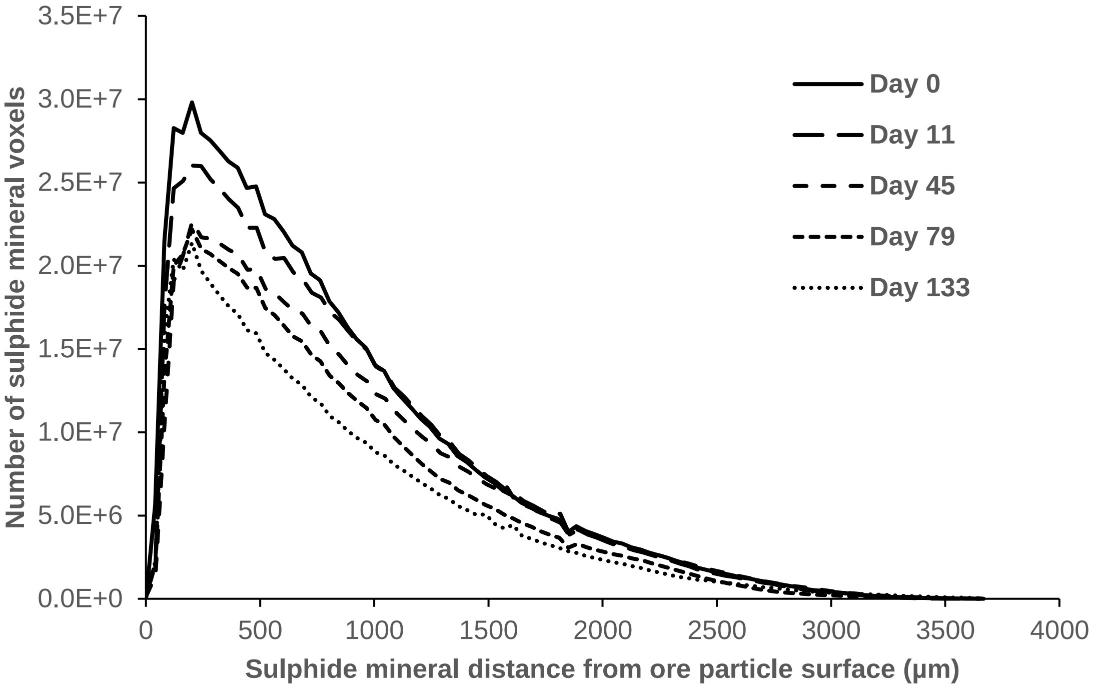

Figure 7-14: Change in the distribution of sulphide minerals as a function of position and time for the waste rock containing pyrite at 37 °C (the sum of three tracked sections). The uncertainty in the grain distance from the ore surface is ±40.2 μm.

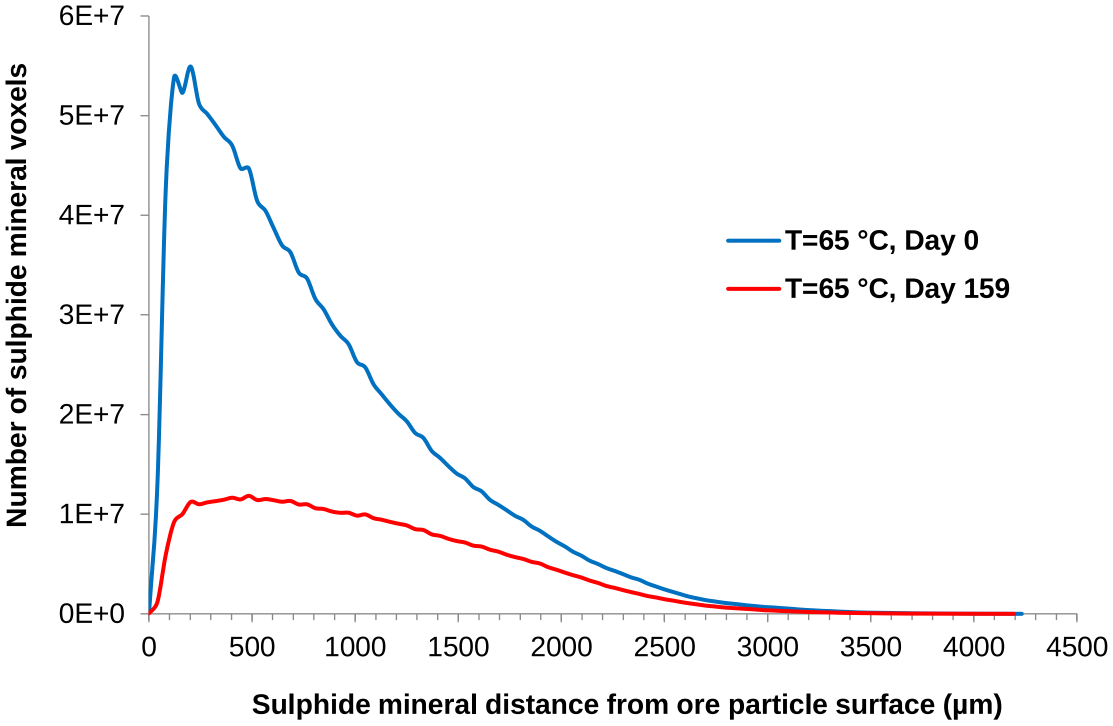

Figure 7-15: Change in the distribution of sulphide minerals as a function of position and time for the waste rock containing pyrite at 65 °C. The uncertainty in the grain distance from the ore surface is ±40.2 μm.

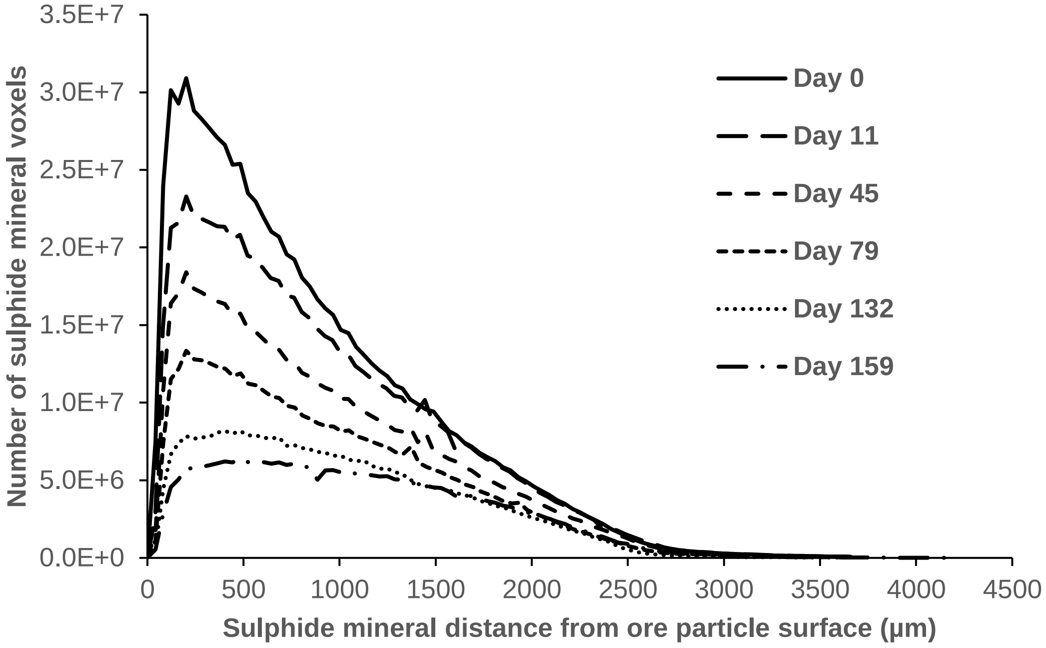

Figure 7-16: Change in the distribution of sulphide minerals as a function of position and time for the waste rock containing pyrite at 65 °C (the sum of three tracked sections). The uncertainty in the grain distance from the ore surface is ±40.2 µm.

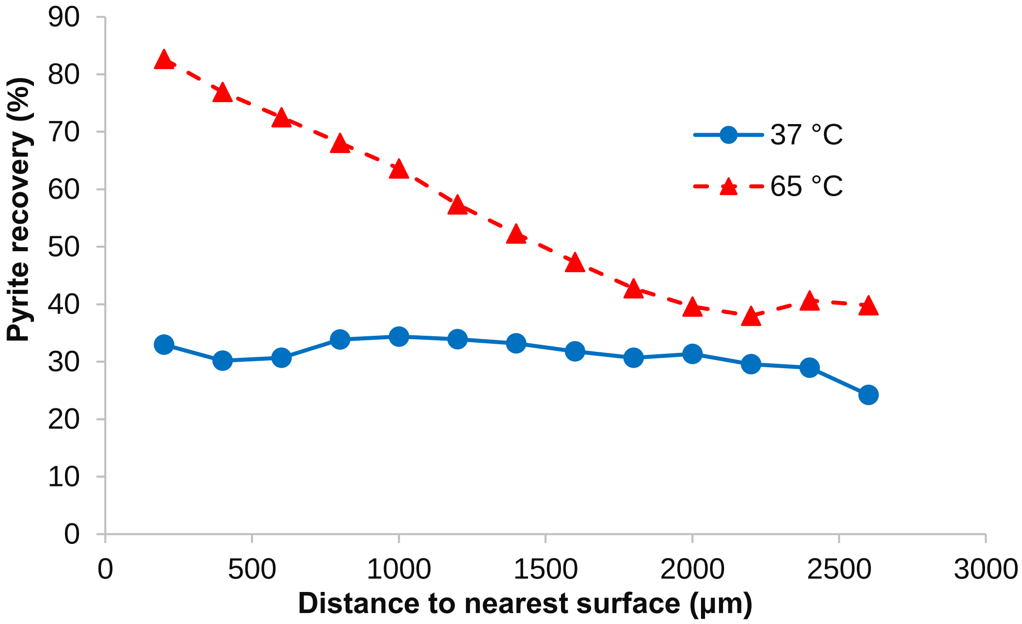

Figure 7-17: Comparison of the iron recovery at different distances to the ore particle surface at 37 °C and 65 °C.

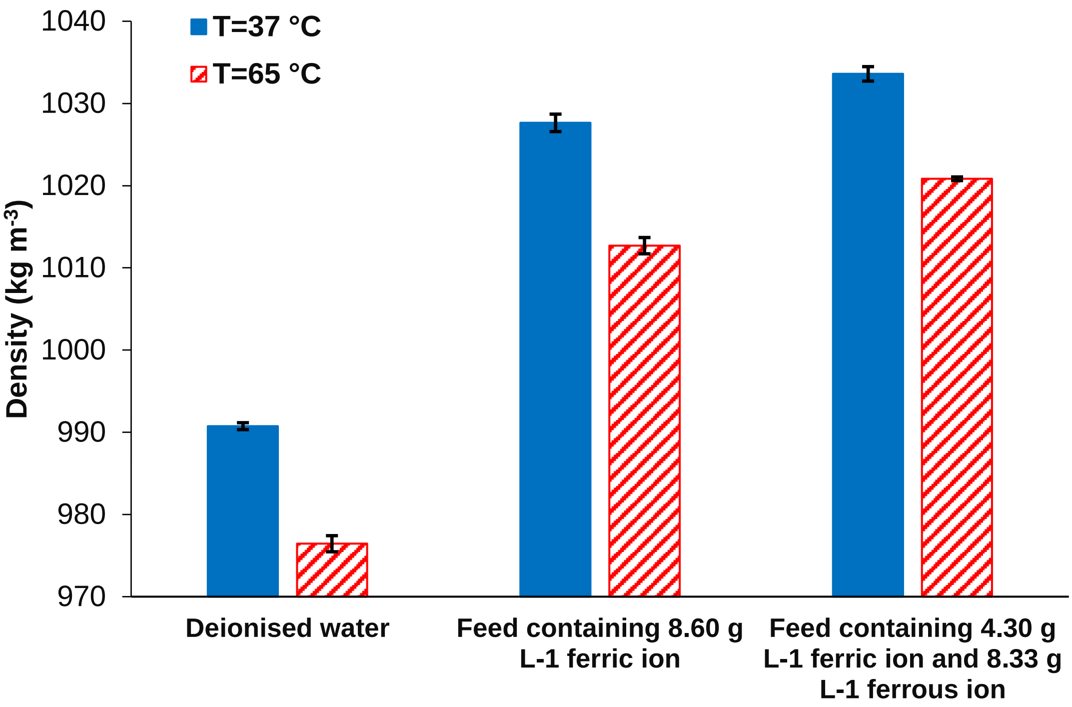

Figure 7-18: Effect of temperature on feed solution density.

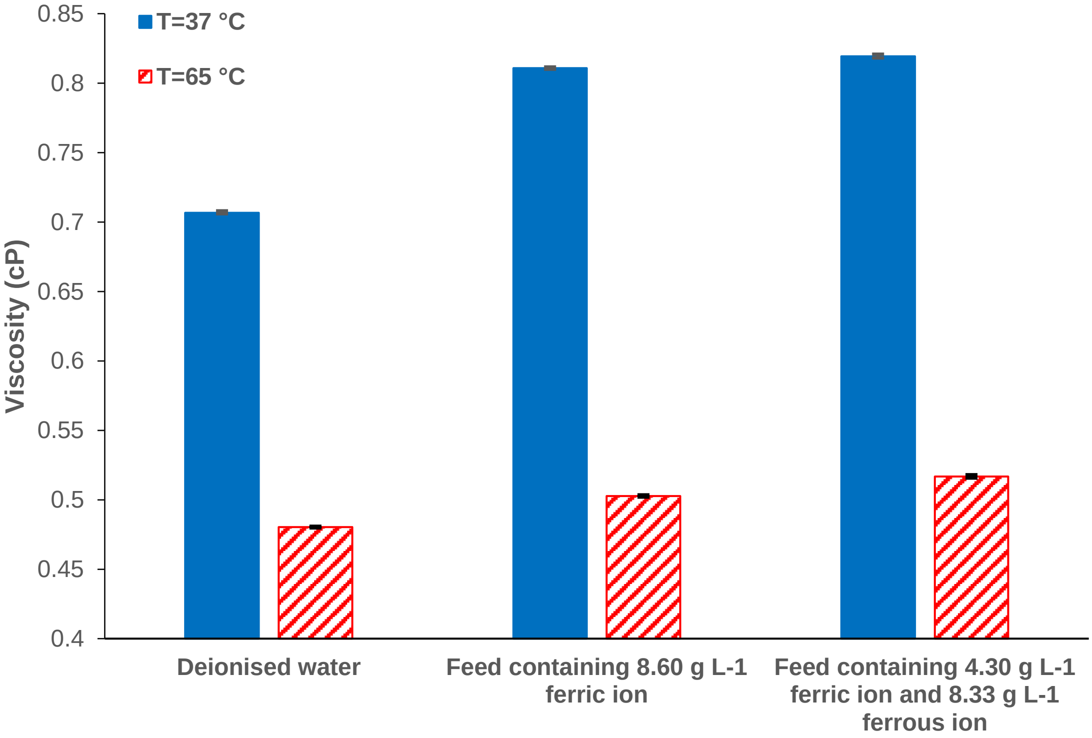

Figure 7-19: Effect of temperature on feed solution viscosity.

7.2.3 Chalcopyrite

Feed solution with 4.3 g L^{-1} Fe^{3+} and 8.33 g L^{-1} Fe^{2+} was introduced from top of the mini-columns for the leaching of the copper from the low-grade chalcopyrite. Changes in pH, redox potential, ferrous ion (Fe^{2+}) and ferric ion (Fe^{3+}) concentrations of the effluent solution over the leaching period are shown in Figure 7-20. It is not possible to see meaningful differences in parameters at two different temperatures. This was due to the high concentration of ferric and ferrous ion in the solution and relatively small amount of mineral in the mini-columns (50 g of ore).

The pH of the effluent during the acid wash (first 5 days) was initially 1.8 and decreased to 1.25, owing to dissolution of acid soluble gangue minerals in the ore. After introduction of the lixiviant feed solution, the pH decreased further and reached approximately pH 1.15 on day 25. The pH subsequently remained between pH 1.14 and 1.17.

The redox potentials increased from 395-400 mV to about 430 mV during the acid washing. In the first 15 days of ferric leaching, the redox rose from 430 to 440 mV. This can be attributed to fast leaching of exposed mineral grains and precipitation of ferric ion because of the high temperature (65°C). It subsequently remained in the range of 443 to 446 mV, slightly higher than the feed redox value of 440 mV. The redox changes were corroborated by ferrous and ferric ion concentrations in the effluent solution.

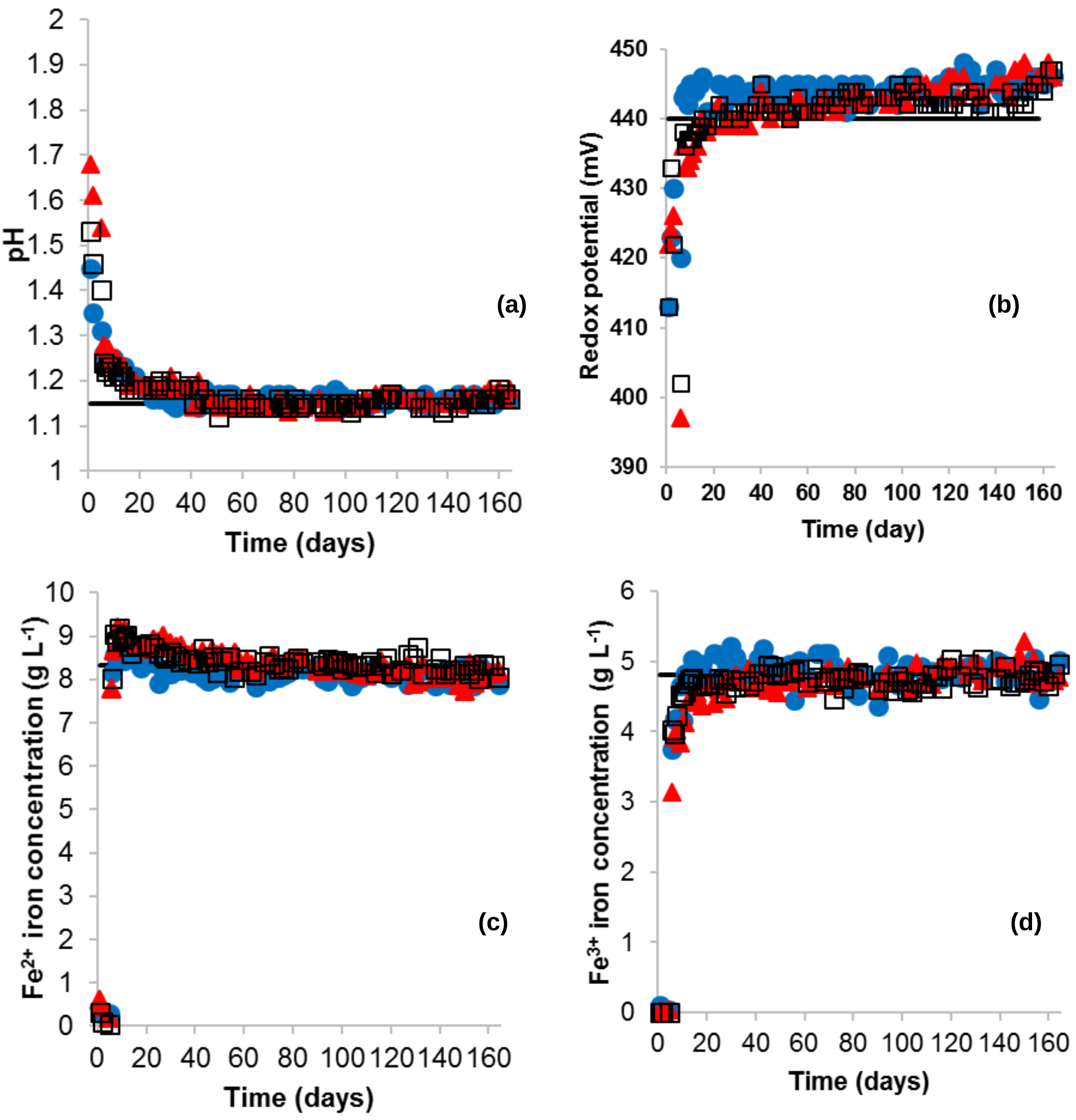

Figure 7-20: Changes of (a) pH profile, (b) redox potential (mV), (c) ferrous ion concentration (g L^{-1}) and (d) ferric ion concentration (g L^{-1}) during chalcopyrite leaching. Feed solution (—), 37 °C (●), 65 °C (▲), 65 °C non-agglomerated (□).

7.2.3.1 *Effect of temperature*

Figure 7-21 shows the copper recovery from the low-grade chalcopyrite ore for the different operating conditions, based on chemistry measurements from AAS as well as the overall percentage sulphide mineral leached calculated from the mineral volume in the X-ray µCT images. The results show rapid and slow ferric ion leaching periods. In the first period, easily leachable minerals led to rapid copper extraction. The copper extraction rate decreased in the second period, due to the depletion of the rapidly leachable and more accessible minerals. This corresponds to the pH, redox and iron concentration data in Figure 7-20, which are indicative of rapid leaching at the start, followed by little consumption of the leaching reagents provided in the feed from circa day 20.

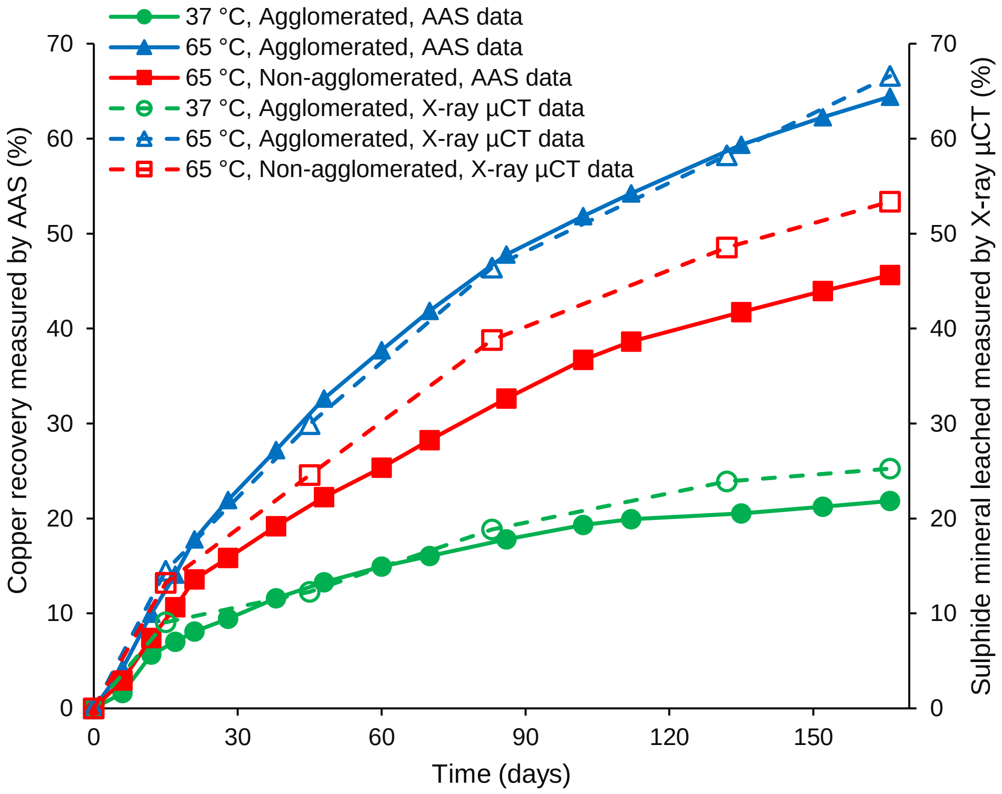

Figure 7-21: Comparison of copper recovery measured by AAS (solid lines) and sulphide mineral leached based on image measurement (dashed lines) for low-grade chalcopyrite.

There are only 3% and 2% differences between the chemistry results and image data for the mini-columns with agglomerated ore at 37 °C and 65 °C respectively. This confirms that the X-ray µCT images are a good measure of copper leaching. This was especially true during the first two weeks (rapid leaching period). There is a deviation between the two analysis methods towards the end of the experimental period. This can be attributed to the cumulative effect of leaching of other non-copper containing minerals present in the ore (e.g. pyrite) which are thresholded along with the chalcopyrite during the X-ray µCT image analysis.

Increasing temperature from 37 °C to 65 °C resulted in clear enhancement of leaching based on both analysis methods, with the copper recovery increasing from 20% at

37 °C to 64% at 65 °C by the end of the leaching period, and the overall sulphide mineral dissolution increasing from 24% to 67%.

Figure 7-22 and Figure 7-24 show the distributions of the sulphide mineral within the ore expressed as the distance from the ore particle surface before the start of leaching (day 0) and at the end of leaching (day 165) for the mini-columns operated at 37 °C, and 65 °C, respectively. The sums of the three tracked sections at different time points are presented in Figure 7-23 and Figure 7-25.

The maximum leaching penetration distance, beyond which no mineral volume change was observed, was 1.7 mm at 37 °C. This increased to 2.5 mm at 65 °C. At the lower temperature, minerals were leached within 0.6 mm of the ore particle surfaces during first two weeks. The leaching penetration distance then increased to 1.2 mm by day 84, with the small amount of leaching at distances between 1.2 to 1.7 mm occurring during the later stages of leaching. Crack development was not observed at 37 °C and the majority of the leaching was carried out in the more porous agglomerate structure, as presented in Figure 7-2.

At 65 °C, the copper minerals located within 1.9 mm of the surface were extracted in the first two weeks of the ferric leaching. Following this, leaching was of chalcopyrite grains at distances closer to the ore surface. The change in mineral content located at distances less than 1.9 mm was seen until day 84. This distance corresponds to the higher porosity region of the agglomerates, as presented in Figure 7-2. But, mineral recovery was observed at distances further than 2 mm from the ore surface on day 165. An example slice from the mini-columns before leaching and at the end of leaching at 37 °C and 65 °C is shown in Figure 7-28. Crack development in the ore particles is evident at the higher temperature. Similar development of ore porosity was not observed in the 37 °C mini-column. The leaching of the deeper mineral at 65 °C correlates to and therefore may be reasonably attributed to this creation of cracks during the later stage of ferric leaching. Formation of the cracks could have been due to dissolution of the mineral lattice, through the sulphide mineral leaching and biotite dissolution, for example.

Significant enhancement of copper recovery with increased temperature, as presented in Figure 7-21, confirms the pronounced effect of temperature on chalcopyrite ferric leaching due to the high activation energies. Chalcopyrite activation energy was reported as 130.7 kJ/mol in the temperature range between 35 and 68 °C (Córdoba et al., 2008a). However, the X-ray µCT acquisitions show that the enhanced recovery was not just due to increased leaching rate, as the maximum penetration distance also increased by 0.8 mm at the higher temperature. Thus, increasing temperature appears to reduce the diffusion limitation to leaching.

The copper recoveries at different distances from the ore surface are presented in Figure 7-29. The mini-column at 37°C had a copper recovery in the range of 30% to 14% at different distance values. The coppery recovery first increased from 24% at the distance value of 200 µm to 30% in the range of 400 to 600 µm then decreased to 14% at a distance value of 1.2 mm. It subsequently remained low, though increased slightly to 17%. The results indicate that the leaching kinetics are the rate limiting factor for the mini-column operated at 37 °C.

The agglomerated mini-column at 65°C had high recovery of the grains closer to the surface, with the same leaching rate observed for the first 600 µm. There would not have been reagent limitation in this region, with the reaction being controlled by kinetics. This distance correlates to the maximum in the agglomerated ore porosity, shown in Figure 7-2. Beyond 1 mm, however, the recovery decreased steadily from 69% to 19%, attributable to lixiviant accessibility limitation.

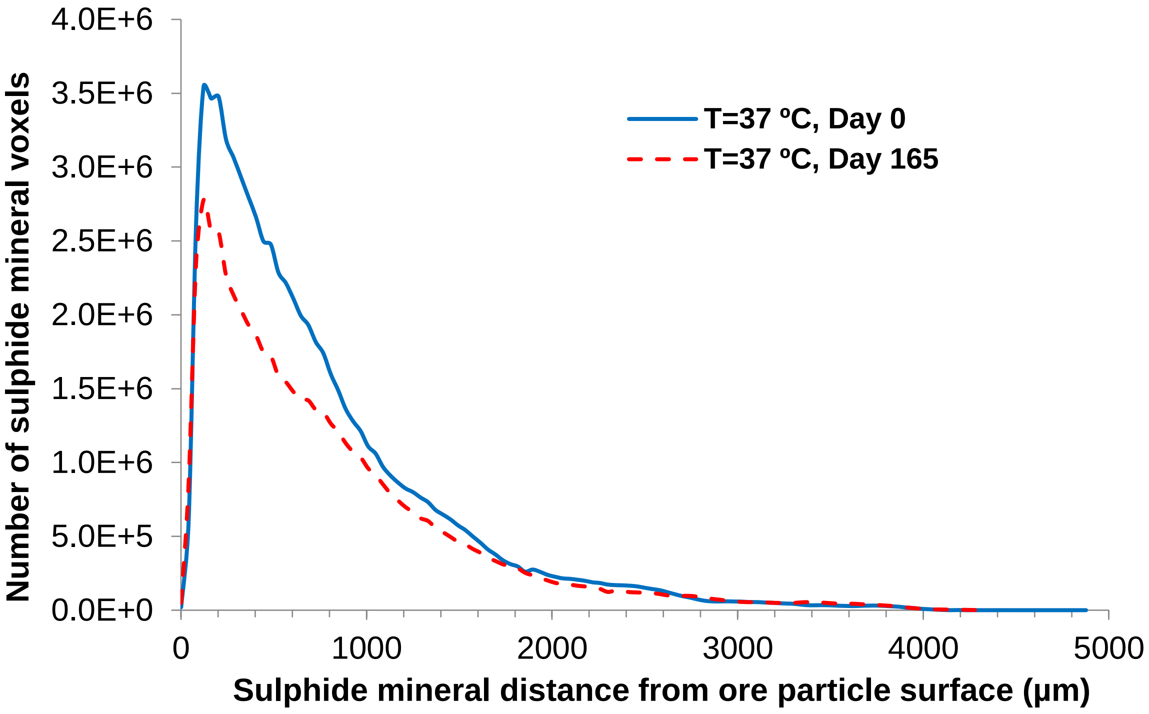

Figure 7-22: Change in the distribution of sulphide minerals as a function of position and time for the chalcopyrite ore at 37 °C. The uncertainty in the grain distance from the ore surface is ±40.2 µm.

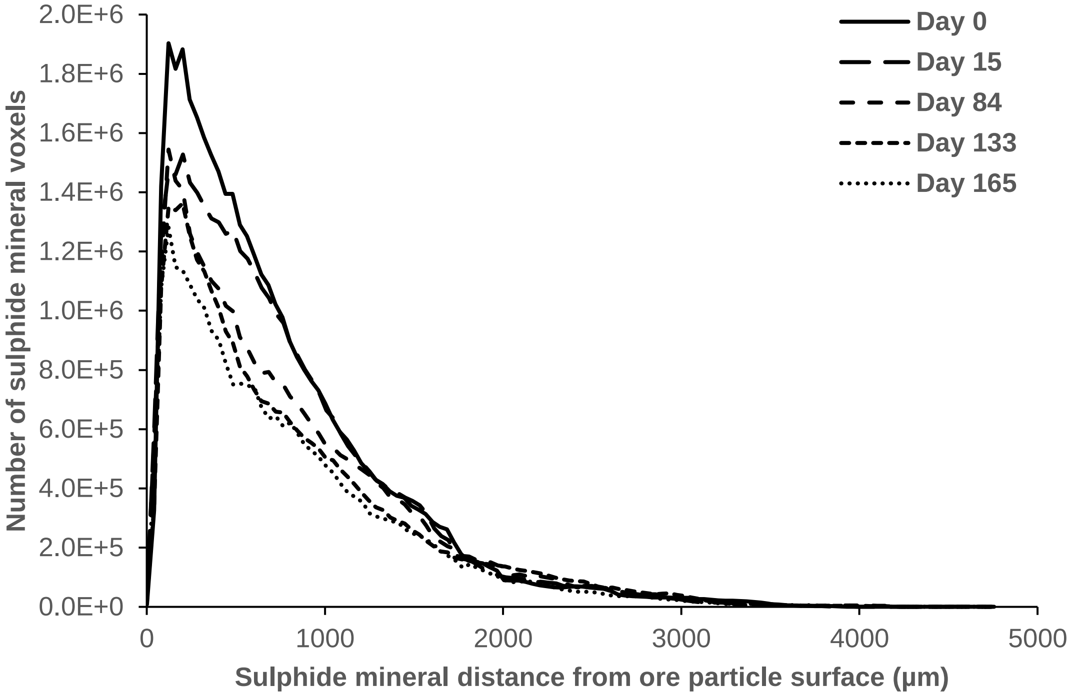

Figure 7-23: Change in the distribution of sulphide minerals as a function of position and time for the chalcopyrite ore at 37 °C (the sum of three tracked sections). The uncertainty in the grain distance from the ore surface is ±40.2 µm.

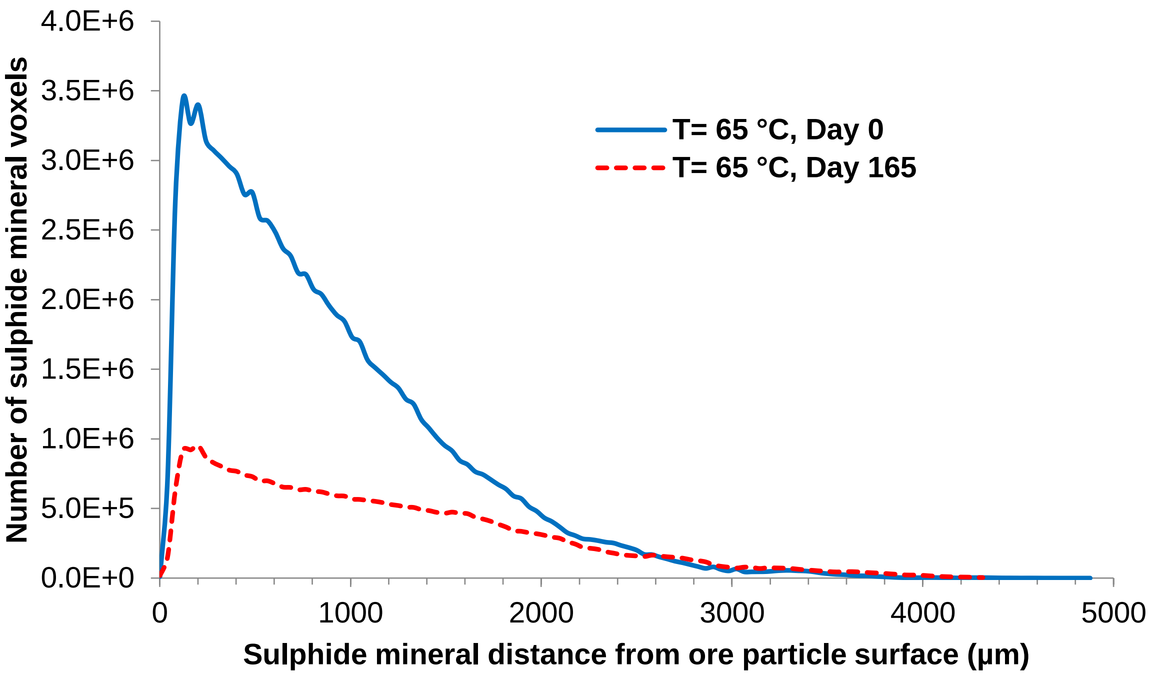

Figure 7-24: Change in the distribution of sulphide minerals as a function of position and time for the chalcopyrite ore at 65 °C. The uncertainty in the grain distance from the ore surface is ±40.2 µm.

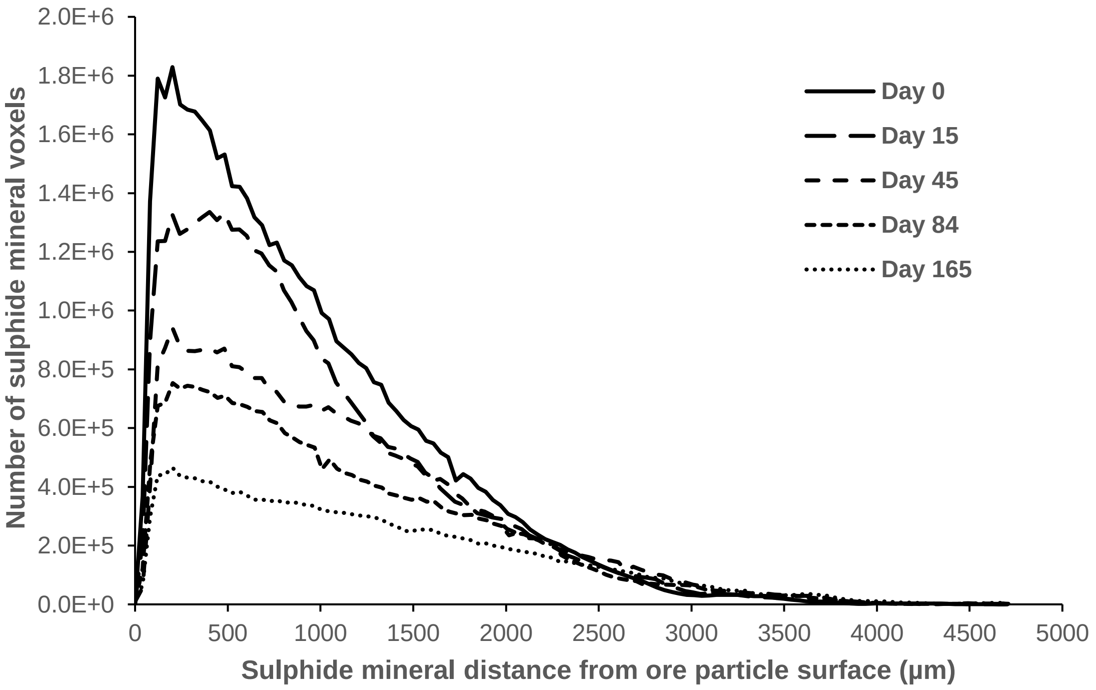

Figure 7-25: Change in the distribution of sulphide minerals as a function of position and time for the chalcopyrite ore at 65 °C (the sum of three tracked sections). The uncertainty in the grain distance from the ore surface is ±40.2 µm.

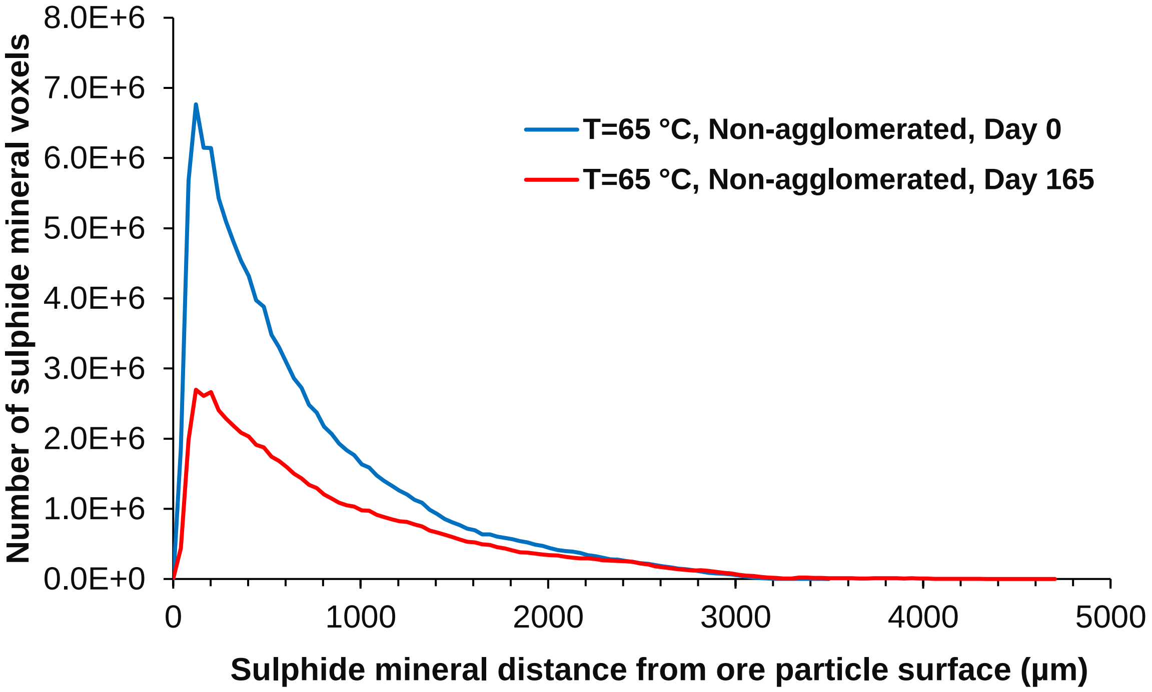

Figure 7-26: Change in the distribution of sulphide minerals as a function of position and time for the non-agglomerated chalcopyrite ore at 65 °C. The uncertainty in the grain distance from the ore surface is ±40.2 µm.

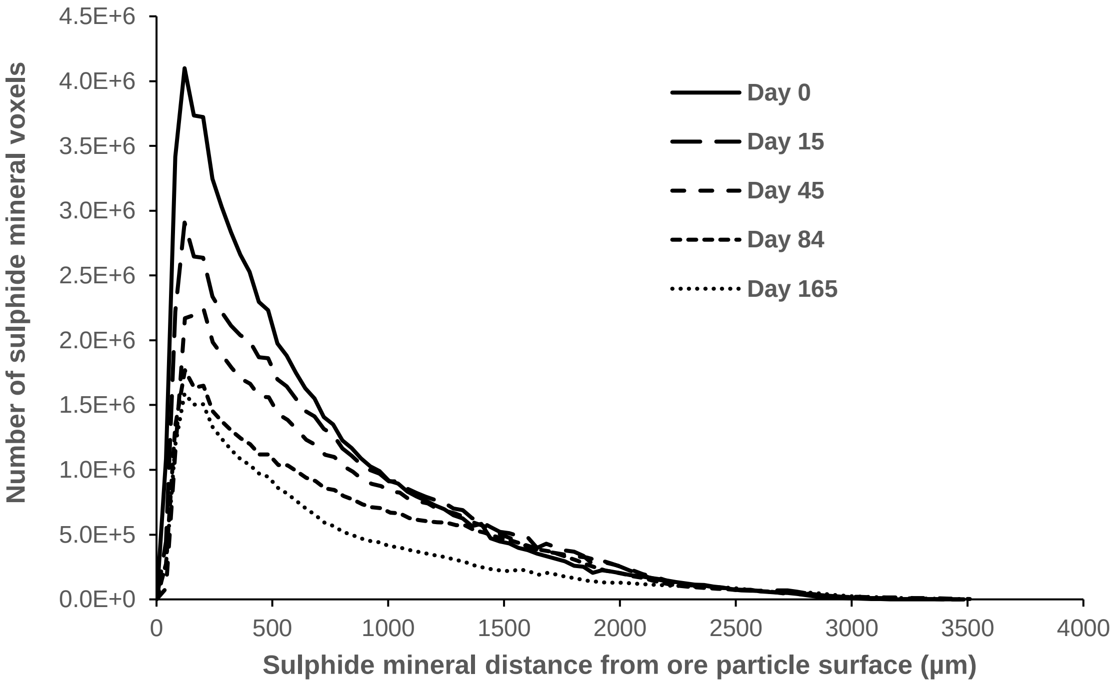

Figure 7-27: Change in the distribution of sulphide minerals as a function of position and time for the non-agglomerated chalcopyrite ore at 65 °C (the sum of three tracked sections). The uncertainty in the grain distance from the ore surface is ±40.2 µm.

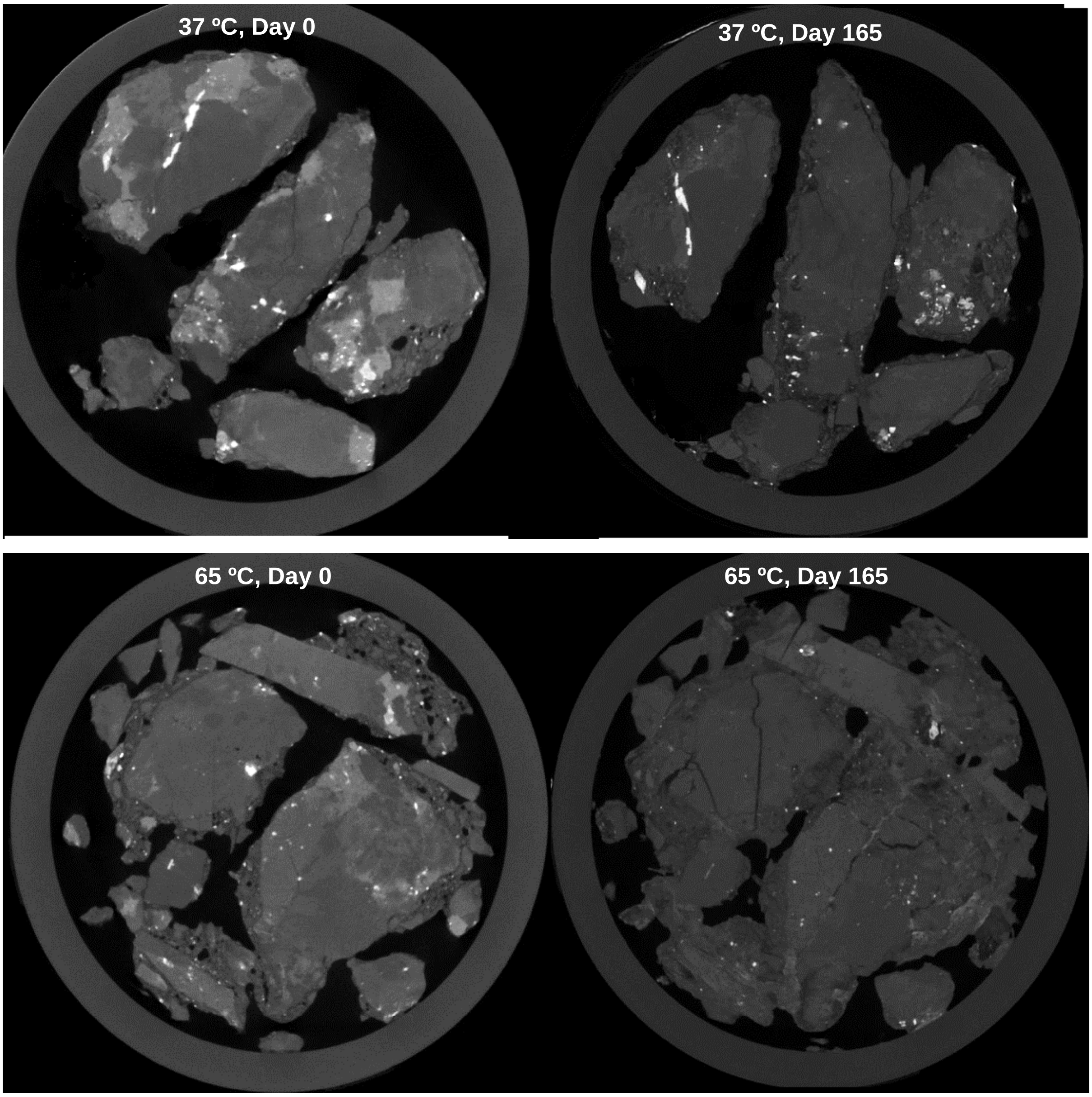

Figure 7-28: Example slices of a scanned leaching column before leaching and at the end of leaching at 37 °C and 65 °C, from a reconstruction image, as evidence of crack development at the higher temperature.

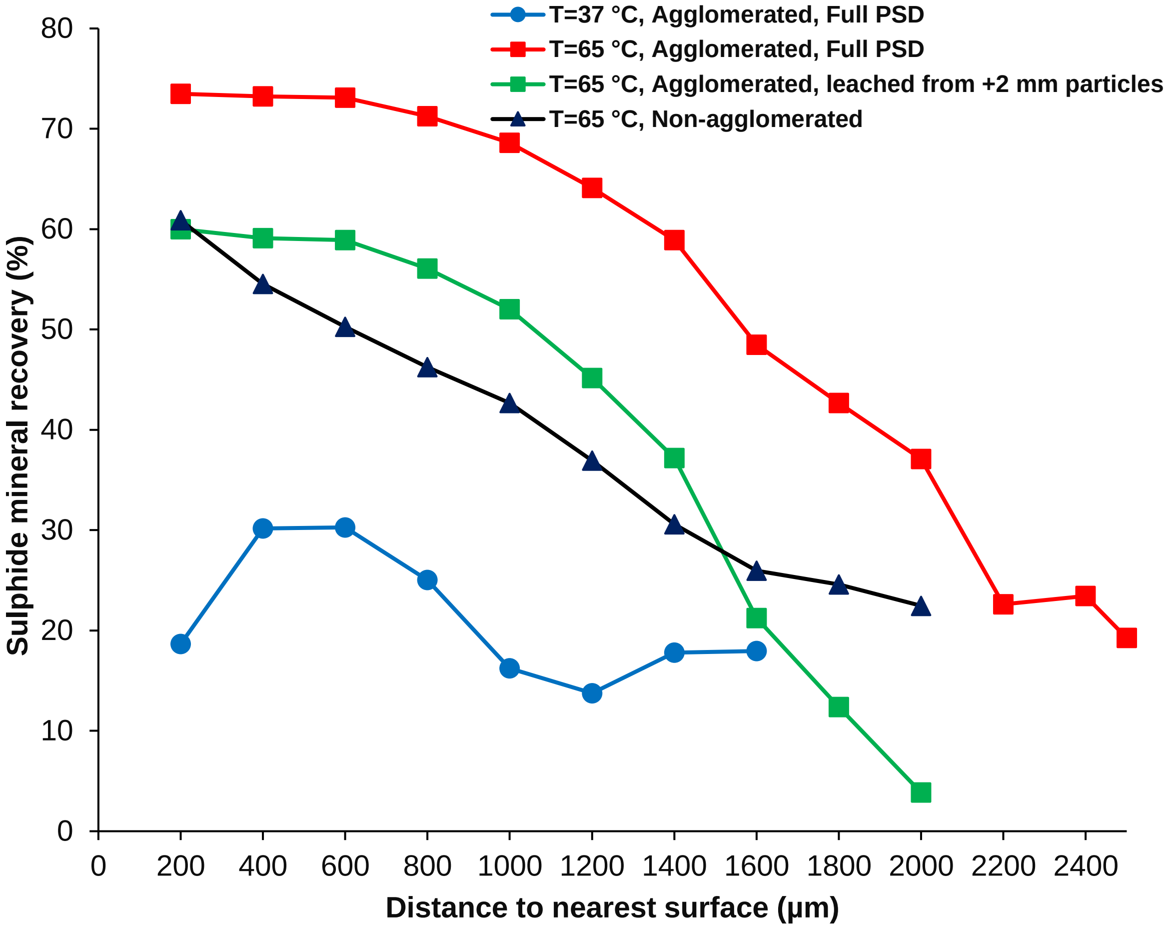

Figure 7-29: Comparison of the copper recovery at different distance to surface values for the low-grade chalcopyrite ore.

7.2.3.2 *Effect of agglomeration*

The copper recovery from a non-agglomerated mini-column (-5.6 mm particles were removed) is also presented in Figure 7-21. The cumulative sulphide mineral dissolution showed a linear increase from day 16 till day 84 for the non-agglomerated mini-column. Thereafter the rate decreased until end of leaching. The sulphide mineral dissolution was 54% at the end of experiment based on the sum of the three sections of the mini-column (Figure 7-21). The sulphide mineral dissolution for the whole non-agglomerated mini-column was 47% and the copper recovery was 45% which showed good consistency. Comparing the copper recovery in the PLS from the agglomerated mini-column at 65 °C with the non-agglomerated mini-column showed that as leaching progressed, the difference in copper recovery became larger. The copper recovery in the non-agglomerated mini-column was approximately 19% lower in comparison to the agglomerated mini-column. While copper leaching from the +2 mm particles in the agglomerated column showed a similar extent of leaching of 60% at 200 µm from the surface, the extent of leaching remained higher with increasing distance from surface in the agglomerated +2 mm compared to non-agglomerated ore over the distance from surface of 400 to 1400 µm. For the small size fractions < 2 mm, the copper minerals are close to the surface and readily leachable. Further the copper content in the smallest size fraction (1.04 %) is high compared to the + 2 mm particles which resulted in high copper recovery in the agglomerated mini-column.

Non-agglomerated and (A) agglomerated (B) particles are shown in Figure 7-30. In the agglomerated case, fine particles become adhered onto coarse particles (white arrows), forming a rim around them. Fine and coarse particles can also combine to produce newly nucleated agglomerates (red arrow). Pores (black points) between adhered particles are visible in the agglomerated particles. The non-agglomerated particles did not have these attributes and thus a different internal structure.

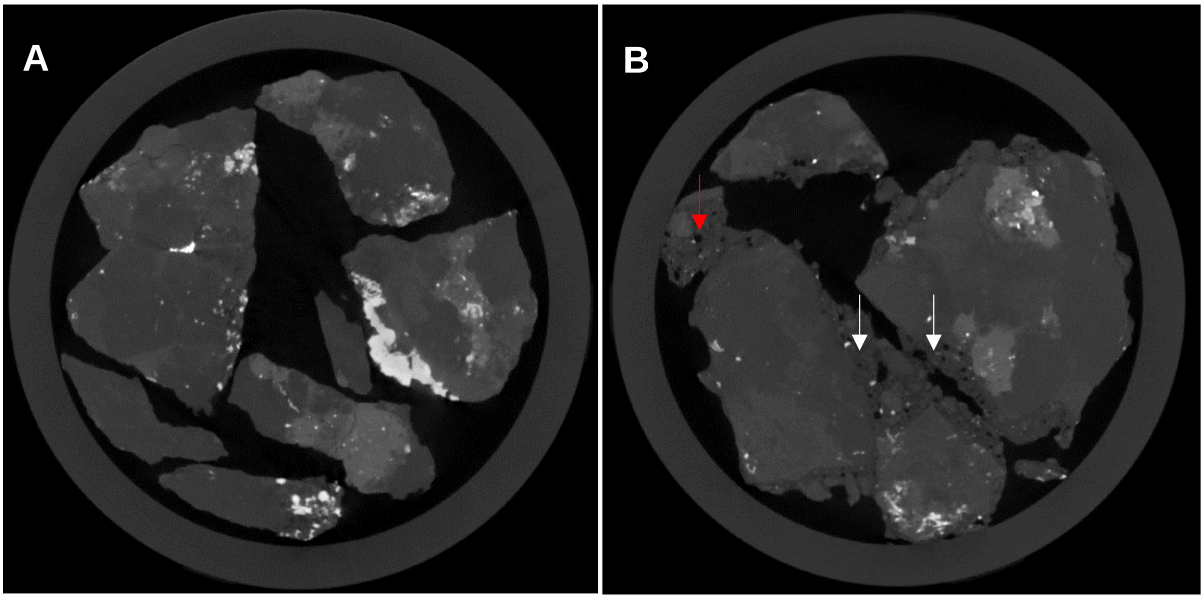

Figure 7-30: The X-ray µCT images of the internal structure of non-agglomerated (A) and agglomerated (B) particles.

Figure 7-26 shows the distributions of the sulphide mineral within the ore expressed as the distance from the ore particle edge before the start of leaching (day 0) and at the end of leaching (day 165) for the non-agglomerated mini-column operated at 65 °C. The sum of the three tracked sections at different time points is presented in Figure 7-27. Mineral leaching was achieved up to a distance of 0.7 mm from the ore surface within 15 days. The leaching penetration distance improved from 1.3 mm to 2.1 mm by 84 days and 165 days respectively. The recovery of deeper sub-surface metal in the non-agglomerated system confirms that the natural low porosity of the ore does not prevent leaching. The final leaching penetration distance for the agglomerated mini-column was therefore 500 µm higher than the non-agglomerate mini-column. The highest porosity value for the agglomerated ore was also at a distance of approximately 500 µm from particles' surface, indicative of the rim of fines that formed around the coarse ore particles (Figure 7-2). Crack development in the coarse particles at the higher temperature was observed in the non-agglomerated particles, akin to the agglomerated observation.

For the non-agglomerated mini-column, a downward trend in copper recovery from 61% to 21% occurred from the region closest to the ore particle surface (0.2 mm) to 2 mm, as shown in Figure 7-29. The sulphide mineral recovery achieved in the agglomerated mini-column at distance of 1.4 mm from ore surface was approximately equal to that achieved at the non-agglomerated mini-column surface. Beyond this depth, there was a similar downward trend for both mini-columns. The 1.4 mm threshold corresponds to the higher porosity region for the agglomerated ore according to Figure 7-2.

The dominant leaching rate liming factor was therefore diffusion. The copper recovery for the whole range of distance values was higher for the agglomerated mini-column compared to the non-agglomerated column. However, approximately the same decrease in recovery was observed in the two columns if the first 1 mm of data is disregarded from the agglomerate mini-column. The different behaviour over the first 1 mm on the agglomerate ore may be attributed to the rims of finer particles on the surface of the coarser particles. Leaching from these finer particles would not have been diffusion limited, with the diffusion limitation only observed once the effect of the boundary of the coarser particles was encountered.

Sulphide mineral recovery from +2 mm particles in the agglomerated ore was determined as follows. The sulphide mineral content was calculated in the -2 mm particle size fractions and it was assumed that all the sulphide mineral was leached from these small size fractions. It was then subtracted from the mineral amount known to have leached from all size fractions (overall result). This was finally divided by the sulphide mineral content in the +2 mm size fractions:

$$Cu\ leached\ from + 2\ mm\ particles = \frac{Cu\ leached - Cu\ content\ in - 2\ mm\ particles}{Cu\ content\ in\ 50\ g\ ore - Cu\ content\ in - 2\ mm\ particles} \qquad (5\text{-}3)$$

The results are provided in Figure 7-29. The sulphide mineral recovery is equal at the edge of +2 mm particles in the agglomerated mini-column and non-agglomerated mini-column. But, the sulphide mineral recovery amount is higher for the +2 mm particles in the agglomerated mini-column that non-agglomerated particles at the distance of 0 to 1.5 mm. This indicates that the porous rim formed around +2 mm particles in the agglomerated mini-column thus provided a more conducive leaching environment for the larger particles, with more Fe^{3+} as the main leaching reagent. It also means that agglomerate pre-treatment could improve the copper recovery from large particles, beyond improvement of ore packing and lixiviant flow characteristics.

7.3 Summary

Ferric leaching of chalcopyrite and pyrite was evaluated in this chapter. There have been many research studies which evaluated ferric ion concentration on chalcopyrite leaching as the main oxidation reagent (Córdoba et al., 2008a; Hirato et al., 1987; Kametani and Aoki, 1985). Hirato et al. (1987) indicated that the enhancement of ferric ion concentration from 0.11 g L^{-1} to 11.17 g L^{-1} resulted in the improvement in chalcopyrite leaching. Increasing the total iron concentration from 0.5 g L^{-1} to 5 g L^{-1} (redox potential of 400 mV) improved copper recovery from 50% to 90% (Córdoba et al., 2008b). The high copper recovery from the chalcopyrite in the abiotic system could therefore have been due to the high ferric ion concentration in the solution as well as the low redox potential (440 mV in the abiotic versus 600 mV in the biotic system).

The leaching of sulphide and oxide ores with different characteristics in terms of mineralogy and internal structure was evaluated with respect to non-surface mineral grain liberation. Porosity overall values and distributions for the three different ores meant that accessibly of target mineral grains was anticipated to be the highest for the malachite ore due to its relatively high porosity. A good porosity was maintained by the malachite ore even beyond 3000 µm from the ore surface, indicating that the ore matrix itself was porous (not e.g. cracked). The pyrite agglomerates had the lowest porosity, with the maximum also occurring earlier at circa 500 µm. The porosity of the agglomerated chalcopyrite ore was less than half that of the malachite, but was two orders of magnitude larger than the pyrite. The non-agglomerated chalcopyrite porosity results showed that the ore itself had a very low porosity.

High temperature is required to break down bonds in the chalcopyrite crystal lattice due to its high activation energy and improve pyrite leaching. Significant enhancement of copper recovery with increased temperature confirmed the pronounced effect of temperature on chalcopyrite ferric leaching due to the high activation energies. For the pyrite, the maximum recovery reached was 32% for 37 °C and 66% for 65 °C based on chemistry data. This was in close agreement with the recoveries of 33% for 37 °C and 68% for 65 °C according to image quantification data. Both methods confirm that the iron recovery was improved with increasing temperature.

Increasing copper recovery by the enhancement of temperature was determined to be because of thermodynamic reasons as well as increasing of maximum penetration distance. However iron recovery enhancement was only due to the expected thermodynamically increased leaching rate. This was concluded because an increase in maximum penetration distance was not observed in the waste rock containing pyrite with increasing temperature. This different behaviour can be due to the difference in the percentage of sulphide minerals in the ore, gangue mineralogy or the ore texture. The reduction of density and viscosity with temperature increasing for both chalcopyrite and pyrite may improve leaching rates. However because it did not influence the final maximum penetration distance for the pyrite, it was not possible to conclude that the increasing in the maximum penetration distance was due to sufficient reduction of physicochemical factors.

8 Conclusions and Recommendations

The literature review identified that non-surface mineral grain behaviour during heap bioleaching is highly important because a significant fraction of the mineral grains is positioned below the surface of ore particles. In order to extract the non-surface mineral grains, the lixiviant has to diffuse through cracks and pores in the ore connected to the surface. The long extraction times and low metal recoveries typical of heap systems are thought to be due to the resultant slow leaching rate of these non-surface grains as well as constraints on their accessibility. X-ray µCT as an imaging technique was selected as a method to quantify the leaching of non-surface minerals grains at different operating conditions, with the aim of enhancing their recovery. The main parameters of interest were agglomeration pre-treatment, ore type, temperature, and surfactant addition into feed solution. Specifically, it was desired to investigate how increasing temperature results in the enhancement of leaching, whether addition of surfactant into the leaching solution increases penetration distance and if it feasible to study heap bioleaching using X-ray µCT. The conclusions from this thesis are now synthesised.

8.1 Combination of mineralogical data, bulk measurements and X-ray µCT imaging

A systematically developed and optimized method was used for the investigation of non-surface mineral grain leaching through the combination of mineralogical data, bulk leaching measurements and X-ray µCT results. The chalcopyrite and pyrite grain size distribution, determined using QEMSCAN, was used as a basis for the design of an acceptably sized leaching mini-column. The outer diameter size (24 mm) ensured that the sulphide mineral dissolution of particles larger than 40 µm (accounting for 92% of the grains) could be tracked. The QEMSCAN data was then used to identify the different gangue, sulphide minerals and high-density minerals in the X-ray µCT images. In the analysis, high density/atomic number minerals visible in X-ray µCT image were identified and confirmed with QEMSCAN to be zircon or monazite. These high-density minerals had very high attenuation coefficients which went to almost highest value of histogram (strong light) and made it easy to identify and orientate them using their size and shape. The position of these high attenuation coefficient minerals as well as markers on the column walls were used for image registration of scans at different time points.

Tracking of the behaviour of the different mineral grains during leaching requires segmentation of the different phases. Simple thresholding using a histogram was not possible due to the X-ray absorbance of the various mineral phases being too similar. Accurate measurement of the sulphide mineral grain volume and correction of partial volume effects using machine learning tools was thus investigated. Trainable Weka Segmentation gave the most accurate results compared with the QEMSCAN data; however, it was too expensive with respect to computer processing and hence too time consuming to use for the multiple image data sets acquired for this thesis. The interactive thresholding function in Avizo® used for segmentation of sulphide mineral grains was found to be the next most accurate, with an error measurement in the sulphide mineral volume of 3.30% obtained.

A technique for distance map analysis was subsequently successfully developed which quantified the sulphide mineral grain distance from ore surface with an accuracy of ±40.2 µm.

8.2 Feasibility of studying biotic heap leaching using X-ray µCT

In light of the potential for X-ray µCT to be used as a 3D and non-destructive tool for the study of heap bioleaching dynamics, it was necessary to establish whether microbial populations used in bioleaching are affected by the X-ray energies required for imaging.

Liquid culture experiments were used to confirm that exposure to X-ray does not affect the microbial activity for energy doses between 35 and 90 kV at 200 to 280 µA. However, X-ray exposure was found to have a slight negative influence at higher voltages of 120 and 150 kV, temporarily reducing ferrous ion oxidation (per cell basis) and suppressing the specific growth rate of the bioleaching microorganisms. The X-ray exposure thus negatively affected both the total microbial population available for leaching (population viability) as well as the metabolic health of the individual microorganisms (population vitality).

The effect of X-ray exposure on bioleaching cultures attached to a mineral surface was examined using pyrite-coated beads packed into mini-columns. The energy dosage limits identified in the liquid culture experiments were found to be compatible with the X-ray µCT imaging conditions (minimum energy dosage and sample position) required for acquisition of complete and accurate images of the columns at a resolution that can allow identification of individual mineral grains. Following X-ray exposure, the performance of the exposed bioleaching mini-columns was equivalent to the unexposed control column. Similarly, the microbial activity and presence on the mineral surface appeared unchanged. The mini-column experiments therefore confirmed that there was no persistent negative effect on the attached archaeal and bacterial populations under the imaging conditions needed for the experimental X-ray µCT imaging to detect mineral grains.

Both sets of results confirm that X-ray µCT can be compatible with heap bioleaching experiments, while still permitting appropriate resolution of the mineral grains to make an X-ray µCT investigation worthwhile. However, cognisance that an upper limit of tolerable X-ray exposure exists must be acknowledged. This may present a challenge if it is desired to image larger or denser ore samples which require a greater X-ray energy level for sufficient penetration of the sample by the X-rays and hence accurate imaging.

8.3 Surfactant effect on non-surface mineral grain leaching

Surfactant addition promotes the lixiviant contact with an ore by decreasing surface tension. This could be highly beneficial in the leaching of mineral grains embedded in larger ore particles, where the grains are only accessible through small cracks and pores in the ore matrix. The response of bioleaching microorganisms to the presence of surfactant in lixiviant was evaluated to assess whether surfactant inclusion in the heap bioleaching process influences the bioleach positively. The effect of five different non-ionic surfactants at different concentrations on thermophilic (65 °C) bioleaching microorganisms was studied in terms of microbial growth, ability for ferrous ion oxidation and chalcopyrite bioleaching.

The thermophilic microorganisms were able to grow and oxidise ferrous ion in the presence of 5 and 10 mg L^{-1} Tween® 20, 5 mg L^{-1} Tween® 80, 5 mg L^{-1} Plurafac® LF 120, and 5 and 10 mg L^{-1} Lutensol® XL 90. Conversely, 10 mg L^{-1} Tween® 80 and

Plurafac® LF 120, and 5 and 10 mg L^{-1} Plurafac® LF 600 inhibited both the growth and ferrous ion oxidation by microorganisms.

In the chalcopyrite bioleaching experiments, 20 mg L^{-1} Tween® 20, 10 and 20 mg L^{-1} Tween® 80, and 5 and 10 mg L^{-1} Plurafac® LF 600 inhibited microbial growth, therefore only permitting abiotic leaching of the copper mineral. The final copper recovery in the presence of these surfactants was lower than the abiotic control, potentially because of reduced diffusion of ferric ion to the ore surface as a result of the formation of an adsorbed surfactant layer. The copper recovery was the same or slightly lower than the biotic control in the presence of 5 mg L^{-1} Tween® 20 and Tween® 80, 5 and 10 mg L^{-1} Plurafac® LF 120, and 5 and 10 mg L^{-1} Lutensol® XL 90. The addition of 10 mg L^{-1} Tween® 20 improved the final copper recovery. There was a direct relationship between copper extraction improvement and microbial growth and ferrous ion oxidation occurrence. The copper recovery obtained was 68.9%, 75.1%, and 47.7% for 5, 10 and 20 mg L^{-1} Tween® 20. This therefore means that an optimal surfactant concentration exists at which the copper recovery is maximised, and below or above which it may be reduced. Lower molecular weight surfactants corresponded to better copper leaching efficiencies, recommending their preferential use.

In all cases, attachment of the thermophilic microorganisms to the concentrate surface was reduced in the presence of surfactant. However, the corresponding pH, redox potential and copper recovery data indicated the relative lack of attachment of the microorganisms did not prevent or reduce the bioleaching activity during batch operation when appropriate surfactant and concentrations were used in the experiment. However, less attachment may be an issue in a larger scale flow-through heap if it results in insufficient retention of microbial cultures in the ore bed (wash-out).

The result of including 10 mg L^{-1} Tween® 20 in the leaching solution feed to a mini-column packed with chalcopyrite ore was an improved final copper recovery of 4% at the end of the experiment period. However, when the availability of sulphide mineral was not rate limiting, the copper recovery and sulphide mineral volume reduction in the mini-column with surfactant was lower than the mini-column without surfactant. This may have been due to depression of diffusion of ferric ion to the ore surface as a result of the formation of an adsorbed surfactant layer on the mineral surface. The performance of the mini-column with surfactant later became superior as the amount of readily leachable mineral became limiting, with the final leaching penetration distance being higher.

Thus, it was confirmed that addition of surfactant can improve sulphide mineral recovery by increasing maximum penetration distance, but the leaching is complicated by a slower initial rate and less microbial attachment.

8.4 Temperature and ore type effect on non-surface mineral grain leaching

This part of the study confirmed that for the chalcopyrite ore, an enhancement of copper recovery and sulphide mineral dissolution with increasing temperature from 37 °C to 65 °C was attributable to an increased leaching penetration distance and crack development in the ore particles in addition to the thermodynamically expected increased leaching rate. The higher operating temperature thus not only increases leaching rate via improved reaction conditions for the high activation energy chalcopyrite dissolution, but also increases the amount of mineral that is leachable from ore particles. This further strengthens the use of higher temperature conditions for the bioleaching of chalcopyrite.

Conversely, it was observed that increasing temperature did not have effect on maximum penetration distance for the waste rock containing pyrite. For this ore the increase in iron recovery was only due to thermodynamic reasons. The different behaviour of chalcopyrite and pyrite with respect to increasing temperature was due to a number of reasons including no observed crack development in the pyrite-containing waste rock.

The experiments thus proved that the operating temperature can influence the maximum penetration distance, but the effect depends on the ore type.

8.5 Future work

In this thesis, a method for the tracking of non-surface grain leaching in an unsaturated system and under bioleaching conditions was developed and demonstrated for the analysis of the effect of processing options on metal recovery from three different ores. The application of the developed approach is recommended for the study of other aspects of heap bioleaching operation.

Options exist to improve leaching penetration through appropriate ore preparation. SELFRAG AG has developed a flexible pilot scale Pre-Weakening Testing Station (PWTS) using high voltage pulses (HVP). HVP breakage is a comminution method that uses high voltage pulses to initiate electrical breakdown inside ore particles that are immersed in water, generating a strong tensile force to disintegrate the particles (Zuo et al., 2015). In addition, microwave heating (Charikinya et al., 2015) and HPGR comminution method (Ghorbani et al., 2012) has proved the formation of cracks which has the potential to improve metal recovery. The percentage of zinc extraction of a sphalerite ore over 11 months of leaching in a saturated system has been evidenced to be higher for an ore when crushed by HPGR rather than with a cone crusher (Ghorbani et al., 2012). X-ray µCT and the method developed in the current research study is thus suggested to investigate and quantify high voltage pulses pre-treatment, microwave heating, and comminution method effects on non-surface mineral grain leaching and maximum penetration distance evolution.

The developed quantification methodology can be further applied to other leaching mini-column configurations and various leaching conditions. One such example is the use of intermittent irrigation. Vries (2013) used intermittent irrigation for chalcopyrite bioleaching and found no major difference between continuous and intermittent irrigation in terms of copper leaching efficiency on a time basis with significant improvement on a volume basis. It was suggested that during intermittent irrigation, inverse capillary effects when solution irrigation stops draws the liquid out of the pores and cracks to the ore surface. It would be useful to use the technique to understand the temporal leaching behaviour of non-surface mineral grains, as their recovery is strongly dependent on capillary wetting of the ore and diffusion of reactant species.

Differentiation of different sulphide minerals (such as pyrite and chalcopyrite) in X-ray µCT images is one of the main challenges in using X-ray µCT for the study of heap leaching processes. Using dual-energy acquisition and the combination of X-ray µCT imaging with an appropriate image analysis methodology (grey level co-occurrence matrices, GLCM) (Jardine et al., 2018) is a suggestion to overcome the problem.

References

Acosta, M., Galleguillos, P., Ghorbani, Y., Tapia, P., Contador, Y., Velásquez, A., Espoz, C., Pinilla, C., Demergasso, C., Variation in microbial community from predominantly mesophilic to thermotolerant and moderately thermophilic species in an industrial copper heap bioleaching operation. Hydrometallurgy, 2014, **150**, 281-289.

Africa, C.-J., van Hille, R.P., Harrison, S.T.L., Attachment of Acidithiobacillus ferrooxidans and Leptospirillum ferriphilum cultured under varying conditions to pyrite, chalcopyrite, low-grade ore and quartz in a packed column reactor. Applied Microbiology and Biotechnology, 2013, **97(3)**, 1317-1324.

Ahonen, L., Tuovinen, O.H., Temperature Effects on Bacterial Leaching of Sulfide Minerals in Shake Flask Experiments. Applied and Environmental Microbiology, 1991, **57(1)**, 138.

Anand H., Balasundaram B., Pandit A. B., Harrison S.T. L., The effect of pre-treatment combined with mechanical disruption on the extent of disruption and subsequent release of intracellular protein from E.coli. Biochemical Engineering Journal, 2007, **35(2)**, 166-173.

Antonijević, M.M., Dimitrijević, M., Janković, Z., Leaching of pyrite with hydrogen peroxide in sulphuric acid. Hydrometallurgy, 1997, **46(1)**, 71-83.

Arganda-Carreras, I., Kaynig, V., Schindelin, J., Cardona, A., Seung, H.S., Trainable Weka Segmentation: A machine learning tool for microscopy image segmentation. Arganda-Carreras, 2014, 73-80.

Avizo User's Guide, Avizo User’s Guide, Avizo 9. Konrad-Zuse-Zentrum fu¨r Informationstechnik Berlin (ZIB), Germany, 2015.

BASF, S., 2008. Plurafac® LF types, In *Technical Information*.

Baum, W., Ausburn, K., HPGR comminution for optimization of copper leaching. Minerals & Metallurgical Processing, 2011, **28(2)**, 77-81.

Berry, V.K., Murr, L.E., Hiskey, J.B., Galvanic interaction between chalcopyrite and pyrite during bacterial leaching of low-grade waste. Hydrometallurgy, 1978, **3(4)**, 309-326.

Bingöl, D., Canbazoğlu, M., Dissolution kinetics of malachite in sulphuric acid. Hydrometallurgy, 2004, **72(1)**, 159-165.

Bobadilla-Fazzini, R.A., Pérez, A., Gautier, V., Jordan, H., Parada, P., Primary copper sulfides bioleaching vs. chloride leaching: Advantages and drawbacks. Hydrometallurgy, 2017, **168**, 26-31.

Bouffard, S.C., Review of agglomeration practice and fundamentals in heap leaching. Mineral Processing and Extractive Metallurgy Review, 2005, **26(3-4)**, 233-294.

Brierley, C.L., How will biomining be applied in future? Transactions of Nonferrous Metals Society of China, 2008a, **18(6)**, 1302-1310.

Brierley, J.A., A perspective on developments in biohydrometallurgy. Hydrometallurgy, 2008b, **94(1)**, 2-7.

Bromfield, L., Africa, C.J., Harrison, S.T.L., van Hille, R.P., The effect of temperature and culture history on the attachment of Metallosphaera hakonensis to mineral sulfides with application to heap bioleaching. Minerals Engineering, 2011, **24(11)**, 1157-1165.

Cathles, L.M., Apps, J.A., A model of the dump leaching process that incorporates oxygen balance, heat balance, and air convection. Metallurgical Transactions B, 1975, **6**, 617-624.

Charikinya, E., Bradshaw, S., Becker, M., Characterising and quantifying microwave induced damage in coarse sphalerite ore particles. Minerals Engineering, 2015, **82**, 14-24.

Chiume, R., Minnaar, S.H., Ngoma, I.E., Bryan, C.G., Harrison, S.T.L., Microbial colonisation in heaps for mineral bioleaching and the influence of irrigation rate. Minerals Engineering, 2012, **39**, 156-164.

Cnudde, V., Boone, M.N., High-resolution X-ray computed tomography in geosciences: A review of the current technology and applications. Earth-Science Reviews, 2013, **123**, 1-17.

Colmer, A.R., Hinkle, M.E., The Role of Microorganisms in Acid Mine Drainage. Science, 1947, **106(2751)**, 253.

Córdoba, E.M., Muñoz, J.A., Blázquez, M.L., González, F., Ballester, A., Leaching of chalcopyrite with ferric ion. Part I: General aspects. Hydrometallurgy, 2008a, **93(3)**, 81-87.

Córdoba, E.M., Muñoz, J.A., Blázquez, M.L., González, F., Ballester, A., Leaching of chalcopyrite with ferric ion. Part II: Effect of redox potential. Hydrometallurgy, 2008b, **93(3)**, 88-96.

Dalton, R.F., Diaz, G., Price, R., Zunkel, A.D., The cuprex metal extraction process: Recovering copper from sulfide ores. JOM, 1991, **43(8)**, 51-56.

Dew, D.W., Van Buuren, C., McEwan, K., Bowker, C., Bioleaching of base metal sulphide concentrates: A comparison of high and low temperature bioleaching. The Journal of The South African Institute of Mining and Metallurgy, 2000, 409-414.

Dhawan, N., Safarzadeh, M.S., Miller, J.D., Moats, M.S., Rajamani, R.K., Crushed ore agglomeration and its control for heap leach operations. Minerals Engineering, 2013, **41**, 53-70.

Dhawan, N., Safarzadeh, M.S., Miller, J.D., Moats, M.S., Rajamani, R.K., Lin, C.-L., Recent advances in the application of X-ray computed tomography in the analysis of heap leaching systems. Minerals Engineering, 2012, **35**, 75-86.

Dixon, D.G., Hendrix, J.L., A general model for leaching of one or more solid reactants from porous ore particles. Metallurgical Transactions B, 1993, **24(1)**, 157-169.

Dobson, K.J., Harrison, S.T.L., Lin, Q., Bhreasail, A.N., Fagan-Endres, M.A., Neethling, S.J., Lee, P.D., Cilliers, J.J., Insights into ferric leaching of low grade metal sulfide-containing ores in an unsaturated ore bed using X-ray computed tomography. Minerals, 2017, **7**, 85.

Duncan, D.W., Trussell, P.C., Advances in the Microbiological Leaching of Sulphide Ores. Canadian Metallurgical Quarterly, 1964, **3(1)**, 43-55.

Duncan, D.W., Trussell, P.C., Walden, C.C., Leaching of chalcopyrite with Thiobacillus ferrooxidans: Effect of surfactants and shaking. Applied microbiology, 1964, **12(2)**, 122-126.

Fagan-Endres, M.A., Cilliers, J.J., Sederman, A.J., Harrison, S.T.L., Spatial variations in leaching of a low-grade, low-porosity chalcopyrite ore identified using X-ray μCT. Minerals Engineering, 2017, **105**, 63-68.

Fagan, M.A., Ngoma, I. Emmanuel, Chiume, Rebecca A., Minnaar, Sanet, Sederman, Andrew J., Johns, Michael L., Harrison, Susan T. L., MRI and gravimetric studies of hydrology in drip irrigated heaps and its effect on the propagation of bioleaching micro-organisms. Hydrometallurgy, 2014, **150**, 210-221.

Firdousi, R., Parveen, S., Local thresholding techniques in image binarization. International Journal Of Engineering And Computer Science, 2014, **3(3)**, 4062-4065.

Fischer, D., Pagenkemper, S., Nellesen, J., Peth, S., Horn, R., Schloter, M., Influence of non-invasive X-ray computed tomography (XRCT) on the microbial community structure and function in soil. Journal of Microbiological Methods, 2013, **93(2)**, 121-123.

Florian, B.M., Sand, W., 2012. Inhibition of bacterial pyrite leaching by surfactants, In *Microbes in Applied Research: Current Advantages and Challenges*, ed. Mendez-Vilas. World Scientific, pp. 140-146.

Garcia, D., Lin, C.L., Miller, J.D., Quantitative analysis of grain boundary fracture in the breakage of single multiphase particles using X-ray microtomography procedures. Minerals Engineering, 2009, **22(3)**, 236-243.

Gardner, J.R., Woods, R., An electrochemical investigation of the natural flotability of chalcopyrite. International Journal of Mineral Processing, 1979, **6(1)**, 1-16.

Gericke, M., Muller, H.H., Neale, J.W., Norton, A.E., Crundwell, F.K., 2005. Inoculation of heap-leaching operations, In *Proceedings of the 16th International Biohydrometallurgy Symposium*, Cape Town, South Africa.

Ghorbani, Y., December 2012. On the progressio of leachig from large particles in heaps, In *Department of Chemical Engineering*. University of Cape Town.

Ghorbani, Y., Becker, M., Mainza, A., Franzidis, J.-P., Petersen, J., Large particle effects in chemical/biochemical heap leach processes – A review. Minerals Engineering, 2011, **24(11)**, 1172-1184.

Ghorbani, Y., Franzidis, J.-P., Petersen, J., Heap Leaching Technology—Current State, Innovations, and Future Directions: A Review. Mineral Processing and Extractive Metallurgy Review, 2016, **37(2)**, 73-119.

Ghorbani, Y., Petersen, J., Becker, M., Mainza, A.N., Franzidis, J.-P., Investigation and modelling of the progression of zinc leaching from large sphalerite ore particles. Hydrometallurgy, 2013, **131-132**, 8-23.

Ghorbani, Y., Petersen, J., Harrison, S.T.L., Tupikina, O.V., Becker, M., Mainza, A.N., Franzidis, J.-P., An experimental study of the long-term bioleaching of large sphalerite ore particles in a circulating fluid fixed-bed reactor. Hydrometallurgy, 2012, **129-130**, 161-171.

Govender-Opitz, E., Kotsiopoulos, A., Bryan, C.G., Harrison, S.T.L., Modelling microbial transport in simulated low-grade heap bioleaching systems: The hydrodynamic dispersion model. Chemical Engineering Science, 2017, **172**, 545-558.

Govender, E., Bryan, C.G., Harrison, S.T.L., A novel experimental system for the study of microbial ecology and mineral leaching within a simulated agglomerate-scale heap bioleaching system. Biochemical Engineering Journal, 2015a, **95(Supplement C)**, 86-97.

Govender, E., Bryan, C.G., Harrison, S.T.L., A novel experimental system for the study of microbial ecology and mineral leaching within a simulated agglomerate-scale heap bioleaching system. Biochemical Engineering Journal, 2015b, **95**, 86-97.

Govender, E., Kotsiopoulos, A., Bryan, C.G., Harrison, S.T.L., Modelling microbial transport in simulated low-grade heap bioleaching systems: The biomass transport model. Hydrometallurgy, 2014, **150**, 299-307.

Gupta, C.K., Mukherjee, T.K., *Hydrometallurgy in extraction processes*. 1990, CRC Press.

Habashi, F., A short history of hydrometallurgy. Hydrometallurgy, 2005, **79(1)**, 15-22.

Han, I., Demir, L., Şahin, M., Determination of mass attenuation coefficients, effective atomic and electron numbers for some natural minerals. Radiation Physics and Chemistry, 2009, **78(9)**, 760-764.

Hansford, G.S., Vargas, T., Chemical and electrochemical basis of bioleaching processes. Hydrometallurgy, 2001, **59(2–3)**, 135-145.

Harrison, S.T.L., Bacterial cell disruption: A key unit operation in the recovery of intracellular products. Biotechnology Advances, 1991, **9(2)**, 217-240.

Harrison, S.T.L., 2016. Biotechnologies that use acidophiles, In *Acidophiles: life in extremely acidic environments*, eds. Quatrini, R., Johnson, D.B. Caister Academic Press, UK, pp. 265-284.

Harrison, S.T.L., Dennis, J.S., Chase, H.A., Combined chemical and mechanical processes for the disruption of bacteria. Bioseparation, 1991, **2(2)**, 95-105.

Heinen, H.J., McClelland, G.E., Lindstrom, R.E., Enhancing percolation rates in heap leaching of gold-silver ores. Report of Investigation 8388, Bureau of Mines: Reno, NV,, 1979, 20.

Heyes, G.W., Trahar, W.J., The natural flotability of chalcopyrite. International Journal of Mineral Processing, 1977, **4(4)**, 317-344.

Hirato, T., Majima, H., Awakura, Y., The leaching of chalcopyrite with ferric sulfate. Metallurgical Transactions B, 1987, **18(3)**, 489-496.

Hiroyoshi, N., Arai, M., Miki, H., Tsunekawa, M., Hirajima, T., A new reaction model for the catalytic effect of silver ions on chalcopyrite leaching in sulfuric acid solutions. Hydrometallurgy, 2002, **63(3)**, 257-267.

Hiroyoshi, N., Kuroiwa, S., Miki, H., Tsunekawa, M., Hirajima, T., Synergistic effect of cupric and ferrous ions on active-passive behavior in anodic dissolution of chalcopyrite in sulfuric acid solutions. Hydrometallurgy, 2004, **74(1)**, 103-116.

Hiroyoshi, N., Nakamura, T., Tsunekawa, M., Hirajima, T., Ito, M., Enhancement in Bacterial Leaching of Chalcopyrite by Polyoxyethylene Sorbitan Monolaurate Addition. Shigen-to-Sozai, 1995, **111(13)**, 943-948.

Hoummady, E., Golfier, F., Cathelineau, M., Truche, L., Durupt, N., Blanvillain, J.-J., Neto, J., Lefevre, E., A multi-analytical approach to the study of uranium-ore agglomerate structure and porosity during heap leaching. Hydrometallurgy, 2017, **171**, 33-43.

Hsieh, C.H., 2012. Procedure and analysis of mineral samples using high resolution X-ray micro tomography, In *Department of Metallurgical Engineering*. The University of Utah.

ICSG, The World Copper Factbook 2018. International Copper Study Group, 2018.

Istiadi Guntoro, P., Ghorbani, Y., Koch, P.H., Rosenkranz, J., X-ray microcomputed tomography (µCT) for mineral characterization: A review of data analysis methods. Minerals, 2019, **9**.

Jansen, M., Taylor, A., Overview of gangue mineralogy issues in oxide copper heap leaching. International Project Development Services Pty Limited, 2003.

Jardine, M.A., Miller, J.A., Becker, M., Coupled X-ray computed tomography and grey level co-occurrence matrices as a method for quantification of mineralogy and texture in 3D. Computers & Geosciences, 2018, **111**, 105-117.

Jerez, C.A., 2011. 3.60 - Bioleaching and Biomining for the Industrial Recovery of Metals, In *Comprehensive Biotechnology (Second Edition)*, ed. Moo-Young, M. Academic Press, Burlington, pp. 717-729.

Johnson, M., Detergents: Triton X-100, Tween-20, and More. Materials and Methods, 2013, **3**, 2163.

Justel, F.J., Claros, M., Taboada, M.E., Solubilities and physical properties of saturated solutions in th copper sulphate+sulfuric acid+seawater system at different temperatures. Brazilian Journal of Chemical Engineering, 2015, **32**, 629-635.

Jyothi, N., Sudha, K.N., Natarajan, K.A., Electrochemical aspects of selective bioleaching of sphalerite and chalcopyrite from mixed sulphides. International Journal of Mineral Processing, 1989, **27(3)**, 189-203.

Kametani, H., Aoki, A., Effect of suspension potential on the oxidation rate of copper concentrate in a sulfuric acid solution. Metallurgical Transactions B, 1985, **16(4)**, 695-705.

Kappes, D.W., Precious metal heap leach design and practice. Proceedings of the Mineral Processing Plant Design, Practice, and Control, Littleton, CO, Society for Mining, Metallurgy, and Exploration, , 2002, 1606–1630.

Kappes, D.W., 2005. Heap leaching of gold and silver ores, In *Advances in gold ore processing. Developments in Mineral Processing,*, pp. 456–478.

Kapur, J.N., Sahoo, P.K., Wong, A.K.C., A new method for gray-level picture thresholding using the entropy of the histogram. Computer Vision, Graphics, and Image Processing, 1985, **29(3)**, 273-285.

Ketcham, R.A., Carlson, W.D., Acquisition, optimization and interpretation of X-ray computed tomographic imagery: applications to the geosciences. Computers & Geosciences, 2001, **27(4)**, 381-400.

Khoshkhoo, M., Dopson, M., Engström, F., Sandström, Å., New insights into the influence of redox potential on chalcopyrite leaching behaviour. Minerals Engineering, 2017, **100**, 9-16.

Khoshkhoo, M., Dopson, M., Shchukarev, A., Sandström, Å., Chalcopyrite leaching and bioleaching: An X-ray photoelectron spectroscopic (XPS) investigation on the nature of hindered dissolution. Hydrometallurgy, 2014, **149**, 220-227.

Klauber, C., A critical review of the surface chemistry of acidic ferric sulphate dissolution of chalcopyrite with regards to hindered dissolution. International Journal of Mineral Processing, 2008, **86(1)**, 1-17.

Kocabag, D., Shergold, H.L., Kelsall, G.H., Natural oleophilicity/hydrophobicity of sulphide minerals, II. Pyrite. International Journal of Mineral Processing, 1990, **29(3)**, 211-219.

Kodali, P., Depci, T., Dhawan, N., Wang, X., Lin, C.L., Miller, J.D., Evaluation of stucco binder for agglomeration in the heap leaching of copper ore. Minerals Engineering, 2011a, **24(8)**, 886-893.

Kodali, P., Dhawan, N., Depci, T., Lin, C.L., Miller, J.D., Particle damage and exposure analysis in HPGR crushing of selected copper ores for column leaching. Minerals Engineering, 2011b, **24(13)**, 1478-1487.

Kolmert, Å., Johnson, D.B., Remediation of acidic waste waters using immobilised, acidophilic sulfate-reducing bacteria. Journal of Chemical Technology & Biotechnology, 2001, **76(8)**, 836-843.

Komadel, P., Stucki, J.W., Quantitative assay of minerals for Fe 2+ and Fe3+ using 1,10 phenanthroline; III, A rapid photochemical method. Clays and Clay Minerals 1988, **36(4)**, 379-381.

Kong, S.M., Bodratti, A.M., Wu, J., Tsianou, M., Alexandridis, P., 2014. Micellization studies of branched alkyl ethoxylate and branched alkyl alkoxylate surfactants, In *Department of Chemical and Biological Engineering*. SUNY University at Buffalo.

Lan, Z., Hu, Y., Qin, W., Effect of surfactant OPD on the bioleaching of marmatite. Minerals Engineering, 2009, **22(1)**, 10-13.

Landis, E.N., Keane, D.T., X-ray microtomography. Materials Characterization, 2010, **61(12)**, 1305-1316.

Lee, D.H., Jung, J.M., Kim, S.Y., Kim, K.T., Cho, Y.I., Comparison tests for plasma viscosity measurements. International Communications in Heat and Mass Transfer, 2012, **39(10)**, 1474-1477.

Li, L., Bergeron, I., Ghahreman, A., The effect of temperature on the kinetics of the ferric-ferrous redox couple on pyrite. Electrochimica Acta, 2017, **245**, 814-828.

Lin, C.L., Garcia, C., 2005. Microscale characterization and analysis of particulate systems via cone-beam X-ray microtomography (XMT), In *Innovations in Natural Resource Processing - Proceedings of the Jan D. Miller Symposium*, eds. Young, C.A., Kellar J.J., Free, M.L., Drelich, J., King, R.P. Society for Mining, Metallurgy and Exploration, pp. 421-432.

Lin, C.L., Miller, J.D., 3D characterization and analysis of particle shape using X-ray microtomography (XMT). Powder Technology, 2005, **154(1)**, 61-69.

Lin, Q., 2015. Use of X-ray computed microtomography to measure the leaching behaviour of metal sulphide ores, In *Department of Earth Science and Engineering*. Imperial College London.

Lin, Q., Barker, D.J., Dobson, K.J., Lee, P.D., Neethling, S.J., Modelling particle scale leach kinetics based on X-ray computed micro-tomography images. Hydrometallurgy, 2016a, **162**, 25-36.

Lin, Q., Neethling, S.J., Courtois, L., Dobson, K.J., Lee, P.D., Multi-scale quantification of leaching performance using X-ray tomography. Hydrometallurgy, 2016b, **164(Supplement C)**, 265-277.

Lin, Q., Neethling, S.J., Courtois, L., Dobson, K.J., Lee, P.D., Multi-scale quantification of leaching performance using X-ray tomography. Hydrometallurgy, 2016c, **164**, 265-277.

Lin, Q., Neethling, S.J., Dobson, K.J., Courtois, L., Lee, P.D., Quantifying and minimising systematic and random errors in X-ray micro-tomography based volume measurements. Computers & Geosciences, 2015, **77**, 1-7.

Lin, Q., Yang, M., Meng, F., Sun, L., Bin, T., Calibration method of center of rotation under the displaced detector scanning for industrial CT. Nuclear Instruments and Methods in Physics Research Section A: Accelerators, Spectrometers, Detectors and Associated Equipment, 2018.

Liu, W., Yang, H.-y., Song, Y., Tong, L.-l., Catalytic effects of activated carbon and surfactants on bioleaching of cobalt ore. Hydrometallurgy, 2015, **152**, 69-75.

Madsen, B.W., Groves, R.D., Using oxygen to reactivate a nearly dormant copper sulfide leach / by BuMines RI 8056, 1975, **9**.

Makaula, D.X., Huddy, R.J., Fagan-Endres, M.A., Harrison, S.T.L., Using isothermal microcalorimetry to measure the metabolic activity of the mineral-associated microbial community in bioleaching. Minerals Engineering, 2017a, **106**, 33-38.

Makaula, D.X., Huddy, R.J., Fagan-Endres, M.A., Harrison, S.T.L., Using isothermal microcalorimetry to measure the metabolic activity of the mineral-associated microbial community in bioleaching. Minerals Engineering, 2017b, **106(Supplement C)**, 33-38.

Mehta, A.P., Murr, L.E., Fundamental studies of the contribution of galvanic interaction to acid-bacterial leaching of mixed metal sulfides. Hydrometallurgy, 1983, **9(3)**, 235-256.

Miller, J.D., Lin, C.L., Cortes, A.B., A review of X-Ray computed tomography and its applications in mineral processing. Mineral Processing and Extractive Metallurgy Review, 1990, **7(1)**, 1-18.

Miller, J.D., Lin, C.L., Roldan, C., Garcia, C., Particle size distribution for copper heap leaching operations as established from 3D mineral exposure analysis by X-ray microCT. COPPER 2003-COBRE 2003, Volume VI-Hydro metallurgy of Copper (Book 1), 2003, 83-97.

Nakazawa, H., Nakamura, S., Odashima, S., Hareyama, W., Effect of carbon black to facilitate galvanic leaching of copper from chalcopyrite in the presence of manganese(IV) oxide. Hydrometallurgy, 2016, **163**, 69-76.

Natarajan, K.A., 2018. Chapter 6 - Bioleaching of Copper and Uranium, In *Biotechnology of Metals*, ed. Natarajan, K.A. Elsevier, Amsterdam, pp. 107-150.

Nazari, G., Dixon, D.G., Dreisinger, D.B., The role of silver-enhanced pyrite in enhancing the electrical conductivity of sulfur product layer during chalcopyrite leaching in the Galvanox™ process. Hydrometallurgy, 2012, **113-114**, 177-184.

Nicol, M.J., The kinetics of the dissolution of malachite in acid solutions. Hydrometallurgy, 2018, **177**, 214-217.

Nosrati, A., Robinson, D.J., Addai-Mensah, J., Establishing nickel laterite agglomerate structure and properties for enhanced heap leaching. Hydrometallurgy, 2013, **134-135**, 66-73.

Nosrati, A., Skinner, W., Robinson, D.J., Addai-Mensah, J., Microstructure analysis of Ni laterite agglomerates for enhanced heap leaching. Powder Technology, 2012, **232**, 106-112.

O'Kane Consultants, I., Demonstration of the application of unsaturated zone hydrology for heap leach optimiztion. Report No. 628-1, The Unsaturated Soils Research Group and M.D. Haug and Associates Ltd., 2000, 1-38.

Otsu, N., A Threshold Selection Method from Gray-Level Histograms. IEEE Transactions on Systems, Man, and Cybernetics, 1979, **9(1)**, 62-66.

Panda, S., Akcil, A., Pradhan, N., Deveci, H., Current scenario of chalcopyrite bioleaching: A review on the recent advances to its heap-leach technology. Bioresource Technology, 2015, **196**, 694-706.

Parbhakar-Fox, A., Lottermoser, B.G., A critical review of acid rock drainage prediction methods and practices. Minerals Engineering, 2015, **82**, 107-124.

Park, J.Y., Levenspiel, O., The crackling core model for the multistep reaction of solid particles. Chemical Engineering Science, 1977, **32(2)**, 233-234.

Partearroyo, M.A., Ostolaza, H., Goñi, F.M., Barberá-Guillem, E., Surfactant-induced cell toxicity and cell lysis: A study using B16 melanoma cells. Biochemical Pharmacology, 1990, **40(6)**, 1323-1328.

Peng, A.-a., Liu, H.-c., Nie, Z.-y., Xia, J.-l., Effect of surfactant Tween-80 on sulfur oxidation and expression of sulfur metabolism relevant genes of Acidithiobacillus ferrooxidans. Transactions of Nonferrous Metals Society of China, 2012, **22(12)**, 3147-3155.

Pesic, B., Olson, F.A., Dissolution of bornite in sulfuric acid using oxygen as oxidant. Hydrometallurgy, 1984, **12(2)**, 195-215.

Petersen, J., Determination of oxygen gas–liquid mass transfer rates in heap bioleach reactors. Minerals Engineering, 2010, **23(6)**, 504-510.

Petersen, J., Heap leaching as a key technology for recovery of values from low-grade ores – A brief overview. Hydrometallurgy, 2016, **165**, 206-212.

Petersen, J., Dixon, D.G., Competitive bioleaching of pyrite and chalcopyrite. Hydrometallurgy, 2006, **83(1)**, 40-49.

Petersen, J., Dixon, D.G., 2007a. Modeling and optimization of heap bioleach processes, In *Biomining*, ed. Rawlings, D.E.a.J.D.B.E. Springer, Berlin, pp. 153-176.

Petersen, J., Dixon, D.G., 2007b. Principles, mechanisms and dynamics of chalcocite heap bioleaching, In *Microbial Processing of Metal Sulfides*, eds. Donati, E.R., Sand, W. Springer Netherlands, Dordrecht, pp. 193-218.

Plumb, J.J., McSweeney, N.J., Franzmann, P.D., Growth and activity of pure and mixed bioleaching strains on low grade chalcopyrite ore. Minerals Engineering, 2008, **21(1)**, 93-99.

Quaicoe, I., Nosrati, A., Skinner, W., Addai-Mensah, J., Agglomeration behaviour and product structure of clay and oxide minerals. Chemical Engineering Science, 2013, **98**, 40-50.

Rodríguez, Y., Ballester, A., Blázquez, M.L., González, F., Muñoz, J.A., New information on the chalcopyrite bioleaching mechanism at low and high temperature. Hydrometallurgy, 2003, **71(1)**, 47-56.

Rohwerder, T., T., G., K., K., W., S., Bioleaching review part A: progress in bioleaching: fundamentals and mechanisms of bacterial metal sulfide oxidation. Appl Microbiol Biotechnol., 2003, **63(3)**, 239-248.

Ruan, R., Zou, G., Zhong, S., Wu, Z., Chan, B., Wang, D., Why Zijinshan copper bioheapleaching plant works efficiently at low microbial activity – Study on leaching kinetics of copper sulfides and its implications. Minerals Engineering, 2013, **48**, 36-43.

Rubio, A., García Frutos, F.J., Bioleaching capacity of an extremely thermophilic culture for chalcopyritic materials. Minerals Engineering, 2002, **15(9)**, 689-694.

Sand, W., Gehrke, T., Extracellular polymeric substances mediate bioleaching/biocorrosion via interfacial processes involving iron(III) ions and acidophilic bacteria. Research in Microbiology, 2006, **157(1)**, 49-56.

Sandoval, S.P., Pool, D.L., Schultze, L.E., 1990. Effect of nonionic surfactants on chalcopyrite leaching under dump chemical condition, In *Report of Investigations 9311,*, Reno Research Center, U.S. Bureau of Mines, Reno, NY, pp. 1-12.

Sandoval, S.P., Pool, D.L., Schultze, L.E., Effect of nonionic surfactants on chalcopyrite leaching under dump chemical conditions, Part 2. Report of Investigations 9381, Reno Research Center, U.S. Bureau of Mines, Reno, NY., 1991, 1-10.

Schindelin, J., Arganda-Carreras, I., Frise, E., Kaynig, V., Longair, M., Pietzsch, T., Preibisch, S., Rueden, C., Saalfeld, S., Schmid, B., Tinevez, J.-Y., White, D.J., Hartenstein, V., Eliceiri, K., Tomancak, P., Cardona, A., Fiji: an open-source platform for biological-image analysis. Nature Methods, 2012, **9**, 676.

Schmidt, H., Vetterlein, D., Köhne, J.M., Eickhorst, T., Negligible effect of X-ray μ-CT scanning on archaea and bacteria in an agricultural soil. Soil Biology and Biochemistry, 2015, **84**, 21-27.

Schmuhl, R., Smit, J.T., Marsh, J.H., The influence of microwave pre-treatment of the leach behaviour of disseminated sulphide ore. Hydrometallurgy, 2011, **108(3)**, 157-164.

Searby, G.E., December 2006. An investigation of the kinetics of thermophilic microbial ferrous iron oxidation in continuous culture, In *Department of Chemical Engineering*. University of Cape Town, p. 201.

Shah, K., 2017. The use of surfactants to aid and improve the leaching of low grade copper ores, In *Materials Engineering Department*. The University of British Columbia.

Silverman, M.P., Mechanism of bacterial pyrite oxidation. Journal of Bacteriology, 1967, **94(4)**, 1046-1051.

Silverman, M.P., Ehrlich, H.L., 1964. Microbial Formation and Degradation of Minerals, In *Advances in Applied Microbiology*, ed. Umbreit, W.W. Academic Press, pp. 153-206.

Simate, G.S., Ndlovu, S., Acid mine drainage: Challenges and opportunities. Journal of Environmental Chemical Engineering, 2014, **2(3)**, 1785-1803.

Smart, M., Huddy, R.J., Edward, C.J., Fourie, C., Shumba, T., Iron, J., L., H.S.T., Linking microbial community dynamics in BIOX® leaching tanks to process conditions: Integrating lab and commercial experience. Solid State Phenom., 2017, **262**, 38-42.

Spiro, C.L., Holmes, D.S., Lobos, J., Maylotte, D.H., Use of x-ray computed tomography to examine microbial desulfurization of lump coal. Energy & Fuels, 1987, **1(1)**, 76-79.

Sprawls, P., AAPM tutorial. CT image detail and noise. RadioGraphics, 1992, **12(5)**, 1041-1046.

Sridevi, M., Mala, C., A Survey on Monochrome Image Segmentation Methods. Procedia Technology, 2012, **6**, 548-555.

Takayanagi, S., Kawasaki, H., Sugimori, K., Yamada, T., Sugai, A., Ito, T., Yamasato, K., Shioda, M., Sulfolobus hakonensis sp. nov., a Novel Species of Acidothermophilic Archaeon. International Journal of Systematic and Evolutionary Microbiology, 1996, **46(2)**, 377-382.

Tan, K., Li, C., Liu, J., Qu, H., Xia, L., Hu, Y., Li, Y., A novel method using a complex surfactant for in-situ leaching of low permeable sandstone uranium deposits. Hydrometallurgy, 2014, **150**, 99-106.

Tapera, T., Sheean, J., Nikoloski, A.N., The effect of silver on the acidic ferric sulfate leaching of primary copper sulfides under recycle solution conditions observed in heap leaching. Part 2: Synergistic additives. Hydrometallurgy, 2018, **179**, 1-7.

Temple, K.L., Colmer, A.R., The autotrophic oxidation of iron by a new bacterium: Thiobacillus ferroxidans. Journal of Bacteriology, 1951, **62(5)**, 605-611.

Torma, A.E., Gabra, G.G., Guay, R., Silver, M., Effects of surface active agents on the oxidation of chalcopyrite by thiobacillus ferrooxidans. Hydrometallurgy, 1976, **1(4)**, 301-309.

Tributsch, H., Gerischer, H., The oxidation and self-heating of metal sulphides as an electrochemical corrosion phenomenon. Journal of Applied Chemistry and Biotechnology, 1976, **26(1)**, 747-761.

Van Geet, M., Swennen, R., Wevers, M., Quantitative analysis of reservoir rocks by microfocus X-ray computerised tomography. Sedimentary Geology, 2000, **132(1)**, 25-36.

van Hille, R.P., van Zyl, A.W., Spurr, N.R.L., Harrison, S.T.L., Investigating heap bioleaching: Effect of feed iron concentration on bioleaching performance. Minerals Engineering, 2010, **23(6)**, 518-525.

Van Staden, P., Naseri, A., Petersen, J., HEAPSIM modelling of high temperature heap bioleaching data. 2007.

Vest, M., Lutzerath, A., Friedrich, B., Seelmann-Eggebert, H.-P., 2009. Improvments in copper heap leaching by use of wetting agents, In *Proceedings of EMC*, pp. 1-12.

Vries, E., 2013. Effects of intermittent irrigation on the extraction of copper from heap bioleaching systems, In *Department of Chemical Engineering*. University of Cape Town.

Wang, Y., Lin, C.L., Miller, J.D., Improved 3D image segmentation for X-ray tomographic analysis of packed particle beds. Minerals Engineering, 2015, **83**, 185-191.

Wang, Y., Lin, C.L., Miller, J.D., Quantitative analysis of exposed grain surface area for multiphase particles using X-ray microtomography. Powder Technology, 2017, **308**, 368-377.

Watling, H.R., The bioleaching of sulphide minerals with emphasis on copper sulphides — A review. Hydrometallurgy, 2006, **84(1)**, 81-108.

Watling, H.R., Chalcopyrite hydrometallurgy at atmospheric pressure: 1. Review of acidic sulfate, sulfate–chloride and sulfate–nitrate process options. Hydrometallurgy, 2013, **140**, 163-180.

Watling, H.R., Collinson, D. M., Li, J., Mutch, L. A., Perrot, F. A., Rea, S. M., Reith, F., Watkin, E. L. J., Bioleaching of a low-grade copper ore, linking leach chemistry and microbiology. Minerals Engineering, 2014, **56**, 35-44.

Xia, L., Uribe, P., Liu, X., Yu, C., Chai, L., Liu, J., Qiu, W., Qiu, G., Comparison of chalcopyrite bioleaching after different microbial enrichment in shake flasks. World Journal of Microbiology and Biotechnology, 2013, **29(2)**, 275-280.

Yeh Daniel, H., Pennell Kurt, D., Pavlostathis Spyros, G., Effect of Tween surfactants on methanogenesis and microbial reductive dechlorination of hexachlorobenzene. Environmental Toxicology and Chemistry, 2009, **18(7)**, 1408-1416.

Zuo, W., Shi, F., van der Wielen, K.P., Weh, A., Ore particle breakage behaviour in a pilot scale high voltage pulse machine. Minerals Engineering, 2015, **84**, 64-73.